STRUCTURAL ANALYSIS OF THE DRAINAGE BASIN OF KENYAN RIFT VALLEY LAKES WITHIN THE ABERDARE DETACHMENT, USING SATELLITE DATA, GIS AND FIELD OBSERVATIONS

BY

SIMON MANG'ERERE **ONYWERE**

A Thesis Submitted to the Faculty of Science, in Fulfilment of the Requirements for the Award of the Degree of Doctor of Philosophy (Geology)

Department of Geology, University of Nairobi,
P.O. Box 30197 Nairobi, KENYA

March 1997

This thesis is my original work and has not been submitted for a degree in any other University.

Signed ---------- date---6th SEPT. 1996

Simon Mang'erere **Onywere**

Department of Geology

University of Nairobi

This thesis has been submitted for the degree of Doctor of Philosophy (Geology) with our knowledge as University Supervisors.

signed ---------- date---11th Sept. 1996

Prof. Steve Jesse **Gaciri**

Professor, Department of Geology

University of Nairobi

signed ---------- date---11/9/96

Dr. Norbert **Opiyo-Akech**

Senior Lecturer, Department of Geology

University of Nairobi

STRUCTURAL ANALYSIS OF THE DRAINAGE BASIN OF KENYAN RIFT VALLEY LAKES WITHIN THE ABERDARE DETACHMENT, USING SATELLITE DATA, GIS AND FIELD OBSERVATIONS

Simon Mang'erere ***Onywere***

Department of Geology, University of Nairobi

ABSTRACT

In addressing the problem of lake-level changes in the drainage basin of the Kenyan Rift Valley lakes (Bogoria, Nakuru, Elmenteita, Naivasha) of the Aberdare Detachment System, a study of the watershed of the basin is made. The study deals with information extraction and representation using digital techniques based on ERDAS image analysis programs and Intergraph, Geographic Information System (GIS) based on Microstation software. A GIS database is designed, and through modelling, has provided the cartographic ability to address the questions posed by the present problem. Because of variation in data types and sources, raster-based GIS and vector-based GIS are used. At first approach, analysis is based on visual interpretation of photographic products. In designing raster-based GIS, satellite imagery is initially digitally enhanced and filtered. Analysis of Landsat-5 TM and SPOT imagery is made and used for interpretation and classification, facilitating analysis of land use and land cover characteristics and patterns. Good ground resolution, and characteristics of the data reveal significant details of the land use cover patterns and linear patterns of fault scarps, with the synoptic view suggesting NNE, NE and NW trending scarps and associated grabens. The spectral analysis has allowed for:

(1) Image classification of Nakuru-Menengai area using supervised image classification programs and Principal Component Analyzed (PCA) image data.

(2) Lineament analysis and drainage pattern analysis using PCA and directionally filtered image data.

(3) Generation of raster GIS data files that are integrated and modelled with vector GIS data files.

The image classification identifies 17 land cover types that show a marked increase in agricultural activity in the study area in the period July 1984 to present. Increased irrigation around lake Naivasha in this period has resulted in increased direct consumption of water from the lake. There is also increased land use in the catchment areas of the lakes, affecting the morphology of the delicate soil structure and the forest cover, and subsequently run-off into the lakes. The loss of vegetation cover on the soils has resulted in decreased infiltration and thus ground discharge into the lakes. This has affected the water levels in the lakes.

For the vector GIS, information concerning five themes, namely structures (faults), lithology, drainage patterns, land use patterns, and topography, is extracted from topographic maps, geologic maps, and tables and reports of the study area. The various digitized elements are given attribute values through Look-up-Tables and referenced to the analyzed satellite data. In the referencing, the imagery products are draped on the vector data and incorporated into the database. The area is divided into three tectonic blocks on the basis of recognized trends of fault patterns. A detailed analysis of selected areas in the three divisions is made, basing the interpretation on a number of measurable and recognizable features in the images, ground truth data, and integration with digitized data sets.

Stored GIS information allows for graphic presentation of the morphotectonic structures of the Aberdare Detachment. Comparison between vector data and raster data, reveal a strong structural control and tectonic involvement on the drainage patterns and the lake basins. There is also strong structural control into the geothermal reservoirs. Step-fault ramps channel water from the marginal escarpments and the platform areas into the rift floor, largely directing the waters away from the nearby lake basins into widely separated basins. Thus, the drainage into lakes Bogoria, Nakuru, Elmenteita and Naivasha cover small areas, poorly recharging these lakes.

* * *

ACKNOWLEDGMENTS

Information from various sources obtained through the courtesy of a number of individuals, were used in this work. First, I am indebted to Egerton University for granting me study leave, without which I could not have effectively carried out this research. I am also indebted to Egerton University for allowing me the use of the University vehicle and driver during the ground truth survey. I express my gratitude to the German Academic Exchange Services (DAAD) for a Research Grant in the first two years of this project. I am also grateful to DAAD for supporting me to work at the Ludwig Maximilians, University of Munich from June to the end of October 1994.

I would like to express my sincere appreciation to Prof. S.J. Gaciri and Dr. N. Opiyo-Akech of the Department of Geology, University of Nairobi, for not only serving as my thesis advisors and supervisors, but also for initiating my study visit to the Centre for Interactive Graphical Computing (CIGC), Department of Geological Sciences, University of Cape Town (UCT), through Prof. Maarten de Wit of that University. The two supervisors together with Prof. de Wit, kindly helped me with the field survey strategy and promoted my interest in GIS database design. Their guidance, comments and criticism greatly helped me in the research methodology followed and in structuring this research effort.

Two periods were spent at the University of Cape Town. The first period was from May to October 1993, with support from South Africa's Fund for Research and Development (FRD). For this period, I am indebted to Prof. de Wit, Mr. Russell Hebert and Miss Armenia Vitali of CIGC, who guided me through, and facilitated the structuring of the vector GIS, based on the Gondwana GIS. The second period is part of a continuing 13 month study visit from May 1996, sponsored by the Universities Science, Humanity and Engineering Partnerships in Africa (USHEPIA). I am grateful to the USHEPIA International Steering Committee and Prof. de Wit, Dr N. Opiyo-Akech, Mr Daniel Wilson and Dr M. Doucoure for their guidance during this period which was used to prepare the illustrations in this thesis. I am also indebted to the Department of Geological Sciences at UCT, for their support.

The outcome of this thesis was also a result of initial training in GIS database design,

at the Regional Centre for Services in Surveying Mapping and Remote Sensing (RCSSMRS) and Department of Resource Surveys and Remote Sensing (DRSRS) to which I owe my gratitude to Mr. L. Isavwa of RCSSMRS and Messrs S. Nga'nga and J. Njuguna of DRSRS. In undertaking the training that led to satellite digital image analysis, I am deeply indebted to DAAD for their support to the Remote Sensing Work Group (AGF), Institute for General and Applied Geology, Ludwig Maximilians, University of Munich. I register my appreciation to Prof. Dr J. Bodechtel and the staff of AGF for taking me through the various stages of image analysis. The production related to imagery is due to the analysis at the AGF.

My gratitude also goes to the Office of the President, Government of Kenya, and the Provincial Administration, for permission to use the topographic maps, and to visit the study area. I thank the Kenya Wildlife Services for giving me unlimited access to the National Parks. Thanks also go to the Kenya Power and Lighting Company, for access to Olkaria Power Station area and for providing unlimited access to their library facilities. I also thank the DRSRS and Mines and Geology Department for consultations. I express my gratitude to the National Oil Corporation of Kenya for aeromagnetic and gravity data and for the geological and structural maps of Kenya.

Comments and critical remarks made by various reviewers, were of great help in writing this thesis. I am deeply indebted to Prof. A. F. H. Goetz of the Centre for Study of Earth from Space, University of Colorado and Prof. P. Wiegand of the Department of Geological Sciences, California State University for their advise on the choice of Landsat-5 TM digital data. Thanks also go to Mr. Guy Neuville of the French Technical Assistance (FTA), at the RCSSMRS who kindly provided me with SPOT digital data used for image analysis. Thanks go to all staff of the Department of Geology, University of Nairobi, who have had direct or indirect impact on the ideas expressed in this thesis.

Finally my appreciation goes to my wife, Margaret K. Omiti, and children, C. Omari and E. Nyaundi for their patience throughout the research period and in the long months I was away. Their love and moral support have been a great source of inspiration. I thank God for His countless blessing throughout the years.

Simon M. Onywere (March 1997)

TABLE OF CONTENTS

TITLE PAGE i

DECLARATION PAGE ii

ABSTRACT iii

ACKNOWLEDGMENTS v

TABLE OF CONTENTS vii

LIST OF FIGURES xi

LIST OF TABLES xiii

LIST OF PLATES xiv

LIST OF PHOTOGRAPHS xv

LIST OF ACRONYMS AND ABBREVIATIONS xviii

CHAPTER 1: INTRODUCTION 1

1.0 OBJECTIVES AND JUSTIFICATION 1

1.1 THE STUDY AREA 2

1.1.1 Geological Setting 2

1.1.2 Physiography 8

1.1.3 Infrastructure 11

1.1.4 Climate 11

1.1.5 Vegetation 13

1.1.6 Volcanic Soils, Alluvium and other Soils 15

1.2 PREVIOUS WORK 16

1.2.1 Rift Evolution and Geological Studies 16

1.2.2: Studies using Satellite Remote Sensing Techniques 20

1.3 METHODOLOGY AND DATA ACQUISITION 22

1.3.1 Preparation of Working Images and Establishing the Vector Database 24

1.3.2 Pre- and Post-interpretation Ground Observation 25
1.3.3 Interpretation Process 26

CHAPTER 2: APPLICATION OF SATELLITE REMOTE SENSING TECHNIQUES IN LAND USE AND LAND COVER PATTERN ANALYSIS OF THE OLOBANITA-NYAHURURU AREA 28

2.0 INTRODUCTION 28

2.1 THE GEOLOGY 31

2.2 HYDROLOGY 33

2.3 AGRICULTURE 36
2.3.1 Sisal Plantations of Olobanita Plain 37
2.3.2 Rangelands and Semi-Arid Northwest 40
2.3.3 Bahati Forest 40
2.3.4 Population Estimates 43

CHAPTER 3: IMAGE ANALYSIS/GIS AND LAND COVER CLASSIFICATION OF NAKURU-MENENGAI AREA 44

3.0 INTRODUCTION 44

3.1 IMAGE ENHANCEMENT OF NAKURU-MENENGAI SUBSCENE 49

3.2 PRINCIPAL COMPONENT ANALYSIS OF NAKURU-MENENGAI SUBSCENE 52

3.3 MULTISPECTRAL IMAGE CLASSIFICATION OF NAKURU-MENENGAI AREA 56
3.3.1 Signature Evaluation 56
3.3.2 Classification Results 62

3.3.3 Menengai Caldera Classification and Interpretation 69

CHAPTER 4: STRUCTURAL ANALYSIS OF THE DRAINAGE BASIN OF CENTRAL KENYAN RIFT VALLEY LAKES (ABERDARE DETACHMENT SYSTEM) USING A VECTOR GEOGRAPHIC INFORMATION SYSTEM (GIS) DATABASE DESIGN 77

4.0 INTRODUCTION 77

4.1: VECTOR GIS DATABASE DESIGN AND ORGANIZATION 79
4.1.1 Data Selection and Entry 79
4.1.2 Data Processing and GIS Information 85

4.2 THE FAULT BLOCKS OF THE ABERDARE DETACHMENT 92
4.2.1 The Sattima-Mau Block 95
4.2.2 Solai-Subukia Block 98
4.2.3 Lake Bogoria Block 100

CHAPTER 5: THE TECTONIC STRUCTURES, HYDROLOGIC REGIMES AND GEOTHERMAL RESOURCES OF THE ABERDARE DETACHMENT 108

5.0 INTRODUCTION 108

5.1 THE RIFT VALLEY FLOOR AND ITS VOLCANIC CENTRES 110
5.1.1 Eburru Volcanic Complex 110
5.1.2 Longonot Volcano 112
5.1.3 Margaret Volcano 116
5.1.4 Suswa Caldera 117

5.2 THE CENTRAL RIFT VALLEY DRAINAGE SYSTEMS 118
5.2.1 Structural Control on the Drainage Systems 124
5.2.2 Lake Naivasha (1885 m a.s.l) 128
5.2.3 Crater Lake 135

5.2.4 Lake Elmenteita (1776 m a.s.l) 135
5.2.5 Lake Nakuru (1758 m a.s.l) 137
5.3.6 Lake Bogoria (985 m a.s.l) 141

5.3 GEOTHERMAL MANIFESTATIONS IN THE ABERDARE DETACHMENT 145

CHAPTER 6: SUMMARY AND CONCLUSIONS 153

6.1 RESULTS AND DISCUSSIONS FOR LAND COVER AND STRUCTURAL-GEOLOGICAL MAPPING 153
6.1.1 Land cover characteristics and classification 155
6.1.2 Errors in radiometric signature classification 157

6.2 CONCLUSIONS AND RECOMMENDATIONS 158

REFERENCES 163

APPENDICES 176

APPENDIX 2.1 Records of various fault azimuths in the Aberdare Detachment 176

APPENDIX 3.1 Image histograms of the original TM data of Nakuru-Menengai area (Image file TMS4.LAN) 181

APPENDIX 3.2 Signature ellipse plots and scatter diagrams of PCA Landsat-5 TM image file T1PCA.LAN of Nakuru-Menengai area 188

APPENDIX 4.1 Projection parameters of 1:50000 topography and 1:125000 geological maps, used to create GIS design files of topography, lithology, and structures of the study area 193

APPENDIX 4.2 GIS attributes of lithology of the Aberdare Detachment area 195

LIST OF FIGURES

Figure 1.1: Schematic map of East Africa Rift System showing the positions of the Cenozoic Eastern and Western Rift Branches and the Proterozoic Aswa, Tanganyika-Rukwa-Malawi (TMR) and Zambezi shear zones 3

Figure 1.2: Structural map of Kenya showing the relationship between the Cenozoic Kenyan Rift Valley, the Precambrian marble outcrops, and the Mesozoic fault systems to the east of the Rift Valley. 5

Figure 1.3: A generalised structural map of the Aberdare Detachment area showing the three main structural trends 6

Figure 1.4: Communication and physiography of the study area 9

Figure 2.1: Morphostructural interpretation of Menengai-Nyahururu area made from SPOT satellite imagery and existing geological and topographic maps 29

Figure 2.2: Tectonic structure of Olobanita-Nyahururu area 32

Figure 2.3: Interpreted land Cover Map of Olobanita plain 38

Figure 2.4: interpreted land cover Map of part of Bahati forest 41

Figure 3.1: Schematic representation of some of the influence on incident electromagnetic (EM) radiation showing the effect of the atmosphere in determining the various paths of energy to the sensor. 46

Figure 3.2: Plot of Ellipse Diagram showing parallelepiped classification of correlated data 58

Figure 3.3: Interpreted land cover map of Menengai crater area 72

Figure 4.1: Flow diagram showing a typical GIS set-up 80

Figure 4.2: Flow diagram showing five steps involved in an individual GIS database design 81

Figure 4.3: Flow diagram showing some attributes of a lithology (silt), and how they are linked to the map design through the MS-link, the litho-centroid 86

Figure 4.4: Lithological map of Central Rift Valley, Kenya, showing the lithology polygon boundaries and the litho-centroids 87

Figure 4.5: Flow diagram showing the process involved in GIS database design and information flow 88

Figure 4.6: Morphotectonic map of the Aberdare Detachment 90

Figure 4.7: Structural elements of the Aberdare Detachment, compiled from existing geological maps, image interpretation results and ground truth survey 93

Figure 4.8: Morphotectonic map of lake Bogoria showing the main structural trends and the drainage patterns 102

Figure 4.9: Structural tectonic map of lake Bogoria area 103

Figure 4.10: Block diagram of the southern part of Lake Bogoria area observed eastward 105

Figure 4.11: Rose diagram depicting azimuth frequencies of faults in the Lake Bogoria Block 106

Figure 5.1: Drainage Patterns and the extend of the watershed in the Aberdare Detachment 122

Figure 5.2: Drainage map of the Aberdare Detachment, showing the relationship between the major fault structures, and the drainage patterns 126

Figure 5.3: Morphotectonic map of lake Naivasha showing the main structural trends and the drainage patterns 130

Figure 5.4: Rose diagram depicting azimuth frequencies of faults in the Lake Naivasha area 131

Figure 5.5: Structural elements of lake Nakuru-lake Elmenteita area interpreted from Landsat-5 TM imagery and existing geological maps 139

Figure 5.6: Rose diagram depicting azimuth frequencies of faults in the Lake Nakuru area 140

LIST OF TABLES

Table 1.1: Monthly and annual rainfall averages (in mm) calculated for the period 1962-1991 for twelve stations in the study area and measured in a standard raingauge 12

Table 2.1: Summary of satellite photographic products used for interpretation of Olobanita-Nyahururu area 30

Table 2.2: Different levels of maturity of sisal plants recognised from the imagery of Olobanita Plains 39

Table 2.3: Extent of forest depletion in a section of Bahati Forest since 1959 42

Table 3.1: Characteristics of SPOT imaging systems 45

Table 3.2: Summary of satellite digital data used for image analysis 49

Table 3.3: Coefficients of principal component analysis for Nakuru-Menengai image 53

Table 3.4: Calculated Correlation Matrix for Nakuru-Menengai image 54

Table 3.5: Coefficients of Principal Component Analysis for Lake Bogoria image 55

Table 3.6: Image classification Contingency Table using Maximum Likelihood classifier and the first 3 Principal Component Bands 59

Table 3.7: Signature Euclidian Distance Measure Generated using the first 3 Principal Component Bands 60

Table 3.8: Signature Separability Listing of all class pairs of PCA image of Nakuru-Menengai area, formed using PC's 1,2,3 and both Jeffries-Matusita Distance and Transformed Divergence Distance Measures 61

Table 3.9: Land use categories and land cover classes of Nakuru-Menengai area 67

Table 3.10: Spectral characteristics of land cover units of Menengai Crater floor lavas 73

Table 4.1: Data elements and sources identified for the GIS database design of Central Kenya Rift Valley 82

Table 4.2: Vector data capture mode 82

LIST OF PLATES

Plate 2.1: SPOT image FCC of 9/2/1987 of Olobanita plain, north of Menengai Crater 38

Plate 2.2: FCC of part of Bahati Forest (TM image 28/5/88) showing dense forest in

dark red to red hues 41

Plate 3.1: A 5x5 Add-Back Box Filtered, standard FCC (bands 7,5,1 in RGB order) image of Nakuru-Menengai area 51

Plate 3.2: Principal Component Analysis image of Nakuru-Menengai area, displaying principal component bands 2,1,3 in RGB order 57

Plate 3.3: Land cover classification image of Nakuru-Menengai area, obtained from applying Maximum Likelihood classifier to the PCA image of the area 66

Plate 3.4: FCC and classification image of Menengai Crater, showing the caldera lavas and the land use patterns around the crater 71

Plate 4.1: Principal Component Analysis image of Lake Bogoria area, formed from a subset of sum average of TM bands 1,2,3 and bands 4,5,7 and displaying principal component bands 2,1,3 in RGB order. 101

Plate 4.2: Principal Component Analysis image of south-eastern part of Lake Bogoria, showing a close-up view of a rhomb-shaped structure 104

Plate 5.1: FCC of Lake Naivasha area, formed by registering Landsat-TM (1/3/1989) bands 5,1,7 in RGB order 129

Plate 5.2: Linear rectified image of lake Nakuru-lake Elmenteita area, showing lithology boundaries as digitized from geological maps of the area 138

LIST OF PHOTOGRAPHS

Photo 1.1: East-downthrown, step-faulted Mau Escarpment 10

Photo 1.2: West-downthrown Marmanet Escarpment, cutting through phonolite lavas 10

Photo 1.3: Depleted natural forest on Mau Escarpment, west of Sakutiek 14

Photo 1.4: The Rift Valley floor at Kedong plain 14

Photo 2.1: Thomson's Falls Waterfall at Nyahururu 35

Photo 2.2: Sisal plantations at Olobanita plain 35

Photo 3.1: Lava flows in Menengai Crater caldera floor 74

Photo 3.2: A low graben (arrow) on the north-east of Menengai Crater, showing a tilted down-faulted block towards the caldera floor 74

Photo 5.1: A pumice cone erupted along the N-S trending faults east of Eburru 111

Photo 5.2: Ol'lolbutot lava flow at Olkaria geothermal field area 111

Photo 5.3: A River section south of the Black Reef of Longonot lava 115

Photo 5.4: Trace of undermined Nguruine fault 115

Photo 5.5: The inner caldera of Suswa Volcano 119

Photo 5.6: A grove of phreatophyte vegetation of the papyrus, indicating presence of sub-surface waters 119

Photo 5.7: Crater Lake, at Crater Lake volcano, Naivasha 136

Photo 5.8: Kariandus diatomaceous deposit 136

Photo 5.9: The dry lake bed of Lake Elmenteita 142

Photo 5.10: Lake Bogoria Escarpment 142

Photo 5.11: Dyke intrusions at Ol Njorowa Gorge 148

Photo 5.12: Ol'lolbutot fissure 148

LIST OF ACRONYMS AND ABBREVIATIONS

AGF: (Arbeitsgruppe Fernerkundung) Remote Sensing Working Group

ARC/INFO: Environment and Remote Sensing Institute (ERSRI) GIS software

ARCVIEW: Environment ad Remote Sensing Institute (ERSRI) GIS software

BIL: Band Interleaved by Line, satellite data storage format

Bpi: Bits per inch

BSQ: Band Sequencial, satellite data storage format.

CIGC: Centre for interactive Graphical Computing.

CLASOVR: ERDAS program that overlays a GIS file on a raw image file for comparison on the display screen.

CMATRIX: ERDAS program, performs contingency matrix analysis of training samples and reports percentages of pixels that are classified as expected.

Colour Composite: A colour image produced by assigning a colour to each of the bands of a scene and digitally superimposing the results.

Contrast Stretching: Increasing the contrast of images by expanding the original range of values or tones to utilise the full contrast range of the display device.

DAAD: (Deutscher Akademischer Austauschdienst) The Germany Academic Exchange Services

Database: A collection of non-redundant data files shared among different applications (a collection of computer programs performing a particular function).

DBMS: Database Management System.

Design: Microstation coverage graphic data file.

DEM: Digital Elevation Model - a 2.5 dimensional representation of terrain as a function of elevation.

DIGSCRN: ERDAS software, display-screen digitizing of vector data against the backdrop of a displayed image.

DISPLAY: ERDAS software that displays GIS files with automatic pseudo colour scheme assignment, class name display, screen mosaic and magnification options.

Directional Filter: A spatial filter applied in a specified direction.

DIVERGE: ERDAS software, computes and reports Transformed Divergence and Jeffreys-Matusita Distance for evaluating signature separability and band combinations.

DN Digital Number

DRSRS: Department of Resources Surveys and Remote Sensing.

ELLIPSE: ERDAS software, plots 2-d ellipses and scattergrams of signature statistics to evaluate signature separability.

EOSAT: Earth Observation Satellite Company

ERDAS: Earth Resources Data Analysis system, an image processing software.

FCC: False Colour Composites

FRD: Fund for Research and Development.

FTA: French Technical assistance

GIS: Geographic Information Systems - Tools for collecting, storing, manipulating and retrieving data from the real world for a particular purpose.

GISOVR: ERDAS software the displays a GIS file in the overlay plane of the display device.

Ground control point: A geographical feature of Known location that is recognisable on the images and can be used during geometric correction.

Ground truth: Supporting data collected on the ground and information derived there from as an aid to interpretation of remote sensed data.

High-pass Filter: A spatial filter that enhances high spatial frequencies and as a result sharpens the image.

HIS: Hue, Intensity, Saturation.

Hue: The attribute of a colour by virtue of which it differs from grey of the same brilliance and allows it to be classified in different classes such as green, red blue etc.

Image registration: The process of geometrically aligning two or more sets of image data such that the image data matches its position on the ground.

IPX: ERDAS software, Image Processing Extension function

Kernel: A pixel array used for image filtering

Landsat: A series of satellites used for remote sensing that were deployed by the United States National Aeronautics and Space Administration (NASA) and which carry RVB, MSS and TM imaging systems.

LUT: Look-up-Tables.

LUTMOD: ERDAS software, Look-up-Table modification tools.

MAXCLAS: ERDAS software, classification program for minimum distance, mahalanobis distance and maximum likelihood decision rules.

MGE: Microstation GIS Environment.

MGE/ISI: Microstation software, MGE ImageStation Imager.

MSPM: Microstation Software, Microstation Projection Manager

Microstation: An Intergraph Cooperation GIS software.

MOMS: Moduler Optical Multispectral Scanner on board the Space Shuttle.

MSS: Multispectral Scanner on board Landsat satellite

Multispectral data: Remotely sensed data in two or more bands.

PCA: Principal Components Analysis - A mathematical method of generating a new set of variables for image bands that are highly correlated, and which describe the variance of the original data set but are independent of each other.

PRINCE: ERDAS software, Principal components analysis for up to 16 input bands.

RCSSMRS: Regional Centre for Services for Surveying Mapping and Remote Sensing.

Relational Model: A data model that uses a table to represent an object in the real world.

Remote Sensing: The use of Electromagnetic radiation sensors to record images of the environment which can be interpreted to yield useful information: i.e. obtaining information about the physical features without any physical contact with the features.

RGB: Red Green and Blue, colour assignments to image bands

Saturation: The purity of a colour or the degree to which all wavelengths correlate to the dominant wavelength (hue).

SIGEXT: ERDAS software, training sample definition based on an input DIG (digitized polygon) file.

SIGMAN: ERDAS software, combines all signature manipulations: rename, delete merge and append.

SPOT: Satellite probatoire de'Obsevation de la Terre - a French satellite system carrying the HRV instrument.

SQL: Structured Query language - A language used in documentation of tables, definitions and retrieval of data tables using structured statements.

TM: Thematic Mapper - A second generation imaging systems used on board the landsat satellites.

Training sample: Data samples of known identity used to determine decision boundaries as part of a supervised classification of a digital image.

THRESH: ERDAS program, interactive classification thresholding using the probability image created by MAXCLAS.

UCT: University of Cape Town.

USHEPIA: Universities Science, Humanity, Engineering Partnerships in Africa.

WFM: (Write Function Memory) Interactive enhancement utility for image contrast stretch.

CHAPTER 1

INTRODUCTION

1.0 OBJECTIVES AND JUSTIFICATION

This project aims to:

(1) create a Geographic Information System (GIS) database design and use it to integrate raster and vector data sets for land use, land cover, structural, hydrological and geological analysis.

(2) interpret satellite imagery and use it for land cover classification and to examine its effectiveness, suitability and capacity for land use pattern analysis and for structural and geological mapping of the Aberdare Detachment area.

(3) evaluate the land resources of the area such as vegetation, hydrology, geothermal resources, settlement patterns and demographic development.

The GIS database would be used to analyze fissure and fracture zones, and drainage termination areas, in order to locate surface water seepage into, or away from Central Kenya Rift Valley lakes and regional groundwater reservoirs in the axial graben of the Aberdare Detachment. It is anticipated that a GIS database could be implemented to analyze and query spatially related data, relevant to the study area. For example, the GIS is expected to be able to correlate faults and fractures, lithology and hydrological regimes, and to make a drainage network analysis with the hope of understanding the dynamics of the Rift Valley lakes. GIS modelling can also be used for identification of the arrangement and orientation of rift floor fault structural elements. This would additionally resolve the direction of stress fields causing rifting, and thus the geological evolution of the Rift Valley.

The project uses a Geographical Information System (GIS) database design and integration of data sets through vector GIS and raster GIS. It uses vector database and image

analysis to establish a methodology of data integration and registration for maximum utilization of available data. The use of remote sensing techniques and data analysis methods for land cover studies are assessed in this project. By applying a digital image analysis programme to enhance and map out lineaments, drainage patterns, land use cover patterns and geomorphological features in the central section of Kenya Rift Valley, faults and fractures are defined based on geomorphological indicators such as abrupt changes in, or termination of, drainage lines and presence of recent fissure flows and volcanic centres.

Interpretation and classification of satellite imagery allows for identification of structural elements, land systems and land cover units in a local and regional scale based on vegetation delineation. Vegetation delineation and land use pattern classification is helpful in developing an organizational framework for resources analyses and planning. It provides information on areal extent of probable water resources and the nature of drainage systems which is of high priority, in the study area, both in terms of assessing rational development in the region and in environmental monitoring.

1.1 THE STUDY AREA

1.1.1 Geological Setting

The terrain under study is a part of a section of the Central Kenya Rift Valley (Gregory Rift Valley - Gregory, 1896), bound by approximately 0°25'N and 0°55'S latitudes and 35°50'E and 36°40'E longitudes. The Rift Valley is a Cenozoic intra-continental oceanic rift system separating the Somalia Sub-plate from the rest of Africa (Chorowicz, 1992; Smith and Mosley, 1993; Delvaux *et al.*, 1992) - Figure 1.1. The Rift Valley system has a linear N-S geographic (sub-meridian) trend delineated by flank faults with individual faults oriented at diverse angles (see Appendix 2.1). Steep scarps mark the flank faults and long fault lines, while the intervening smaller faults are in places marked by low, narrow horst-graben structures (Baker *et al.*, 1972).

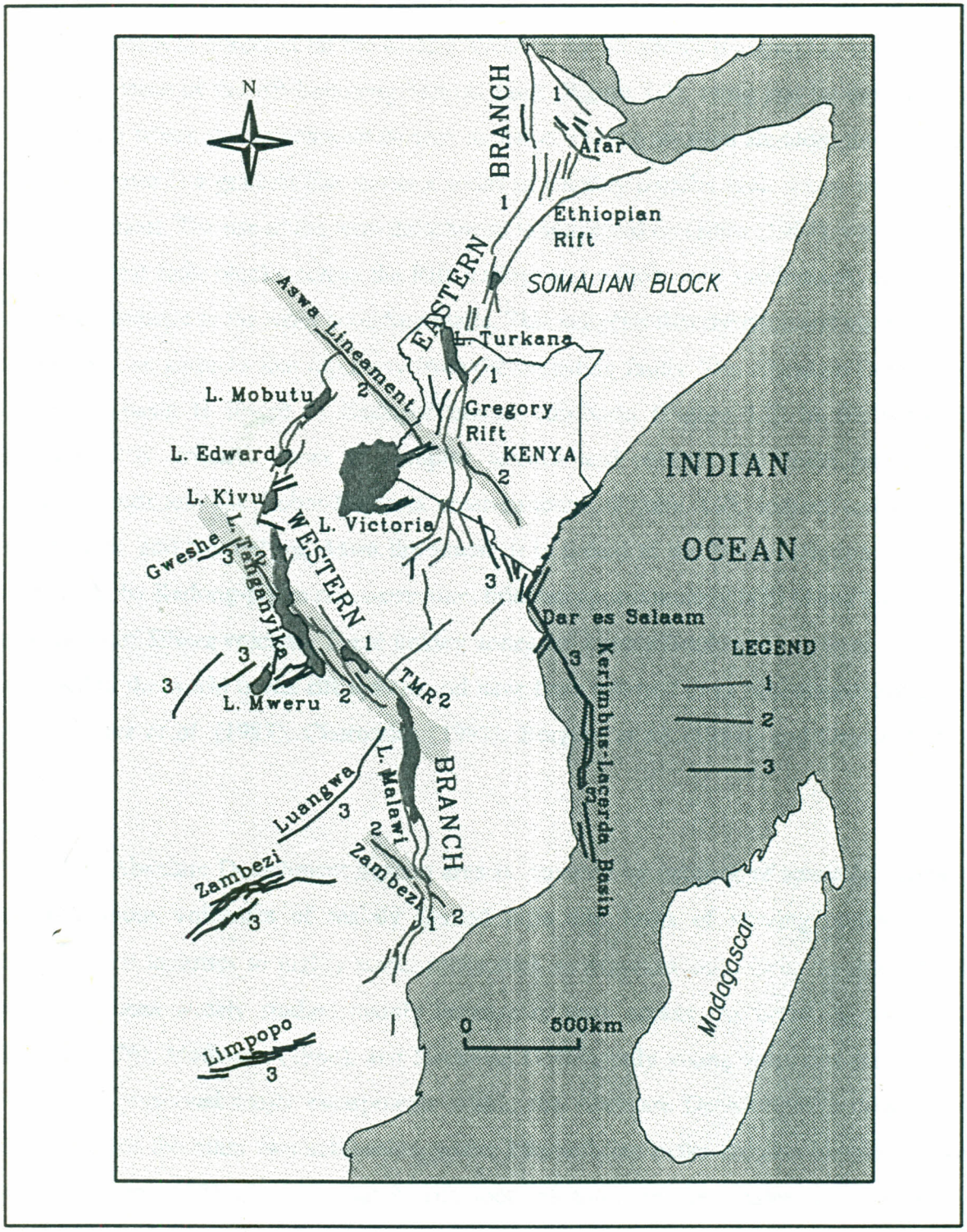

Figure 1.1: Schematic map of East African Rift System showing the positions of the Cenozoic Eastern and Western Rift Branches, and the Proterozoic Aswa, Tanganyika-Rukwa-Malawi (TMR) and Zambezi shear zones. *(Modified from Chorowicz, 1992; Smith and Mosley, 1993; and Delvaux, et al., 1992).*

1 - Cenozoic Main Rift faults; 2 - Proterozoic-Cenozoic shear zones; 3 - other Proterozoic-Cenozoic fault structures. The position of Kenya (see Figure 1.2) is indicated on the map.

The rift system in the study area lies within the Aberdare Detachment System sub-basin (Figure 1.2) that is occupied by lakes Naivasha, Elmenteita, Nakuru and Bogoria (Figure 1.3). The system is bordered on the eastern shoulder by an abrupt topographic break, which is a surface trace of the rift-bounding Sattima fault (Figure 1.3), lying just by the Aberdare Ranges from where the detachment derives its name. On the western shoulder the boundary of the sub-basin is a gradual rise across a series of roughly parallel fault scarps marking the Mau escarpment. The use of the term detachment is suggested by Gibbs (1984), who indicates that the largest fault blocks across the Rift Valley, and within each subdivision, are rotated in a sense synthetic to the main bounding faults. This suggests that the rift-trend normal faults are detached on surfaces that dip away from the bounding faults. The Aberdare Detachment System sub-basin is linked to Baringo/Turkana sub-basin (Figure 1.2) in the north, by N60°W-N30°W oriented zones of complex wrench and oblique slip faults forming the Marmanet fault and the Loboi-Kamasia cross-structure (Figure 1.2), located around Lake Bogoria area, and parallel the Aswa lineament. It is linked to the Magadi/Natron sub-basin in the south, by Kedong-Ngiro cross-structure, oriented approximately N30°E and located just to the south of Suswa volcano. These linking zones are kinematically analogous to transform faults within the world ocean rift system and have been referred to as accommodation zones by Chorowicz *et al.* (1987); Chorowicz (1992); Burgess *et al.* (1987); and Grimaud *et al.* (1994).

The Aberdare Detachment System area is covered by bedrock of spatially extensive and voluminous volcanics of mainly faulted tuffs and lavas of varying composition - undersaturated tephrites to highly acidic rocks such as rhyolites and silicic rhyolites. These rocks have been widely studied mainly because of easy access. As noted by Baker and Mitchell (1976), Matheson (1966), and Hackman (1988), only young volcanics are exposed on the well preserved major escarpments within the Aberdare Detachment, unlike on the escarpments of the other two sub-basins, where Precambrian rocks are also exposed. Baker and Wohlenberg (1971), indicate that the rift floor volcanics are due to later extrusion of lava flows and pyroclastics which in-filled a formerly much deeper graben and concealed the fault structures. The thicknesses of the young volcanics are thus much greater than the present topographic relief of 2000 m above the rift floor. Deep wells at Olkaria area (2000 m a.s.l),

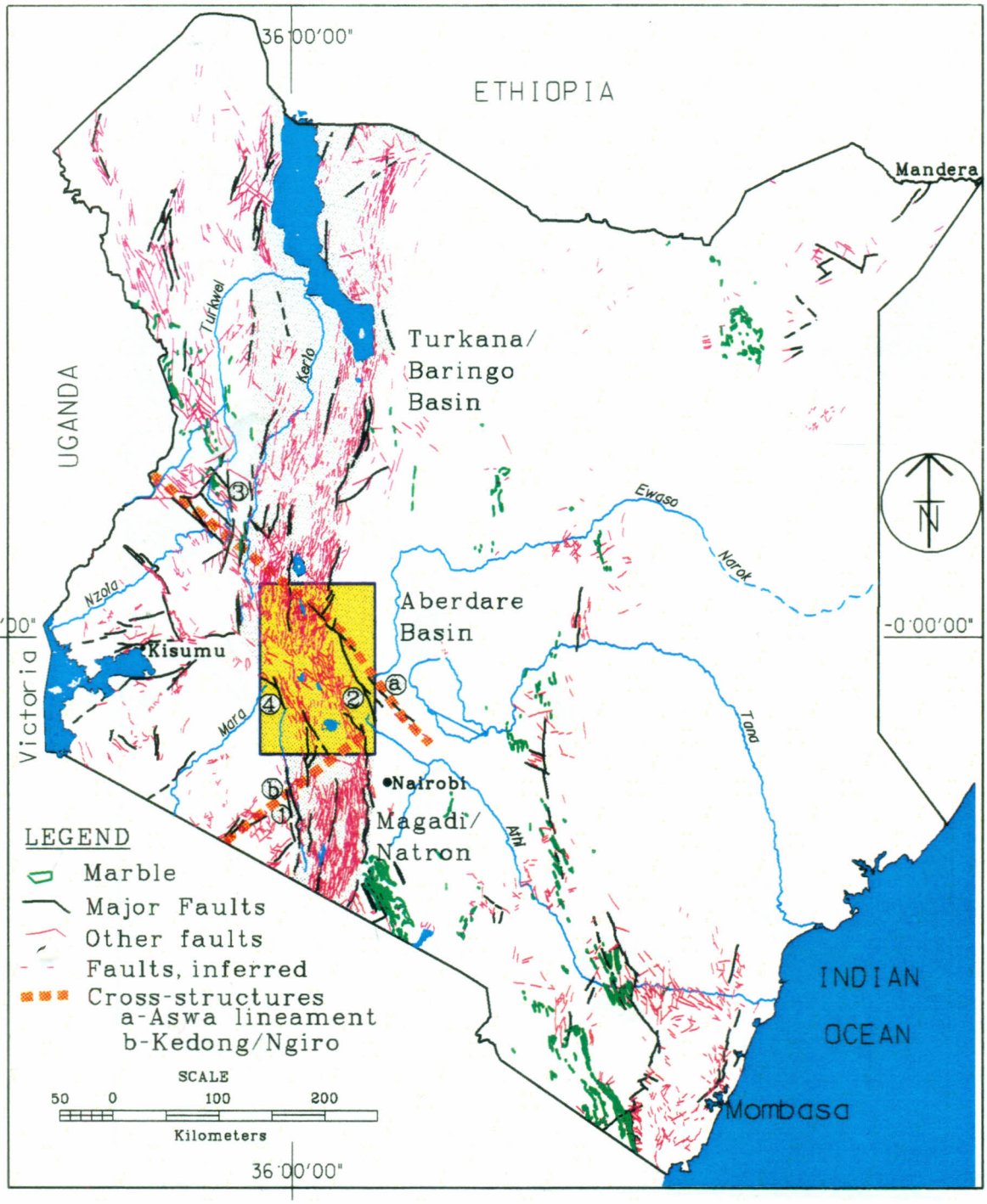

Figure 1.2: Structural map of Kenya showing the relationship between the Cenozoic Kenyan Rift Valley, the Precambrian marble outcrops and the Mesozoic fault systems to the east of the Rift Valley. The location of the study area (the Aberdare Detachment sub-basin) is indicated by the yellow *arae.* The grey outline is the Rift Valley zone. Major detachment faults are: 1-Nguruman, 2-Sattima and 3-Elgeyo. 4 is the Mau fault zone.

(redrawn at CIGC from 1:1 000 000 Geological Map of Kenya, National Oil Corporation of Kenya, Nairobi, 1987).

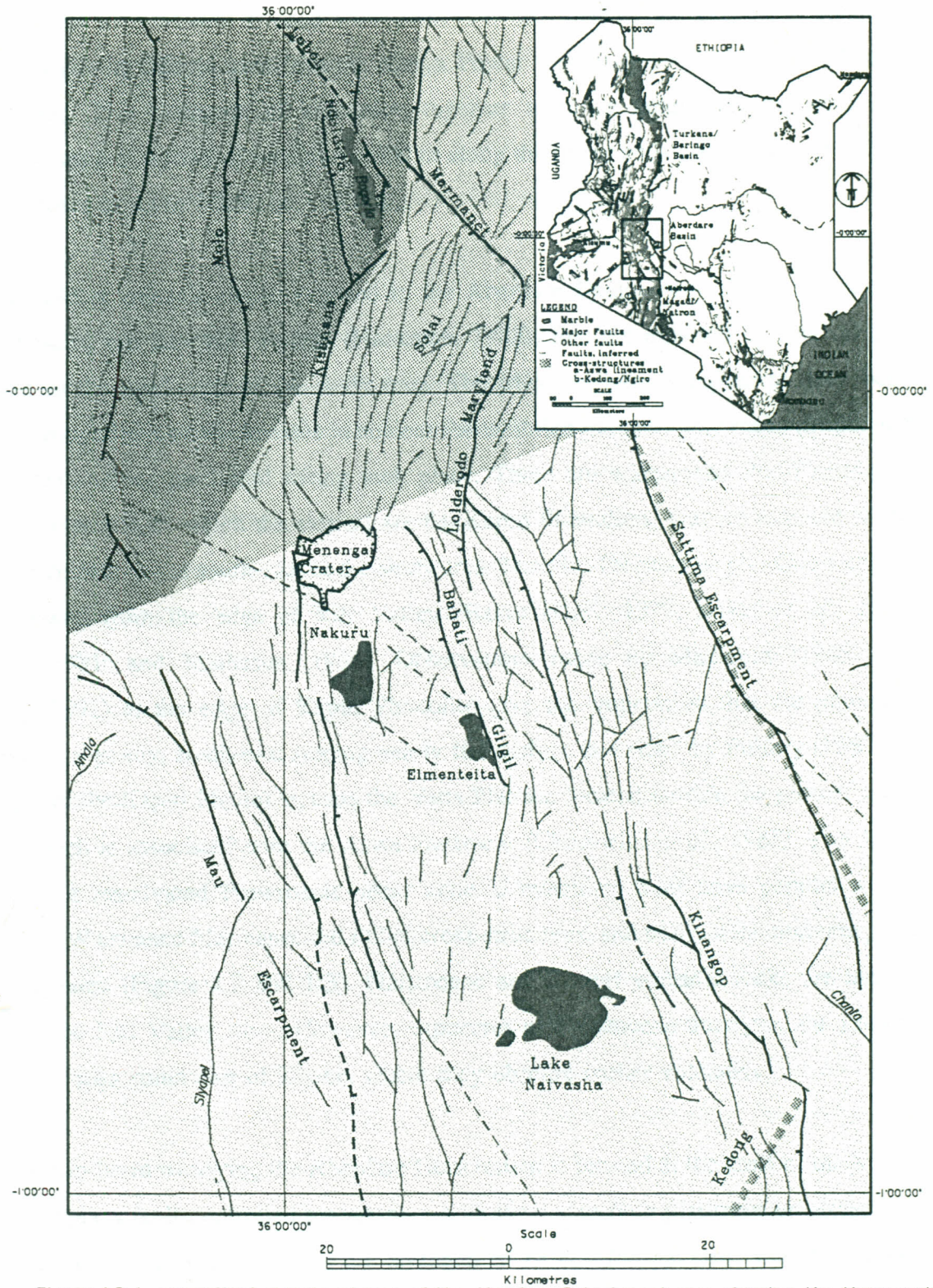

Figure 1.3: A generalised structural map of the Aberdare Detachment area showing the three main structural trends forming: 1 - Sattima-Mau Block, 2 - Solai-Subukia Block, 3 - Lake Bogoria Block. Also indicated are the position of Loboi-Marmanet and Kedong shear zones, part of Aswa and Kedong-Ngiro lineaments respectively.

reveal volcanics in a 2484.6 m deep well (well OW-18), one of the deepest geothermal exploration wells in Olkaria area (source: Kenya Power Company Limited, Olkaria Power Station, 1992). This thickness of volcanics, together with the heights of the adjoining escarpments, suggest throws of well over 4000 m along the major escarpments. Baker (1986) proposed throws of up to 10000 m (10 km).

The oldest volcanic rocks, exposed in the Aberdare Detachment area, form part of Miocene basalts, the Samburu Basalts (Hackman, 1988), that are exposed on the Laikipia escarpment to the north-east of the study area. The Miocene basalts appear to have been emplaced through lines of weaknesses in ancient Precambrian metamorphic rocks (Smith and Mosley, 1993), where the initial rifting took place. There are widespread Plio-Pleistocene volcanic occurrences of which the earliest are the Kapiti Phonolites, that are exposed at the Kikuyu escarpment in the south-east of the study area. The Plio-Pleistocene phonolites appear to have flowed from the edge of Rift Valley (Baker *et al.*, 1977; Baker *et al.*, 1972; Saggerson, 1991; and Matheson, 1966). Observations made by Matheson (1966) and Saggerson (1991) at the edge of Kapiti Phonolite give the impression that the phonolite flowed across a gently, south-east sloping nearly flat surface described by Pulfrey (1960). A similar lava to the Kapiti Phonolite, caps the Yatta Plateau, located outside the present study area, and which is associated with the Aswa lineament (Chorowicz *et al.*, 1988). The Aswa lineament is a reactivated Proterozoic shear zone, a transform fault zone parallel to the N60°W-N30°W oriented Marmanet and Loboi cross-structures, and transect the northern parts of the study area (Figure 1.2 and 1.3). Pleistocene and Recent volcanic rocks are mainly confined to the Rift Valley floor. However, exposures of Pleistocene trachytes, the Limuru trachytes, are seen south-east of Kijabe, where they obscure earlier volcanics.

The sub-basin overlying the Aberdare Detachment is located at the crest of the Kenya dome and displays fault-controlled topography, with local step-fault platforms on either side of the main graben. The major faults are arranged in *en échelon* patterns, with the blocks between overlapping faults broken up and stepped down in numerous smaller faults, instead of forming simple strike ramps. Complex minor fault systems are also seen in synthetic transfer zones within the rift floor. In the Solai-Subukia, Bahati and Gilgil areas, they form polygonal fault-bound structures (box faults) and rhomb-shaped structures. Locally, the main

faults show three major orientations, defining three major fault blocks (see Figure 1.3 and appendix 2.1):

(1) The Sattima-Mau Block, located south of Menengai crater and Bahati fracture zone, with the main fault structures on the block, conforming to the orientation of Sattima fault scarp, (N18°W).

(2) The Solai-Subukia Block, located north of Menengai crater and Bahati fracture zone, but to the east of Kisanana-Chemasa-Emsoss fault scarps, with the fault structures on the block, conforming to Solai, Iguamiti, and South Arabel fault scarps (N10°E).

(3) The Lake Bogoria Block, located west of Kisanana-Chemasa-Emsoss and Lake Bogoria escarpments and bordered to the west and north, by the northern sections of Mau escarpment and Kamasia Ranges, respectively, with the trend of fault structures, conforming to the orientation of Molo, Ndoloita, Ngusero and Sandai faults due north.

1.1.2 Physiography

The physiography of the Aberdare Detachment varies greatly over the area. The marginal escarpments are characterized by high and steep escarpments, up to 2000 m above the rift floor. The Sattima, Marmanet (Photo 1.1), Lake Bogoria and Mau (Photo 1.2) escarpments are the most prominent of these escarpments. Within the rift floor are found isolated volcanic centres of Menengai, Eburru, Olkaria, Longonot, Kijabe and Margaret located along the axis of the Rift Valley; and Kipipiri and ll Kinangop at the edge of the eastern rift margin (Figure 1.4). Kilombe and Suswa are other volcanic centres located just outside the present study area. These rift floor volcanoes are mainly composed of volcanic ashes, pyroclastics and tuffs with layers of trachytes. The youngest volcanic centres are located at Elmenteita "Badlands" (basaltic), Olkaria (obsidic), and Eburru (obsidic and rhyolitic) areas and although many and piling on one another, they are much smaller, and show some pyroclastic occurrences.

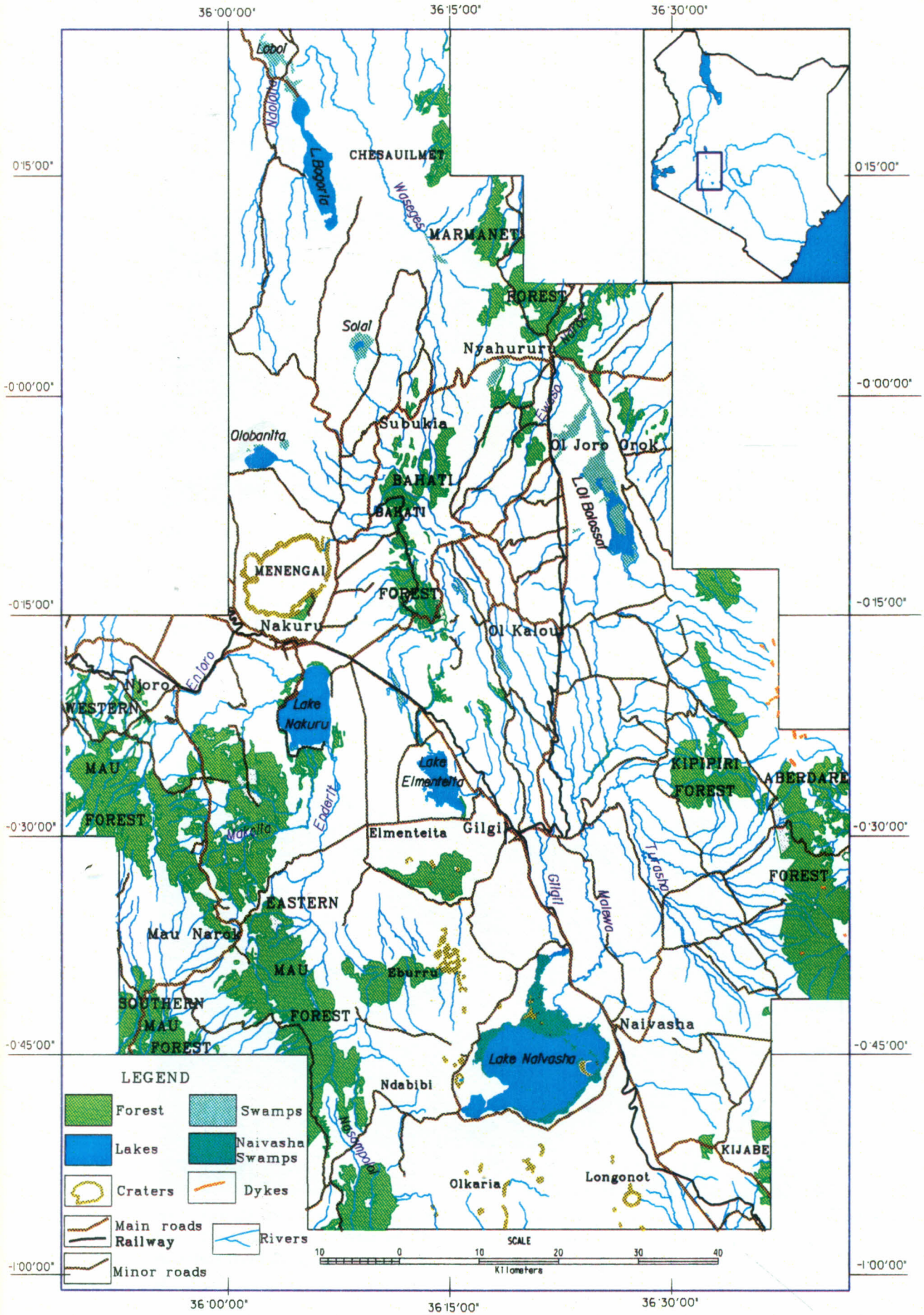

Figure 1.4: Communication and physiography of the study area.

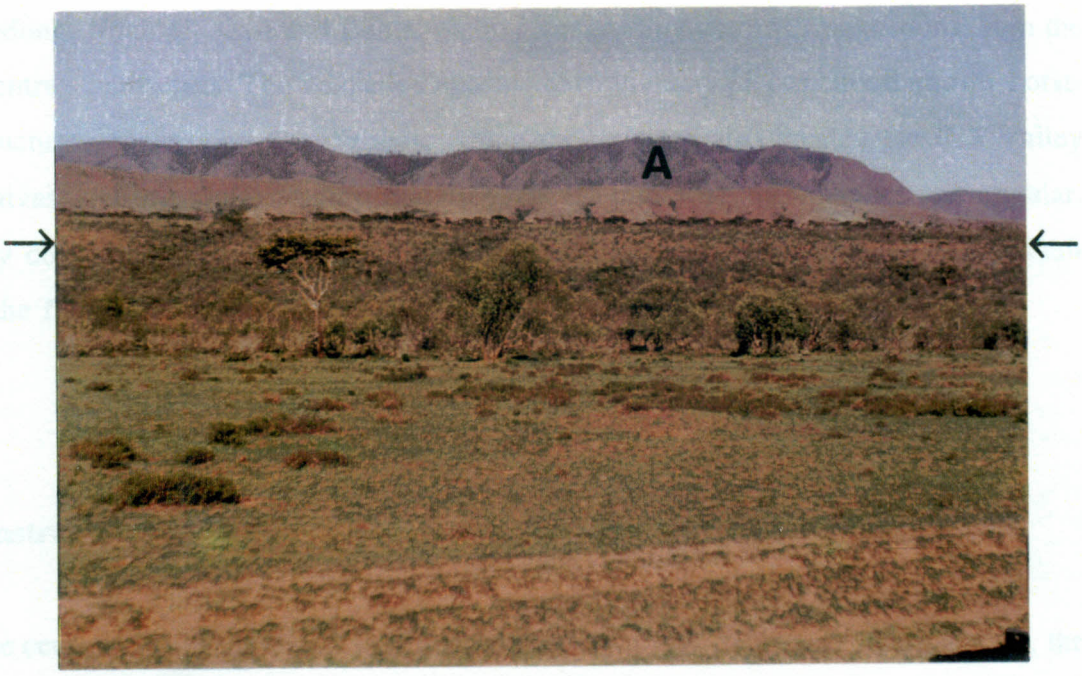

Photo 1.1: *East-downthrown, step-faulted Mau escarpment.* This section of the escarpment cut through volcanic ashes and is located west of Olkaria. It controls drainage south through Nasampoloi, which cross the Rift Valley north of Suswa to join Kedong drainage. Note the deep gorges on the steepest part of the escarpment marked "A", that is about 1000 m high. Note also a rejuvenated fault (shown by arrows) in the middle section of the photograph.

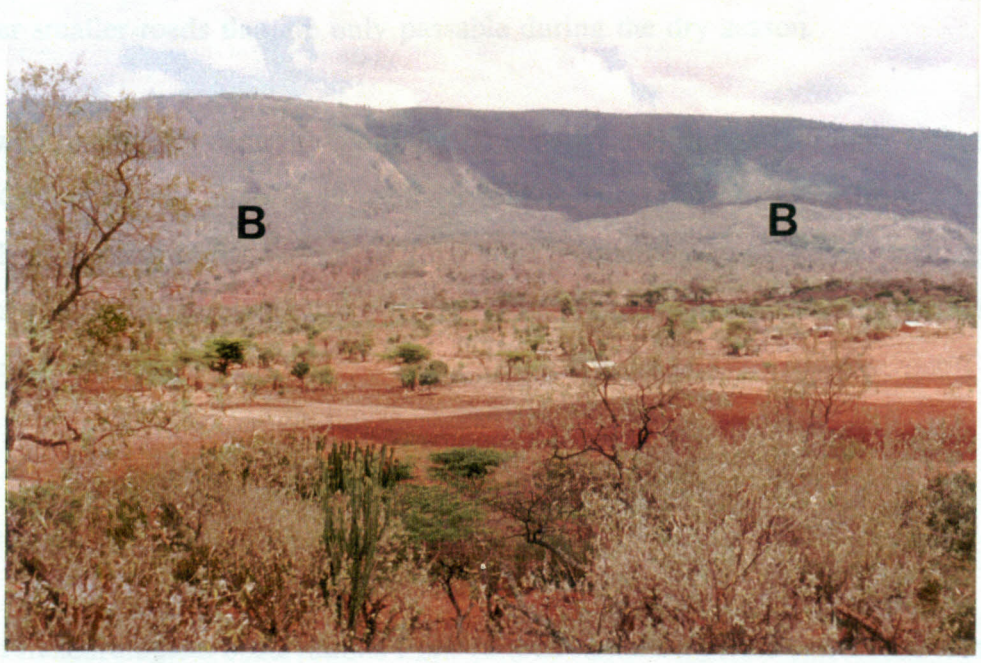

Photo 1.2: *West-downthrown Marmanet escarpment, cutting through phonolite lavas.* The location is south east of Lake Bogoria, west of Shamenek Farm. Note the mass of material marked "B", detached from the escarpment, at the foot of the escarpment. The height of the escarpment is about 800 m.

The axial volcanic centres are separated by extensive areas of smooth topography (Akira, Kedong, Ndabibi, Kiwi and Bahati plains), covered by volcanic depositions from the eruptive centres themselves. The volcanic deposits, have in many places buried narrow horst-graben structures, underlying the rift axis. Along the axis are also located the Rift Valley lakes - Naivasha, Elmenteita, Nakuru and Bogoria (Figure 1.4). Sub-parallel and angular, structurally controlled drainage patterns and aligned sinkholes, mark lines of buried fault scarps in the flattened out areas.

1.1.3 Infrastructures

The central part of the study area is transected by a NW-SE running tarmac road, the Trans-Africa Highway, that links Naivasha to Gilgil and Nakuru - three major towns in the study area (Figure 1.4). From Nakuru, the main town, two tarmac roads run north to Nyahururu and Marigat, through Subukia and Mogotio, respectively. Another branch of a tarmac road runs west to Njoro and Elburgon. Nyahururu is linked to Gilgil by another tarmac road that passes through Ol Joro Orok and Ol Kalou. Along these routes are smaller settlements. Other smaller market centres within the study area are accessible by loose surface roads and other smaller roads that are only passable during the dry season.

A railway line passes centrally along the Trans-Africa Highway and links Nakuru to Nairobi and Kisumu. In the study area, Nakuru is the main railway station from where a disused branch of the line formerly lead to Solai sisal plantations. From Gilgil, a branch of the railway line runs north, through Ol Kalou, Ol Joro Orok to Nyahururu where it serves the farmlands along the route.

1.1.4 Climate

Data of meteorological observations from various stations indicate that annual rainfall, from averages taken over a 30 year period (1962-1991), varies between 1000 - 1400 mm in

the forested areas of the rift escarpment shoulders, and 600 mm - 800 mm in the plains of the rift floor (Table 1.1).

Table 1.1: Monthly and annual rainfall averages (in mm) calculated for the period 1962-1991 for twelve stations in the study area and measured in a standard raingauge (12.7 cm diameter and set 30 mm above the ground) - *the figures are courtesy of the Kenya Meteorological Department.*

Station name	number	Alt(m)	Jan	Feb	Mar	Apr	May	Jun	Jul	Aug	Sep	Oct	Nov	Dec	Total
Perkerra i.s.	8935163	1067	21.5	28.7	49.7	97.4	73.4	59.5	97.0	83.0	31.4	36.7	44.5	24.8	647.4
Marmanet f.s.	8936023	2300	34.0	38.5	62.3	131.4	86.8	93.8	134.0	143.3	54.3	50.3	75.2	66.4	930.4
Nyandarua as	9036135	2378	34.9	31.5	52.4	119.3	106.5	106.0	137.0	147.3	73.3	48.8	67.0	50.8	979.2
Nakuru r.s.	9036020	1851	29.7	37.8	57.8	123.9	123.0	73.7	80.6	100.0	75.9	64.7	63.3	41.2	874.1
Elburgon f.s.	9035011	2378	42.9	51.4	74.9	176.5	128.1	86.4	107.7	131.1	71.6	62.6	95.6	51.9	1081.0
Njoro BPS	9035021	2165	36.7	43.5	65.0	158.3	118.0	72.8	85.8	120.0	66.9	55.0	79.1	44.4	938.1
Kwetu farm	9036029	2348	35.3	34.8	57.5	154.0	118.9	82.5	105.0	118.7	80.1	88.1	86.4	49.7	1020.9
Gilgil r.s.	9036034	2008	29.7	31.1	49.3	96.7	67.3	46.8	57.4	51.6	44.2	56.8	66.7	43.3	635.5
Kinangop f.s.	9036025	2631	49.0	53.3	85.1	172.6	154.9	95.9	73.8	95.7	100.7	103.7	104.0	67.8	1154.6
Naivasha KCC	9036073	1936	33.1	38.3	56.9	105.8	82.7	50.8	39.5	49.3	29.7	44.2	52.5	40.1	631.2
Naivasha D.O.	9036002	1900	32.7	38.0	58.7	124.0	81.8	40.0	35.6	45.3	40.1	55.2	61.7	45.4	670.9
Kerita f.s.	9036061	2439	72.0	73.8	126.3	325.2	234.3	65.2	49.1	38.2	40.2	108.6	164.6	93.8	1382.1

The latitudes and longitudes of the various stations are:

Station	Latitude	Longitude	Station	Latitude	Longitude
Perkerra Irrigation Scheme	0°28'N	35°58'E	Kwetu Farm, Gilgil	0°21'S	36°18'E
Marmanet Forest Station	0°06'N	36°18'E	Gilgil Railway Station	0°30'S	36°20'E
Nyandarua Agricultural Station	0°02'S	36°21'E	Kinangop Forest Station	0°35'S	36°38'E
Nakuru Railway Station	0°17'S	36°04'E	Naivasha KCC	0°40'S	36°23'E
Elburgon Forest Station	0°19'S	35°51'E	Naivasha D.O.	0°43'S	36°26'E
Njoro Plant Breeding Station	0°20'S	35°57'E	Kerita Forest Station	0°59'S	36°38'E

Except for local rainfall variations at the major volcanic centres, there is a general decrease of rainfall from the rift shoulder escarpments into the rift floor and from the highest part of the rift floor at Menengai, towards the south and north. A large part of the study area receives less than 700 mm annual rainfall, with Elmenteita "Badlands", Gilgil and Marigat areas receiving the least (< 500 mm). Rainfall reliability is also very low in Solai and Lake Bogoria areas and in the plains around Lake Naivasha and Longonot volcano.

Annual mean evaporation (1580 mm) is higher than annual mean precipitation (912 mm) for all the stations, accounting for high (73 %) losses of moisture. Daily sunshine hours are on average 8.6 hours for most of the area, making the area warm and sometimes hot

throughout the year. There is a marked hot spell in January-February, when the area is dry, and the average maximum monthly temperatures are higher then than in the other months, reaching monthly average of 34°C around Lake Bogoria. A cold spell is observed in the months of July and August when maximum mean temperatures are lower than in the other months. Generally, drier areas experience higher temperatures and wetter areas lower temperatures. There are, however, extreme variations with a daily range of over 14°C, sometimes resulting in frost at the highest parts of Mau, in the months of January and June.

1.1.5 Vegetation

Vegetation in the Aberdare Detachment takes various forms; dense near-tropical forest in the sections of the Sattima escarpment at the Aberdare Ranges and Mau escarpment; clumped trees in grassland areas of the plains in the rift floor; and shrub or thicket at the valley bottoms, around Lake Nakuru, on the volcanic hills, at Elmenteita "Badlands" and around Gilgil and Bahati escarpments. At some depressions such as at Loboi, Olobanita, Ol Bolossat and Solai, are found swamp grassland and wet grassland. Locally, natural forests cover the steep faces of the fault scarps and some areas on the highest parts of the escarpments. Small natural forests presently form part of Mau, Bahati, Ol Bolossat, Marmanet and Aberdare forests (Figure 1.4), and occupy the areas which receive an annual average rainfall of slightly over 1000 mm. In places, however, the natural forests have been replaced with cultivated forests of eucalyptus, cinder, cyprus and wattle trees, especially at the Bahati and Mau escarpments. Most of the escarpment areas have also over the years, been cleared off forest for cultivation (Photo 1.3) of wheat, maize, potatoes and other vegetables. Both large and small scale farming of these crops, together with beans and napier grass are carried out at the plains around Menengai, Mau plateau, Subukia, Bahati and Ol Kalou areas. Coffee, tea and sisal are under cultivation at Bahati and Solai areas. The rich volcanic soils and ashes in these areas and ample rainfall, result in high agricultural yields.

Evergreen and semi-deciduous bushland cover large areas along stream valleys and the inhospitable areas of Bogoria, Olkokwe, and Ndoloita. This type of vegetation is found in the 600 mm rainfall zone. Grassland, mainly *Combretum savanna* (grass with scattered low

Photo 1.3: *Depleted natural forest on Mau escarpment, west of Sakutiek.* The forest has been burnt down to give way to cultivation of potatoes (seen in the foreground) and maize, thus reducing the catchment potential of the area.

Photo 1.4: *The Rift Valley floor at Kedong plain.* In the foreground is the forested Kikuyu escarpment, and at the far right, background is the form of Mau escarpment. The hill to the left, background (arrow) is Suswa volcano. Note the lines of riverine vegetation on the otherwise featureless plain, defining the drainage lines.

acacia trees - *Acacia drepanolobium*), and wooded grassland, cover the plains in Gilgil, Longonot, Kiwi, Ndabibi and Kedong (Photo 1.4), also in the 600 mm rainfall zone. In these areas, riverine forests are occasionally seen defining river valleys. These semi-arid parts of the Rift Valley are used for ranching and wildlife conservation.

1.1.6 Volcanic Soils, Alluvium and other Soils

The wide variation in climate, geology and topography in the Aberdare Detachment is reflected in soils, which vary from slightly altered volcanic ashes and pyroclastics in Longonot-Nakuru area to dark friable clays, to red and strongly brown clays with occasional lateritic horizons in Ol Kalou-Bahati area (Scott *et al.*, 1971). In the high rainfall areas, the volcanic soils have developed dark red friable clays and greyish brown mottled clays forming deep fertile soils, suitable for agriculture. In the plains of Ol Bolossat and at Kinangop plateau (Figure 1.4), the soils are mainly dark grey to brown clay loam with dark clays of varying depths. The dark clays change to dark grey to black cracking clay developed over calcium carbonate or tuff in swampy places at Lake Ol Bolossat and parts of Kinangop Plateau. The dark clays are seasonally water-logged making cultivation impossible in the rainy seasons.

Volcanic soils derived from reworked pyroclastics and ashes, cover most of the plains between volcanic cones and craters on the rift floor, along the axis of the Rift Valley. Around Longonot, and as a result of the latest eruption from it, the soils are mainly ashy and pumiceous. Around Menengai they are also pumiceous as a result of explosive eruption from Menengai prior to the latest lava flows in the caldera floor. As indicated by Scott *et al.* (1971), the Kedong, Kiwi, Ndabibi and Bahati plains, and the narrow grabens north of Olobanita, are in places covered by flood lacustrine deposits intercalated with, or covered by volcanic ashes, pyroclastics or alluvium. At the plains close to the escarpments the alluvial deposits are soils, originating from the rift floor volcanism and from talus material eroded from the escarpments.

1.2 PREVIOUS WORK

1.2.1 Rift Evolution and Geological Studies

The East Africa rift is an onshore extension of a Tertiary-Quaternary tectonic system that has caused continental breakup and formation of passive continental margins (Bosworth, 1986a). Evidence of the early tectonic style are seen in the broad half-graben depressions at Lake Turkana, and lakes Magadi/Natron in the Kenya Tertiary Rift Valley, also known as the Gregory Rift Valley. The Rift Valley here, follows a marked sub-meridian trend controlled by Proterozoic structures, along the margins between the Tanzanian Craton and the Precambrian Mozambique Belt (Smith and Mosley, 1993). The Baringo/Turkana and Magadi/Natron broad half-graben depressions as well as the Aberdare Detachment graben are sub-meridian and traversed by major antithetic tilted blocks of Late Miocene to Early Pliocene (Bosworth *et al.*, 1986). These sub-meridian structures are separated by transverse fault structures interpreted by Smith and Mosley (1993) to have developed along areas of weaker crust caused by E-W regional extension on the major escarpments.

The events leading to the formation of the Kenya Tertiary Rift Valley are suggested by Baker (1986), and Baker and Wohlenberg (1971) to be related to three phases of epeirogeny and crustal flexuring. Periodic up-arching lead to the formation of a dome 300 m high in the Late Miocene. This was followed by a major uplift of up to 1400 m in the Late Pliocene to Mid-Pleistocene, reaching at least 1700 m in mid-Tertiary. Bosworth (1986b) indicates that the periodic uplift resulted in the crest of the Kenya Dome being raised to elevations of 1800 m. According to Baker (1986), the doming was due to sub-crustal processes, probably intrusion of basaltic or gabbroic magma. The domal uplift is elliptical in plan and about 1000 km wide. Major faults cut through the dome, resulting in a complex sub-meridian graben along the N-S major axis of the uplift. The graben in the central section of the Kenya Rift Valley, is 60-70 km wide and approximately 450 km long, passing laterally into widening zones of splayed step-faults in the Turkana and Magadi/Natron half-graben depressions.

The apex of the Kenya Dome is at the Aberdare Detachment sub-basin. Here, extreme crustal thinning has taken place resulting in a long wavelength negative Bouguer anomaly with some sharper gravity lows along the margins of the Rift Valley and an axial gravity high along the axis. Baker (1986), suggests that the long wavelength anomaly is due to large deposits of low density lava and pyroclastics at the flanks of the Rift Valley. He also points to a positive peak under the inner graben indicating presence of an intra-continental intrusive body, 10 km wide with specific gravity contrast of 0.15 mgals, that is 1500 m below sea level. Lambiase (1989), estimates that the positive short wavelength gravity anomaly is at least 1000 m below sea level and 40-80 km wide, and associated with axial intrusive volcanism and small scale faulting. The near north-south gravity high anomaly is also interpreted by Ndombi (1981), Baker and Wohlenberg (1971) and Fairhead (1976). The underlying process producing this anomaly seems to have been the rise of geotherms in the upper mantle leading to partial melting and regional up-doming of the crust. From the anomaly, a crustal model by Fairhead (1976) suggests, there has been 10 km of crustal separation under the central part of Central Kenya Rift Valley. Baker (1986) points to the presence of Precambrian rocks in the Turkana, Magadi/Natron depressions indicating crustal extension of 2-3 km. Injection of basic igneous rocks from a hot and partially molten zone of low density in the upper mantle is suggested. The trend of this mantle body is NNW-SSE and centred south of Menengai crater. Williams *et al.* (1983) also suggest that the area of domal uplift is underlain by mantle of low density and high temperatures.

The surface geology in the Aberdare Detachment does not show features related to the 10 km separation. This is because the pre-Quaternary structures are largely concealed under piles of pyroclastics. Williams *et al.* (1983), for example, reports that faults south of Olkaria are buried below thick pyroclastics and volcanic ashes and are thus visually less numerous. Volcanic rocks, together with associated structures along the axis of the Rift Valley, are hidden under a blanket of syn- or post-volcanic pyroclastics and ashes from Kilombe, Longonot, Olkaria, Eburru, Menengai, Kijabe, Margaret and Suswa. Baker and Wohlenberg (1971) predict that the 10 km separation took place in the Tertiary, its effects subsequently being obscured by later faulting, subsidence, volcanism and sedimentation, concentrated in a narrowing complex graben in the central part of the Rift Valley. The phenomenon of this rift spreading is also predicted by Girdler *et al.* (1969) using the ages of off-rift volcanicity

which gets younger away from the Rift Valley. Girdler *et al.* (1969), however, point out that the off-rift volcanicity is not symmetrical with respect to the rift axis, there being more volcanoes to the east of the Rift Valley than to the west. This renders the prediction of spreading unreliable.

A major episode of Gregory Rift faulting occurred at least 7 Ma ago (Nyambok, 1985; Baker, 1986). The period of major domal uplift (Late Pliocene to Quaternary), downwarping and formation of deep grabens at 4 Ma (Clarke *et al.*, 1990), was accompanied by extensive ignimbritic trachyte and plateau volcanism. Baker *et al.* (1972) notes a change in composition of the volcanics from basaltic (Miocene) to phonolitic (Early Pliocene) and trachytic (Quaternary). McCall (1967), Fairhead (1976), and Wendlandt and Morgan (1982), have suggested, for the change in volcanic composition in the evolution of East African Rift Valley, a possibility of development of higher than normal temperatures in the mantle, with crustal arching, thinning, intense dyke injections, fracturing and collapse of the rift floor, accompanied by derivation of partial melts from the mantle and their contamination with sialic crust. Baker and Wohlenberg (1971) point to absence of basaltic activity in the Quaternary and indicate that this probably represented that period of crustal separation leading to basic igneous injection in Pre-Upper Pliocene.

Baker and Mitchell (1976), Fairhead *et al.* (1972), Clarke *et al.* (1990), Bosworth *et al.* (1986) and Baker and Wohlenberg (1971) suggest that the main evolution of the escarpments in Central Kenya Rift Valley took place from 1.9-0.8 Ma and was followed by plateau trachyte lava emplacement. The faulting of the plateau trachytes occurred at 0.8-0.4 Ma, marking the last major tectonic episode. The Quaternary period represented a phase of sub-parallel faulting and crustal separation in the Rift Valley floor, followed by intensive central volcanic activities which gave rise to a number of trachytic and silicic calderas represented in the Aberdare Detachment by Suswa, Longonot, Menengai, Olkaria and Eburru. The mechanisms of producing silicic volcanism are not clear, but according to Baker (1986), are possibly due to anatexis of tenitized sialic rocks or some form of crustal assimilation. The silicic volcanism (trachytes, rhyolites, comendites, obsidian), that succeeded the period of crustal separation concealed its volcanic and tectonic effects. Some of the fault structures are, however, comparatively young and cut through, and offset pumiceous pyroclastics and

ignimbrites from the Late Quaternary central volcanoes.

Present dynamics of the rift in the Aberdare Detachment correspond to NW-SE trending divergent movement of intra-continental blocks. Morley *et al.* (1990), Bosworth *et al.* (1986) and Chorowicz (1990), all suggest that these NW-SE transfer zones parallel the Aswa lineament, a major extensional region cutting through the East African Rift Valley. NW-SE structures also occur between faults that display *en échelon* patterns and act as minor transfer faults. Along strike, as displacement along one edge of *en échelon* arranged faults decreases to zero, the opposite fault boundary increases its displacement and vice versa. This gives rise to intervening ramp structures (see discussion in Chapter 2). The change of extension from a full graben to half-graben may thus involve transfer of displacement across major and minor faults. The degree of overlap of *en échelon* patterns with the NW-SE fault terminations affects the type, orientation, and sense of displacement of fault structures within the minor-transfer zones. Chorowicz (1990) distinguishes three types of structures which give rise to transfer zones:

(1) A typical early strike-slip regime (extension NW-SE, compression NE-SW).

(2) A regional extension regime (extension NW-SE compression vertical due to intrusion).

(3) A local extension regime (extension at right angles to the main scarp, compression vertical due to local intrusion).

Work on structural and petrological evolution of the Rift Valley as reviewed by Fitton and Upton (1987) is mainly concentrated in the Olkaria geothermal field. Bhogal (1980) and Furgerson (1972) have carried out electrical resistivity studies in Olkaria area. The interpretation made from these studies indicate that the continental lithosphere is greatly thinned beneath the axis of the rift floor. Seismic data interpreted by Swain *et al.* 1981 and Khan *et al.* (1987) point to a very broad zone of domed deformation. Clarke *et al.* (1990) and Bosworth (1985) suggest that the main structural faulting is more intense on the rift bounding margins and in the Olkaria, Eburru and Lake Bogoria areas. Work directed to geothermal

potential is reported by Mason (1967), Naylor (1972), Ndombi (1981), Odongo (1982), Onacha (1989) and Nderitu (1993). Clarke *et al.* (1990) lays emphasis on geothermal influence. From observations made from borehole data and geothermal springs at Olkaria, Eburru and Lake Bogoria, Haukwa (1986) and Torfeson (1987), interpret high rate of heat flow. Microseismicity studies by Girdler *et al.* (1969) and Tobin *et al.* (1969), show that there are up to 47 low magnitude seismic events per day in some parts of the Rift Valley, with epicentres mainly along the Late Pliocene eastern margin faults and along the Pleistocene grid faults at the axis of the Rift Valley. They also found out that some earthquakes have their epicentres lying along the axial volcanic centres of Suswa, Longonot, Olkaria, Eburru and Menengai. This points to a more active tectonic involvement in these locations than at the Late Miocene/Early Pliocene rift border faults.

1.2.2: Studies Using Satellite Remote Sensing Techniques

Studies on structural interpretation and geologic mapping using satellite remote sensing techniques are limited in the area. The few studies done have proved the technique useful for lineament studies. Jutz and Chorowicz (1993) have applied SPOT/Landsat data to map extensional oblique structures in the Kenya Rift Valley. Chorowicz *et al.* (1988) have applied MOMS imagery to redefine the Aswa lineament in the Lake Bogoria area. Hackman (1988) describes the use of Landsat imagery in identifying parallel, curvilinear, and grid faults in the Baringo-Laikipia area. Miller (1975) used Landsat imagery to map out lineaments in a large sedimentary basin in eastern Kenya. From his interpretations, the full extent of the Lagh Bogal lineament was identified as a sub-surface fault. Onywere (1990) has used Landsat-TM imagery to map Precambrian metamorphic major lineaments (foliations) and the contact between the Precambrian metamorphic rocks and the Rift Valley volcanics in Nairobi-Kajiado area. Grimaud *et al.* (1994) have used remote sensing techniques to study the geometry and extension mechanism of Central Kenya Rift Valley. From their morphostructural study, they interpret two trends of rift structures (N0°-20° and N150°) in the Baringo-Bogoria half-graben.

Environmental monitoring and land cover classification of the Menengai-Nyahururu area is reported by Onywere and Gaciri (1993). Geobotanical studies done in the Kerio Valley by Odhiambo (1988), and lake condition monitoring at Lake Naivasha by Gaudet and Falconer (1982), found satellite imagery useful in environmental monitoring. Norconsult Engineers, in collaboration with IBM/Norway (1977), carried out a project in the northern parts of Kenya and southern Sudan and have shown how remote sensing techniques, combined with field measurements, could play a central role in data collection processes for transport planning and highway engineering.

In other studies done elsewhere, Siegal and Gillespie (1980) devised a method of determining geological information from vegetation studies. They describe remote sensing aspects which involve using spectral reflectance to define geologic differences depicted in the landscapes. Goetz *et al.* (1975), shows that features seen on satellite images and airborne and ground geophysical measurements frequently coincide, lending evidence to the assertion that subsurface features are expressed at the surface and can be detected if proper perspective is used. Goetz (1976a) and Goetz (1989) also outline the use of remote sensing for geological exploration. Elachi (1980) discusses an important use of spaceborne imaging radar for geologic and oceanographic application. Cole *et al.* (1974) on the other hand, have used Landsat (MSS) and aerial photography, to map plant communities which correspond to specific geologic formations. Labovitz *et al.* (1983) have also investigated the use of remote sensing data for studies of geobotanical anomalies. They indicate that spectral signatures, especially observation in infrared, could be exploited in remote sensing units delineations. Harris (1987) points to "clues" found in topographic expressions, structural relationships, outcrop patterns and contextual associations in deciding on the identity of distinct remote sensing units which thus provide a mechanism of indirectly understanding geological processes in an area. D'Hoore (1977) indicates that variations in soil constituents and characteristics directly influenced plant canopy development and hence their spectral signatures. He concludes that climatic variation influences plant phenological behaviour which is amenable to studies employing satellite imagery. Saad (1979) has also used satellite imagery to study temporal changes in a section of the Meghna River in Bangladesh.

Sabins (1986) and Hunt (1977) have shown that reflectance of rocks and minerals in the wavelength regions 0.5 μm - 1.1 μm is dominated by the quantity and oxidation state of iron. This wave band can thus be used in exploring for iron ore mineralization. Sabins (1986) also points out that hydrothermal alterations are marked by distinctive assemblages of secondary minerals that are laterally and vertically zoned, and in good exposures the lateral zoning can be mapped using satellite imagery. Bhattarai (1983) and Goetz (1976b) conclude that use of Landsat images for mineral exploration leans heavily on structural interpretations and particularly mapping of lineaments. They point out that mining districts are often associated with intersection fractures and that the synoptic view recorded by Landsat imagery facilitates their statistical correlation on a regional scale. The lineaments are used to extrapolate from known mining districts, into less prospected areas. Ilyin *et al.* (1983) have also given an account of the application of space images to mineral exploration and in studying Recent tectonics. Fillipone (1986) gives an account of the use of enhanced, filtered, transformed and statistically analyzed Landsat data in grey tones and false colours to derive definitive lineaments. He shows that long lineaments are related to deep-seated basement faulting. Kowalik and Glenn (1987) have also used digital image processing for structural interpretation.

1.3 METHODOLOGY AND DATA ACQUISITION

Population increase and its pressure on land resources has resulted in intensified research related to environmental studies. The methodologies of these researches are varied, but the need to use automated, real-time data outweighs any other data sources and analysis methods. In this regard, remote sensing has rapidly developed to address multiple environmental related problems. The advantage of remote sensing is its ability to capture and preserve land details (to the resolution limits of the system) exactly as it were at an instant in time. Its spatial resolution and scale compresses data, providing the researcher with a synoptic view, and facilitating analysis of local, regional and inter-regional patterns and relationship. Because of its nature, processing of remote sensing data is part of the interpretation. The theory behind the interpretation is well documented and a survey of world literature such as American Society of Photogrammetry (1975), Lo (1986), Curran (1985),

Andrews and Hunt (1977), Richards (1986), Thomas *et al.* (1987), Drury (1987), Pratt (1977), Short (1982), Sabins (1986), and Harris (1987) reflect elaborate and varied techniques used for image analysis.

To facilitate the development of raster-based GIS, thematic image classification, lineament analysis and image manipulation through digital image analysis were performed using ERDAS (Earth Resources Data Analysis System) software applied to SPOT (Satèllite Probatoire d'Observation de la Terre - the French satellite system carrying high resolution visible instrument), and Landsat-5 TM (Thematic Mapper) data. Digital image enhancement, directional edge enhancement (derivative) and convolution filtering, were performed on the image data. These methods of image processing were particularly suitable in delineating linear features and land use boundaries which were checked against vector GIS, by registration and integration of the two data sets.

In the context of the present study, rock composition, age determination and chemical data were obtained from previous studies in the area. In many areas, these data sets are incomplete and an extensive field check was made to ascertain rock unit boundaries. A morphostructural interpretation of Lake Bogoria, Menengai-Nyahururu and Lake Naivasha is made based on satellite image classification and ground truth survey. Interpretation of the relative ages of Menengai post-caldera lavas and that of some volcanic hills is also made. Detailed tectonic mapping required a combined study of tectonic, geomorphologic and sedimentology structures and detailed image interpretation.

The principal source of information used for vector GIS database design were: topographic, geological and structural maps; climatic data; natural resources data; and geological and environmental publications. An intensive search of these materials is made, reviewed, and used to digitize and design the vector GIS. The information contained in the topographic maps, geological reports, environmental related publications, and climatic data from the Aberdare Detachment area, cover a full range of environmental, agricultural, and socio-economic topics and describe in substantive detail these aspects. In consulting these data, special emphasis was placed on topics pertaining to geology, structures, and data on resources. In the geological reports, composition and origin of rock types, geological

structures, the general geological history and the economic potential of the area are described. These data was assessed, digitized and put into the GIS database. Accompanying each geological report is a 1:125,000 scale, coloured 30'-quadrangle, geological map with a vertical cross section diagram. A mosaic of digitized geological maps revealed discrepancies in rock unit boundaries and in structural continuity within adjacent maps. These discrepancies required image interpretation and field checks for correction. In some areas such as at the forested parts of Mau escarpment between Maela-Enosupukia and Mau Narok-Elmenteita road (Figure 1.4); southern and western parts of Eburru volcanic centres; Marmanet escarpment; Waseges-Lake Bogoria escarpment area; the sections of Sattima escarpment at Kipipiri; and the eastern and southern parts of Longonot volcano, image interpretation proved to be useful since it was virtually impossible to verify lithologic boundary discrepancies and structural discontinuities in the field as these areas were inaccessible. In these areas image classifications and visual image interpretation results, and draping of this data on vector data were heavily relied on, in assessing the geology, structures and drainage patterns.

The first few months of this project were initially spent training in GIS database design using Arc/Info software on PC and Prime Workstation. This was followed by a six months vector data capture and database design using Microstation software on PC and Intergraph Workstation. In the months that followed, digital image processing, classification and analysis were performed using TM and SPOT satellite data. These were then integrated with the vector GIS data sets for structural analysis of the area.

1.3.1 Preparation of Working Images and Establishing the Vector Database

A full scene (scene 169/060) of Landsat-5 TM digital data in 1/4 scenes on four 9-track magnetic tapes was obtained from the Earth Observation Satellite Company (EOSAT). Two 1/4 scene frames, sufficiently covered the study area and were, together with SPOT digital data (see Table 3.2), digitally analyzed. The images were processed after experimentation using several image filters and edge enhancement procedures. The most effective colour combinations were determined, and images with optimal colour balance

selected. The digital data was then transferred to a magnetic film, from where positives were printed. These positives were then used to make false colour composites (FCC) and other colour composites at a desired scale for visual interpretation and use in the field.

Seventeen 1:50,000 topographic maps covering the study area, were digitized to extract drainage patterns, contours, infrastructure and data on land use. Similarly, seven 1:125,000 geological maps covering the study area, were digitized to extract and normalize the lithology and structured data. Each category of digitized information formed a theme of vector information that was stored in different layers (levels) to facilitate independent evaluation and for easy registration and integration with image interpretation results and other data sets. In the digital vector database, attribute data associated the digital data and were tabulated and linked through identification links in Look-up-Tables (LUT). The vector data was initially compared with photographic image interpretation results and verified in the field to correct lithologic boundaries and structural discontinuities. The image colour composites were of special use in structural analysis and in the evaluation and interpretation of the macrorelief, and determination of land use patterns. The task of image interpretation required a multi-disciplinary approach, requiring consultation with agronomists, rangelands ecologists, foresters, geo-hydrologists and geologists.

1.3.2 Pre- and Post-interpretation Ground Observation

Field work involved two separate trips of two months and one and half months respectively to the study area. The first field trip (February to April 1994) was subsequent to initial photographic image interpretation and vector GIS data design and the second (December 1994 to February 1995) subsequent to digital image analysis, classification and integration with vector data sets. The ground truthing was for support observations and data gathering and involved checking several uncertainties on the geological maps. The field visits to various localities were also to establish the drainage divides, volcanic morphology, geothermal manifestation and to ascertain the cause of the drainage termination, especially around lakes Bogoria, Nakuru, and Naivasha and at the Olkaria and Eburru geothermal fields.

1.3.3 Interpretation Process

In the Chapters that follow, vector and raster data sets are spatially geo-referenced, with respect to one another, allowing for their registration. This data integration process result in ability to relate known ground observations to specific image types. Mapping guidelines involving legend systems that serve as the framework for inventorying, are tabulated. In making an inventory for image classification and interpretation, three groups of image features are considered:

(a) Narrow, elongate, distinct delineations representing linear features of fault zones.

(b) Smooth uniform textures, natural patterns and land features, boundaries marked by natural vegetation also marking structural features and lithological contacts.

(c) Textures, shapes and patterns showing modified landscape that point to anthropogenic changes dominating the image scene and resulting from different habitation densities and settlement patterns, grouped into:

(i) Large agricultural fields with distinct, regular outlines, that show straight edges, with a uniform texture used to map classes of well developed land use cover types.

(ii) Small agricultural fields with indistinct edges, or with a few straight edges and indistinct angular corners, identified as areas showing a dot and small blob, stippled (salt and pepper) tone and texture. These areas are considered as complex agricultural mapping units showing intricate land features with more than one land use cover type.

Using these three guidelines, remote sensing unit boundaries are traced as accurately as possible. Where the boundary is intricately incised or dendritic, averaging is made by visual smoothing. Mapping (tracing) is done on clear mylar overlay so that image characteristics are not masked or altered by the overlay material. Advantage is also taken of

the flexibility in digital image analysis that allow for band combinations and ratio image analysis and interpretation. On the basis of ground truthing, changes are made to remote sensing image interpretation where necessary. Occasionally, sub-divisions separated on the basis of subtle tone or hue, are combined after ground examination.

* * * *

CHAPTER 2

APPLICATION OF SATELLITE REMOTE SENSING TECHNIQUES IN LAND USE AND LAND COVER PATTERN ANALYSIS OF OLOBANITA-NYAHURURU AREA

2.0 INTRODUCTION

SPOT and Landsat-5 TM images are utilised to analyze land cover characteristics and patterns in the Olobanita-Nyahururu area, a section of the Aberdare Detachment sub-basin. The interpretation is first based on visual interpretation of image photographic products. The synoptic view from the imagery suggest, NW, NNE, and NE (N23°W-N38°E) striking linear patterns and associated grabens and plateaus. Ground work resolved details of land cover patterns and linear patterns. Based on image characteristics, the ground truth survey, and reference to collateral data of topographic and geologic maps, three morphostructural areas are recognized (Figure 2.1) namely, (1) Bahati, Olobanita, Solai low plateaus, marked by low escarpments and lying on the western part of Olobanita-Nyahururu area; (2) steep escarpments in the middle section of the area, marked by high escarpments of Solai, Lolderodo, Iguamiti and Subukia; (3) the plain of the fault-angled Lake Ol Bolossat, bordered by the Sattima rift border escarpment. The three morphostructural areas mark three agricultural areas: (a) high agricultural and forest areas of Bahati, Subukia, Marmanet, and Ewaso Narok, (b) semi-arid Olobanita and Solai areas, covered by shrub and bushes, (c) water-logged Ol Bolossat plain and the Sattima escarpment plateau.

In studying Olobanita-Nyahururu cultural and biotic environment, remote sensing is applied to collect information for a better understanding of the spatial distribution of population, its density and its impact on the living environment. Interpretation is influenced by the size of the settlements and the radiance characteristic of the cover patterns. Land units, geomorphology, physiography, and vegetation also influence interpretation.

Figure 2.1: Morphostructural map of Menengai-Nyahururu area constructed from SPOT satellite imagery and existing geological and topographic maps.

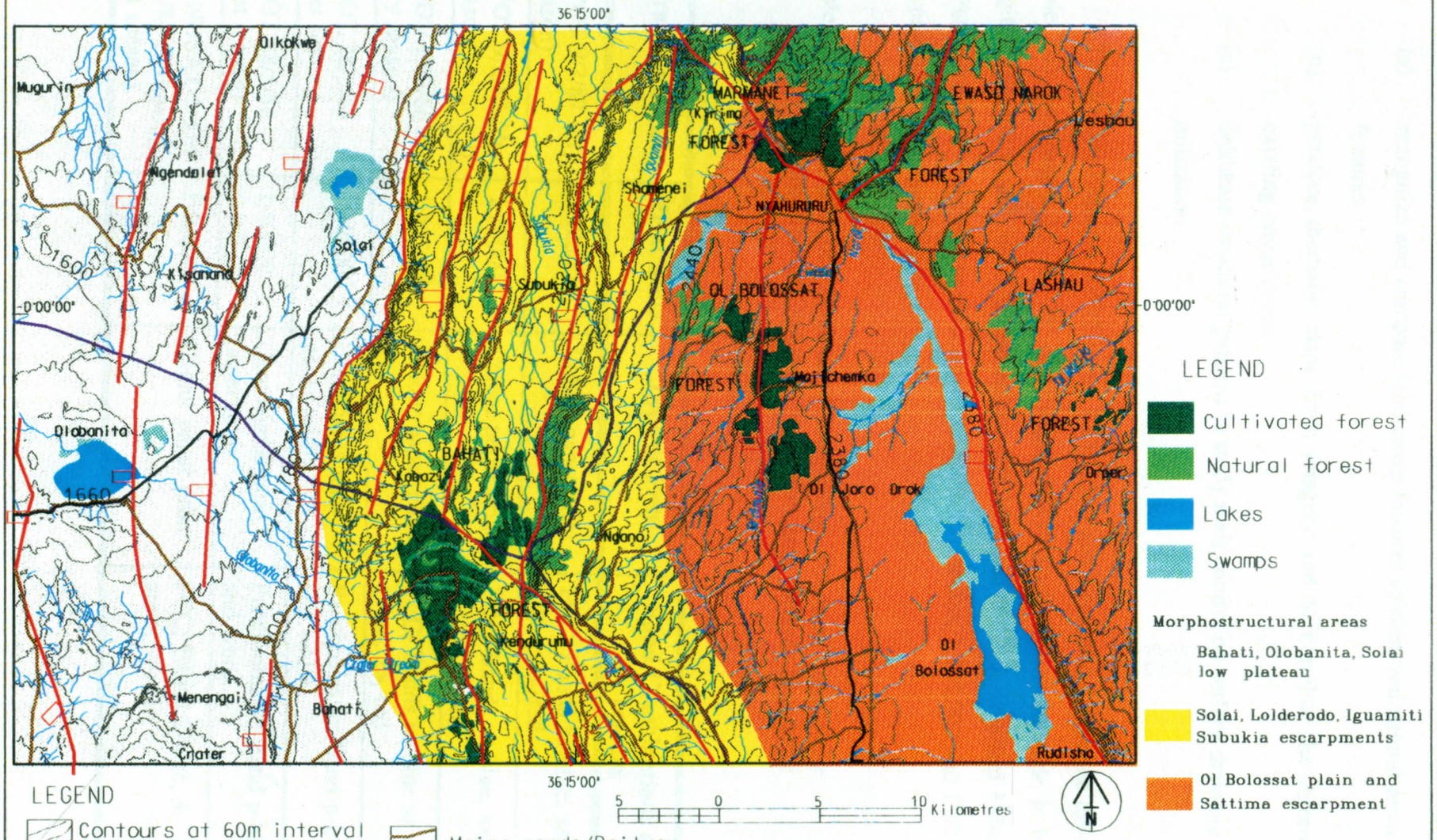

The procedure followed in the interpretation, sought to:

(a) recognize and compare land cover features to observed natural environmental features

(b) produce thematic maps from imagery and to correlate the information to existing cover types.

(c) delineate structural patterns to study their control on surface drainage and land utilization.

The images used are SPOT scene K137-J350 and Landsat-5 TM scene 169-060 (see Table 2.1), covering a 25' by 25' quadrangle (≈2170 km^2). The quadrangle is bound by longitudes 36°00'E and 36°25'E and latitudes 0°15'S and 0°10'N. Standard False Colour Composite (FCC) and panchromatic image prints in two scales, 1:125,000 and 1:50,000, are processed for the interpretation.

Table 2.1: Summary of Satellite Photographic Products used for Interpretation of Olobanita-Nyahururu area (*images processed at RCSSMRS, Nairobi).*

Frame and date	Print Scale	Type of Print	Band Combinations and colours
SPOT 9/2/87 (dry season)	1:125000	Colour paper print	FCC; Bands xs-blue, xs_1-green, xs_2-red
SPOT 9/2/87 (dry season)	1:50000	Colour paper print	FCC; Bands xs-blue, xs_1-green, xs_2-red
SPOT 23/9/86 (dry season)	1:125000	Colour paper print	FCC; Bands xs-blue xs_1-green, xs_2-red
SPOT 28/5/88 (wet season)	1:125000	Continuous tone paper print	Panchromatic; Band p-black and white
SPOT 28/5/88 (wet season)	1:50000	Continuous tone paper print	Panchromatic; Band p-black and white
LANDSAT-5 TM 1/7/84 (following wet season)	1:50000	Colour paper print	FCC; Bands 2-blue, 3-green, 4-red

Selected SPOT multispectral and panchromatic data covered 0.5 μm to 0.89 μm (green - near infrared) and 0.51 μm - 0.73 μm (visible) regions of the electromagnetic spectrum respectively, whereas Landsat-5 TM data covered 0.52 μm - 0.9 μm, visible to infra-red regions of the electromagnetic spectrum. The ground resolution cells of these data are 20 m (SPOT multispectral), 10 m (SPOT panchromatic) and 30 m (TM multispectral) pixel sizes. The photographic products are optically enlarged to permit maximum detection of variations in tone, hue, texture, pattern, shape and related characteristics.

2.1 THE GEOLOGY

The geology of Olobanita-Nyahururu area is reflected in contrasting step-fault volcanic morphology of the East African Rift Valley in Kenya (the Gregory Rift Valley), which crosses a crest of an elongate dome in the Aberdare Detachment (Olkaria-Lake Bogoria area - Figure 1.3 in Chapter 1). Rifting in the Gregory Rift Valley, occurred in Mid-Miocene in the north and Early Pliocene in the south, accompanied by a change in composition of volcanism from phonolitic to trachytic (Baker *et al.*, 1977; Nyambok, 1985). The major domal uplift and formation of deep grabens occurred in the Late Pliocene and was followed by extensive ignimbritic trachyte volcanism in the Quaternary (Baker, 1986). The area of domal uplift is suggested by Williams *et al.* (1983) as being underlain by mantle of low density and high temperature. Bosworth (1986b) indicates that the elongate dome has been raised to elevations of 1800 m by periodic uplifts.

The Gregory Rift Valley is divided into three faulted, north-south elongate sub-basins, Magadi-Natron (Nguruman Detachment), Naivasha-Elmenteita-Nakuru-Bogoria (Aberdare Detachment), and Baringo-Turkana (Elgeyo Detachment), separated by accommodation zones of complex wrench and oblique slip faults (Chorowicz *et al.*, 1987; Bosworth, 1986a) centred at Marmanet-Kamasia and Kedong-Ngiro cross structures. This study covers the central, north-east part of the Aberdare Detachment, the Olobanita-Nyahururu area. In this section of the Rift Valley, down-faulting to the west, the N-S trend of faults, and low sun azimuth of 3° to 5° at imaging time, enhances subtle differences in heights of features. Conspicuous fault lines, striking from about N15°W to N38°W (see Appendix 2.1) are prominent (Figure 2.2).

Figure 2.2: Tectonic structure of Olobanita-Nyahururu area. The faults azimuth frequencies rose diagram is shown below. The vector mean of N10.3°E reflect the percieved fault trends (N11°E) in the *Solai-Subukia Block.*

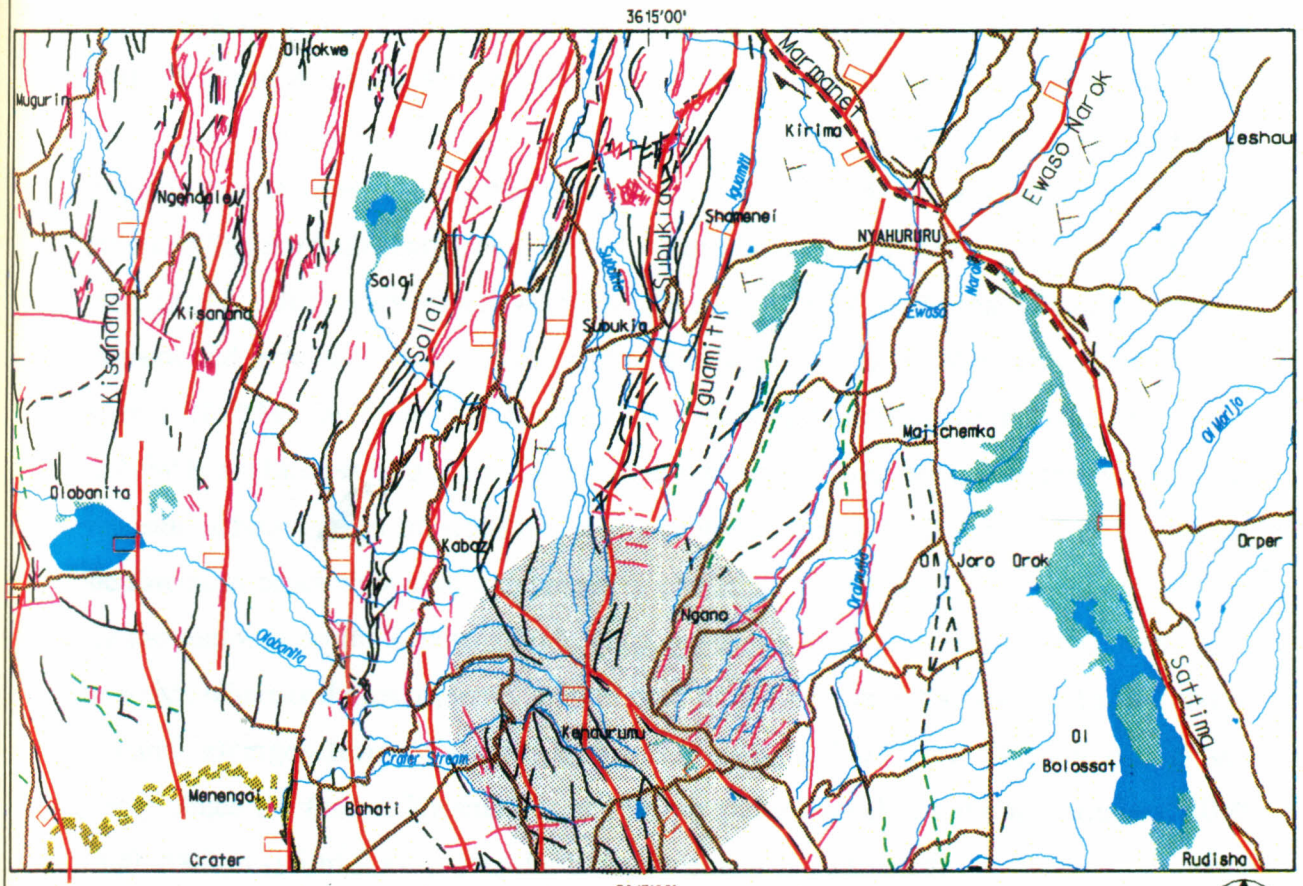

LEGEND

- Major faults with tick on downthrow
- Faults, west downthrow
- Inferred faults, west downthrow
- Faults, east downthrow
- Inferred faults, east downthrow
- Faults, unknown throw direction
- Menengai caldera fracture zone
- Direction of strike-slip motion
- Marmanet accommodation zone
- Tilt of fault block
- Lakes
- Swamps
- Bahati fracture zone

Rose diagram depicting azimuth frequencies of faults in the Solai-Subukia Block.

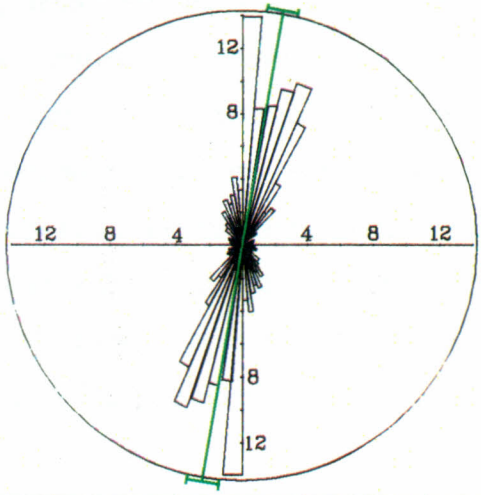

Calculation Method .. Frequency
Class Interval ..... 5 Degrees
Data Type ..... Bidirectional
Rotation Amount ..... 0.0 Degrees
Population 688
Maximum Percentage . 13.4 %
Mean Percentage ..... 2.9 %
Standard Deviation ..... 3.30 %
Vector Mean ..... 10.30 Degrees
Confidence Interval ..... 4.11 Degrees

These have a vector mean azimuth frequency of 10.3°, and coincide with the perceived fault trends in the Solai-Subukia Block discussed in Chapter 4. The main fault lines are Kisanana (N11°E), Solai (N13°E), Maryland-Lolderodo (N9°E) that border to the west, Solai, Subukia, Iguamiti-Ol Bolossat plateaus respectively. The plateaus are tilted towards the east at low angles of 5-15° and dissected by a series of smaller, near parallel faults. In the Bahati escarpment area, however, the trend of faults is N15°W with Mbaruk, Sebugo, Oloebar, Karindo and Sapuko fault scarps, at their foot, controlling Mbaruk, Sebugo, Oloebar or Gilgil, Karindo and Nyaioko rivers respectively. The Sattima (N23°W) is the main bounding eastern escarpment and is replaced towards the north, at its approach to the Marmanet forest, by the Marmanet (N38°W) fault line. The Kisanana and Maryland faults curve in to their north and trend N38°E as Emsoss and Chui faults. These curving faults are down-thrown on their convex side. Chorowicz *et al.* (1988) refers to them as "spoon" faults. All the faults die out in one direction or another with a decrease in elevation from Bahati Fracture Zone (Figure 2.2) in the south, to north. Kisanana fault scarp, for example, rises to 1885 m at Kisanana Hill in the south, whereas the escarpment is 1500 m at its northern end. Sattima fault scarp on the other hand, emerges from Marmanet forest and rises to 2975 m at Beacon Hill in the southeast. Since the foot of Kisanana is at 1500 m and the level at Lake Bogoria is at 1000 m, 1500-2000 m (1.5 to 2 km) total fault displacement is suggested.

2.2 HYDROLOGY

The main drainage basin in Olobanita-Nyahururu area, is the Lake Ol Bolossat fresh water lake (Figure 2.1 and 2.2). The lake is a fault-angled, shallow ephemeral lake, resting on Kinangop step-fault platform, at the foot of Sattima escarpment. The lake is the only Rift Valley lake in the Aberdare Detachment area with evident surface outlet located at Nyahururu (Figure 2.1). The lake owes its existence to the north-east tilt of the Kinangop plateau and to runoff from the well-watered Sattima escarpment and the Aberdare Ranges. Recharge into the lake is also from springs at the foot of the Sattima escarpment. The lake drains north through Ewaso Narok, the only drainage system originating in the Rift Valley and flowing out of it. The Ewaso Narok also takes water from the southern parts of Marmanet forest, Ol Bolossat forest, and the Bahati Fracture Zone. The fracture zone marks a high part of the Rift Valley

floor in the Aberdare Detachment, from where the Rift Valley slopes to the south and to the north. Thus, the area form the drainage divide for all the drainage basins in the Aberdare Detachment area. At Nyahururu, the Ewaso Narok falls over 30 m across a ledge of Thomson's Falls phonolite (Photo 2.1), and out of the Rift Valley; from there it flows northeast into Ewaso Narok swamp. The rest of the drainage in the Aberdare Detachment is internal, flowing into the Rift Valley.

At Olobanita, volcanic rocks show good permeability due to fractures and high porosity. Interpretation from satellite imagery show aligned vegetation, seen from the red hues, marking the path of the drainage lines. The fracture lines and permeable lithology that alternate with impermeable lithology are also marked by aligned vegetation. Vegetation concentration also mark near circular features along the stream lines, and at points of water concentration. Areas of emergence of springs, along fault lines, at the foot of the fault scarps are found to be always marked by these circular features. The near circular features are also seen at lakes Ol Bolossat, Olobanita and Solai, marking swampy areas. These swamps are regulators of river discharge for down-stream supply of water and a direct source of the water itself.

On the satellite imagery, clear water displays blue hues, while turbid water is in the light blue to white hues. These distinctions can reflect the condition of lakes with high sediment influx, and thus poor land use methods in the surrounding environment. As reflected in Photo 2.2, taken during the dry season, the land surface under sisal plantations is bare of any intervening vegetation and any flush rainfall is likely to wash away the soils. Using the blue hues, the extent of water surfaces are mapped and the size of the water bodies determined based on the dry season and the wet season images. In the instance of Lake Ol Bolossat, aquatic vegetation complicated easy recognition of its extent based on the blue hues, because the vegetation imparts a red hue. For this lake, dry season and wet season imagery are compared and ground truth verification made. Lakes Olobanita and Solai are ephemeral, shallow water pans that act as sediment traps. The extent of sediment accumulation in them is mapped from the white hues which indicated how large the lakes could grow during exceptional conditions of high rainfall.

Photo 2.1: *Thomson's Falls Waterfall at Nyahururu.* The Ewaso Narok at Nyahururu closely follows the lowest part of Sattima escarpment (where it is displaced by a north-east trending fault). The river falls in a drop of 30 m over the ledge of Thomson's Falls Phonolite, out of the Rift Valley, cutting a deep valley along the displacing fault. Note the dense Ewaso Narok forest.

Photo 2.2: *Sisal plantations at Olobanita plain.* The rows of sisal crop give a distinctive contrast between the ground and the crop itself, leading to stripped patterns on the imagery (see Plate 2.1). The photo was taken facing north-west. At the background is a N-S trending rift floor horst structure.

2.3 AGRICULTURE

In a crop production process, physical, biological and chemical factors when measured, allow monitoring and surveillance of agro-ecosystems. In mapping these systems in the Olobanita-Nyahururu area, a visual photographic image classification is made based on vegetation, soil cover structure and type and their spatial distribution. The classification is found to be useful in feasibility studies of the land development process. Crop types and coverages are identified by the size of green vegetation biomass which is estimated using a vegetation index involving red and near infrared colour image ratios. The intensity of the spectral reflectance is dependent on vegetation density and the nature of its leaves, topography of its canopy, the soil substrate, and the shadow effect. The influence of seasonal changes on vegetation is also reflected in the red hues. By using SPOT images of 23/9/86 (wet season) and of 9/2/87 (dry season) and the red hues, permanent crop types are recognised and mapped. The wet season image as expected, produces a rather dense vegetation cover. Where the vegetation density is greater than 30% cover, the hue on the image is dark red to red. The areas with less than 10% vegetation cover show on the dry season imagery in shades of green and grey-blue. The semi-arid area north of Olobanita plain reflect this hue. The vegetation associations in the Olobanita area is closely related to lithological variations in the area. The different green to grey-blue hues are used to differentiate between the trachytes and the phonolites mapped in this area.

Variations in crop density and type in Olobanita-Nyahururu area are related to thicknesses of superficial deposits, soil moisture and local relief, forming much denser vegetation at the well watered escarpments than at the Olobanita plain or the Ol Bolossat plain. The image of the area exhibits a clear sensitivity to these variations and to regular patterns of crop fields. Multi-date imagery and different spatial resolutions and scales are adopted in the actual land cover analysis and interpretation, enabling identification of five classes of land use cover patterns:

(a) settlements (large, medium, small scale, crop fields), located in the Bahati and Olobanita plains

(b) forest located along the escarpments transecting the middle part of the area.

(c) scrub bush (rangelands) located at the Olobanita plain and the fault scarps bordering the plain to the west.

(d) water, swamp, wetland and riverine vegetation located in the Lake Ol Bolossat plain

(e) barren land (bare rock) located in the northern parts of Olobanita plain and the north-western slopes of Menengai crater.

The locations of these land cover patterns lead to identification of (see Figure 2.1):

(a) The sisal plantations of Olobanita plain that are seen on the imagery as consistent stripped patterns of rows of brown, dark red, to red hue (Plate 2.1 and Figure 2.3). The area around the sisal plantations shows some bare rock occurrences.

(b) Forest, coffee and tea covered areas, sub-divided into (1) forest areas seen on the imagery as irregularly outlined, persistent dense dark red, red, to brown hue on multidate FCC covering Marmanet, Ol Bolossat, and Bahati escarpment (Plate 2.2) areas, (2) coffee covered areas of a similar hue, also persistent on multidate imagery but with regular artificial outline, and (3) tea farms depicting bright red to red hues, persistent on multidate imagery, and confined to higher altitudes in the areas bordering the coffee plantations north of Bahati and just before the Bahati forest line.

(c) Ploughed areas showing green hues on SPOT imagery, and although also appearing in a similar hue on TM imagery, are inconsistent. Where the area changes in the green hue, it is probably under a perennial crop of maize or wheat at various stages of maturity. These are often utilised as pasture ground when not under crop cover or ploughed.

2.3.1 Sisal Plantations of Olobanita Plain

Variation in vegetation density and crop cover is best exemplified by SPOT multispectral image of Olobanita plain (Plate 2.1). When this image is compared to TM data, crop fields of dense dark red, red, to brown hue are found to be persistent on the FCC's of both images and as mentioned earlier, represented permanent crop. Areas under perennial crop appear in different hues in both scenes, varying from greenish, through light red to white depending on the state of the crop and the type of cover and whether the crop had just been harvested or not. Ploughed areas, however, show consistent green hue in the imagery of all seasons, although inconsistent in the same reference areas. The grey-green hue reflect the background soil, which bear characteristic red to brown soils. The green hue is the characteristic reflectance of iron rich soils. More conspicuous on the imagery of Olobanita plain, however, is the sisal plantations. The sisal fields appear in stripped patterns of rows of the crop (Photo 2.2). The various shades of red hue of the stripes reflect different levels of maturity of the sisal (Table 2.2 and Figure 2.3).

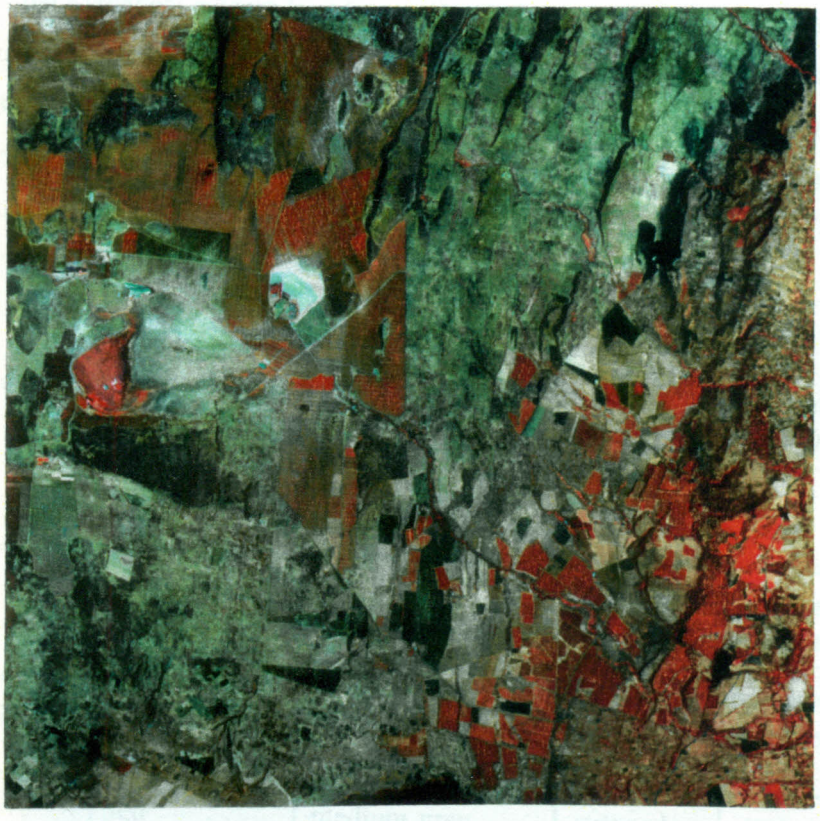

Plate 2.1: SPOT Image FCC of 9/2/1987 of Olobanita plain, North of Menengai Crater (*image processed at RCSSMRS, Nairobi).*

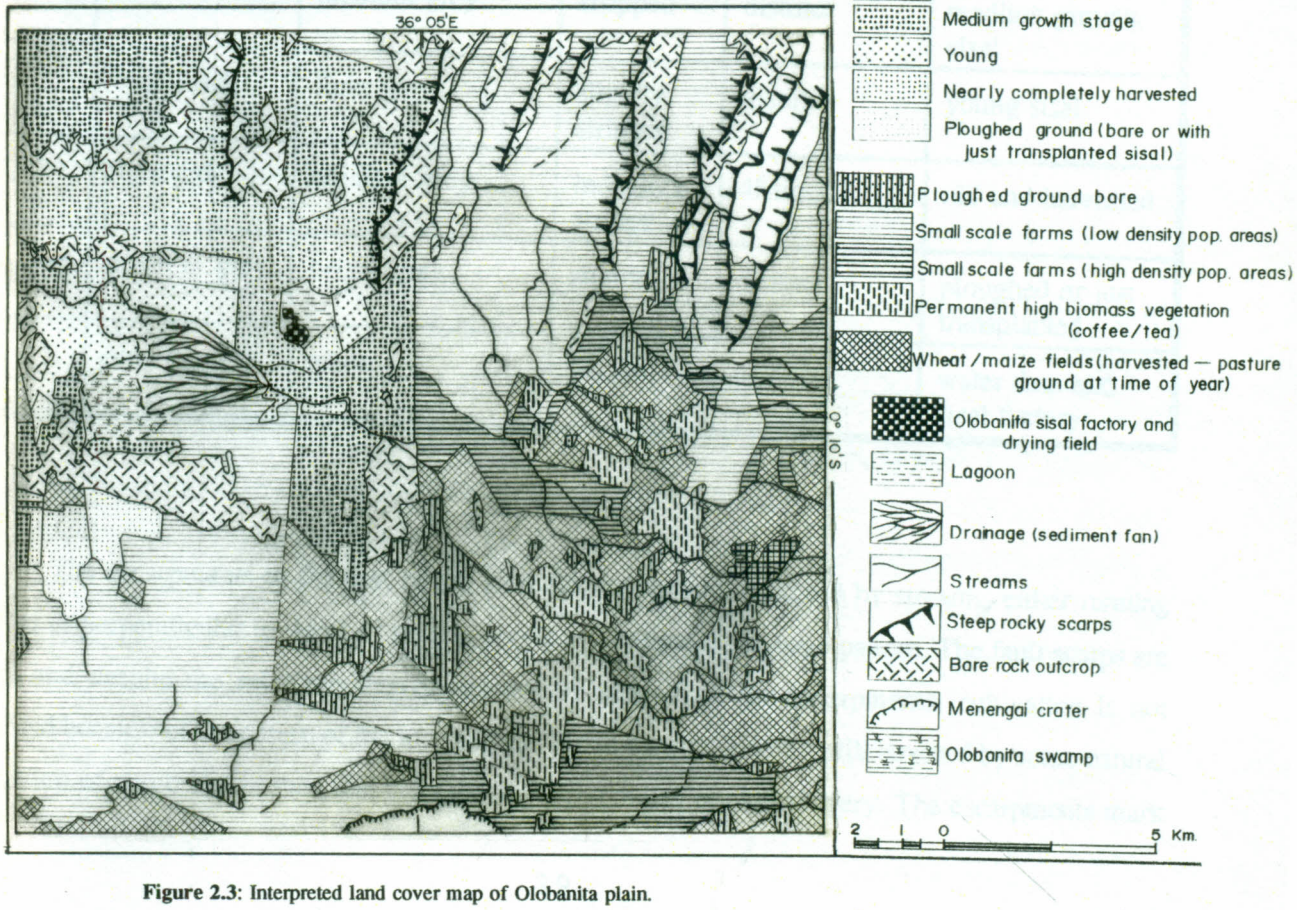

Figure 2.3: Interpreted land cover map of Olobanita plain.

The Olobanita plain is underlain by faulted phonolitic trachytes with poor soil development. The area receives very low rainfall (<700 mm) which supports few other crops, other than the sisal. The plantations are bordered to the south by a rugged texture running into lobes, and representing one of the Menengai caldera lava flows. On the image, the lobate patterns show grey to near brown-green hue which reflect the nature of the rock and the vegetation cover on it, in contrast to the plantation environment. The rocks are mapped as welded vitreous tuffs and ignimbrites of the Menengai volcanic series. The rocks have a poor soil cover, and any cultivation is in small pockets of soil among the rocks.

Table 2.2: Different levels of maturity of sisal plants recognised from the imagery of Olobanita plains (*extracted from SPOT image of 9/2/87 and 28/5/88*).

Unit	SPOT FCC 9/2/87	SPOT panchromatic 28/5/88	Texture/ Pattern	Boundary definition	Interpretation supported by field check
S_1	brown/dark red	light grey	stripped	distinct	mature sisal
S_2	red	medium grey	stripped	distinct	medium growth sisal
S_3	bright red	light grey	slightly stripped	distinct	young sisal
S_4	light red	medium grey	indistinct stripes	distinct	old and harvested
S_5	green to grey	bright grey	smooth	distinct	ploughed or just transplanted
S_6	blue to white	white	smooth	distinct	water dam and sisal factory

The escarpments to the east of the sisal plantations are dissected by streams, either running parallel or perpendicular to the fault scarps, giving a rectangular drainage pattern. The fault scarps are steep, and despite the relatively higher amount of rainfall on the escarpments, cultivation is not practised because of the nature of the topography. These escarpments are still covered by some natural vegetation of shrub and bushes that enhance the escarpments on the imagery. The escarpments mark

small plateaus used for farming in 5 ha. to 20 ha. plots. The cultivated crop reflect different soil thickness developed on vitreous pumiceous tuffs and phonolite, under differing relief and slope conditions, and soil moisture.

2.3.2 Rangelands and Semi-Arid Northwest

The north western parts of Olobanita-Nyahururu area are little cultivated and are covered by sparse vegetation (<10%) consisting mainly of shrub, bushes and grass. The area falls in the 600 mm rainfall regime, and supported minimal cultivation and grazing of nomadic nature. Because of lack of demographic pressure on the land, the vegetation cover reflects geobotanical associations to rock types. Rock alteration and soil cover, for example, impart a brown hue to the FCC of the Subukia-Marmanet area. This area is found to be underlain by porphyritic phonolite rocks. A green to grey-blue hue is, however, imparted to the terrain north and west of Lake Solai. This area is underlain by analcitic phonolites and porphyritic trachytes. In both areas, thin debris accumulation represent *in-situ* soil cover units directly derived from the parent rocks, and reflect the chemistry, permeability and texture of the underlying rocks. The variations in hue and tone is sharp between the two units, facilitating their subdivision.

2.3.3 Bahati Forest

In the Bahati forest area, the intensity of red hues on the FCC reflect the density of vegetation (>30% cover) and the level of maturity of the forest. Other dense vegetation with similar reflectance is located along some stream lines and at Ol Bolossat forest, Lashau forest, Ewaso Narok forest, and South Marmanet forest (Figure 2.1). Some steep fault scarps, such as the Subukia escarpment, also bear a similar density of forest. The Bahati forest itself occupies the steep faulted terrain of Bahati Fracture Zone. FCC of this area (Plate 2.2) appears in dark red hue for a mature forest of indigenous trees and in red hue for youthful and cultivated forest. The granular texture on the red hues indicates variation in height of the trees and the tree crown types. Boundary delineation of part of the forest was made by visual interpretation using SPOT imagery of 28/5/1988. This compares favourably to the classification results, discussed in chapter 3, and field verification. As shown in Figure 2.4, the forest boundary on the 28/5/1988 image differs significantly from that of the old forest boundary (McCall, 1967, 1959 Geological map of Nakuru-Lake Hannington area). In Table 2.3, it can be seen that in the

Plate 2.2: FCC of Part of Bahati Forest (TM image 28/5/88) showing Dense Forest in dark red to red hues (*image processed at RCSSMRS, Nairobi*).

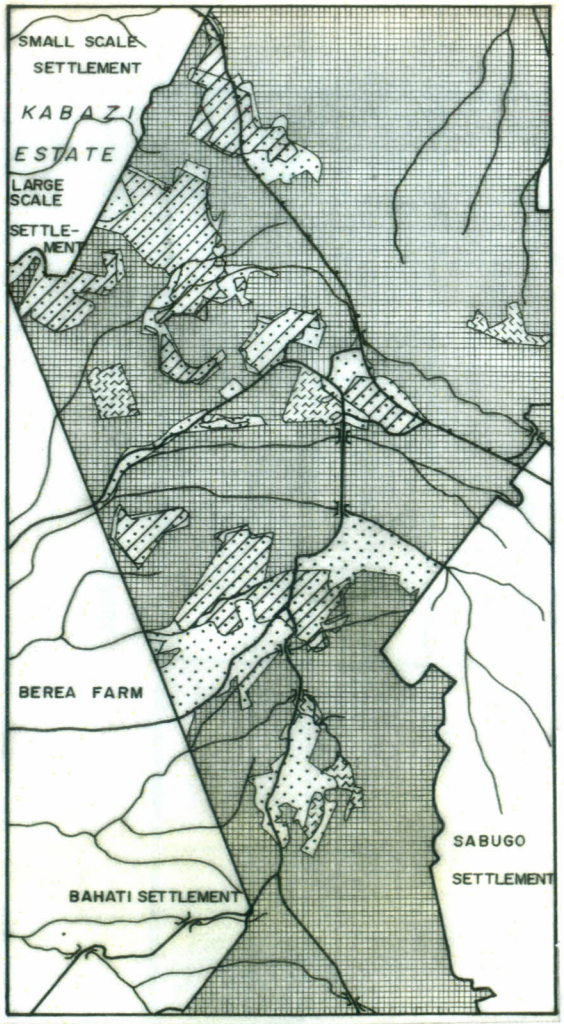

Figure 2.4: Interpreted land cover map of part of Bahati Forest. The 1959 geological map of the area was used to delineated the old forest boundaries. Overlays on Plate 1 and the Landsat TM image of 1/7/84 and SPOT image of 9/2/87 were used to determine the extent of forest depletion.

period 1959 to 1984 the forest had been depleted by 357.5 ha. and 601.25 ha. by 1988. Thus, from July 1984 to May 1988 alone, the annual depletion in the forest zoned area, is about 61 ha.

In theory and in practice, rapid increase in population would result in deforestation, starting first with areas suitable for subsistence farming, then the proximity of the area (weighted distance) from roads and settlement. The most likely places are predicted as being along major roads and close to large scale farms where the need for cheap labour inevitably leads to squatter settlement. Evaluation of the area shows that population increases can not be contained in the existing cultivated areas, even if efforts for a more intensive land use are made, hence the deforestation.

Table 2.3: Extent of forest depletion in a section of Bahati forest since 1959.

Data	Depletion (km^2)	Depletion (ha.)	Existing Forest (ha.)
Geological Map (1959)	-	-	2965.0
Landsat TM of 1/7/84	3.575	357.5	2607.5
SPOT FCC of 9/2/87	5.5425	554.25	2410.7
SPOT Panchromatic of 28/5/88	6.0125	601.25	2363.7

Rate of depletion = 61 ha/year

The Bahati forest and its environment is an important catchment area for all the drainage basins in the Aberdare Detachment (see also Figure 5.1 in Chapter 5). The Meroronyi and Mbaruk rivers that recharge Lake Elmenteita to the south originate from this forest. The Ngosorr river is also sourced at the forest and probably feeds Lake Nakuru to the south through underground channels. The Crater stream, Olobanita and its tributaries, flow east from the forest to feed Menengai crater and subsequently the geothermal reservoir underlying the crater floor lavas, and the Olobanita swamp, respectively. There is evidence from hot springs and steam fumaroles located along fractures north of Olobanita swamp that the swamp discharges underground through intervening fault structures, and subsequently emerge as hot springs feeding Ndoloita river and other springs in the Olkokwe area. The steam fumaroles were mapped in the field along the near N-S trending fault lines, running very close to the swamp and extending north as part of Lake Bogoria Block fault structures. The Olobanita

swamp, despite being seasonal, maintains relatively fresh waters due to underground discharge. The Subukia, a tributary of Waseges is also sourced at the Bahati forest and drains north through Waseges into Lake Bogoria. As mentioned earlier, part of the source waters of Ewaso Narok are from the Bahati forest. Lake Solai also gets its recharge waters from the forest and from percolating waters from Subukia plateau, emerging as springs at the foot of Solai escarpment.

The hydrological regimes in the Aberdare Detachment are thus conditioned by rainfall occurring in the Bahati forest catchment area where runoff retention capacity is controlled by the forest cover. Deforestation is therefore presently causing loss of water catchment, potentially leading to considerably decreased surface and underground recharge waters into the rift floor drainage basins.

2.3.4 Population Estimates

In the settled areas and as interpreted from high resolution SPOT panchromatic imagery of the area, circular white specks represent reflective corrugated iron sheet roofed dwelling units. These units are particularly conspicuous in Bahati and Olobanita settlements. The panchromatic imagery is used to estimate counts of dwelling units per grid cell area, by running a window of one hectare grid cells. The counts are computed at one dwelling unit per 3.58 ha. in the densely populated parts of Olobanita and Bahati settlements, and one dwelling unit per 13.14 ha. for the medium to sparsely populated areas around Olobanita, Bahati, and Ol Joro Orok settlements. Ground truth records indicated that one dwelling unit, on average, contained one house hold of five persons. Population density estimates made from the above data are: 170 persons/km^2 for the densely populated areas, and 5 persons/km^2 for medium to less densely populated areas. A greatly reduced figure of population density is to be expected for the sparsely populated semi-arid areas north of Olobanita and in the terrain occupied by crop fields of 8 to 20 ha. However, this cannot be estimated from the imagery, as the reflectance contrast in these areas is insufficient for the dwelling units to show up on the panchromatic imagery.

In making the population estimates, errors associated with dwelling units having more or less than one household; presence of traditional grass thatched houses that do not have sufficient reflectance contrast to show up on the imagery; and the presence of new and unoccupied dwelling units, provide difficulties in precise population estimates. A ground truth survey is required to establish accurate population estimates, an exercise that is beyond the present study effort.

* * * *

CHAPTER 3

IMAGE ANALYSIS/GIS AND LAND COVER CLASSIFICATION OF NAKURU-MENENGAI AREA

3.0 INTRODUCTION

A technique of information extraction and representation using digital techniques based on ERDAS image analysis programs has been applied to the Landsat-5 TM and SPOT images. Integration with supplementary data using a Geographic Information Systems (GIS), was completed to obtain a land cover classification of Nakuru-Menengai area. Principal components analysis (PCA) and a "maximum-likelihood" classifier are also applied to the data. Most image pixels are a complex mixture of pure components, and the maximum-likelihood classifier uses the mean spectral values for iterations. From the iterations, the informative value of the first 3 principal component bands of the imagery contained most information for characterization of 17 land use categories. The estimate in the supervised classification is not, however, able to classify all samples distinctly. Non-spectral knowledge GIS data such as geology, structures and drainage patterns are georeferenced and registered on to the image GIS data to eliminate this indistinction.

In the digital format of the satellite data, a nominal instantaneous field of view (IFOV) in the satellite data, is a cell, stored as a pixel that is the spectral signature of a reflecting object (American Society of Photogrammetry, 1975). The analog output of the detectors is recorded in computer compatible magnetic tapes which are used at a receiving station to transform and process the imagery (Richards, 1986). The dynamic range of Landsat-5 TM data used in this study is 8-bit with each pixel having a possible range of 0-255 grey values. The data is multispectral, reflected radiation, recorded in 7 channels of assigned ranges: 0.45-0.52 μm - blue; 0.52-0.60 μm - green; 0.63-0.69 μm - red; 0.76-0.90 μm - reflected infrared; 1.55-1.74 μm - mid-infrared; 10.4-12.5 μm - thermal band; 2.08-2.35 μm -mid-infrared (Richards, 1986), used to detect earth features. SPOT multispectral data is recorded in 3 multispectral bands and 1 panchromatic band (Table 3.1).

The wavelength range of the channels constitute the spectral resolution bands. Since the image data values are quantitative and unrelated, each value specifies some degree of reflectance of the study area parameters. As shown by Ilyin *et al.* (1983), reflectance characteristic of materials is a consequence of the chemistry and physics of the material modified by environmental factors and physical conditions.

Table 3.1: Characteristics of SPOT imaging systems (*after ERDAS Field Guide, 1990*)

Sensor parameters	Spectral range (μm)	IFOV (m)	Features Detected
panchromatic black/white	0.51-0.73	10 x 10	(sensitive to all visible colours) cultural features, geological boundaries
XS1-blue	0.50-0.59	20 x 20	healthy vegetation
XS2-green	0.61-0.68	20 x 20	plant species; soil, geological boundaries
XS3-infrared	0.79-0.89	20 x 20	vegetation biomass, crop identification; soil/crop, land /water contrast

The presence of the atmosphere, as shown in Figure 3.1, significantly modifies both incident and reflected radiation. If, for example, the sun radiates energy isotropically so that its spectral irradiance (measured in Watts per m^2 per wavelength - λ) i.e. its power density at the earth, in the absence of the atmosphere is E_λ and $E_\lambda \cos\theta$ if the solar zenith angle measured from the normal to the surface is θ (Richards 1986), the available irradiance between λ_1 and λ_2 is:

$$E_{sensor} = \int_{\lambda_1}^{\lambda_2} E_\lambda \cos\theta \, d\lambda \qquad \text{(i)}$$

since $\Delta\lambda$ is very small, $E_{sensor} = E_{\Delta\lambda} \cos\theta \, \Delta\lambda$ (ii)

Where $E_{\Delta\lambda}$ is the average spectral reflectance in the band $\Delta\lambda$ (i.e. λ_2-λ_1, the wave band used in remote sensing).

If the reflecting surface is diffuse and has reflectance R, then the radiance scattered into the upper atmosphere and available for measurement is:

$$L = E_{\Delta\lambda} \cos\theta \, \Delta\lambda R/\pi, \text{ for ideal case of no atmosphere.} \qquad \text{(iii)}$$

When an atmosphere is present, Rayleigh and Mie scattering and absorption by atmospheric particles must be taken into account and this considers transmittance T of the atmosphere (see Figure 3.1). This modifies the equations significantly, and equation (ii) becomes:

$$E_G = E_{\Delta\lambda} T_\theta \cos\theta \, \Delta\lambda + E_s$$

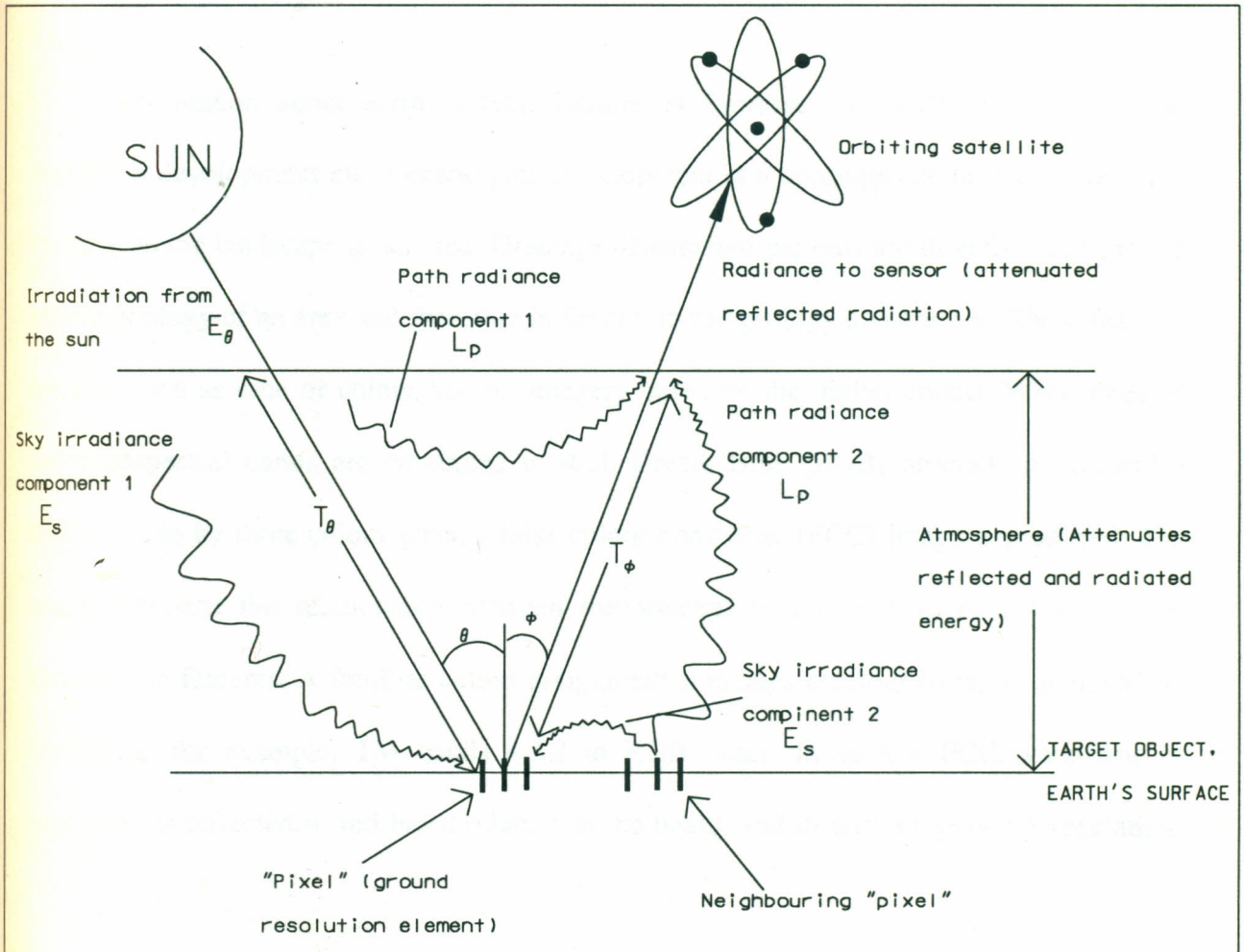

Figure 3.1: Schematic representation of some of the influences on incident electromagnetic (EM) radiation showing the effect of the atmosphere in determining the various paths of energy to the sensor *(modified from Richards, 1986).*

whereas equation (iii) becomes:

$$L_T = R/\pi \{E_{\Delta\lambda} T_\theta \cos\theta \Delta\lambda + E_s\}$$ Where E_s is the sky irradiance

The total irradiance available to the sensor is then;

$$L_{sensor} = RT_\phi/\pi \{E_{\Delta\lambda} T_\theta \cos\theta \Delta\lambda + E_s\} + L_p \quad \text{(iv)}$$

which reduces to $L_{max} = Ck + L_{min}$, where L_{max} and L_{min} are the maximum and minimum measurable radiances of the sensor and relate the digital count value C to measured radiances.

The digital count, C, gives the power detected by the sensor, and thus the grey level in the image which is directly related to the radiance of the scene and has a grey range between 0 and 255.

Information about earth surface features is expressed in landform, drainage and vegetation development etc. Geomorphic development is a consequence of earth processes, recorded in the landscape of an area. Drainage density and patterns are directly related to the geomorphology of an area and therefore indirectly to the geology and climate. These features are expressed as tone or colour hue on imagery based on the digital counts. When three of the multispectral bands are combined in Red, Green, Blue (RGB) ordered colours and a display made by three colour guns, a false colour composite (FCC) image is produced. The image represent the relationship between the spectral bands by colours and hence the variations in features. A familiar colour assignment simulates a colour infrared, achieved by combining, for example, TM bands 4,3,2 in RGB order. In such a FCC, variations in vegetation is reflected in red hues, relating to the health and density of growing vegetation.

In analysing remote sensing data for land cover classification, three main issues are of importance. First, there is the model that represent signature extraction; second, the

quantification of different classes facilitate integration of information from image signatures; and third, there is the use of geographic and geometric information in a GIS data base. The reasoning capability of GIS can be integrated with image classification results to attach a meaning to classified signatures. In the classification, computer assisted analysis utilizes reflected radiation, as a digital number (DN) located in a feature space. Pattern recognition techniques based on mathematical probabilities are then applied to build classification models for discriminating land cover. Kartikeyan *et al.* (1995) points out that, though digital methods are fast and accurate when the model assumptions are true, their success is limited by natural variability of the landscape and over-simplicity of the model assumptions. Different land use categories have different probability models and the spectral signature of a class varies dynamically. In adopting to land cover variations, visual interpretation of images is handy, and indeed, digital methods for supervised classification depend on visual intervention to define signatures from land use categories.

In the present study, a 512 x 512 pixel size subset of Landsat-5 TM scene 169/060 of 1/3/1989 of Nakuru-Menengai area is georeferenced by bilinear interpolation algorithm, trained on ground control points. Several image enhancement and manipulation techniques outlined in ERDAS Field Guide (1990) and by Richards (1986) are then employed to modify image data and to enhance subtle features. The enhancements provide increased apparent spatial resolution and more precise reflectance information, greatly improving the accuracy of land cover mapping. A summary of the working images used to process data for this study is given in Table 3.2. Optically enlarged paper prints of these images were made available at two scales, 1:50000 and 1:125000, permitting for comparison with topographic and

Table 3.2: Summary of Satellite Digital Data used for Digital Image Analysis.

Data type	Path/Raw	Acquisition date	Format/ Density	Band and Scene Coverage
[1]TM	169/060	01/3/1989	[2]BSQ, 6250 bpi	Seven bands, multispectral, quarter scenes of Lake Naivasha-Lake Bogoria area
[3]SPOT	K137/J350	22/3/1988	[4]BIL, 1600 bpi	Panchromatic data in two tapes of Lake Ol Bolossat area
SPOT	K136/J350	21/3/1991	BIL, 1600 bpi	3 bands, multispectral, in two tapes of Menengai crater
SPOT	K136/J351	02/2/1991	BIL, 1600 bpi	3 bands, multispectral, in two tapes of Mau-Narok area

[1]TM - Thematic Mapper of Landsat-5 satellite.
[2]BSQ - Band Sequential.
[3]SPOT- Système Probatoire d'Observation de la Terre (The French satellite system carrying the HVR- High Resolution Visible, instrument).
[4]BIL - Band Interleaved by Line.

geologic maps and for maximum detection of variations in tone, hue, texture, pattern, shape and related characteristics, used to describe the terrain and land cover features.

3.1 IMAGE ENHANCEMENT OF NAKURU-MENENGAI SUBSCENE

To enhance features on Nakuru-Menengai subscene, data file values are stretched using look-up-table modification (LUTMOD) and write function memory (WFM) tools in ERDAS programs. The process involves suppressing the lowest and highest brightness values in the image and stretching the dynamic range of the remaining values. Image histograms used in this task represent a count of the number of pixels, DN (grey value), with specific data file values in each band. In unstretched data, the DN are represented in small portions of 0-255 range histograms (Appendix 3.1). A trial and error approach was adopted in defining minimum and maximum brightness values and linear contrast stretch, saturated linear contrast

stretch, piecewise stretch and saw toothed stretch tested on the image. Non-linear stretch such as logarithmic, exponential, Gaussian and ramp stretch functions were also tested on the image. Other contrast stretch programs applied, involved algebra functions such as rescaling, mapping, differencing, ratioing, linear combinations and colour transformations. In these functions, the continuous tone of the image was converted into a series of density intervals corresponding to specific range of reflectance values, in a manner similar to that described by Haydn *et al.* (1982) and Goetz (1989). The result of the modifications on 3 combined bands of the image were displayed and images with the right contrast and highlighted features written to a file for analysis, interpretation and printing of photographic products.

Image filter programmes are also run on the Nakuru-Menengai subscene to enhance structural features. These involve using stored image processor extension functions of IPX ERDAS program to perform mathematical convolutions on displayed images. The process involve, separating satellite imaging lines into their component wavelengths which are then filtered using a convolution kernel (matrix) selected from a library of kernels, depending on the spatial frequency of the wavelength. Zero sum kernels are used for a complete directional filter analysis in the 8 principal compass directions, enabling detection of both artificial and natural linear features aligned in various directions. The filtered image products are used for structural analysis discussed in Chapter 4 and 5. A 5 x 5 add back box filter (BOXFILT ERDAS program) developed by J. Henkel of AGF, University of Munich (1994, personal communication) is applied on the image of Nakuru-Menengai area to produce the false colour composite (FCC) shown in Plate 3.1. Features, especially edges and fault lines are more pronounced and sharper on this image, and the image is used for principal component analysis (PCA) to prepare the image for supervised classification.

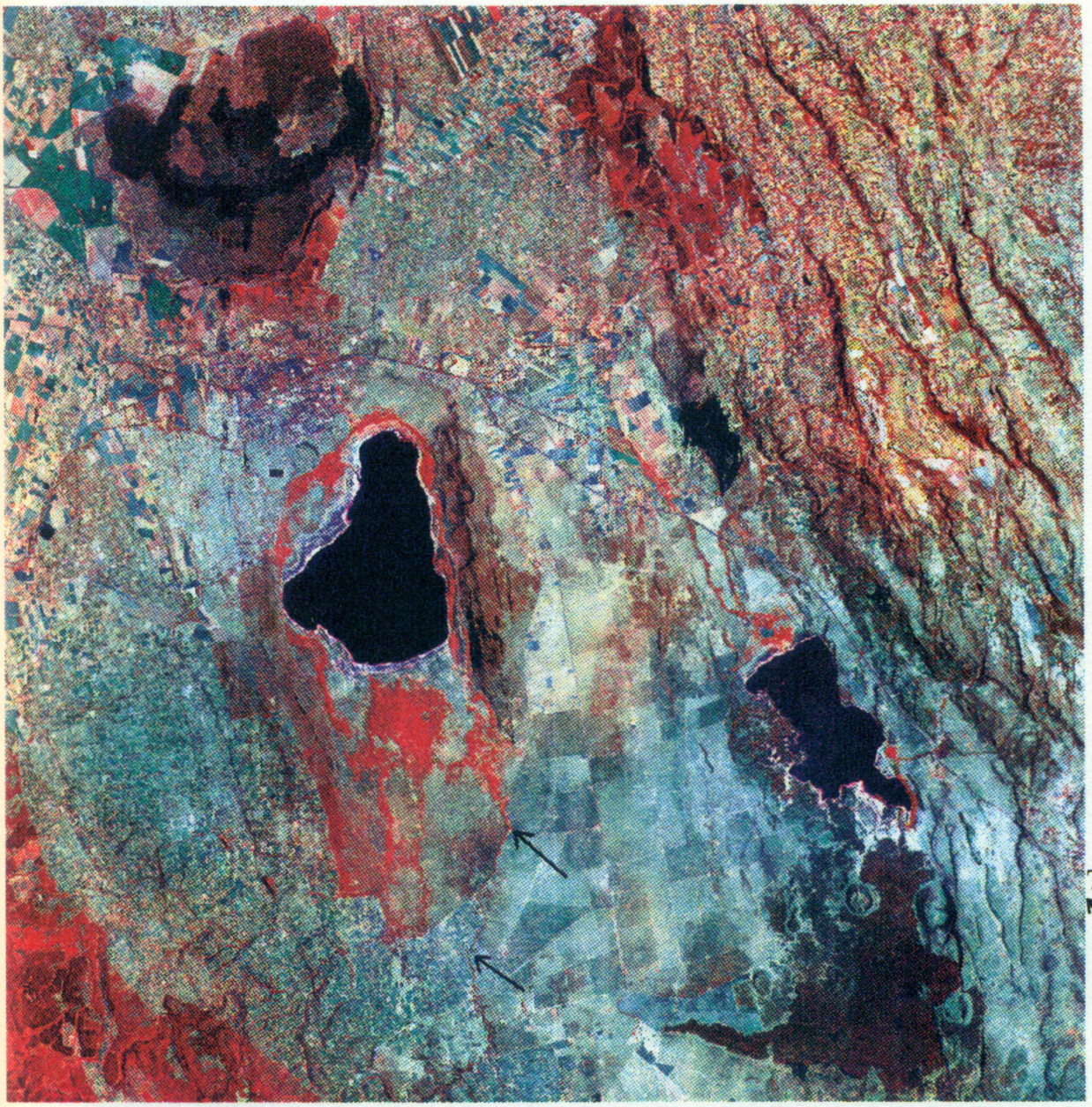

Plate 3.1: A 5x5 Add Back Box Filtered, Standard FCC (bands 7,5,1 in RGB order) image of Nakuru-Menengai area. The image is linear rectified and shows Lake Nakuru - in the middle; Menengai crater as a circular feature in the north-west; and the basalt flows of Elmenteita "Badlands in the south-east. Note the angular drainage (arrowed) into Lake Nakuru and the fault lines on the east of the image. The Nairobi-Nakuru road (marked TH) runs across the image. Nakuru Town is located between Menengai Crater and Lake Nakuru.

3.2 PRINCIPAL COMPONENT ANALYSIS OF NAKURU-MENENGAI SUBSCENE

PRINCE ERDAS program is used to calculate covariance matrices that are applied to image data to produce principal component bands (PC's - linear combinations of image bands along some orthogonal axes featuring the direction of maximum variance), that are used to assess the suitability of the image for classification. In a normal distribution of image data in all the bands, a bivariate scatterplot of "n" bands shows the relationship in the data file values, and n-dimension hyperellipsoid plots can be made. The axis along which there is most spread in the scatterplots is the 1st PC's (PC's 1). This is the longest axis and describes the most variance in the data. The other axes describe the variance in the data that are not already described. For "n" input bands there are always "n" output bands described by Eigenvalues (Table 3.3). It can be seen from Table 3.3, that there is a rapid fall in the Eigenvalues, indicating a high degree of correlation in the original bands. The percentage of the total variance accounted by the Eigenvalues is shown and since most detail in the data is contained in the first 3 PC's (98.59%), these PC's could be used for classification. It is also seen from the Eigenvectors in Table 3.3, and taking the most positive value, that Eigenvector PC 1 is dominated by input band 5, PC 2 by band 4, PC 3 by band 1, PC 4 by band 6 (7), PC 5 by band 3 and PC 6 by band 2, where band 6 corresponds to band 7 of the TM imagery (the thermal band 6 is excluded from this analysis).

Table 3.3: Coefficients of principal component analysis for Nakuru-Menengai image.

Principal Components
File: T1.LAN

Covariance Matrix

	1	2	3	4	5	6(7)
1	165.12	87.28	149.70	95.27	286.95	175.80
2	87.28	52.22	87.93	68.14	175.66	102.05
3	149.70	87.93	159.17	113.32	342.69	202.86
4	95.27	68.14	113.32	315.60	394.47	146.81
5	286.95	176.66	342.69	394.47	1116.58	605.75
6(7)	175.80	102.05	202.86	146.81	605.75	390.61

File: T1.LAN - Eigenvalues

	Eigenval.	Variance%	Total%	Angle	Scale
1	1826.34	83.04	83.04	20.76	1
2	213.06	9.69	92.73	83.92	4
3	128.89	5.86	98.59	71.85	5
4	20.54	0.93	99.52	88.87	14
5	8.85	0.40	99.93	97.37	21
6	1.63	0.07	100.00	88.73	49

File: T1.LAN - Eigenvectors

	PC 1	PC 2	PC 3	PC 4	PC 5	PC 6
1	0.23	-0.20	0.68	-0.04	-0.66	-0.10
2	0.14	-0.05	0.35	-0.04	0.28	0.88
3	0.26	-0.16	0.46	-0.10	0.69	-0.46
4	0.28	0.87	0.18	0.35	0.00	-0.04
5	0.77	0.03	-0.36	-0.51	-0.09	0.03
6(7)	0.43	-0.41	-0.21	0.78	0.01	0.02

The covariance matrix is used to generate a correlation matrix (Table 3.4) used to assess the extent to which the bands are correlated. The value of the correlation matrix C_{ij}, at position $_{ij}$ (row, column) value, in the same position as the covariance matrix, is given by:

$$C_{ij} = \frac{V_{ij}}{(V_{ii} \cdot V_{jj})}$$

Where V_{ij} is the value of the covariance matrix at position $_{ij}$
V_{ii} is the value of the covariance matrix at position $_{ii}$
V_{jj} is the value of the covariance matrix at position $_{jj}$
in the covariance matrix table.

Table 3.4: Calculated Correlation Matrix for Nakuru-Menengai image.

File: T1.LAN - Correlation Matrix

	1	2	3	4	5	6(7)
1	1.000	0.940	0.923	0.417	0.668	0.692
2	0.940	1.000	0.964	0.531	0.732	0.715
3	0.923	0.964	1.000	0.506	0.813	0.813
4	0.417	0.531	0.506	1.000	0.665	0.418
5	0.668	0.732	0.813	0.665	1.000	0.917
6(7)	0.692	0.715	0.813	0.418	0.917	1.000

From the correlation matrix, data values in bands 1,2,3, in the range 0.45-0.70 μm are correlated. This is the region where reflectance curves of natural materials is relatively smooth, leading to redundancy in the data. PCA is run to reduce this redundancy. Two of the bands could also be effectively ignored in image classification or the three bands could be averaged to produce a single band. Band averaging was utilized in performing PCA of Lake Bogoria (Table 3.5) by averaging bands 1,2,3. For PCA of the lake, band 4 is first calculated as the sum average of bands 1,2,3 of the original TM data to avoid most of the redundancy in the data provided by the three bands.

The sum average is calculated using image algebra AOIALGE ERDAS program, to create a single band 4. This band is then subset into a new image file together with bands 4,5,7 of the original image data, to create new bands that are labelled 1,2,3,4. Bands 1,2,3 of the new image correspond to bands 4,5,7 but band 4 of the new image correspond to the sum average of bands 1,2,3 of the original TM data respectively. It can be seen from the Eigenvalues that the first 3 PC's account for nearly all the variance in the data (99.69%). PCA was run on the new image bands to produce the values shown in Table 3.5.

Table 3.5: Coefficients of Principal Component Analysis for Lake Bogoria Image.

Principal Components
File: BOGORIA3.LAN

Covariance Matrix

	1(4)	2(5)	3(7)	4(1+2+3)
1(4)	208.41	281.64	144.90	416.07
2(5)	281.64	755.26	475.25	1321.53
3(7)	144.90	475.25	337.45	937.38
4(1+2+3)	416.07	1321.53	937.38	2512.25

File: BOGORIA3.LAN - Eigenvalues

	Eigenval.	Variance%	Total%	Angle	Scale
1	4381.81	91.03	91.03	19.43	1
2	320.65	6.66	97.70	72.07	1
3	96.09	2.00	99.69	82.79	1
4	14.83	0.31	100.00	89.24	1

File: BOGORIA3.LAN - Eigenvectors

	PC 1	PC 2	PC 3	PC 4
1(4)	0.12	0.50	0.81	0.29
2(5)	0.37	0.70	-0.29	-0.54
3(7)	0.25	0.28	-0.49	0.79
4(1+2+3)	0.89	-0.44	-0.15	-0.04

File: BOGORIA3.LAN - Correlation Matrix

	1(4)	2(5)	3(7)	4(1+2+3)
1(4)	1.000	0.710	0.546	0.486
2(5)	0.710	1.000	0.941	0.811
3(7)	0.546	0.941	1.000	0.861
4(1+2+3)	0.486	0.811	0.861	1.000

From the correlation matrix, bands 2 and 3 are correlated. This compares favourably with the result shown in Table 3.4 where the corresponding bands 5 and 7 are also correlated. The Eigenvectors of Lake Bogoria image, indicate that PC's 1 is dominated by input band 4, PC's band 2 by input band 2, PC's band 3 by input band 1 and PC's band 4 by input band 3. PCA image of Lake Bogoria, (Plate 4.1), produced using the first 3 PC's was used for structural interpretation of Lake Bogoria area discussed in Chapter 4 and Chapter 5.

To prepare the image of Nakuru-Menengai test area for classification, 6 TM bands are utilized, omitting thermal band 6, to perform PCA. The first 3 PC's are used for classification

without loss of detail since they are related to scene brightness, greenness and wetness respectively. PC's 1 is a weighted average of all the bands and represent the scene brightness; PC's 2 represent a contrast between the visible and the infrared bands and can be used for vegetation delineation; and PC's 3 represent a more variable contrast between visible and near infrared bands and can be used for mapping water bodies. PC's 4,5,6 are problematic to interpret, but seem to contain small residue variances related to bands 1,4,5, and 7. PC's 1,2,3 thus contain most information and are output in PC's 2,1,3 RGB order (Plate 3.2). The PCA image data, however, have no one-to-one mapping relation between the bands. The colours are thus not used for interpretation as in the standard FCC. The PCA image colours are, however, more interpretable to the eye, allowing for distinction between features where one is familiar with the image area. The image is also good for edge detection and structural interpretation since fault lines, escarpments, and lava flow edges are enhanced.

3.3 MULTISPECTRAL IMAGE CLASSIFICATION OF NAKURU-MENENGAI AREA

3.3.1 Signature Evaluation

Supervised image classification of Nakuru-Menengai area provides a framework for organizing and categorizing image information. Training samples are chosen based on vegetation and soil-rock cover, taking into account their spatial distribution, type and structure. DIGSCRN ERDAS program is used to digitize the training samples on the image display. To avoid problems due to georeferencing errors, boundary pixels are avoided during digitization. The resulting digital polygon file is the input file for signature extraction, using SIGEXT ERDAS program, that create signatures from image data, based on the pixels corresponding to training sample polygons. In the signature extraction, image pixels are grouped according to their spectral values, outputting a signature file and a name file. Using these files, spectral values are manipulated and evaluated using SIGMAN ERDAS program, to predict the accuracy of classification. In the quick ALARM evaluation, a display of one or more classification clusters on the image overlay is carried out and pattern recognition used to assess the classes on the display.

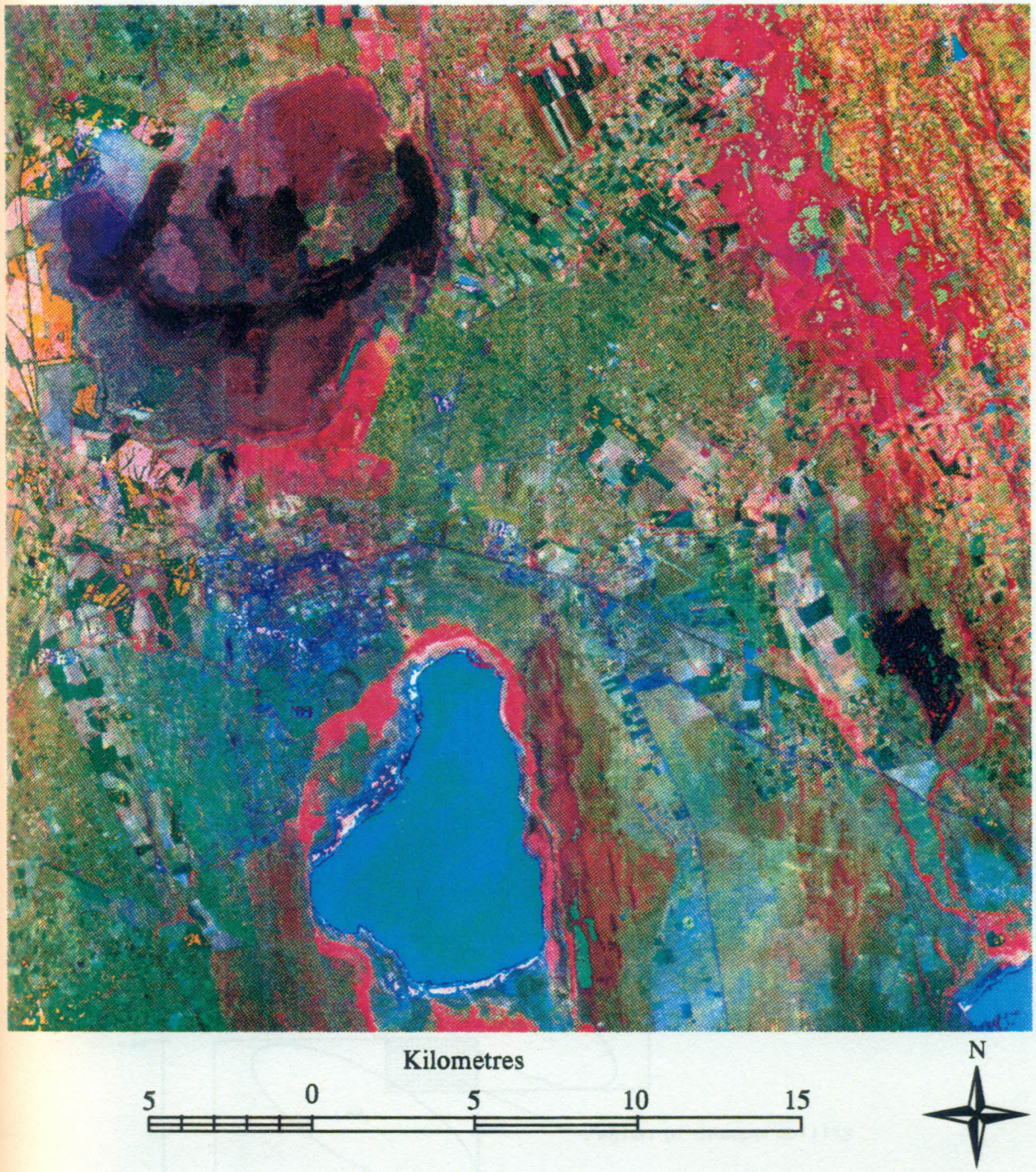

Plate 3.2: Principal Component Analysis Image of Nakuru-Menengai area, displaying principal component bands 2,1,3 in RGB order.

In the ELLIPSE evaluation, a pair-wise scatterplot of ellipse diagrams in two dimension, represented all classes. Each ellipse is based on the mean, μ, and standard deviation, σ, of one signature in two bands, say x_1 and x_2 (Figure 3.2) for all band pairs (Appendix 3.2) of the PCA image of the test area and using 17 evaluated classes. To create an ellipse diagram requires access to image file with a statistical trailer file. As seen in Appendix 3.2, there is overlap of the ellipsoids in band pairs 2,4 3,4 1,5 2,5 3,5 4,5 1,6 2,6 3,6 4,6 5,6 since image data in these band pairs are correlated and the spectral axes of the classes are not separated well enough. The ellipse evaluation indicate that significant classification results would only be achieved using PC's pairs 1,2 or 1,3 or 1,4 or 2,3 for classification. These band pairs show signatures that represent a relatively distinct set of pixels on the ellipse plots, with minimal or no overlap in the ellipse plots.

On carrying out CMATRIX evaluation, a contingency matrix analysis, a table of matrices with the number of pixels sampled and the percentage of those sampled pixels located to each signature are produced (Table 3.6). The pixels of each training sample are

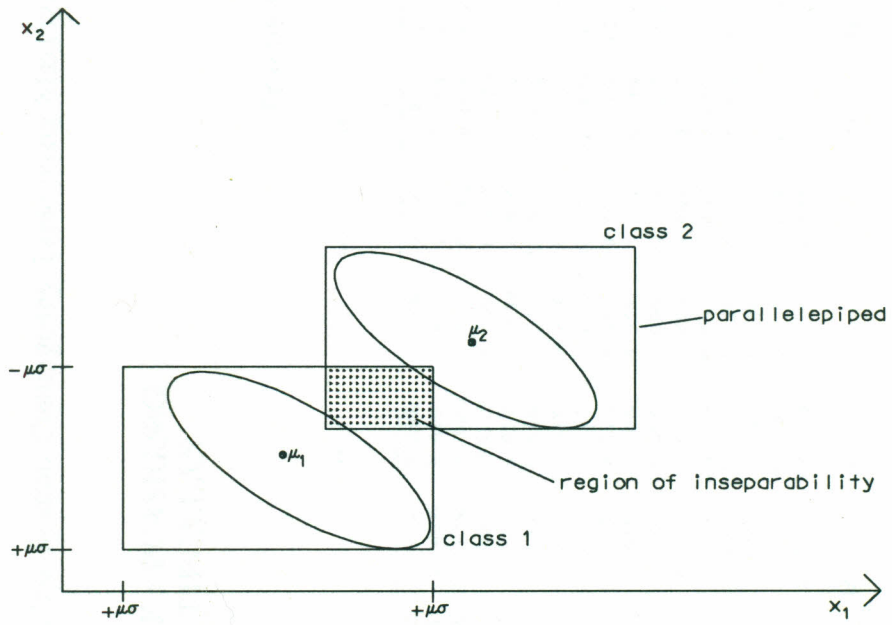

Figure 3.2: Plot of Ellipse Diagram showing parallelepiped classification of correlated data. The sides of the parallelepiped are parallel and consequently there are some data which cannot be separated.
(modified from ERDAS Field Guide,1990)

Table 3.6: Image Classification Contingency Table using Maximum Likelihood Classifier and the first 3 Principal Component Bands

SIGNATURE FILE : PCASIG.SIG
IMAGE FILE : T1PCA.LAN

Training Polygon Names

signature name	s1	S2	s3	s4	s8	s10	s11	s12	s13	s14	s19	s24	s56225	s67	s915	s1718	s2123
s1	793 95.5%	437 11.8%	0 0.0%	0 0.0%	0 0.0%	0 0.0%	0 0.0%	0 0.0%	0 0.0%	0 0.0%	0 0.0%	0 0.0%	0 0.0%	0 0.0%	0 0.0%	0 0.0%	6 0.4%
s2	20 2.4%	2990 80.7%	1 0.0%	0 0.0%	0 0.0%	0 0.0%	0 0.0%	0 0.0%	0 0.0%	0 0.0%	0 0.0%	0 0.0%	0 0.0%	0 0.0%	0 0.0%	0 0.0%	0 0.0%
s3	0 0.0%	132 3.6%	2255 99.1%	0 0.0%	0 0.0%	0 0.0%	0 0.0%	0 0.0%	0 0.0%	0 0.0%	0 0.0%	0 0.0%	0 0.0%	0 0.0%	0 0.0%	0 0.0%	0 0.0%
s4	0 0.0%	0 0.0%	0 0.0%	1250 66.2%	0 0.0%	0 0.0%	5 0.2%	0 0.0%	8 1.8%	1 0.1%	0 0.0%	0 0.0%	35 0.7%	0 0.0%	0 0.0%	0 0.0%	0 0.0%
s8	0 0.0%	0 0.0%	0 0.0%	0 0.0%	491 98.8%	0 0.0%	0 0.0%	0 0.0%	0 0.0%	0 0.0%	0 0.0%	0 0.0%	0 0.0%	0 0.0%	0 0.0%	0 0.0%	0 0.0%
s10	0 0.0%	0 0.0%	0 0.0%	0 0.0%	0 0.0%	1028 89.2%	0 0.0%	1 0.1%	0 0.0%	0 0.0%	0 0.0%	0 0.0%	0 0.0%	0 0.0%	0 0.0%	0 0.0%	0 0.0%
s11	0 0.0%	0 0.0%	0 0.0%	2 0.1%	0 0.0%	0 0.0%	1614 71.0%	31 2.9%	0 0.0%	1 0.1%	0 0.0%	0 0.0%	0 0.0%	0 0.0%	0 0.0%	0 0.0%	0 0.0%
s12	0 0.0%	0 0.0%	0 0.0%	0 0.0%	0 0.0%	89 7.7%	322 14.2%	957 91.1%	5 1.1%	1 0.1%	0 0.0%	0 0.0%	0 0.0%	0 0.0%	0 0.0%	0 0.0%	0 0.0%
s13	0 0.0%	0 0.0%	0 0.0%	0 0.0%	0 0.0%	0 0.0%	0 0.0%	62 5.9%	324 72.8%	10 0.7%	0 0.0%	0 0.0%	0 0.0%	0 0.0%	0 0.0.%	0 0.0%	0 0.0%
s14	0 0.0%	0 0.0%	0 0.0%	0 0.0%	0 0.0%	0 0.0%	32 1.4%	0 0.0%	80 18.0%	1036 76.4%	0 0.0%	0 0.0%	0 0.0%	0 0.0%	0 0.0%	0 0.0%	0 0.0%
s19	0 0.0%	0 0.0%	0 0.0%	0 0.0%	0 0.0%	36 3.1%	0 0.0%	0 0.0%	25 5.6%	0 0.0%	590 100.%	0 0.0%	21 0.4%	0 0.0%	0 0.0%	0 0.0%	0 0.0%
s24	0 0.0%	0 0.0%	0 0.0%	0 0.0%	0 0.0%	0 0.0%	0 0.0%	0 0.0%	0 0.0%	0 0.0%	0 0.0%	968 100.%	0 0.0%	0 0.0%	0 0.0%	230 5.0%	0 0.0%
s56225	0 0.0%	0 0.0%	0 0.0%	171 9.1%	0 0.0%	0 0.0%	0 0.0%	0 0.0%	3 0.7%	39 2.9%	0 0.0%	0 0.0%	5279 99.0%	0 0.0%	1 0.2%	0 0.0%	64 4.3%
s67	0 0.0%	0 0.0%	0 0.0%	0 0.0%	1 0.2%	0 0.0%	0 0.0%	0 0.0%	0 0.0%	0 0.0%	0 0.0%	0 0.0%	0 0.0%	1911 99.1%	0 0.0%	0 0.0%	0 0.0%
s915	0 0.0%	0 0.0%	0 0.0%	0 0.0%	5 1.0%	0 0.0%	0 0.0%	0 0.0%	0 0.0%	1 0.1%	0 0.0%	0 0.0%	0 0.0%	17 0.8%	521 99.8%	0 0.0%	0 0.0%
s1718	0 0.0%	0 0.0%	0 0.0%	81 4.3%	0 0.0%	0 0.0%	0 0.0%	0 0.0%	0 0.0%	6 0.4%	0 0.0%	0 0.0%	0 0.0%	0 0.0%	0 0.0%	4373 95.0%	826 55.8%
s2123	17 2.0%	146 3.9%	19 0.8%	384 20.3%	0 0.0%	0 0.0%	301 13.2%	0 0.0%	0 0.0%	261 19.2%	0 0.0%	0 0.0%	0 0.0%	0 0.0%	0 0.0%	0 0.0%	583 39.4%
T o t a l points	**830**	**3705**	**2275**	**1888**	**497**	**1153**	**2274**	**1051**	**445**	**1356**	**590**	**968**	**5335**	**1928**	**522**	**4603**	**1479**

Table 3.7: Signature Euclidian Distance Measure generated using the first 3 Principal Component bands

Image file : T1PCA.LAN
Signature File: PCASIG.SIG

	s1	s2	s3	s4	s8	s10	s11	s12	s13	s14	s19	s24	s56225	s67	s915	s1718	s2123
s1	0.0	70.68	127.97	158.60	240.07	238.07	146.14	181.38	179.26	119.18	255.04	214.08	271.84	255.67	268.54	126.01	61.38
s2	70.68	0.0	81.34	169.46	219.43	220.74	133.16	169.79	173.42	131.58	250.99	258.27	292.23	235.18	292.01	173.45	73.77
s3	127.97	81.34	0.0	131.51	176.10	146.49	73.06	103.76	114.41	106.89	184.63	243.64	246.36	172.13	265.36	172.03	84.18
s4	158.60	169.46	131.51	0.0	232.22	125.76	74.65	77.97	96.70	102.47	129.02	156.46	128.68	200.33	234.44	105.42	115.84
s8	240.07	219.43	176.10	232.22	0.0	165.18	166.74	166.77	139.42	152.26	183.31	247.99	277.66	72.11	170.28	229.73	190.14
s10	238.07	220.74	146.49	125.76	165.18	0.0	92.77	58.24	68.60	137.17	51.75	209.97	154.88	104.72	213.88	192.61	177.85
s11	146.14	133.16	73.06	74.65	166.74	92.77	0.0	36.99	50.69	67.73	118.68	183.67	174.79	142.07	215.74	128.95	87.42
s12	181.38	169.79	103.76	77.97	166.77	58.24	36.99	0.0	36.38	88.66	83.15	181.26	151.34	126.84	208.13	145.69	122.33
s13	179.26	173.42	114.41	96.70	139.42	68.60	50.69	36.38	0.0	69.38	81.90	162.63	155.08	104.68	173.68	132.82	118.53
s14	119.18	131.58	106.89	102.47	152.26	137.17	67.73	88.66	69.38	0.0	145.49	42.44	185.32	149.38	169.75	85.62	63.39
s19	255.04	250.99	184.63	129.02	183.31	51.75	118.68	83.15	81.90	145.49	0.0	178.70	114.36	121.58	187.55	182.94	196.20
s24	214.08	258.27	243.64	156.46	247.99	209.97	183.67	181.26	162.63	142.44	178.70	0.0	137.07	232.41	138.45	90.49	184.96
s56225	271.84	292.23	246.36	128.68	277.66	154.88	174.79	151.34	155.08	185.32	114.36	137.07	0.0	227.70	216.28	166.04	227.64
s67	255.67	235.13	172.13	200.33	72.11	104.72	142.07	126.84	104.68	149.38	121.58	232.41	227.70	0.0	171.74	223.13	196.92
s915	268.54	292.01	265.36	234.44	170.28	213.88	215.74	208.13	173.68	169.75	187.55	138.45	216.28	171.74	0.0	184.19	227.37
s1718	126.01	173.45	173.03	105.42	229.73	192.61	128.95	143.69	132.82	85.62	182.94	90.49	166.04	223.13	184.19	0.0	103.15
s2123	61.38	73.77	84.18	115.84	190.14	177.85	87.42	122.33	118.53	63.39	196.20	184.96	227.64	196.92	227.37	103.15	0.0

Table 3.8: Signature Separability Listing of all class pairs of PCA image of Nakuru-Menengai area, formed using PC's 1,2,3 and both Jeffries-Matusita Distance and Transformed Divergence Distance Measures

Image File : T1PCA.LAN
Signature File: PCASIG.SIG

Class Pairs, Jeffries-Matusita Distance Measure :						
1:2	1:3	1:4	1:5	1:6	1:7	1:8
1:9	1:10	1:11	1:12	1:13	1:14	1:15
1:16	1:17	2:3	2:4	2:5	2:6	2:7
2:8	2:9	2:10	2:11	2:12	2:13	2:14
2:15	2:16	2:17	3:4	3:5	3:6	3:7
3:8	3:9	3:10	3:11	3:12	3:13	3:14
3:15	3:16	3:17	4:5	4:6	4:7	4:8
4:9	4:10	4:11	4:12	4:13	4:14	4:15
4:16	4:17	5:6	5:7	5:8	5:9	5:10
5:11	5:12	5:13	5:14	5:15	5:16	5:17
6:7	6:8	6:9	6:10	6:11	6:12	6:13
6:14	6:15	6:16	6:17	7:8	7:9	7:10
7:11	7:12	7:13	7:14	7:15	7:16	7:17
8:9	8:10	8:11	8:12	8:13	8:14	8:15
8:16	8:17	9:10	9:11	9:12	9:13	9:14
9:15	9:16	9:17	10:11	10:12	10:13	10:14
10:15	10:16	10:17	11:12	11:13	11:14	11:15
11:16	11:17	12:13	12:14	12:15	12:16	12:17
13:14	13:15	13:16	13:17	14:15	14:16	14:17
15:16	15:17	16:17				

Jeffries-Matusita Distance Measure Separability Listing :						
1262	1414	1414	1414	1414	1414	1414
1414	1414	1414	1414	1414	1414	1414
1414	1405	1414	1414	1414	1414	1414
1414	1414	1414	1414	1414	1414	1414
1414	1414	1406	1414	1414	1414	1414
1414	1414	1414	1414	1414	1414	1414
1414	1414	1410	1414	1414	1414	1414
1414	1414	1414	1414	1414	1414	1414
1414	1404	1414	1414	1414	1414	1414
1414	1414	1414	1414	1414	1414	1414
1414	1399	1414	1414	1409	1414	1414
1414	1414	1414	1414	1058	1407	1414
1414	1414	1414	1414	1414	1414	1410
1341	1414	1414	1414	1414	1414	1414
1414	1412	1414	1413	1414	1414	1414
1414	1414	1414	1414	1414	1414	1414
1414	1414	1400	1414	1414	1414	1414
1414	1414	1414	1414	1414	1414	1414
1414	1414	1406	1414	1414	1414	1414
1414	1414	1410				

Ave.value=1409, Min.Value=1058

Class Pairs, Transformed Divergence Distance Measure						
1:2	1:3	1:4	1:5	1:6	1:7	1:8
1:9	1:10	1:11	1:12	1:13	1:14	1:15
1:16	1:17	2:3	2:4	2:5	2:6	2:7
2:8	2:9	2:10	2:11	2:12	2:13	2:14
2:15	2:16	2:17	3:4	3:5	3:6	3:7
3:8	3:9	3:10	3:11	3:12	3:13	3:14
3:15	3:16	3:17	4:5	4:6	4:7	4:8
4:9	4:10	4:11	4:12	4:13	4:14	4:15
4:16	4:17	5:6	5:7	5:8	5:9	5:10
5:11	5:12	5:13	5:14	5:15	5:16	5:17
6:7	6:8	6:9	6:10	6:11	6:12	6:13
6:14	6:15	6:16	6:17	7:8	7:9	7:10
7:11	7:12	7:13	7:14	7:15	7:16	7:17
8:9	8:10	8:11	8:12	8:13	8:14	8:15
8:16	8:17	9:10	9:11	9:12	9:13	9:14
9:15	9:16	9:17	10:11	10:12	10:13	10:14
10:15	10:16	10:17	11:12	11:13	11:14	11:15
11:16	11:17	12:13	12:14	12:15	12:16	12:17
13:14	13:15	13:16	13:17	14:15	14:16	14:17
15:16	15:17	16:17				

Transformed Divergence Distance Measure separability listing						
1806	2000	2000	2000	2000	2000	2000
2000	2000	2000	2000	2000	2000	2000
2000	2000	2000	2000	2000	2000	2000
2000	2000	2000	2000	2000	2000	2000
2000	2000	2000	2000	2000	2000	2000
2000	2000	2000	2000	2000	2000	2000
2000	2000	2000	2000	2000	2000	2000
2000	2000	2000	2000	2000	2000	2000
2000	1997	2000	2000	2000	2000	2000
2000	2000	2000	2000	2000	2000	2000
2000	1995	2000	2000	2000	2000	2000
2000	2000	2000	2000	1280	1991	2000
2000	2000	2000	2000	2000	2000	2000
1904	2000	2000	2000	2000	2000	2000
2000	1999	1999	1999	2000	2000	2000
2000	2000	2000	2000	2000	2000	2000
2000	2000	1987	2000	2000	2000	2000
2000	2000	2000	2000	2000	2000	2000
2000	2000	2000	2000	2000	2000	2000
2000	2000	1997				

Ave. value=1992, Min. value=1280

not always homogeneous enough for every pixel in the training sample to be classified to its corresponding class. The sampled pixels only weigh the statistics that determined the class.

If the signature statistics for any one sample are distinct from those of the other samples, then a high percentage of the sampled pixels are classified as expected.

Signature Euclidian Distance Measure (Table 3.7) and Divergence measure (Table 3.8) of every class pair are computed in band combinations of PC's 1,2,3, to determine their suitability for classification. The Signature Euclidian Distance Table shows the spectral distance between vectors of each pair of signature means. Where the spectral distance is not significant, that is, equal to zero or very small, then the signatures are not distinct enough to produce a successful classification. The measure allows one to rule out any sample points that diminishes the result of classification. In the Euclidian measure, computed values are high and confirmed expected good classification results using principal components bands 1,2,3 for classification.

In the Divergence Measure, all class pairs are evaluated using Transformed Divergence Distance Measure with values from 0-2000 (Table 3.8) and Jeffries-Matusita Distance Measure with values from 0-1414 (Table 3.8). Both measures are statistical distances between a pair of signatures and are used to determine the separability of class sample pairs in a specified band subsets that can be used to maximize classification. The divergence measures fall in the appropriate upper bound when the first three principal component bands are used for classification. All the signatures are considered totally separable as they show Transformed Divergence Distance Measure average value of 1409 and Jeffries-Matusita Distance Measure average value of 1992. These values are within the 1414 and 2000 upper limits respectively. The selected bands are therefore useful in classification of the selected training samples.

3.3.2 Classification Results

Twenty five training samples are initially selected for classification. These are reduced to 17 training sample, after assessing the signatures using SIGMAN ERDAS program and merging those sample with low percentage in their classification. First, a test classification is constructed using four decision rules; Mahalonubis Distance, Maximum Distance, Minimum Distance and Parallelepiped, in which the relative likelihood for each pixel in the image

belonging to a class is computed. Final classification is made using MAXCLAS ERDAS program and Maximum Distance decision rule, in which the relative likelihood for each pixel in the image is computed and labelled according to its highest likelihood to belong to a class.

As explained in the ERDAS Field Guide (1990) and following the mathematical operations and pattern recognition techniques outlined by Richards (1986), the technique of image classification delineate multispectral patterns in imagery using a set of rules. For each class e.g. 1, 2, 3, 4, ... i, the computer constructs mathematical pixel vectors (F_x) for the pixel signatures in bands (a, b, c, d ...j) such that for class 1, for example:

$$F_x = \begin{vmatrix} F_1a \\ F_1b \\ F_1c \\ F_1d \\ . \\ . \\ F_ij \end{vmatrix}$$ is the prototype vector

and the elements of the vector are means of the corresponding training sets for class 1 and represent the brightness of the pixels. Unknown vector (f_x) is also constructed such that:

$$f_x = \begin{vmatrix} f_1a \\ f_1b \\ f_1c \\ f_1d \\ . \\ . \\ f_ij \end{vmatrix}$$ is the unknown vector

Using these vectors, and the Maximum Likelihood Decision rule, a set of maximum distances, D_1, D_2, D_3, ... D_i, are calculated against the prototype vector, such that for class 1, for example, and in all bands;

$$D_1 = (F_1a - f_1a)^2 + (F_1b - f_1b)^2 + (F_1c - f_1c)^2 + ... (F_ij - f_ij)^2$$

The highest value (threshold) T_1, T_2, T_3, ... T_i for each class is also defined and is included in the calculation to ensure that a pixel is closest to a candidate class, and also that it is within the prescribed distance D_i for that class. The pixel is rejected if not within that distance. The distance threshold T_i is specified according to the number of standard deviations from the class mean.

This mathematical principals are utilised in making a supervised classification of the Nakuru-Menengai area. The training classes are employed in a 4-dimension space parallelepiped. The training set for the classification contains 17 training classes (land use categories) used to train the maximum likelihood classifier. The result is the classification image shown in Plate 3.3. The classification legend consists of a class number and a descriptor which characterized the class. Each land use category belongs to one of the five land cover types - agriculture, forest, barren, urban and water (Table 3.9).

As seen from the contingency matrix table, Table 3.6, it is not possible to resolve all pixels into unique classes solely on spectral information. Some pixel samples remain with some degree of uncertainty between the identified land use categories. From the maximum likelihood classification result, some training samples, however, give good results. Classes 1, 3, 5, 11, 12, 13, 14, 15 and 16 have over 95% of the spectral points properly classified and the classes truly represent the range of variations of features over the test samples. The majority of classes that showed this belong to the water environment or planned land use categories. Classes 4, 16 and 17 are slightly better classed when all the 6 principal component bands are used for classification. The other training samples show no significant change in classification when using either all principal component bands, or 3 principal component bands. Where more than 90% of spectral points are put to one class, the training samples and extracted signatures are considered separable from other classes.

Classes 2, 4, 6, 7, 8, 9, 10, and 17 present significant uncertainty in their classification since the classes contain some degree of generalized information. In these classes, less than 90% of spectral points are classified to assigned classes. In the land use category, fallow

Bahati (class 4), for example, 66.2% of the 1888 spectral points are properly classified, whereas 9.1% of the points are misclassed as ploughed ground and soils, 20.3% as shrub, and 4.3% as fallow rangelands. Bare ground, exposed soils, and variations in vegetation cover density, exerted the uncertainty inherent in the class. Because of variation in the soil colours (ranging from red to ashy white) and ground texture, and because of the presence of patches of trees, or hedges, or patches of fallow ground, uniform fields are not apparently always defined by the classification. Having more training samples within the class did not improve the result, indicating that more refinement is necessary: the training classes, even in small samples, are too broad.

The classifier performed poorly for the urban (Nakuru Municipality) land use category. The uncertainty in this is due to the lake-shore (lakes Nakuru/Elmenteita) environment (see Plate 3.3) of silts, which provide highly reflective surfaces. Because of lack of distinction between the lake-shore and urban land cover types, these classes are merged to achieve the 99.8% of points in the classification (class 15) which is an erroneous representation. It is, however, not surprising that the performance is poor in these two land cover categories as it is well known that spectral features are insufficient to separately classify their samples (Kartikeyan *et al.* 1995). Visual interpretation and vector GIS, designed following methodologies explained in Microstation II-32/pc 2D Graphics Training Course Guide (1991) and Microstation I-32 2D Graphics Training Course Guide (1992), are used to separate the two classes. Non-spectral knowledge parameters such as transport network; secondary features such as shape and size; and other features such as texture and patterns are also taken into account in trying to separate the build-up area from the lake-shore.

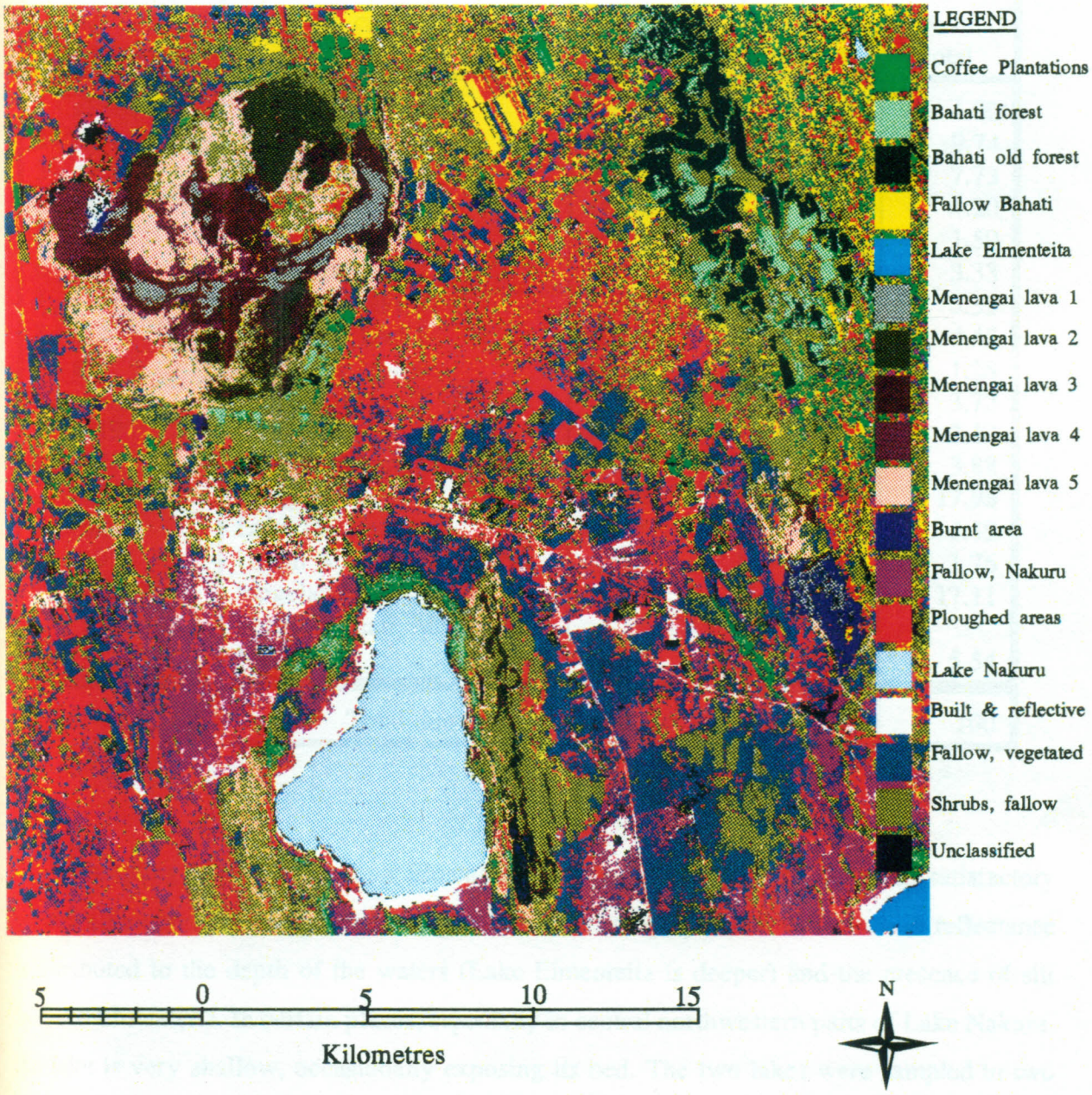

Plate 3.3: Land cover classification image of Nakuru-Menengai area, obtained from applying Maximum Likelihood Classifier to the PCA image of the area.

Table 3.9: Land use categories and land cover classes of Nakuru-Menengai area. Shown on the table are the number of spectral points classified to each land use category and the percentage of the area represented by each class.

Class/ signature name	Land use category	land cover type	spectral points	% of total
1 - s1	coffee	agriculture	1236	4.00
2 - s2	Bahati forest	forest	3011	9.74
3 - s3	Bahati old forest	forest	2387	7.73
4 - s4	Fallow, Bahati	agriculture	1299	4.20
5 - s8	Lake Elmenteita	water	491	1.59
6 - s10	Menengai lava 1	barren	1029	3.33
7 - s11	Menengai lava 2	barren	1648	5.33
8 - s12	Menengai lava 3	barren	1374	4.45
9 - s13	Menengai lava 4	barren	396	1.28
10 - s14	Menengai lava 5	barren	1148	3.72
11 - s19	burnt areas	barren	672	2.17
12 - s24	Fallow Nakuru	barren	1198	3.88
13 - s56225	ploughed, soils	agriculture	5557	17.98
14 - s67	Lake Nakuru	water	1912	6.19
15 - s915	Urban & reflective fallow,	urban	544	1.76
16 - s1718	rangelands	barren	5286	17.11
17 - s2123	Shrub (Bahati, Menengai, Nakuru)	forest	1711	5.54
	Total number of points classified		30899	100

Sampling lakes Nakuru and Elmenteita to one class could also not yield satisfactory results although both categories belong to the water category. Their difference in reflectance is attributed to the depth of the waters (Lake Elmenteita is deeper) and the presence of silt in Lake Elmenteita. In certain places, especially in central northwestern parts of Lake Nakuru, the lake is very shallow, occasionally exposing its bed. The two lakes were sampled to two different classes.

Using the contingency matrix table (Table 3.6), and referring to the summary in Table 3.9, it can be seen that 26963 spectral points are properly classified, representing 87.26% of the total number of spectral points. It is also deduced that, of the total land area shown in

Plate 3.3, 7.78% is under water; 1.76% is under urban development; 23.01% is under some form of vegetative cover mainly shrub and forest; 26.18% is under agriculture; and 41.27% is considered barren, as the land cover type is not under cultivation although it had the potential for it. This is composed of 18.11% lava flow, 20.98% fallow grazing ground, and 2.17% burnt areas.

The Nakuru-Menengai area predominantly comprises cultivated land and fallow ground. Cultivation in this area is conditioned by climate and soil types that reveal differences in the parent rock (local geology). Different physical surfaces in terms of macro-relief, landforms and soil thickness also determine areas used for cultivation. Structural patterns influence the kind of agriculture practised, as they control the slope condition and the surface drainage, thus affecting the availability of water for cultivation and vegetation growth. Classification of cultivated areas is influenced by the size of settlement and the observed hue due to radiance characteristic of the land cover. In the PCA image, dwelling units offered problems in the classification of small scale farming areas, such as at the Bahati Settlement, south-west of Menengai crater. The contrast of features in this area is very low. The areas covered by poorly weathered lavas such as at Olobanita Settlement also offered problems in the classification. In these areas, cultivation is confined to pockets of soil among the rocks, making it difficult to choose representative training samples. Here, patches of trees, hedges, ploughed ground, grassed fields, or dwelling units gave very low reflectance contrast. These two areas were ignored in choosing the training samples and the various land units were classified either as ploughed, fallow, shrub, or built and reflective.

Larger fields (8-20 ha.) are grouped into four classes, displaying regular patterns of cultivated land represented by classes 4, 12, 13, and 16, representing fallow ground or ploughed areas of Bahati, Menengai and Kiwi plains. Class 13 represent truly ploughed areas, whereas class 16 represent true rangelands. Comparison of observed features in class 16 using image characteristics and ground truth record, enable addition of high, medium and low biomass indicators to the mapping units in this class, allowing for characterization of grass maturity, grazing pressure, and localized draught areas. In many instances, however, ground truth in this area is not truly reflected in the classification, as land use category keeps changing.

In using Maximum Likelihood classifier, every pixel is assigned to its nearest class. After the classification it is necessary to introduce a threshold to eliminate those pixels with a low likelihood to belong to the class. Use is made of a probability file and Chi-Square graphs from THRESH ERDAS program, to screen misclassed pixels. The sieved out pixels are lumped to class 18. They reflect boundary areas of the edge of the lakes; the shadow areas of Menengai caldera wall, Lion Hill and Bahati escarpment and the small cloud cover, over north west of Menengai crater (Plate 3.3). Isolated water dams and odd pixels on the image are also sieved out as misclassed elements. These areas show indistinct Chi-Square graphs, with no definite peak associated with the main class. They have high threshold values attributed to a wider statistical distribution at the boundaries than at the centre of the classes.

The accuracy of classification is finally tested using overlay (CLASOVR, GISOVR and DISPLAY ERDAS programs) which displayed the GIS file, over the original image, allowing for comparison and inspection of the classification. Colour highlights are modified in the overlay plane and stored for reference and printing of the classification map. Ground truth windows are generated and used to verify the samples. The ground truthing is available for permanent crop categories such as forest and coffee, and for some land cover classes such as the Menengai lava flows, discussed in section 3.3.3 below, and the lakes. Since much data in the study area was not collected at the time of imaging, an attempt is not made to separate annual crop categories such as wheat or maize. To detect changes in the annual crop categories and map them, use of real time multi-date/multi-data sets would be justified.

3.3.3: Menengai Caldera Classification and Interpretation

Menengai crater, Plate 3.4 and Figure 3.3, show at least five classes of lava flows on the crater floor (Table 3.10) delimited by rugged texture running into lobes at their edges. Geobotanical associations in the crater floor lavas is closely related to lithological variations. Because of these associations, some lavas in Lion Hill, east of Lake Nakuru, and at the Bahati escarpment area, are grouped to the crater floor classes, contributing to some uncertainty in classification of, especially lava 2 (class 7) and lava 5 (class 10). In the wide caldera such as that of Menengai, microclimates also develop due to variations in topography and the

proximity of the caldera to the rift bounding escarpments, further leading to some uncertainty in the classification of the crater floor lavas.

The crater rises to 2278 m at the caldera rim and covers ≈90 km² with a diameter of 9 to 11.5 km at its near circular floor. The caldera is encircled by steep, to vertical slopes that at their deepest, measure 450 m. Its wall shows stratified lithology of pumice, welded tuff, tuff, trachyte and columnar jointed trachyte exposed due to the central section undergoing a volcano-tectonic collapse. The caldera walls are the surface expression of ring faults, which Leat (1984) indicates are due to local crustal anomalies. The subsidence caldera is complicated by recent renewal of the crater floor eruptions of trachytic flows whose structures were aa, glassy, ropy and blocky.

The flow structures, and the different periods of eruptions are reflected in the texture, colour and tone on imagery of the crater. Judged from the vegetation on the lavas, most of it is very young. The youngest lava is fresh and the scant vegetation and absence of soils on it pointed to a very young age, not more than 200-400 years, from the local legend. At least five periods of volcanic eruptions on the caldera floor were interpreted from FCC of the crater and the image classification results shown in Plate 3.3. The caldera rim is distinct and delimited by the crater floor lavas.

Scoria and cinder cones dot the caldera floor, marking the centres of eruption. The main alignment of the centres form an active arc, centrally running east-west along a major fissure and associated with the major axis of the pre-caldera shield ridge. The mode of eruption of the caldera floor lavas was apparently very quiet, through the fissure and the volcanic vents. The youngest lavas indicate presence of four source vents from three cinder cones, and along the fissure. From the nature of lavas, the eruptions from the source vents indicate occurrence near the same time. The individual flows are differentiated from the flow patterns marked by ripple-like structures, and the lobate patterns (tongue-like flows) and structures (Photo 3.1). A number of centres of eruption are also identified for the lavas where craters or cones are absent but the source of the lavas is in no doubt, as the shape of the flow and the presence of fumaroles, pointed to such a source. Some of these lavas appear as big low patches on the caldera floor (Plate 3.4 and Figure 3.3).

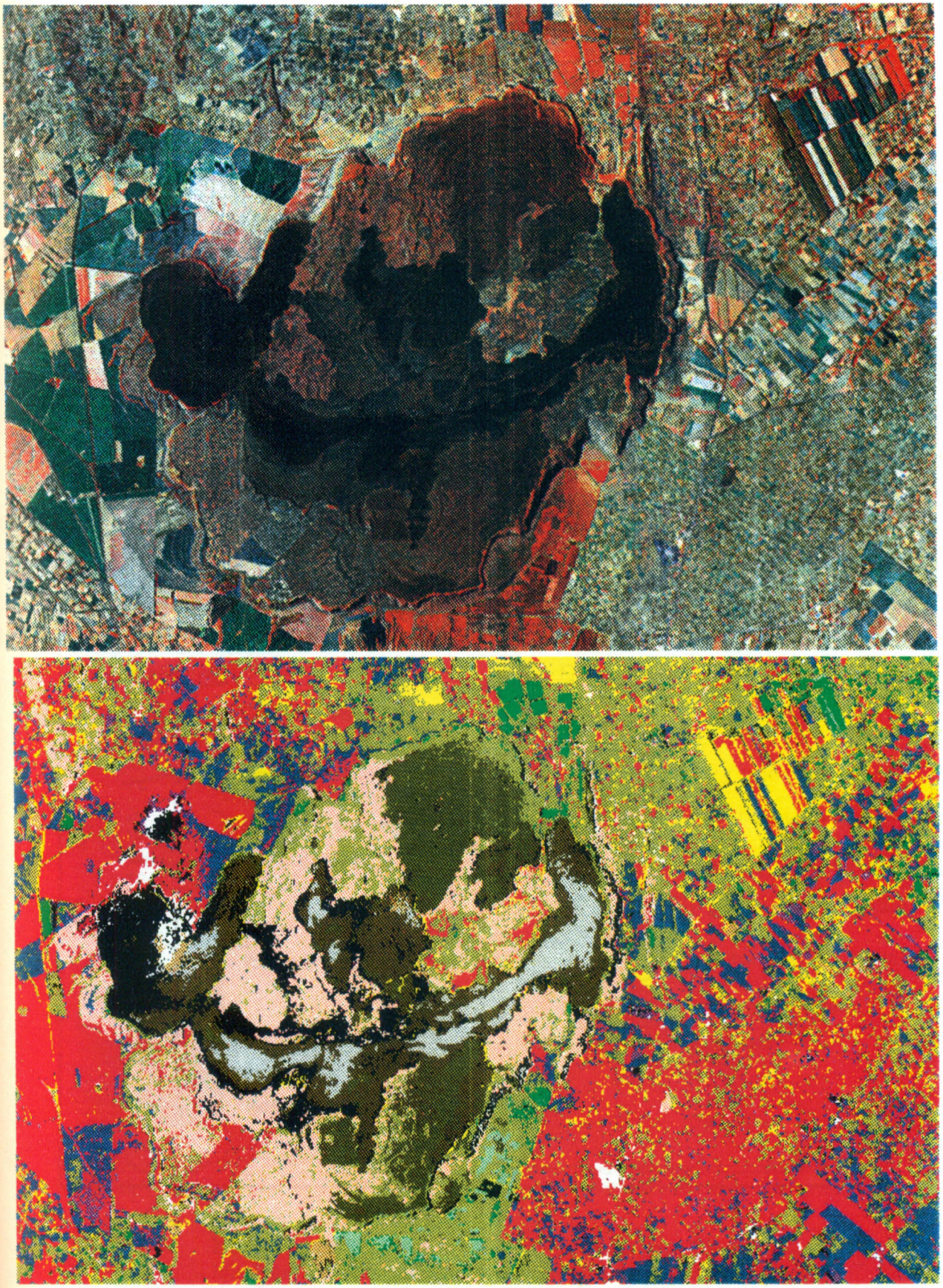

Plate 3.4: FCC and classification image of Menengai crater, showing the caldera lavas and the land use patterns around the crater. The interpretation of the image is shown in Figure 3.3 and the legend of the classes in Plate 3.3.

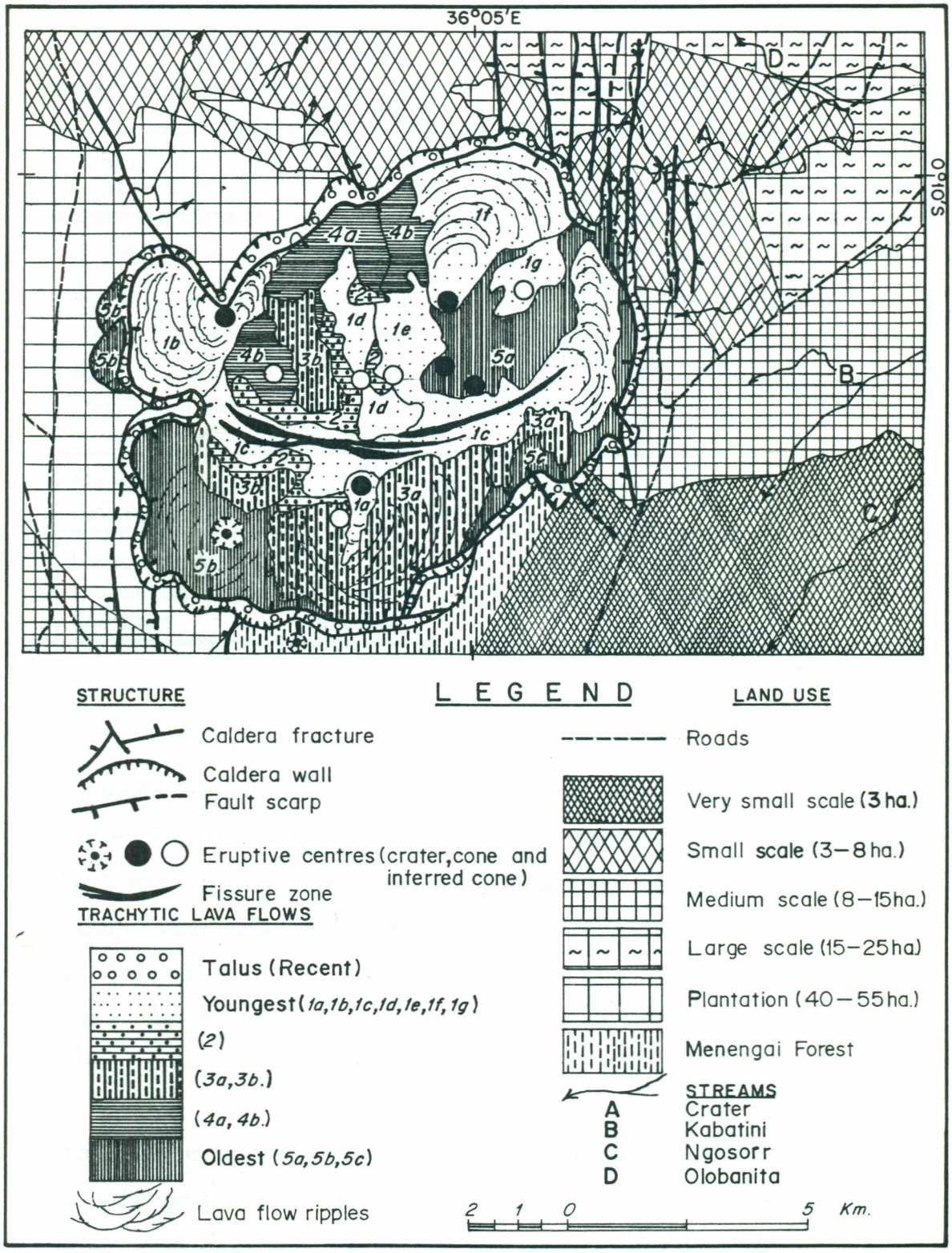

Figure 3.3: Interpreted land cover map of Menengai crater area. The crater floor lithologic units and the land cover classes were interpreted from the FCC and classification image of Plate 3.4 and ground truth survey.

Table 3.10: Spectral characteristics of land cover units of Menengai crater floor lavas. Five relative ages of the lava were interpreted.

Unit (Fig. 7)	Spectral Characteristics and Texture			Relative age
	SPOT FCC of 9/2/87	SPOT FCC of 23/9/86	SPOT (28/5/88) Panchromatic	
5a,-b	red/brown, ragged	red, spotted grey	grey, curvilinear lineations	oldest lava flow
4a,b	red/brown, spotted green	grey/blue, smooth	grey, smooth curvilinear lineations	overlies 5a, b, c
3a,b	grey/blue, tinted red/brown	grey/blue spotted light grey	dark grey	overlies 4a, b
2	bluish grey to dark brown, smooth	grey/blue with reddish brown,	light grey, smooth	overlies 3a, b
1a,-g	black to dark red, smooth curvilinear lineations	dark red, curvilinear lineations	black to dark grey, curvilinear lineations	youngest

On the south-west outer slopes of Menengai caldera and running to the edge of the caldera wall, are four small phreatic eruptive centres, falling on a N-S fissure. On the imagery, this fissure is traced to the western shore of Lake Nakuru, forming part of Baboon Cliffs fault scarp. One of these eruptive centres has formed a parasitic cone just by Menengai caldera edge. The cone issued a trachyte lava flow, traced south to Nakuru, by the Nakuru-Kabarnet road and left behind a volcanic tube (cave), 30 m deep and 10 m across. The crater in the parasitic cone is 100 m across.

The north-east part of Menengai caldera is cut by rift floor grid faults that are more pronounced in this area, where they form a tilted graben structure. The low, down-faulted graben structure, tilted towards the crater (Photo 3.2) indicates larger downward displacement in the crater. Underlying the ashes and pyroclastics in the graben, are welded tuff and tuff of the Menengai series. These are also exposed on the upper reaches of the caldera wall. The main fault line is the west downthrown Menengai fault, described by Leat (1984) and

Photo 3.1: *Lava flows in Menengai crater caldera floor.* The lavas show surfaces marked by flow ripples and lobate forms at the edges. The youngest lava (the dark central band on the photo) show no vegetation growth, and originate from the centre of the caldera. The form of Mau hills can be seen at the background. The photo was taken from the south-west highest point on the caldera edge.

Photo 3.2: *A low graben (arrow) on the north-east of Menengai crater, showing a tilted down-faulted block, towards the caldera floor.* The photo was taken facing north, and Menengai fault is to the right. The faults are in the general trend of fault structures in the lake Bogoria area. Menengai crater is hidden in the foreground.

Grimaud et al. (1994) as belonging to Lake Bogoria grid faults dated at 0.3 Ma. This fault structure therefore post-dates the caldera collapse which must have then occurred in the prior to 0.3 Ma.

Initial trachyte flow from Menengai, occurred just before the major pre-0.3 Ma eruptive event, creating the caldera. The last major eruption in the collapsed caldera occurred at 12000-10000 years before present (B.P.) (McCall, 1967). The initial lava from the infant caldera flowed south and its edge can be traced in the area just north of Lake Nakuru. The lavas and pyroclastics appear to have concealed dyke-like trachy-phonolite intrusives and block structures, of which Hyrax Hill and Lion Hill are remnants. These intrusives were probably associated with initial upsurge of magma before the eruption of Menengai. During the formation of the caldera, trachyte flows occurred, whose nature and form can be observed on the caldera wall, and to the south-east of the crater at Bahati Maili Tatu area where there is quarrying for road ballast. The trachyte flows are confined, and overlay a soil, baked red by the lava flow itself.

Superficial deposits of volcanic ashes, pumice and vitreous tuff and ignimbrites from Menengai, mantle the trachyte flows and cover the larger part of the outer slopes of the crater. These superficial deposits are dated by Leat (1984) at 29000-12800 B.P., and obscure the fault structures in the Bahati plain, Olobanita plain and the area between Lake Nakuru and the Menengai caldera, leaving no impression of the faulted relief. The Menengai slopes are gentle, with little or no drainage pattern development. The soils support a forest on the southern slopes of the crater, and a thriving agriculture (Plate 3.4 and Figure 3.3).

The Crater Stream, flowing in from the Bahati escarpment crosses the fault line and takes a sharp bend to flow south along the foot of Menengai fault scarp into the crater. The river is ephemeral, but during prolonged rainfall, it carries substantial runoff into the crater. This runoff immediately percolates through the permeable caldera floor lavas and pyroclastics, probably to feed an underlying geothermal reservoir. The foot of the caldera wall also forms a "valley" that collects surface runoff crossing from the central Menengai caldera "cone" and the internal slopes of the caldera, further recharging the geothermal reservoir discussed in Chapter 5.

Menengai resistivity data analysis done by Nderitu (1993) identifies four geoelectrical units within the caldera floor, with contrasting thickness and depth. These units are: a laterally heterogenous surface unit, 100-200 m thick; a resistive cap rock at 200-800 m depth; a conductive unit (5-10 Ωm) at 500-1500 m depth; and a geoelectrical substratum (50-300 Ωm) at >1500 m depth. The interpretation of the units envisages a deep conductive unit underlying Menengai geothermal field. The unit contain a potential geothermal reservoir which has a general discharge of fluids to the north and northwest, explaining the presence of steam fumaroles and hot springs observed during ground truth survey at Olobanita, Maji Moto near Mogotio and at Ndoloita.

* * *

CHAPTER 4

STRUCTURAL ANALYSIS OF THE DRAINAGE BASIN OF CENTRAL KENYAN RIFT VALLEY LAKES (ABERDARE DETACHMENT SYSTEM) USING A VECTOR GEOGRAPHIC INFORMATION SYSTEM (GIS) DATABASE DESIGN

4.0 INTRODUCTION

In order to address the problem of lake-level changes in the drainage basin of the Central Kenyan Rift Valley lakes namely, Bogoria, Nakuru, Elmenteita, and Naivasha, a study of the entire watershed of the Aberdare Detachment System is made. The approach adopted was to use the cartographic ability provided through a Geographic Information System (GIS) database to correlate and study the relationship between fault structures, drainage patterns, land use patterns, topography and to some extent lithology. Merging and manipulation of cartographic and remotely sensed data as outlined by Carter-Bonham (1994) is required for identification of potentially mineralized areas and environmentally sensitive areas, and to support decision making. Satellite imagery, topographic maps, geologic maps, and tables and reports of the study area are used to extract information required for themes (grouped data elements) that are needed for this study. Variation in these data types lead to development of two GIS database types, a raster-based GIS and a vector-based GIS. Elmasri and Nevathe (1989) have recognised the integration of the two database types as powerful tools that can help in understanding geological structures, lithological distribution and improved efficiency in exploration.

Interpretation and classification of information for raster GIS and digital image analysis used Landsat TM and SPOT data, discussed in Chapter 2 and 3. Information for the vector based GIS is digitized from the other data sets. The various digitized elements are assigned attribute values through Look-up-Tables (LUT) using links of unique identifiers generated by the GIS system. To facilitate for integration of the various themes, each set of information of a specified theme was designed in a specified layer in the GIS. Since the themes possess a spatial reference they can be accessed and referenced to one another and managed using the GIS, which is the essence of intelligent spatial computing (Wilsher *et al.*,

1993).

Interpretation and visual comparison of raster and vector GIS data sets reveal structural control and tectonic involvement on the drainage systems into the Aberdare Detachment lake basins. The lakes have a generally poor surface and sub-surface recharge because the step-fault ramps of the Rift Valley floor channel water from the high rainfall and forested areas of the marginal escarpments and the rift floor platforms, into lakes Baringo-Turkana, and Natron, located to the north and south of the study area respectively. Image interpretation and field investigation also reveal a marked increase in agricultural activities in the catchment areas of the lakes, and around the lakes. Deforestation in the catchment areas has led to decreased vegetation cover over the soils, raising questions about infiltration of runoff into the regional water table that feed the springs and rivers recharging the lakes. Concern is also raised about the water balance in the area that relate to human influence on the water containment areas and over-exploitation of these resources. Exchange of water and demographic and agricultural pressure on the land and the effects of climatic factors are matters of great interest in understanding the hydrological regimes in the area. Structural control on the surface and sub-surface water into and out of the lake basins has a great influence on the nature of the water reservoirs in the area.

Detailed tectonic mapping of surface features require a combined study of tectonic and geomorphological structures. In accessing cryptic structures -(volcanic rocks, and associated structures are, to a large extent, hidden under a blanket of syn- and post-rifting volcanic pyroclastics and ashes) - filtered images, image classifications results, and vector GIS data, are applied. Satellite imagery offer some distinct advantages since it provides a wide synoptic view of the Kenyan Rift Valley, making it possible to see enough landscape to characterize fault networks, and the macro-relief and landforms, for regional mapping and geo-hydrological analysis. When all the information is incorporated into a database, rapid assessment of hydrological conditions in the area is made.

4.1 VECTOR GIS DATABASE DESIGN AND ORGANIZATION

4.1.1 Data Selection and Entry

In designing a GIS database, a typical work flow follows the steps outlined in Figure 4.1 and 4.2. The actual steps taken in designing the GIS of Central Kenya Rift Valley, follow three general procedures:

(a) Data selection and input, that involve data acquisition, digitizing, conversion of imported data and data storage.

(b) Data processing that involve retrieval of archive data, analysis, modelling and output of the data. The database is created and accessed by a software system linked to a GIS using Database Management System (DBMS) (Burrough, 1986). Through the system, the data can be stored, retrieved, modified or deleted.

(c) Data information, where queries are applied to the GIS database. Fernandez and Rusinkiewicz, (1993) point out that information stored in the database can only be manipulated and interrogated to meet the user's needs if captured, stored and structured in a certain format in the process of database designing.

The information required for the Aberdare Detachment GIS database is extracted from 17, 1:50000 topographic maps and 7, 1:125000 geologic maps (Appendix 4.1). Satellite imagery, some aerial-photographs, tables and reports of the study area are also used to extract some data elements. For ease of manipulation and grouping of data elements, special use and requirement of each of the map topology features are identified and digitized onto different levels. The features are organized into specified themes (coverages) in design files. Up to 63 levels (layers) are available in Microstation GIS Environment (MGE) for map designs. Contours, rivers, lithologic boundaries, forest boundaries, infrastructures and land use cover types, Table 4.1, constitute the major classes of spatial elements or themes (coverages) identified for this project.

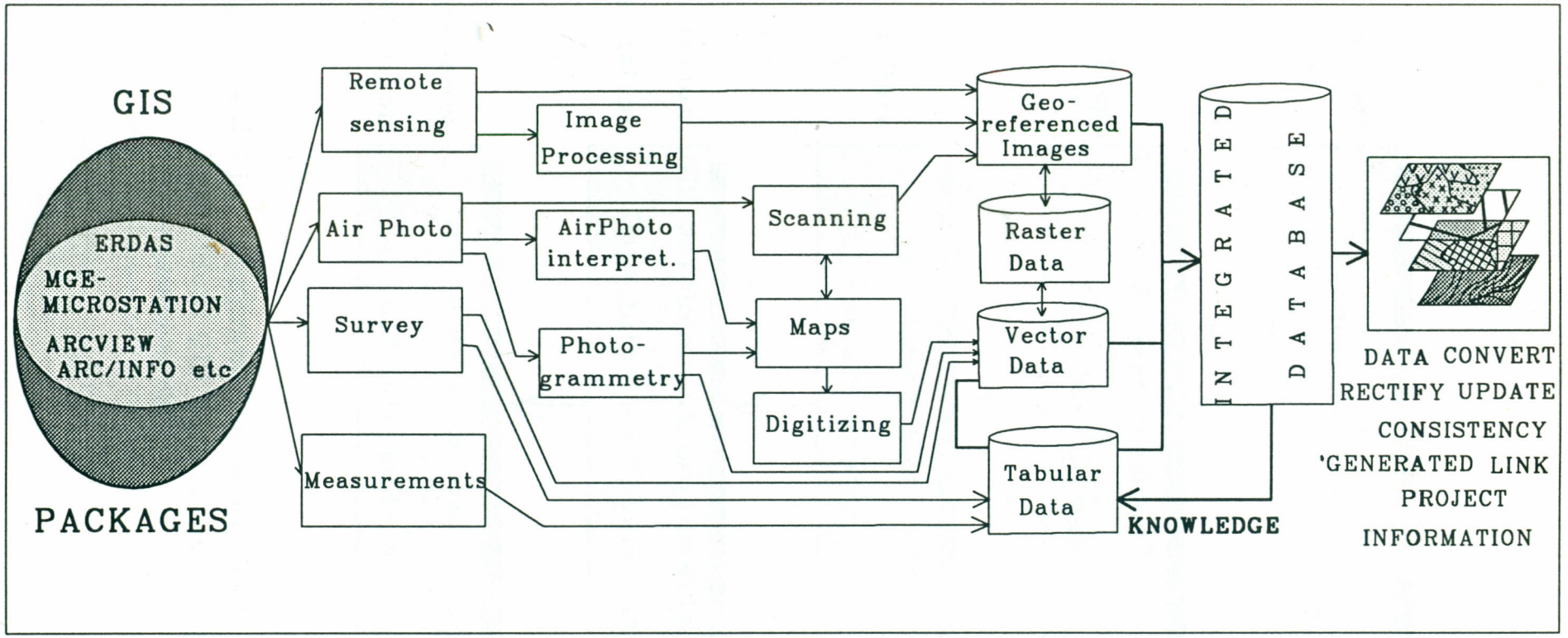

Figure 4.1: Flow diagram showing a typical GIS set-up. In "Survey", geological, hydrological, geophysical, vegetation mapping, soil mapping etc., are involved whereas in "measurements", chemical, mineralogical, gravity, water quality, climatic etc., measurements are involved.

(Compiled from Illustrations In the GIS Laboratory, Information Technology Services, University of Cape Town).

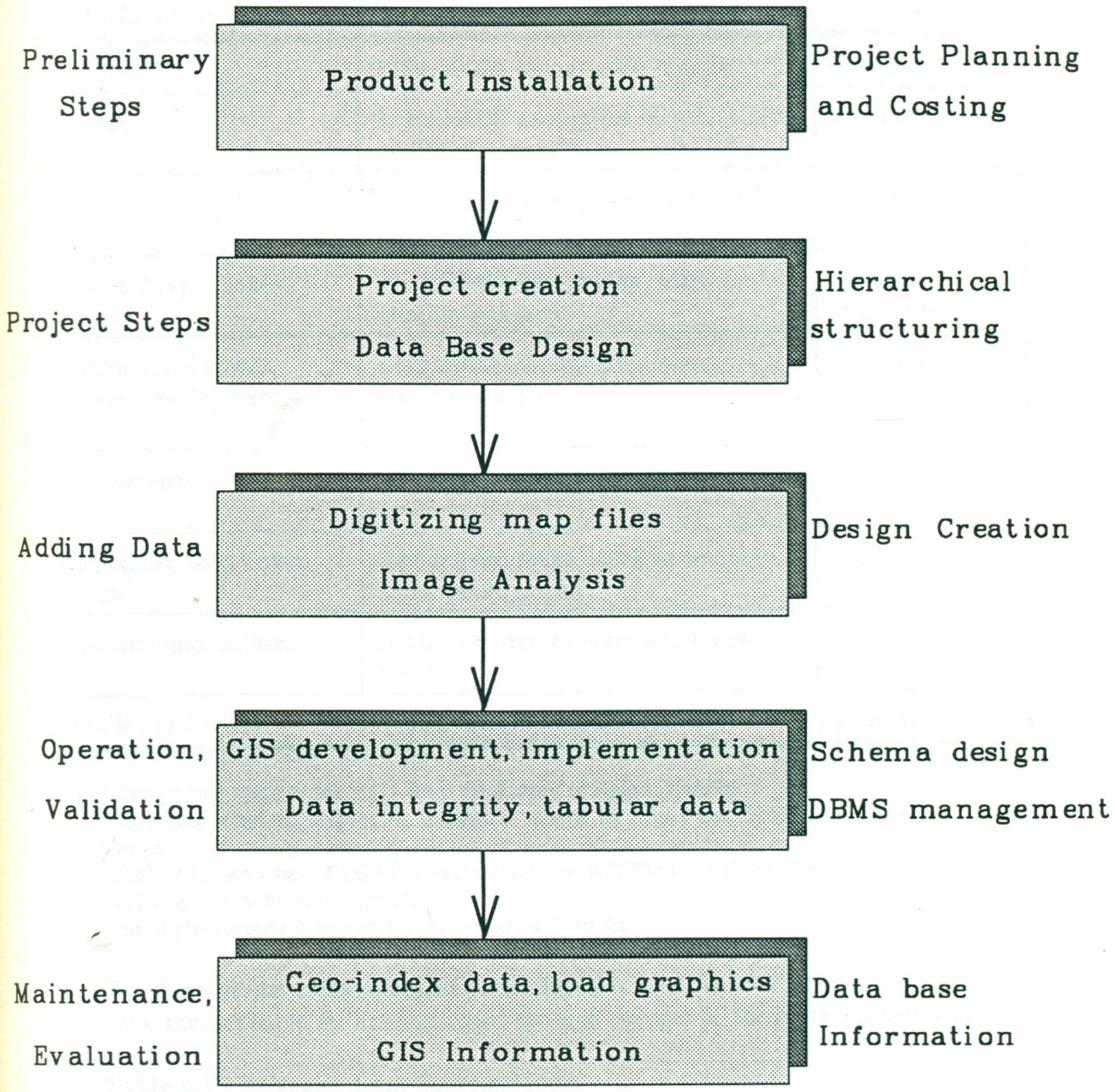

Figure 4.2: Flow diagram showing five steps involved in an individual GIS data base design *(Modified from Fernandez and Rusinkiewicz, 1993).*

Table 4.1: Data Elements and Sources Identified for the GIS Datadase Design of Central Kenya Rift Valley.

Data Elements	Data source	Theme
contours	17, 1:50000 topographic maps[1]	topology
lithology	7, 1:125000 geological maps[2], satellite imagery[3]	lithology
faults	7, 1:125000 geological maps, satellite imagery	structures
drainage (rivers, lakes, swamps)	17, 1:50000 topographic maps, satellite imagery	geography, structures
infrastructures (roads, railways development zones)	17, 1:50000 topographic maps, satellite imagery	geography
soil boundaries	soil maps[4], satellite imagery,	geography, lithology
land parcels, land cover, land use	topographic maps, satellite imagery, aerial photographs[5]	geography
population and utilities	census reports, topographic maps, reports	geography
boreholes and wells	maps and reports	geography

[1]Topographic maps series Y731 from the Survey of Kenya, Nairobi.
[2]Geological maps accompanying geological reports by Mines and Geological Department, Nairobi, Kenya.
[3]Satellite imagery from EOSAT, Dakota, USA and RCSSMRS, Nairobi, Kenya.
[4]Soil maps by Scott et al. (1971).
[5]Aerial photographs from the Survey of Kenya, Nairobi.

The theme to be created, edited or displayed is specified for reference. The coverage data capture mode (Table 4.2) is facilitated through the use of Microstation software

Table 4.2: Vector Data Capture Mode.

data source	entry mode	on line data elements
geological, topographic and soil maps	digitizing, keying-in networking, conversion	topologic features of spatial data (point, line and polygon data)
satellite imagery	digital conversion	raster digital data
lists and reports	keying-in	attribute data tables (descriptive)

products outlined in Microstation II-32/pc 2D Graphics Training Course Guide (1991) and Microstation I-32 2D Graphics Training Course Guide (1992). The first step in establishing spatial coordinates for the coverages is to set up and initialize the hardware environment and prepare the maps for digitizing. Digitizing tolerance and controls are initialized and the extent of the area established by registering control points before designing 2-dimensional (2-D) design files with the required themes. Appropriate working units are established by taking into consideration the scale of the map, such that for the topographic maps used for this study, for example:

Working Units		Settings for 1:50000	
master units (mu)	= meters(m)	**Stream Delta**	= 12.5 m
sub-units (su)	= centimetres (cm)	**Stream Tolerance**	= 37.5 m
sub-units per meter	= 100 cm per m	**Stream Angle**	= 12°
positional units per cm	= 1 positional cm^{-1}	**Stream Area**	= 0

The working units give the resolution of the digitized elements, whereas the stream settings determine the accuracy of digitizing. Considering a hard copy map at the scale of the above settings, a stream delta of 12.5 m meant, sampling points every 12.5 m on the ground or 0.25 mm on the map. The stream tolerance and the stream angle are parameters required so that two points, the limits of which data points closer than the tolerance distance and angle would snap together or a straight line drawn. Every time digitizing is started, at least four known control (monument) points with assigned identities are established to set the digitizing environment and to define the extent of the design files. For accurate digitizing, only root mean square (RMS) errors less than 0.05% are accepted. The stream area used is usually one-half of the square of the stream delta, which in the map units is very close to zero. Three basic data types are handled:

(a) Point data that represent spot heights and location of utilities in the study area such as market centres, schools, hospitals and boreholes.

(b) Line data (arcs) that represent topographic contours, drainage lines, fault lines, roads and railway lines.

(c) Polygon data (closed arcs) that represented lithologic boundaries, soil boundaries, land parcels, forest cover, and land use cover patterns.

The features to be drawn or added are specified and digitized. Digitizing arcs, for example, gave vector data represented by a string of (x,y) coordinates that defined the topology of the features, and the spatial relationship of the coverages. Microstation environment automatically determines the coordinates of digitized vertices relative to the control points and displays them on the screen in plain coordinates of digitizing units (inches/centimetres). As one digitizes, the data is displayed by levels, and specified view configuration (there were 8 views to choose from) and is edited either iteratively or by defining a zoom-in window for close-up editing. Precautions includes assigning labels to features by making a coding form for the features. Start/stop points along arcs, where arcs do not clearly intersect, and where attributes of the arcs change, are marked to avoid duplication.

To facilitate working with Informix relational database on Intergraph's Unix Workstation, the design files that were created on PC Microstation, were transferred to the Workstation, where MGE, MicroStation Projection Manager (MSPM) Primary Coordinate System Geodetic Calculator was used to convert the planer (x,y) coordinates of design files to geographic coordinates (longitude, latitude) by projecting the control points into base coordinate system in degrees, minutes and seconds (dms units - see Appendix 4.1). MSPM is initially used to create a grid of longitudes and latitudes of the study area at 15' interval. These are then used to project the coverages to the real world coordinates (longitudes, latitudes) using Universal Transverse Mercator Projection, thus allowing for the creation of a mosaic of the design files in their correct relative positions.

In the creation of a mosaic of the study area, item definition and attribution features are used to visually compare the coverages and to help in edge matching. Where boundary discrepancies are encountered in adjacent maps, manual extension and joining of data along the edges is performed. A snapping distance is then established to facilitate for joining of corresponding features and merging of the topology of the design files, by running MGE Line Cleaner. In the line cleaning, any errors such as dangling nodes, too many labels, or missing labels, are plotted and fixed. The Line Cleaner also perform geometric corrections on the new

design file graphics by solving undershoot and overshoot errors at the line intersections, at the boundaries, and within the design files. Links are added where appropriate and polygons merged to make a "rubber sheet" by making a topology of the maps.

4.1.2 Data Processing and GIS Information

GIS analysis of the Aberdare Detachment involve analysis using Informix relational database, based on MGE programs as outlined in MGE Projection Manager (MSPM) Operator training Guide (1991); MGE Terrain Modeler (MSM) Reference Manual (1991); and Microstation GIS Environment/ImageStation Imager-2 (MGE/ISI) User's Guide (1992). The analysis enable creation of categories for the data sets and defining of features, and their attributes. This is, besides other map design procedures involving positioning of coverages patterning and colouring using symbolized geographic and geologic elements, inserting neat-lines, titles, legend, scale bar and north arrow. Feature categories are grouped into four: lithology, structures, topology and geography. The coverages with their item codes and annotations are related using 63 levels in the Database Management System (DBMS). Alphanumeric (textual) attribute data, describing spatial topology features of the categories, are related and attached to each of the themes via unique identifiers in the category attribute catalog of Look-up-Tables (LUT) in a manner similar to relational data model that employs two dimensional tabular data (Carter-Bonham, 1994). Item definition and codes are first determined for the attribution data and new, empty data files to which attribution data are defined or tabulated and created, were generated. Verification of the tabulated data sets are made by building topology of the coverages. The attribution data is then joined and related to a feature on the coverage by building query sets.

Lithology boundaries (Litho-boundaries) features, defining area boundaries of the lithology, are identified using litho-centroid (area-centroid) that uniquely identifies the lithology polygons and the attribute feature and link them to the table (Figure 4.3). The record containing the attribute data about the lithology, is shown in the attribute table in Appendix 4.2. This table is linked to the map design (recognised for a particular map by the Map-ID) through Microstation System Links (MS-Links - unique for each element).

To make the maps usable, correction and calculation of spatial measurements and reconstruction of the topology of the maps is performed. The lithology polygons are quantified for perimeter and area of each polygon using MGE Area Builder. The lithologies of the Aberdare Detachment area shown in Figure 4.4, comprised of 1739 polygons representing 96 lithologic divisions. This lithology database is queried using MGE Query Builder, that builds query sets in the topology of the lithology, through spatial feature identifiers (litho-values). The query provided a geo-relational model between a particular lithology and its attribution and is used to retrieve the data from the database, such as that illustrated in Figure 4.4.

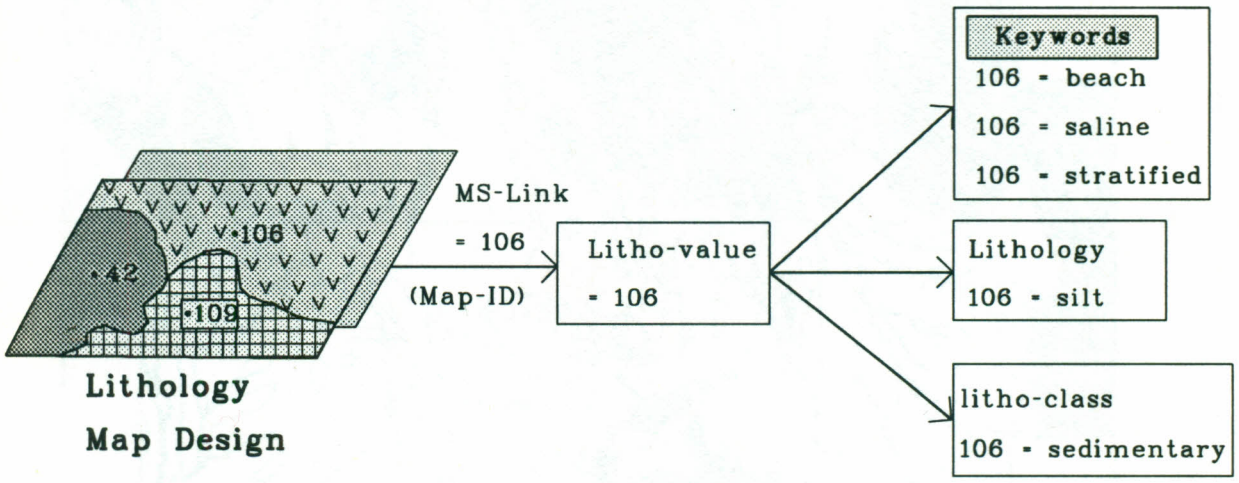

Figure 4.3: Flow diagram showing some attributes of a lithology (silt), and how they are linked to the map design through the MS-Link, the litho-centroid.

Data information involves dissemination and use of relevant GIS information to analyze and model data relations, and to produce maps and reports (Figure 4.5). In the simplest of the data query models, the cursor is used to select any feature displayed on the screen, e.g. a fault line, a litho-value, etc, and that feature's attributes are analyzed,

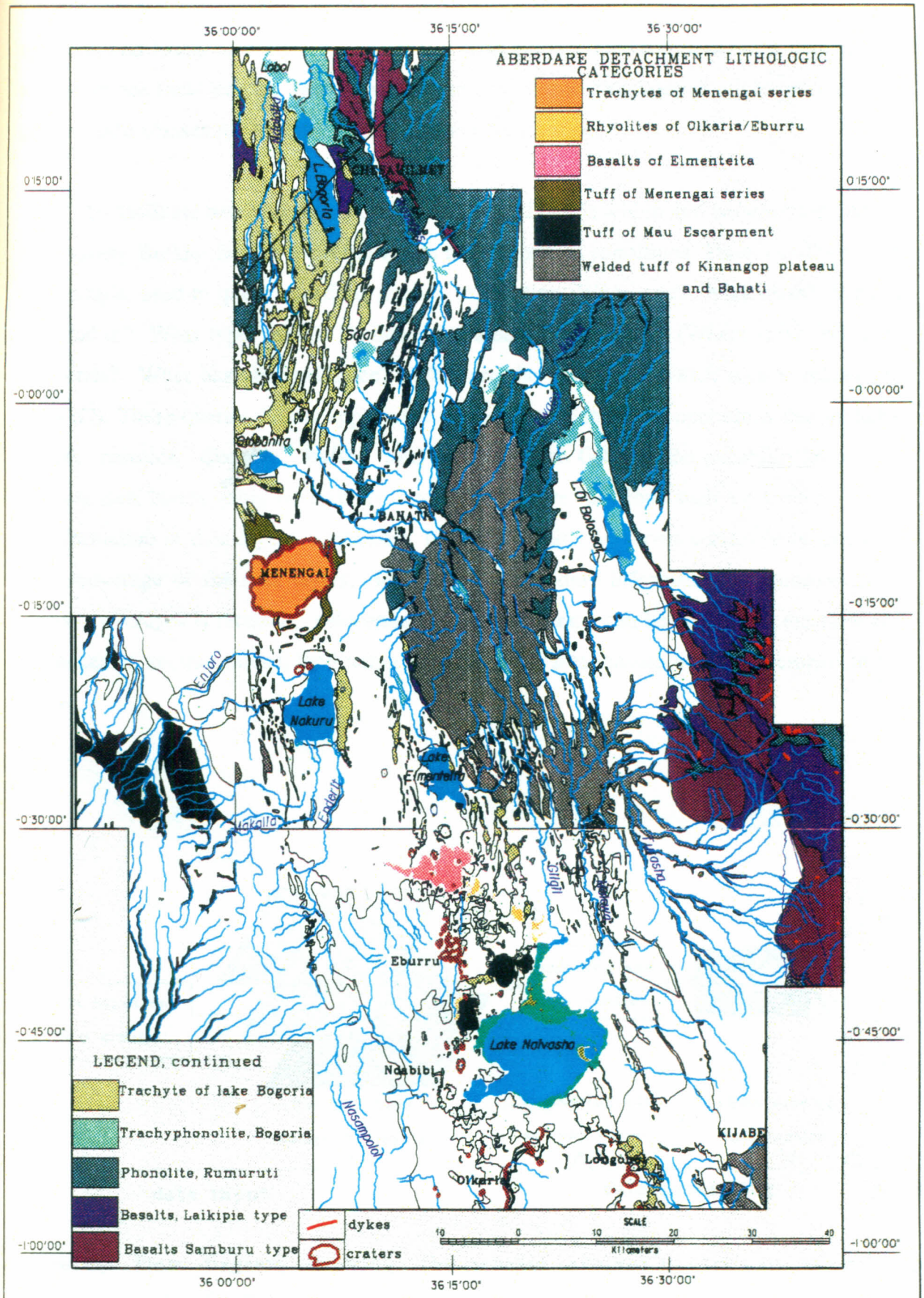

Figure 4.4: Lithological map of Central Rift Valley, Kenya, showing the lithology polygon boundaries, and the litho-centroids. The main volcanic ashes and soils are unshaded. The shaded areas involved query sets on litho-values 103, 123, 105, 420, 410,421, 423, 425, 615, 616, 611,610 and 620 (refer to Appendix 4.2 for explanation).

retrieved, and listed, or printed out. A statistical analysis of the fault patterns is thus queried to identify the fault lengths, fault densities and fault throw directions. Fault lengths are also grouped into classes for analysis related to their distribution.

To facilitate determination of relationships and trends within and between the themes, MGE Query Builder feature identifier has to meet specified conditions. These conditions are, for example, used to query questions relating to **location** (What is at? What class? What is it related to? What type? Area? Perimeter? Value?); or **condition** (Where is it? What are the trends? What has changed since? What are the Patterns? Which data is related to? What if?). These queries follow application of common spatial data operations that included **merge, reselect, dissolve, buffer and overlay**. The GIS has the capability to overlay different data layers using overlay operation that involve functions such as, **Union** - where all information in data layers is retained; **identity** - which preserves certain features within the in-coverage of the data layers; **intersect** - where only information in common to all overlay coverages is retained; **reference** - where any theme can be brought to the view and referenced to another theme, facilitating for analysis of relationship between elements in the themes.

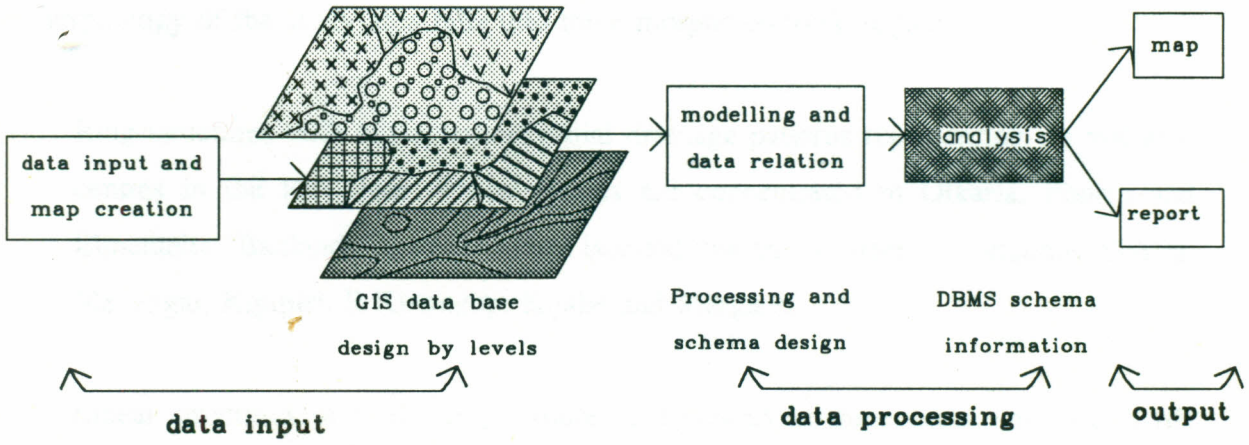

Figure 4.5: Flow diagram showing the process involved in GIS data base design and information flow.

An information index is first prepared by recording longitudes and latitudes on the imagery and georeferencing it to the individual map coverages. Using this information index, one can go from a point or an area on satellite imagery to its topographic or geologic map representation on the coverage, since the cursor indicated the real field coordinates. Registration and integration of spatially geo-referenced vector data sets are further related with respect to one another and with specific image types of the raster data sets. The modelling of the data sets allow for spatial analysis of archive data and on-line data in the GIS, facilitated for viewing of complex relationships and trends between the faults, lithology, drainage patterns and other features. The fault structural elements and the lithology when overlaid on the drainage system, in the first instance, reflect their control on the drainage patterns. Modelling of the behaviour of the drainage flowing through a particular lithology require the use of attributions such as the lengths of streams, the order of the stream, and their flow direction. These helped in answering queries such as those related to finding the density of drainage patterns in lithology of pyroclastic sediments, or locating pyroclastic sediments traversed by perennial rivers, or locating pyroclastic sediments bordered by faults longer than say 20 km with the drainage lines running along the boundary, etc.

Contours were plotted at 60 m intervals. They are represented by 9642 line strings that depict the relief of the area which range from 1000 m to 4020 m a.s.l. It can be seen from the 2-dimensional diagram of the contours (Figure 4.6) and the drainage network map (Figure 5.1) both interpreted and compiled from the imagery and the existing geological maps, that the morphology of the study area falls into three morpho-tectonic regions:

(1) Ring structures with characteristic radial drainage patterns representing the volcanic centres in the Rift floor. These centres are concentrated in Olkaria, Eburru and Elmenteita "Badlands", and also form isolated volcanic centres of Longonot, Eburru, Menengai, Kipipiri, Il Kinangop, Kijabe and Margaret.

(2) Linear structures of fault scarps, more conspicuous in three areas: (a) eastern rift margin fault structures that are downthrown to the west and represented by Sattima and Marmanet escarpments; (b) western rift margin fault structures that are downthrown to the east and represented by Mau fault; and (c) fault structures

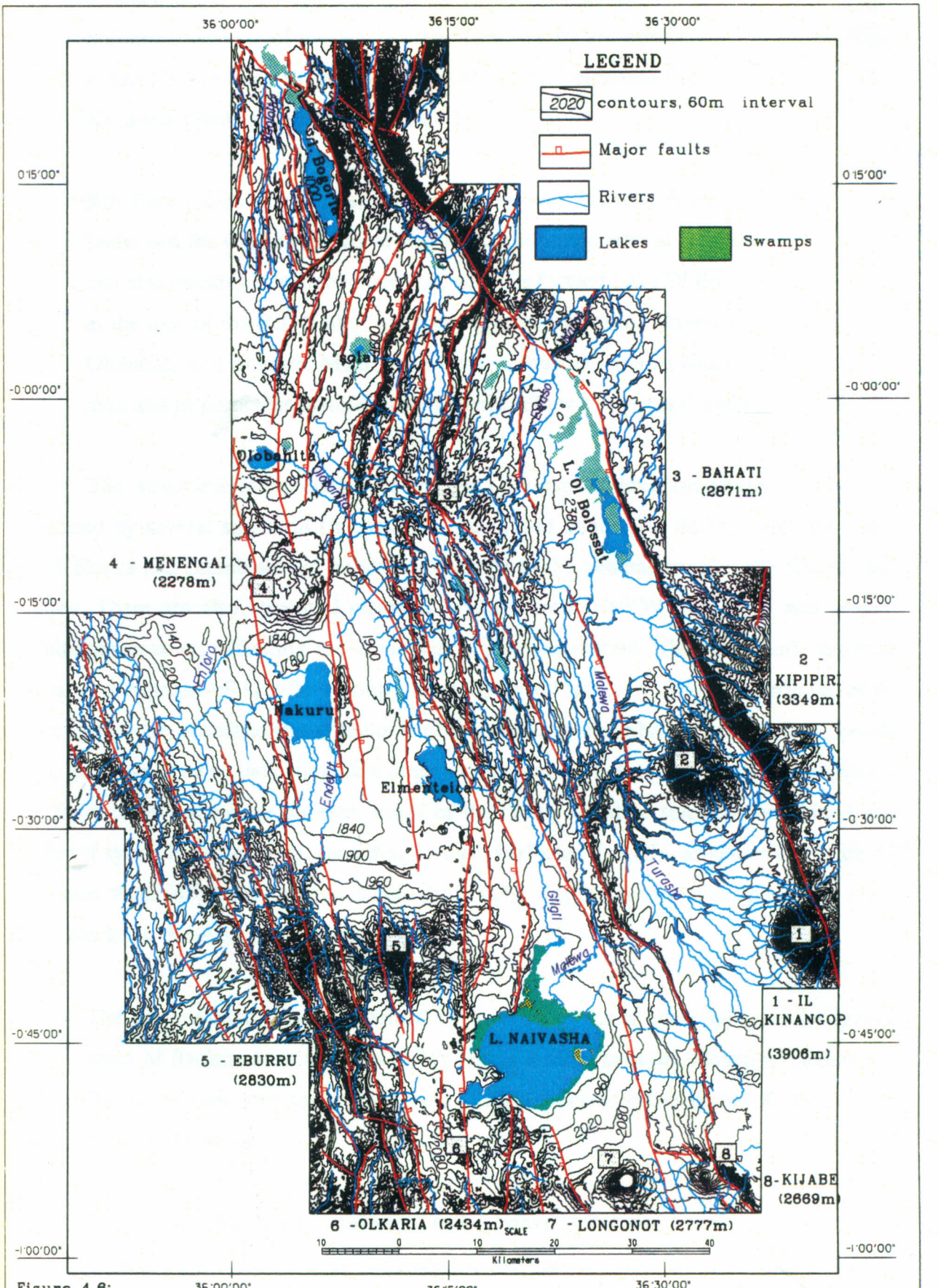

Figure 4.6: Morphotectonic map of the Aberdare Detachment. The contours are at 60m interval and range from 1000m at lake Bogoria to 3900m at Il Kinangop, on the Aberdare Ranges. Note the main fault structures marked by steep escarpments shown by closely spaced, linearly arranged contours (see Figure 4.7 for names); and the relatively flat topography occupied by the lakes.

concentrated at the western part of the eastern half of the Rift floor and immediately bordering the axis of the Rift Valley. These faults are downthrown to the west and marked by the main Kinangop, Bahati, Maryland-Lolderodo-Chui, Solai, Iguamiti and Kisanana-Chemasa-Emsoss and Lake Bogoria faults.

(3) Rift floor plains or plateaus, marking the region between the east downthrown step faults and the west downthrown step faults and interpreted to be at the axis of the rift and also marking Kinangop plateau in which is located Lake Ol Bolossat. In the plains at the axis of the Rift Valley, are located lakes Naivasha, Elmenteita, Nakuru, Solai, Olobanita and Bogoria. Major geothermal resources are also concentrated along this axis and in particular manifested at Olkaria, Eburru, Menengai and Lake Bogoria.

The structural interpretation of the area illustrates three morphotectonic regions enhanced by several structural frameworks - major and minor grid faults, major and minor tilted blocks and rhomb-shaped horsts, all oriented in the general trend of the Kenyan Rift Valley. There are also structural elements oriented from N60°W to N30°W and seen as displacement zones offsetting the main Rift Valley orientation. The main fault structural elements comprised of 3229 line strings, represented in Figure 4.7. The GIS attributes of the fault system are contained in the faults attribute-table and describe their azimuth (Appendix 2.1), length and status, indicating their direction of downward displacement. Map graphics of the faults, representing the different status of the faults, could be selected and plotted with different symbols and colours, according to their attributes. Locally, as shown in Figure 4.7 (see also Appendix 2.1), the main faults show three major trends that defined three major fault blocks in the Aberdare Detachment area:

(1) The Sattima-Mau Block is defined by a series of faults conforming to the general trend of Sattima fault scarp (N18°W) and is located between Menengai caldera and Bahati fracture zone to the north, and Olkaria volcanic complex and Kijabe fracture zone to the south.

(2) North of Menengai caldera and Bahati fracture zone, but east of Kisanana-Chemasa-Emsoss fault scarps, the general trend of the faults is N11°E,

conforming to Solai, Iguamiti, and South Arabel main fault scarps. The fault block defined by this trend of faults was the Solai-Subukia Block.

(3) The Lake Bogoria Block is defined by fault structures generally trending N0° (N-S), and conforming to Kipngatip, Ndoloita, Ngusero and Sandai main fault scarps. The block is located west of Kisanana-Chemasa-Emsoss and Lake Bogoria escarpments and bordered to the north by the Kamasia Ranges and by N90° (E-W) - N30°W trending cross structures in the Loboi plain.

When the block structures were studied in conjunction with the lithology of the area, different periods of volcanic activities were interpreted. This marked different periods of rift deformation, and allowed for determination of geochronology of events in the rift evolution.

4.2 THE FAULT BLOCKS OF THE ABERDARE DETACHMENT

The Aberdare Detachment show fault-controlled topography of near sub-parallel varying N-S striking linear patterns (Figure 4.7). On satellite imagery, subtle differences in heights of these linear patterns are enhanced by the sun azimuth angle of 3° to 5° at imaging time. These angles are much less than the slopes of the fault scarps on the ground. Down-faulting to the west, and near N-S trend of the faults also result in their enhancement on the imagery. The linear features are perceived as specimens in geomorphology and structural geology, representing fractures and fault patterns in the area.

A number of horst-graben structures and plateau blocks that vary in length from a few meters to tens of kilometres, mark three trends of morphotectonic structures in the Aberdare Detachment. These morphotectonic structures defined the Sattima-Mau, Solai-Subukia and Lake Bogoria blocks. Major faults border these blocks and form the initial faults in the formation of the Rift Valley. Initial rifting in Central Kenya Rift Valley was along initial N-S orientations marked by fault trends in the Elgeyo and Nguruman detachments to the north and south respectively. It has been suggested by Grimaud *et al.* (1994) that this general N-S orientation of the Kenyan Rift Valley reflects the foliation direction of Precambrian

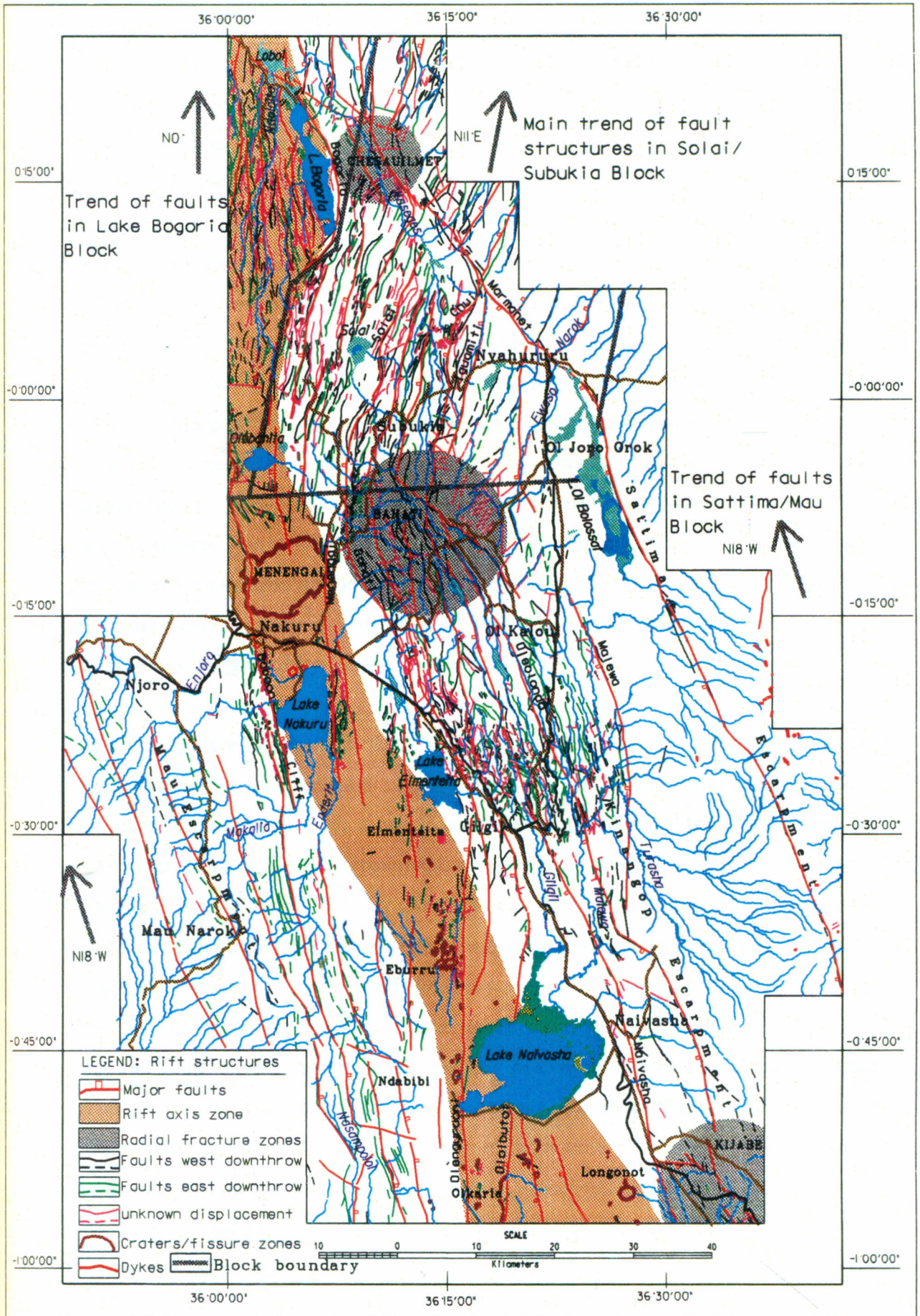

Figure 4.7: Structural elements of the Aberdare Detachment, compiled from existing geological maps, image interpretation results and ground truth survey.

metamorphic rocks, through which the rift cuts, probably following weak zones. The Elgeyo and Nguruman detachments are separated from the Aberdare detachment by cross structures in the Marmanet-Loboi-Kamasia and the Kedong-Ngiro accommodation zones respectively. These accommodation zones show complex displacements, dividing the Kenyan Rift Valley into three broad basins - Turkana-Baringo (Elgeyo Detachment), Bogoria-Nakuru-Elmenteita-Naivasha (Aberdare Detachment), and Magadi-Natron (Nguruman Detachment). The Marmanet-Loboi-Kamasia accommodation zone is represented in the study area by Marmanet-Siracho-Loboi cross structure and separates the Turkana-Baringo basin from the Aberdare Detachment basins. To the north of the accommodation zone, the displacements are complex, showing double rift floor graben structures forming the Kerio graben (between Kamasia Block and the Elgeyo escarpment) and the Baringo-Suguta graben (between the Kamasia Block and the Laikipia escarpment). In the Baringo-Suguta graben, lies Karosi, Peka, Silali, Emaruangogolak and Barrier central volcanoes among others, marking the axis of the Rift Valley in this region. The axis here shows a bias of the shallow mantle underlying the Rift Valley to the east, in contrast to the location of the axis in the Aberdare Detachment, which is biased to the west (Figure 4.7). This fits well with the Rift plate motion model, away from detachment zones, suggested by Bosworth (1986a).

In the Aberdare Detachment there has been an overall spreading of the detachment towards the west, due to strike slip movements along the accommodation zones. These westward displacements and other tectonic movements in the Aberdare Detachment have caused further faulting within the detachment, creating three general homogeneous structural areas with fault orientations at , N18°W (Sattima-Mau Block), N11°E (Solai-Subukia Block) and N-S (Lake Bogoria Block). There are other fault trends within the detachment (see Appendix 2.1), forming N30°W to N60°W cross structures that mark the Marmanet fault zone, the Loboi-Siracho cross structure, and other short faults at Kijabe, Bahati, Gilgil, Menengai and Chesauilmet fracture zones, causing discontinuities that have interfered with the general orientation of the Rift Valley fault structures. The main Marmanet-Siracho-Loboi fault zone falls on the Aswa fault zone and shows transverse shear displacement offsetting the sub-meridian rift fault structures. Shorter faults are observed on directionally filtered, edge enhanced satellite imagery. Many of these faults form short near E-W cross structures seen mainly along the major faults separating the three blocks from one another and also seen in

the main zones separating the Aberdare Detachment from the other detachments, pointing possibly to similar tectonic involvement in the shear structures. There is also a marked orientation of N38°E trending faults, associated with what Chorowicz (1990) refers to as "spoon-fault" structures. The down-throw on the "spoon" faults is on the convex side of faulting giving detachments and a slip to the west on the downthrown blocks.

Later tectonic movement on the Marmanet, Lake Bogoria, Maryland-Lolderodo-Chui and Emsoss-Chemasa-Kisanana fault lines probably followed intrusive magma leading to doming of the Bahati, Chesauilmet and Kijabe fracture zones (Figure 4.7), and at the volcanic centres at Menengai, Longonot-Olkaria and Eburru which subsequently erupted, leading to the formation of cones and craters. The movements at Maryland-Lolderodo-Chui and Emsoss-Chemasa-Kisanana fault lines are marked by "spoon" fault collapse that are very similar and can be superimposed on one another. Along their length, both these faults show trends varying from N11°E, N38°E, and N30°W, at their north-most end where Emsoss merges into Lake Bogoria fault and Chui fault into the Marmanet fault. Because of the tectonic collapse, that is largest at the fault line, there is a tilt towards the east, on the horst and graben structures on the Lake Bogoria Block and the Solai sub-plateau.

4.2.1 The Sattima-Mau Block

The main eastern rift shoulder bounding fault is the Sattima-Lariak fault, defining the break away zone marking the main Aberdare Detachment. The Sattima escarpment is very steep or vertical, reaching 2975 m a.s.l at Beacon Hill, 3791 m at Table Mountain, and 3907 m at Il Kinangop Hill and shows local relief, relative to the immediate rift floor (2340 m a.s.l at the foot of the escarpment), of 100 m to 1500 m along its length. Thus the apparent total relief of 1500-2200 m (1.5 km to 2.2 km) above Lake Bogoria (985 m a.s.l.), indicate throws of similar heights across the eastern rift bounding faults. Their actual displacement could not, however, be determined in the field since large deposits of pyroclastics have buried them.

To its south, the Sattima dies out into the Aberdare, at Il Kinangop Hill, and is replaced further south by the N-S trending Kikuyu fault that is outside the present study area.

Separating the Kikuyu fault from the Sattima fault are the Kijabe cross structures which have offset both these faults, and also affected the Kinangop fault, indicating that the cross structures are of later tectonic involvement. The Kijabe fracture zone forms a dome encompassing Kijabe Hill. It shows a dip-slip to the east at the top of the hill due to later tectonic movements. Three general morphological structures are recognised in the Kijabe area, the first is the main escarpment area that appears to have three strike trends; N18°W (Kinangop fault), N-S (Kikuyu fault) and N50°W (Kijabe fault). The N50°W trending faults conform to the trend of cross-structures cutting across the other two trends of the faults and offsetting them. The second morphological feature forms the Kedong Valley fault systems that are buried under pyroclastics. The faults reflect the trend of faults in the Sattima-Mau Block. Further north and west of Kijabe, in the Gilgil area, the morphology reflects the rift floor grid faults, showing a series of micro-grabens, most of which are cut by short E-W trending cross structures that at Gilgil area are broken up into polygonal or box structures.

On the section of the Sattima trending N18°W, the fault borders the Sattima-Mau Block to the east. The block is bordered on its extreme west by the Mau fault, whereas the southern parts are delimited by the east-west line of volcanic centres of Olkaria, Longonot and Kijabe. Menengai caldera and the Bahati fracture zone border this block to the north. Kinangop, Gilgil, Lion Hill, Baboon Cliff and Bahati faults are the most conspicuous of the series of sub-parallel faults trending in the same direction as the Sattima. In the Bahati fracture area, the faults tend to form ring structures (see Figure 4.7) similar to those seen at Menengai caldera. The ring structure has an E-W elongate ridge with a 15-20 km long axis, probably indicating an intrusive anomaly underlying the area. The intrusive anomaly lead to northerly and southerly tilted fault blocks north and south of the fracture zone. Similar fracture zones are seen at Chesauilmet and Kijabe where there is a multi-directional trend in the rift floor fault structures.

As seen on the drainage network map (see Figures 5.1 and 5.2), the terrain is deeply incised over the Kinangop plateau by the Makungi, Kitiri, Engare Mugutyu and Muruaki, tributaries of the Turasha, which together with Malewa Ndogo and Wanjohi rivers, form tributaries of Malewa. The drainage at Kipipiri is radial on the mountain. Away from Kipipiri, there is a general north-westerly flow of the tributary rivers, following more or less the trend

of Sattima escarpment and controlled by the back tilt on the Kinangop plateau and the drop in elevation from south to north. These trend of streams are, however, confined to the section of the plateau between Malewa and Sattima faults. At Malewa fault line and at the confluence of the tributaries with the Malewa Ndogo, the Kinangop drainage is diverted to south-easterly. The reversal in flow direction is indicated by Thompson and Dodson (1963), to be due to the capture of Kipipiri and Aberdare Ranges sourced rivers by the Malewa. Wanjohi river, for example, flows north in the trend of the Sattima escarpment but changes direction to flow west on its approach to Ol Bolossat swamp. Here it meets the Malewa Ndogo which join Dundori, and changes direction to flow south-easterly along Malewa fault as Malewa river. The rivers west of Malewa fault flow south-easterly in the trend of Malewa fault, closely following the foot of, and running parallel to, Ol Kalou, Simba, Nyaioko, Karindo (tributaries of Malewa), and Gilgil (Muriandati), Baruku and Meroronyi (tributaries of Gilgil) bordered by fault scarps of the same names. Both the Malewa and Gilgil recharge Lake Naivasha. The water-shed between lakes Elmenteita and Naivasha drainages is marked by Sebugo-Oloebar fault scarp and the Gilgil escarpment.

The rest of the drainage into Lake Naivasha basin out of the Kinangop plateau and south of Muruaki, is poor despite the area falling in the 1000 mm annual rainfall zone. The plateau is relatively flat and is absent of surface traces of faults. The Karati river that traverses this section of the plateau is sourced at the Kikuyu escarpment and initially has a north-westerly flow in the trend of the Sattima. It changes direction at Mara Ngishu where it meets the Kinangop fault, and flows down smaller escarpments before flowing south through the Naivasha gorge where it tapers off and does not reach Lake Naivasha by surface drainage. There is a marked decrease in density of the drainage south of Karati and in the section of the Rift Valley occupied by the lakes and the central volcanoes. Around lakes Naivasha, Elmenteita and Nakuru, most of the drainage from the eastern and western escarpments, taper off before reaching the lakes. It is also observed that at Eburru, Kijabe, Longonot and Olkaria volcanoes, short streams form radial patterns around the volcanoes, but taper off at the foot of the volcanoes, never reaching the lakes by means of surface runoff. These morphotectonic controls on the drainage have some consequences (discussed earlier in Chapter 2 and in next Chapter 5) on the recharge of the geothermal reservoirs and the lakes. The section where there is a low density of drainage patterns is considered to be the axis of

the Rift Valley. The fault analysis show N-S oriented faults occupying these sections and perceived to be part of the post-0.3 Ma rift floor faulting.

4.2.2 Solai-Subukia Block

The Solai-Subukia Block lies in-between the Sattima-Mau Block and the Lake Bogoria Block, and is separated from the two blocks by the Kisanana-Chemasa-Emsoss fault, and the Menengai caldera-Bahati fracture zone respectively. The major fault trends in this block are on the main, N11°E. These faults die out in one direction or another, but in their northern extremities, extend onto the Laikipia plateau where they cut across the Marmanet fault (N30°W). The main Marmanet escarpment is steep and on average 500 m above the foot of the escarpment (1740 m a.s.l), reaching 2609 m a.s.l. (870 m above the rift floor) at Marmanet Hill. Three major faults, Iguamiti, South Ol Arabel and Ngusero, cut through the escarpment displacing it. These faults are thus considered to be of later tectonic age than the Marmanet. They are wavy and trend from near N-S to N11°E.

The trend on the Kisanana-Chemasa-Emsoss and the Lolderodo-Maryland-Chui vary from N11°E, N38°E and N30°W, marking three sections on the faults. The faults merge into the Marmanet fault on their approach to the Marmanet. Grimaud *et al.* (1994), have indicated that these faults form sigmoidal-shaped structures due to oblique, dextral shear along Lake Bogorja and Marmanet faults. A number of back-tilted sub-plateaus mark the Solai-Subukia Block. These are the Solai, Subukia, Iguamiti, and Ol Bolossat sub-plateaus that are bordered on their west by the Kisanana-Chemasa-Emsoss, Solai, Chui-Maryland-Lolderodo, and Ol Joro Orok faults, respectively.

Within the sub-plateaus on the block, numerous smaller faults, open gushes, and rhomb-shaped horst structures were present. The main faults die out laterally in one direction or another and show maximum displacement at their centres with a general decrease in elevation from south to north. Kisanana fault scarp, for example, is 1885 m a.s.l. at Kisanana Hill, but falls to 1787 m at Kamaech Hill and 1634 m at Sirken Hill on Emsoss escarpment. The foot of this escarpment is at 1620 m at Kisanana, falling to 1020 m at the foot of Emsoss

at Lake Bogoria area. Similarly, the Solai escarpment is 2173 m a.s.l. at Hamp Hill but falls to 1931 m at Solai Hill. Where the faults die out within the plateau, their trends are picked by other faults, leading to ramp-like structures arranged in *en échelon* patterns. Instead of the faults forming simple strike slip ramps, they show blocks between overlapping faults that are broken up and stepped down in other minor faults. The rhomb structures are morphotectonic features, representing the configuration of the fault movements and thus the E-W extensional forces operating on the blocks.

The drop in relief from south to north accounts for channelling of the drainage on the block, north into lakes Bogoria and Baringo (Lake Baringo is outside the study area). There is, however, a marked low density of drainage lines in the block, explained by sudden termination of the drainage at the open fault lines. The runoff drains through the open gushes to feed the underlying water table that recharges the geothermal reservoirs in the Olobanita Lake Bogoria area.

The Sattima fault dies out into the Marmanet forest at Nyahururu and re-emerges as Lariak escarpment east of Ol Arabel river. In the section of the Sattima-Lariak fault, between Nyahururu and Ol Ngarua, the fault is marked by a low ridge that is a trace of the Marmanet fault. Here it is offset by Ewaso Narok, South Ol Arabel, and Melwa faults and other smaller faults that trend N11°E. Thus, where the Sattima dies out, it is replaced by the Marmanet fault zone that is part of N60°W-N30°W oriented cross structure, cutting the earliest faults on the Solai-Subukia Block. The Marmanet fault shows complex displacements with two major "spoon" fault structures marked by Chui fault at Shamenek, and Emsoss fault at Murgor.

The "spoon-fault" structures show wavy concave features along the length of Chui-Maryland-Lolderodo and Emsoss-Chemasa-Kisanana faults. The faults show curved surfaces leading to convex structures. The Chui fault merges into the Marmanet (N30°), which further north, is offset and changes orientation to N60°W where it enters the Chesauilmet fracture zone. The Emsoss fault on the other hand merges into Lake Bogoria fault (N30°W), which further north also changes orientation to trend in the direction of Siracho (N60°W) fault. At Chesauilmet fracture area, several other faults loose form and are replaced by N-S trending eastern Laikipia border faults represented by Ngusero, Waseges and Sandai faults. The nature

of the detachment along the length of the Chui-Maryland-Lolderodo fault, may have hastened a landslide located at the foot of a section of its escarpment. The landslide is conspicuous on satellite imagery because of its mud-flow structure and form. The flow has been attributed to a large earthquake that occurred in January 6, 1928. As indicated by Girdler *et al.* (1969) and McCall (1967), the earthquake was of magnitude 7.0 on the Richter scale with its epicentre located at 00°20'N, 36°22'E, on the Laikipia escarpment. This earthquake also lead to an open fault structure, 2.4 m wide, reported by McCall (1967) as lying below the Marmanet fault at Subukia. Present tectonic activities are underlain by micro-earthquakes, associated with geothermal resources that can be located along the axis of the Rift Valley (Figure 4.7).

4.2.3 Lake Bogoria Block

Lake Bogoria Block is separated from Solai-Subukia Block by the Kisanana-Chemasa-Emsoss fault, that merges into Lake Bogoria fault along the Emsoss "spoon" fault structure at Sirken Hill. The Kamasia Range (foliation and fault orientation on the range are N-S) and the section of Mau fault at Londiani broadly border the block to the north and west, respectively. Within the study area, the block is, however, delimited to the north by the Loboi cross-structure (orientation N60°W-N30°W) and to the west by Kipngatip fault with a downthrow to the west (Plate 4.1 and Figure 4.8 and 4.9). The Kipngatip fault is one of the series of west-downthrown faults, of which the Molo fault, located further west, is the longest in the Lake Bogoria Block.

Interpretation established from satellite imagery and existing geological maps, as well as field studies, suggests rift offsets in the area, coinciding with the intersection of the Laikipia plateau faults with the Loboi-Siracho-Marmanet cross structures. This cross structure forms part of the Aswa fault zone. The offsets in the Rift Valley orientation also coincide with the junction of the Kavirondo rift, with an E-W to WSW orientation. The Kavirondo graben structure (located to the west of Lake Bogoria Block) is interpreted by Chorowicz *et al.* (1988) as a large tensional joint related to tectonism in Central Kenya Rift Valley.

Plate 4.1: Principal Component Analysis image of Lake Bogoria area, formed from a subset of sum average of TM bands 1,2,3 and bands 4,5,7, and displaying principal component bands 2,1,3 in RGB order. The yellow feature to the NW is the Loboi swamp and next to it is the sediment fan of Waseges as it enters the Loboi plain. Lake Bogoria escarpment is just to the east of the lake, while Marmanet escarpment can be located further east. Note the near N-S faults marking the Lake Bogoria Block to the west of the lake. The arrowed feature to the east of Emsoss escarpment is a rhomb-shaped horst resulting from interference between N-S and NW trending faults (refer to Plate 4.2 and Figure 4.10 for further interpretation using this feature).

Figure 4.8: Morphotectonic map of lake Bogoria showing the main structural trends and the drainage patterns. A detailed structural map is shown in Figure 4.9

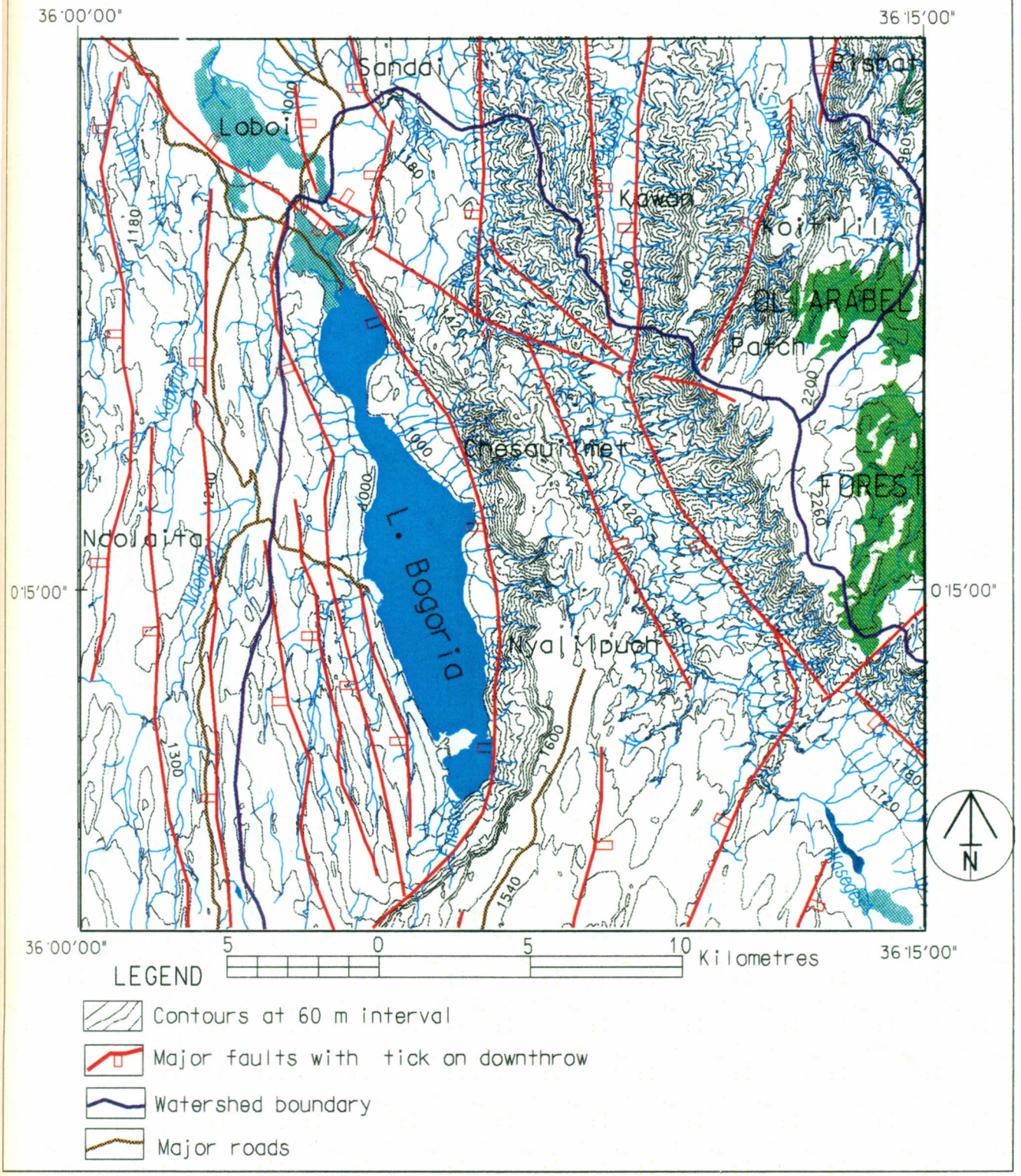

Figure 4.9: Structural tectonic map of lake Bogoria area. Refer to Figure 4.10 for a block diagram of the southern section of the area. A rose diagram of the fault azimuths west of the lake are shown in Figure 4.11.

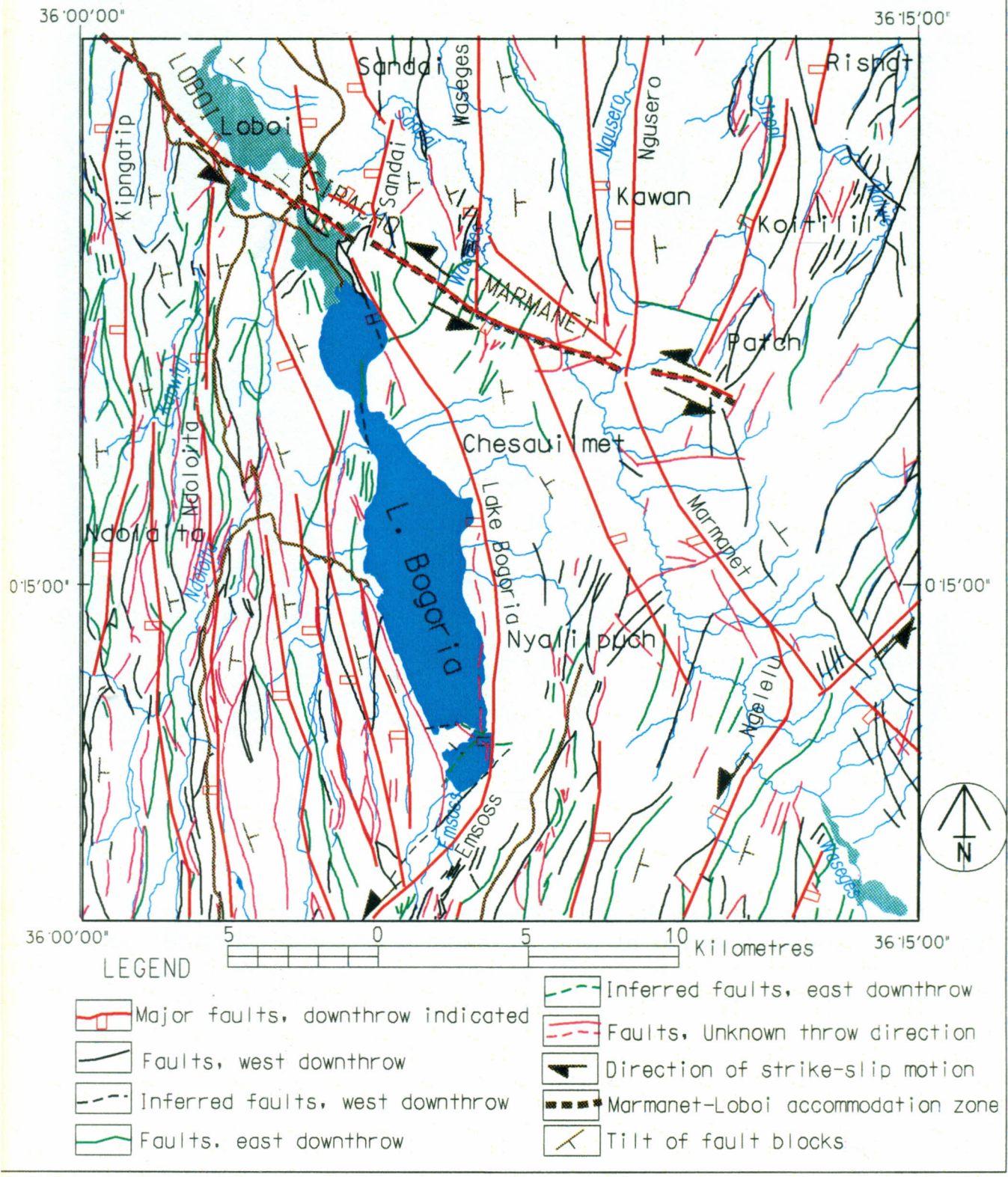

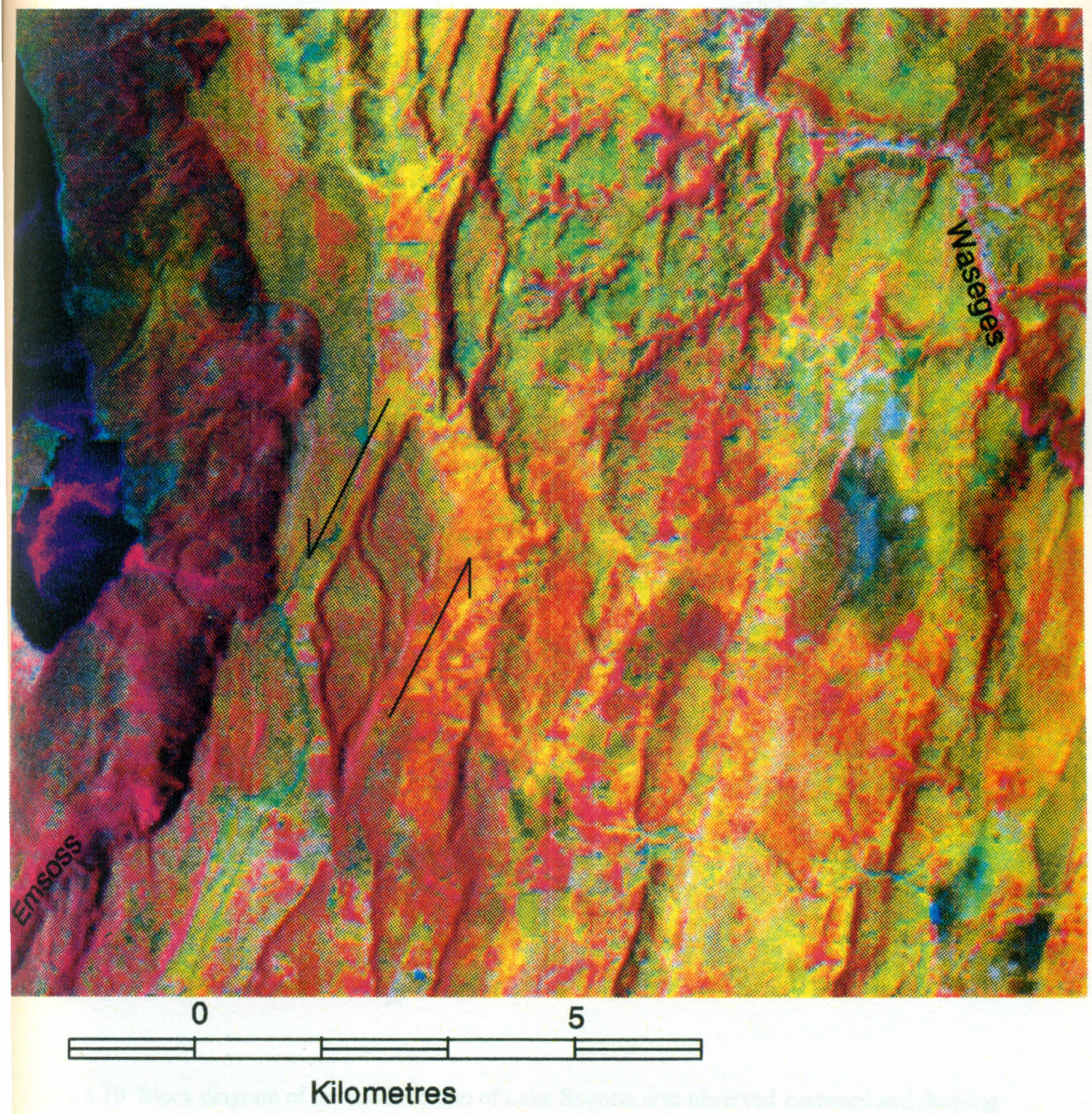

Plate 4.2: Principal Components Analysis image of south-eastern part of Lake Bogoria, showing a close-up view of a rhomb-shaped structure. Inferred relative motion of the fault blocks (Figure 4.10) on either side of the horst is shown by the arrows.

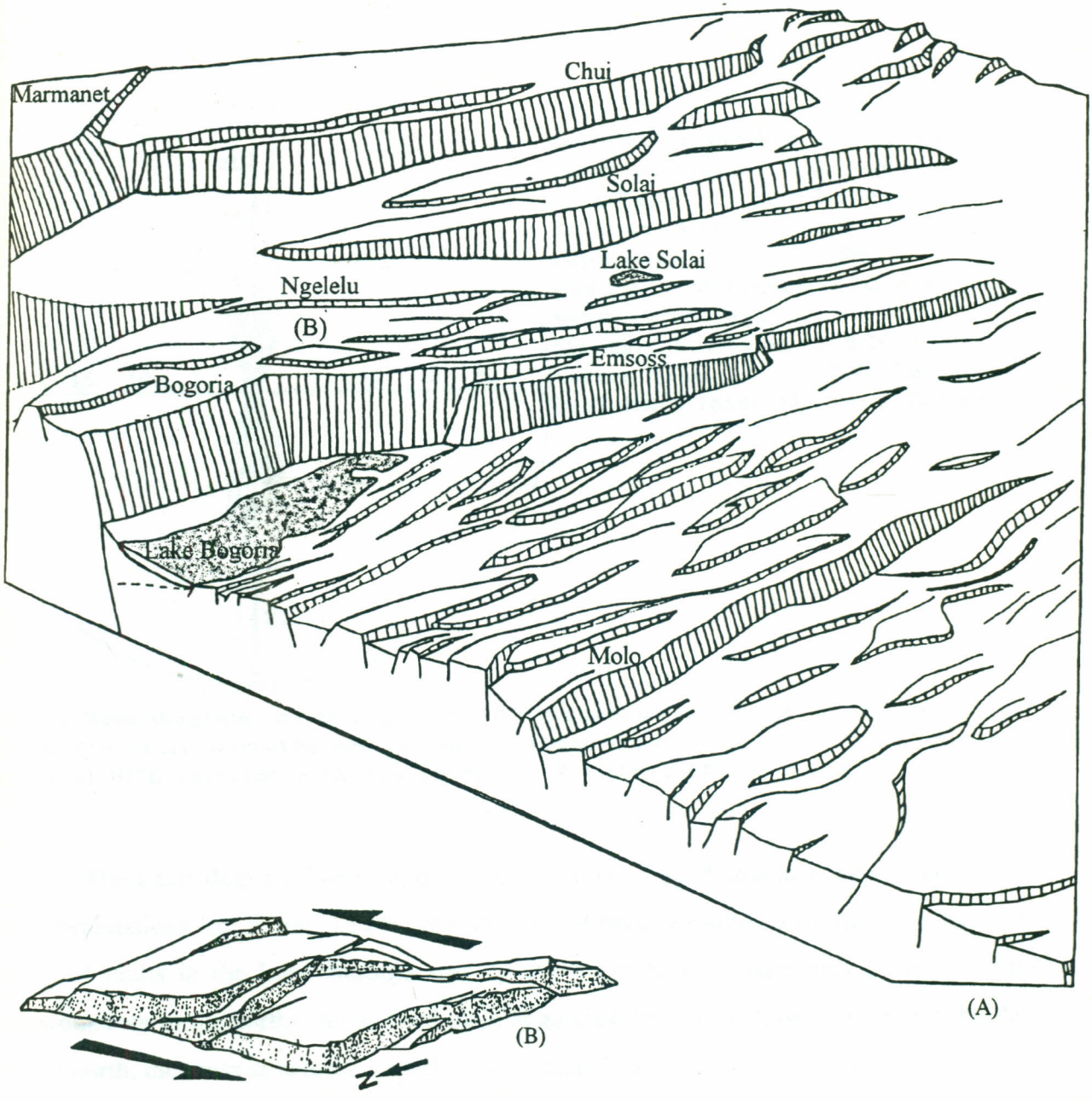

Figure 4.10: Block diagram of the southern part of Lake Bogoria area observed eastward and showing:

(A) Molo, Emsoss, Solai, and Chui strike or relay ramp structures *(modified from Grimaud et al., 1994).*

(B) Structural interpretation of the rhomb-shaped horst structure located west of Ngelelu ("B" on the block diagram) and identified in plate 4.2.

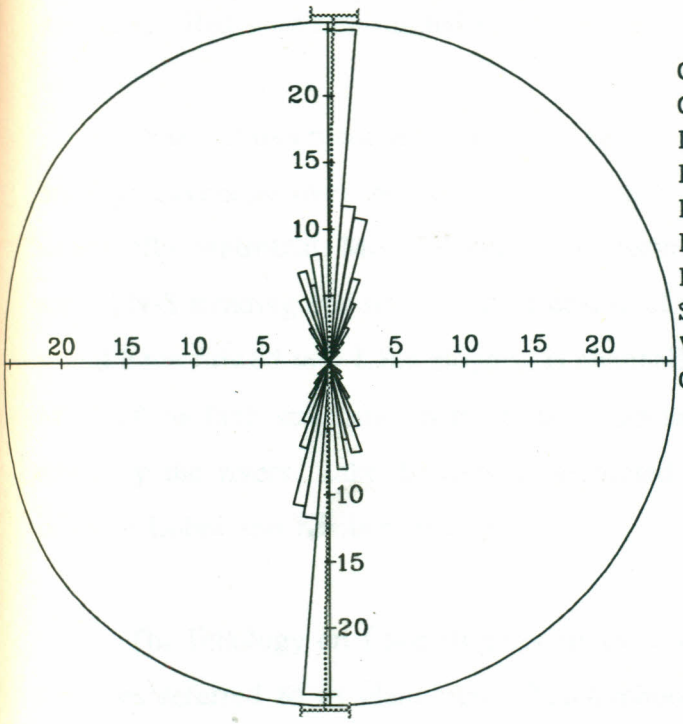

Calculation method ... Frequency
Class Interval .....5 Degrees
Data Type ..... Bidirectional
Rotation Amount ..... 0.0 Degrees
Population 288
Maximum Percentage . 23.6 %
Mean Percentage ..... 4.2 %
Standard Deviation .... 5.20 %
Vector Mean ..... 0.96 Degrees
Confidence Interval .... 4.12 Degrees.

gure 4.11: Rose diagram depicting azimuth frequencies of faults in the Lake Bogoria Block. The fault azimuths considered are those from west of the lake, and the vector mean of N1°E coincide with the percieved N-S trend of the faults in this block.

The Lake Bogoria Block appears as a "spoon" shaped structure, controlled by N0° fault orientations (see Figure 4.11 for rose diagram of fault azimuths) separated from similarly oriented faults in the Lake Baringo area by the Loboi-Siracho-Marmanet cross structures (downthrown to the north). An alluvial plain at an elevation of 1020 m at its highest borders to the north, the cross structures . A left lateral sinistral movement on the Lake Bogoria Block is interpreted, and is of later tectonic involvement than the faulting causing the Loboi cross structure. The block is bordered to the east by several step faults forming ramp structures (Figure 4.10) and belonging to the Laikipia, N-S border fault, north of Marmanet fault and the Sattima border fault, south of Marmanet.

At the foot of Lake Bogoria escarpment is the fault angled Lake Bogoria (Plate 4.1), discussed in chapter 5, that is elongate in the trend of the escarpment. The escarpment stands 600 m above the lake. To the west of the lake are faults that are some-what more pronounced and trending N-S. The block show antithetic tilt to the east. Rhomb-shaped structure forms

mark the block (plate 4.2), and are enhanced by smaller N60°W-N30°W and the N0° orientations. Sharp boundaries border the horsts (faulted lavas), enhanced by the graben structures filled with non-faulted Quaternary fluvial lacustrine sediments.

Observations made on satellite imagery (Plate 4.1) and the overlay of structural and drainage coverages over the image indicate that all the drainage in Lake Bogoria Block are structurally controlled. Most of them drain north along the narrow grabens between closely spaced N-S trending opposing faults. Because of the structural control, most of drainage that would have flowed into Lake Bogoria is channelled into Lake Baringo through Loboi plain. Many of the fault structures in the Loboi plain are obscured by lacustrine deposits brought down by the rivers. Lake Bogoria is separated from Lake Baringo by a low fault scarp between Loboi and Kisibor swamp.

The lithology on Lake Bogoria Block is mainly analcitic phonolites and porphyritic trachytes referred to as Hannington Trachyphonolites and dated 0.3 My by Griffiths and Gibson (1980). The terrain is covered by sparse vegetation of shrub, bush and occasional grass and reflect different permeability and texture that imparted to the image a green-grey to blue hue. The thin debris accumulation on the lithology represents *in-situ* soils. The area east of Kisanana-Chemasa-Emsoss fault scarp is underlain by porphyritic phonolite whose rock alteration and soil cover impart a brown hue to the image.

* * * *

CHAPTER 5

THE TECTONIC STRUCTURES, HYDROLOGIC REGIMES AND GEOTHERMAL RESOURCES OF THE ABERDARE DETACHMENT

5.0 INTRODUCTION

The Gregory Rift Valley in Kenya, as mentioned in the previous chapters, is divided into three tectonic terrains of contrasting age, size and type - the splay faulted northern depression of Baringo-Turkana basin; the southern depression of Magadi-Natron basin; and the step faulted central basin of Bogoria-Nakuru-Elmenteita-Naivasha. The Baringo-Turkana and Magadi-Natron basins are separated from one another by Bogoria-Nakuru-Elmenteita-Naivasha basin. E-W tensional movement along major, normal Rift Valley displacements have caused near N-S elongate block structures to be detached from the main bounding faults. All the basins are bordered by a major fault detachment on one side and a fault flexure on the other side. The major detachment block in Central Kenya Rift Valley is the Aberdare Detachment (Bosworth 1986a). This detachment is along the eastern border rift margin of Marmanet-Sattima-Kikuyu escarpment, and derives its name from the Aberdare Ranges, bordering the Sattima escarpment. The Baringo-Turkana and Magadi-Natron basins occupy the Elgeyo and Nguruman detachments respectively, and derive their names from Elgeyo and Nguruman fault scarps, bordering the detachments on the western side of the Rift Valley margin, and located outside the present study area. The main Rift Valley graben is thus asymmetrical and bordered by major normal faults on one side and fault flexures on the other side with interpreted rift axis biased towards the fault flexure, and showing a swing from the eastern side in the Elgeyo Detachment, to the western side in the Aberdare Detachment, and swinging again to the eastern side in the Nguruman Detachment.

The three detachments are separated, by zones of cross-structures, multi-fractures and displacements, representing accommodation zones of complex wrench and oblique slip faults (Chorowicz *et al.* 1987; Bosworth, 1986a). The wrench and oblique slip faults are associated with lateral offset on the main Rift Valley faults. Where the offsets occur on the Aberdare

Detachment, such as at Chesauilmet, Nyahururu and Kijabe (see Figure 4.7), all falling along Marmanet-Sattima-Kikuyu escarpments, there is a definite deflection in the sub-meridian course of the main rift. It is noted, for example, that the Kikuyu escarpment, oriented N-S, is offset at the Kijabe fracture zone and replaced to the north by Sattima escarpment, oriented N18°W. The Sattima is offset at Nyahururu and replaced to the north by Marmanet, trending N30°W. The junctions where there is a change in orientation of the fault scarps, appear to be the focus of intense tectonic activity evidenced by multi-direction trending faults and doming.

In the Aberdare Detachment, major fault structures are associated with large accumulations of pyroclastics and trachyte lavas, intercalated with tuffs and welded tuffs. As noted by Morley *et al.* (1990), the major faults in the detachment display large scale structural domains with a consistent structural style, controlled by the geometry of the interaction among those fault displacements showing more than 1000 m throw. The fault flexures, on the other hand, have isostatically uplifted footwalls giving monoclinal flexures on the western rift bounding Mau escarpment. Baker and Mitchell (1976) have indicated that the rift margin bounding faults form the earliest faults in Central Kenya Rift Valley, 1.9-1.4 Ma, or earlier. Basalts, underlying the plateau trachyte of the rift floor, are exposed at the Laikipia escarpment and, as suggested by Baker and Mitchell (1976), they were faulted before at least 1.4-0.8 Ma when the plateau trachytes were emplaced. The trachytes were subsequently also faulted. The original fault structures had a near N-S trend which in the study area is maintained east of Lake Bogoria and south-east of Longonot volcano. Subsequent faulting and tectonic structure have led to other trends in the fault systems. These faults are arranged in *en echélon* patterns giving rise to individual fault blocks, discussed in Chapter 4. In a large part of the rift floor along Mau escarpment, and at the Kinangop plateau at the foot of Sattima escarpment, and in the area between Olkaria-Longonot and Menengai crater, the earlier fault structures and lava flows are concealed by grey to white volcanic ashes and pyroclastics from the rift floor eruptive centres, leaving less than 10% rock exposures. These eruptive centres form an arc, defining the axis of the Rift Valley (see Figure 4.7 and 5.2). Some of the rift floor volcanic ashes and pyroclastics are consolidated or welded to tuff, but others are incoherent ashes and pumice.

5.1 THE RIFT VALLEY FLOOR AND ITS VOLCANIC CENTRES

The Rift Valley floor in the study area is diverse in its structure and topography, and is characterised by numerous volcanic cones, craters, hosts, grabens, and intervening plains. The volcanoes are of striking appearance and vary greatly in the nature of the rocks they are built of, ranging from volcanic ash, pyroclastic and trachyte built cones to obsidic and basaltic cones. Many of the volcanoes occur along major faults, occupying the arc of the Rift Valley axis in the Aberdare Detachment. Suswa Caldera, located just to the south of the study area, and Menengai crater (2278 m), are the largest of the volcanic centres, and are composed mainly of sodic and peralkaline trachytes. The other volcanoes include the basaltic and pyroclastic cinder cones of Elmenteita "Badlands" (highest peak at 2128 m a.s.l.); comenditic and rhyolitic Eburru volcanic vents (2820 m at Ol Doinyo Eburru); agglomeritic Crater Lake volcanic cones (2220 m, highest peak); comenditic, rhyolitic and obsidic Olkaria volcanic complexes (2434 m at Olkaria Hill); and isolated volcanic massif of Longonot (2777 m and of mainly trachytes); Kipipiri (3349 m and basaltic to phonolitic); Kijabe (2669 m and basaltic); and Margaret volcano (phonolitic to trachytic). These volcanic centres post-date the pre-0.3 Ma rift faulting, and have thus been active over the same period although varying in the length of time over which they have been active. Lavas from them have been intermittently erupted with ashes and pyroclastics.

5.1.1 Eburru Volcanic Complex

The Eburru volcanic massif forms a ridge against the Mau escarpment. The main volcanic complex is marked by centres of trachytic, rhyolitic, pumiceous and welded tuff that have been intermittently erupted. N-S oriented fault lines cut through the eastern parts of the volcanic complex. The fault lines were traced north into the basaltic cones and lava flows of Elmenteita "Badlands", and south through the Crater Lake volcanoes into Olkaria volcanic cones. The larger number of eruptions extruded along these N-S fault lines. The small ridges of coalescing pumice cones and vents of obsidian flows on the summit of Eburru and at the western flanks of the volcano (Photo 5.1) are, for example, traced along the fault lines (see Plate 5.1).

Photo 5.1: *A pumice cone erupted along the N-S trending faults east of Eburru.* The small escarpment on the left of the photograph, is a section of the low Gilgil escarpment, along which there has been extrusion of a number of small cinder cones. Because of their form and lack of vegetation on them, these cones were easily traced on the images.

Photo 5.2: *Ol' lolbutot lava flow at Olkaria geothermal field area.* The buildings in the middle section of the photograph are the Geothermal Production Station. The mass of rock behind the Station is the youngest lava flow in the area (Ol'lolbutot lava). Ol Njorowa Gorge can be located at the far left. The gorge was a Pleistocene outlet of Lake Naivasha. Fine ash deposits and pumiceous pyroclastics from Longonot had dammed the lake in the Pleistocene. The photo was taken facing west.

The earlier eruptions of the cinder cones of Elmenteita "Badlands" and those located at Olenguruoni area west of Olkaria, and at the Crater Lake, are composed of pyroclastic and were extruded and emplaced along the N-S fault lines. There is evidence of earlier basaltic eruptions and emplacement in Elmenteita "Badlands" area, following the emplacement and faulting of the plateau trachytes. The plateau trachytes and the faulting in them, as suggested by Thompson and Dodson (1963), and Sutherland (1974), are of Lower to Middle Pleistocene, at least 0.3 Ma. The authors also give details of the petrography and mineralogy of the Eburru rocks. The plateau trachytes form the oldest rocks in the Eburru area, and are only exposed at the Gilgil escarpment. There is field evidence of later tectonic movements along the Gilgil and the associated fault lines affecting the post-0.3 Ma emplaced basalts and pyroclastic cones of Elmenteita "Badlands", the Crater Lake area, and the Olenguruoni area. Since the Eburru lava flows abut against these pyroclastics and the cinder cones, they are of later extrusion and are thus much younger.

The youngest cones are a result of the latest upsurge of magma along the Rift Valley axis, leading to a phase of phreatomagmatic eruptions centred at Ol Doinyo Eburru, Olkaria, and Elmenteita "Badlands", probably causing the youngest eruptions on Menengai and Longonot. Many of the young lava cones are extruded along the fault lines, but they are not faulted, indicating absence of tectonic movements in the last 200 years or more, when they were emplaced. The rhyolite and obsidian flows of Ol Obonge at Eburru, and Ol'lolbutot (Photo 5.2) at Olkaria, are the most recent, dating less than 200 years. The extrusion of the youngest lavas was during a period of declining tectonic activity and mark the last major episode of magmatic upsurge in this part of the Rift Valley.

5.1.2 Longonot Volcano

Longonot crater is build of trachytes, pyroclastics and ashes, intermittently erupted and intercalated with one another. The earliest eruption from Longonot was probably basaltic and flowed north towards Lake Naivasha where traces of it can be seen. Trachyte lava extrusions have since been intermittently extruded with pyroclastics and ashes to build the present composite cone. The trachytes are confined to the vicinity of the volcano, with the longest

flow, the Black Reef, running south-east towards Kedong Valley, stopping just by Nairobi-Mau Narok road where it forms Mlima Panya. Kagasi (1983) indicates that Mlima Panya trachyte lava is dark grey, fine grained with greasy phenocrysts of alkali feldspars, and shows vesicles elongated in the flow direction. Thompson and Dodson (1963), Washbourne (1967), Scott (1980), and Scott and Bailey (1986), suggest that Longonot volcano has grown in stages, at least since Upper Pleistocene, with a pre-crater succession of trachyte and pyroclastics. The youngest Longonot lavas pre-date the latest ash producing event and post-date the crater collapse which was accompanied by pyroclastic eruption. The post-crater eruptions are trachytic and occur on the northern flank of the crater, and extruded from the Longonot parasitic cone. Another flow of a similar age is located on the south-western flank of the volcano. These younger post-crater flows lie on a linear feature interpreted as part of the N-S fault structures which are obscured by ash and pyroclastic eruptions from Longonot itself. The post-crater eruptive vents have left secondary lava cones with pit craters. The floor of the near-circular main crater is covered by trachyte boulder-breccia. The crater is elongate in east-west trend with a long axis diameter of about 7 km.

Stream gulleys cutting down the slope of Longonot have exposed sequences of layers of pyroclastics and ashes. The layers mark sequences of eruptive events, determined from the various colours of ashes and pyroclastics and varying in thickness from 7-10 m to a few millimetres and in most cases thinning out completely. In some parts, where the surfaces of the ashes, pyroclastics and palaeo-soils came into contact with lava flows, they are seen baked brown. From interpretations made using satellite imagery, and field checks, a pile of pyroclastics and ashes are deposited to the west of the Longonot volcano, adjacent to the Olkaria dome area. These have formed an arc-like structure that in recent studies by Clarke *et al.* (1990), has been referred to as Longonot outer caldera. However, other than the satellite image impression of an outer caldera, there is no field evidence to indicate caldera collapse that could have possibly generated the structure. Instead, the pile seems to form dune-like structures indicative of wind deposition, persistently to the west.

The bulk of the formations in a vast area around Longonot volcano are covered by grey to white pumiceous pyroclastics and ashes from Longonot. Torfeson (1987), notes that pumice beds believed to be originating from Longonot, are seen in the uppermost successions

on the northern flanks of earlier formed Suswa volcano, thinning uphill. Scott (1980) has also reported these ashes as forming the uppermost succession on the Mau escarpment to the west. Because of the ash and pyroclastic deposits, there are hardly any rocks or structures exposed in the featureless plain around Longonot volcano. In a few deep gulleys, however, recently excavated by accelerated erosion, pyroclastics are seen intercalated with palaeo-soils (Photo 5.3). The pyroclastics are unconsolidated, grey in colour with unsorted, sub-angular grains of various sizes. The exposures indicate intermediate periods of no volcanic activity, and therefore, weathering to form the palaeo-soils. Numerous weathered surfaces are traced, and although representing surfaces of unconformity, their inter-beddings are conformable to one another, indicating emplacement and deposition by wind in a quiet environment. Lacustrine sediments, probably representing Pleistocene lake deposits, cover the pyroclastics/palaeo-soils intercalations and these are in turn overlain by ashes that form the uppermost formations in the area. The ashes and dust are thus the most recent deposits and occupy much of the area around Longonot, extending eastward to Kedong Valley, and up Kinangop plateau.

At the plains, and very close to the volcano, are 5-10 m deep gulleys that have only developed since 1990, following opening up of the area to agricultural settlement in the mid-1980's. Most of the gulleys follow depressions that define near N-S fault patterns, buried under ashes and pyroclastics. Along the depressions the water quickly percolates or disappears into the ground through sinkholes. Due to undermining of the buried fault structures, they have in recent years been exposed, revealing structural elements that provide an idea of the underlying formations. One such undermined fault line (Photo 5.4) is located between Kijabe and Longonot, at Nguruine (Kwa Kihika) and is oriented in the trend of the Kikuyu escarpment, N-S.

The Nguruine fault structure is an open fault exposed for at least 1.5 km and located some 3 km to the north of Margaret volcano and directly extrapolated onto the line of the fault structures on Margaret volcano itself. Grey-white pumice and ashes are exposed on the eastern side of the open gush with the ashes overlying the pumice. On the western side of the gush wall, yellow-buff pumiceous tuff of unknown thickness is exposed (at least 10 m to the depth of the exposed surface in the fault gush). The yellow-buff tuff represents the fault displacements that are now buried under a blanket of pyroclastics and ashes from Longonot.

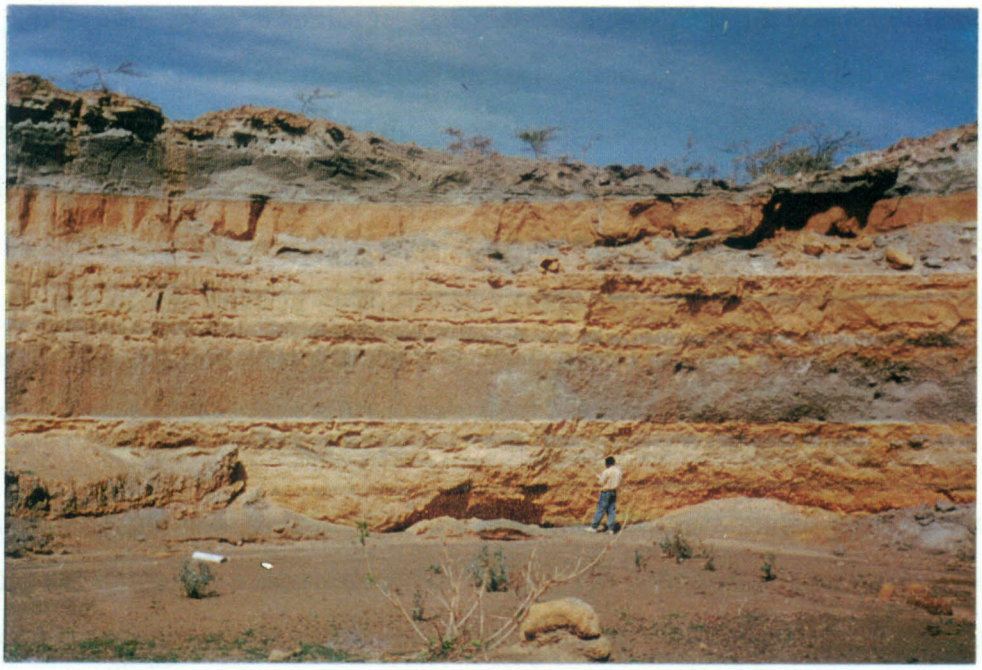

Photo 5.3: *A river section south of the Black Reef of Longonot Lava.* The section shows interbedding of palaeosoils-ash-pyroclastic-lacustrine deposits. The brown layers are the palaeosoils, the grey layers are mainly pyroclastics. The lacustrine sediments form the uppermost layer underlain by ash (burrowed).

Photo 5.4: *Trace of undermined Nguruine fault.* This fault line is located 10 km to the southeast of Longonot volcano extending for about 3 km. The fault is one of the many buried faults in the study area that are now being exposed by runoff which find its way underground through sink holes along the fault lines.

Since the eastern side of the gush-walls exposes no tuff, and the tuff is believed to be much older that the pumice and ashes (Thompson, 1964; and Kagasi, 1983), a down-throw of the fault to the east is implied. There are possibly other rock sequences overlying the yellow-buff tuff and laid down before the deposition of the Longonot pumice and ashes. At a river section near Mai Mahiu, for example, lacustrine sediments unconformably overly the yellow-buff tuff. Kagasi (1983) suggests that Kijabe basalts overlie the lacustrine sediments and the buff tuff, and post-date the major rift faulting episode that caused the step-fault topography on the eastern rift flank. He suggests that Margaret and Longonot eruptions occurred after the faulting and that Longonot eruptions are younger than Margaret ones.

The Nguruine fault gush structure lies in a shallow valley, draining the eastern slopes of Longonot and the south and western slopes of Kijabe. The runoff in this valley disappears through sinkholes developed along the valley. Other drainage lines also show no sustained water flow and any flow in them only occurs during periods of prolonged rainfall for a few hours following heavy downpour. Major rejuvenation of Nguruine gush followed the heavy rains of 1991, leading to the structure shown in Photo 5.4. The drainage lines that flow into this structure, drain to the south through a 2 m diameter hole at the southern end of the structure. The structure apparently controls the drainage towards Margaret volcano and into the Kedong Valley, never crossing to Lake Naivasha. Development of gush structures has increased in recent years especially in the northern parts of Kedong plain between Kijabe and Longonot, in Ndabibi plains, and at Kwa Rodha near Nakuru Town. These areas have recently opened to subsistence agriculture and associated urban development. The sudden agricultural activities have disturbed the delicate structure of pyroclastics and soils covering the fault structures in these areas. Although imposing environmental problems these settlements, are facilitating increasing awareness about hidden structure underlying the rift floor.

5.1.3 Margaret Volcano

Margaret volcano is a small central volcano of complex structure, just to the south east corner of the study area. The volcano stands 100 m above the rift floor, and from satellite imagery is seen as a ring structure forming a rim of an in-filled crater. The base of the

volcano is dominated by volcaniclastic rocks and welded tuff overlain by layered agglomeratic trachy-phonolites. Kagasi (1983) indicates that the volcano is composed of pyroclastics and tuffs. On the other hand, Torfeson (1987) suggests that the formations on the volcano are of four groups; feldspar-phyric ignimbrites, porphyritic phonolite, welded tuff and pyroclastics, all of local origin. To the south-west of the volcano, the welded tuff is quarried for building stone.

The formations on the volcano are densely faulted, with the faults cutting through the volcanic cone and displacing the various rock units. Kagasi (1983) points out that tectonic movements on these faults have caused the rocks in the Kedong Valley, to the south and north of Margaret, to be tilted by about 26°C to the south-west. This tilt, and the fact that the Nguruine fault is downthrown to the east, controls the drainage crossing in from the eastern bounding escarpment and direct it south to Kedong basin. Concentrated on the south-east lower slopes of the volcano, and lying along the fault structures, are hydrothermal alterations and steam fumaroles with temperatures close to 80°C. This is evidence of meteoric water flow underground from the north to the south, being heated by the still hot plug of the Margaret volcano. Some sulphur is seen as yellow coatings on the lavas and pyroclastics close to the steam vents, and is interpreted as resulting from sublimation of slightly sulphur-charged vapours.

5.1.4 Suswa Caldera

Suswa is a dormant caldera located south of the present study area, and mentioned here because of its association with the axial rift volcanoes and its possible connection with the drainage from the Olkaria and Eburru geothermal fields. Work related to the caldera has been reported by Nyamweru (1980). The volcano, as indicated by Nash *et al.* (1969) and Naylor (1972) started its activity 0.5 Ma ago, just as the grid faulting of the Rift Valley floor took place. After the main eruption and volcano-tectonic collapse, the central part subsided in stages at 0.24 Ma (Nyamweru, 1980), to form a caldera, now filled with lava of varying composition - obsidian, porphyritic phonolite, phonolite, some trachytes and ignimbrites. During the later period of subsidence, another caldera formed inside the older caldera,

terminating in a resurgent episode during which a block was uplifted in the central part (Photo 5.5) as a result of intrusion at depth. Johnson (1969) suggests that at Suswa volcano, the annular ring graben at the centre of the volcano is due to a third collapse formed after the pit crater collapse. The resurgent episode also culminated in eruption of Recent phonolite lava through fissures located on the south-east end of the volcano, leaving behind lava tubes.

At the foot of the volcano, the formations include tuff, pyroclastics, reworked volcanics and sub-aqueously deposited pyroclastics from Suswa volcano itself and from Longonot volcano. Rocks on Suswa caldera floor show an evolutionary trend with decreasing silica content, so that there is a gradual change from the original trachyte lava to phonolitic lava. This is attributed by Torfeson (1987), to magma differentiation.

5.2 THE CENTRAL RIFT VALLEY DRAINAGE SYSTEMS

The substrate in the Aberdare Detachment is composed of porous, permeable surfaces of volcanic ashes, pumiceous pyroclastics and faulted lava and tuff. Digitally treated images were instrumental in identifying enhanced features of some subtle zones, reflecting porosity, permeability and soil moisture of the substrates (Photo 5.6). The porous permeable surface provides for percolation of runoff, leading to potentially high groundwater storage. Likely areas where groundwater may concentrate was judged from the density of fracturing on the rocks, the substrate type, the size of the drainage basin and the proximity of the areas to the water catchment. One step in judging this was to delineate the drainage basin morphology by considering the texture of the drainage divides and the density of the drainage channels using the imagery. Landforms such as: the alluvial fans at Loboi, Akira and Ndabibi plains; interior drainage basins of lakes Bogoria, Nakuru, Elmenteita and Naivasha; swampy depressions of lakes Ol Bolossat, Solai, and Olobanita; volcanic centres of Menengai, Longonot, Kijabe, Il Kinangop, Kipipiri, Eburru and Olkaria; influenced the movement and the accumulation of surface and sub-surface waters and subsequently the process of interpretation. Vegetation is a useful indicator of hydrological regimes, with the riparian vegetation being used to delineate the drainage lines. Some sub-surface waters are determined from the presence of phreatophyte vegetation (Photo 5.6). Vegetation also gave an indication of the relative amounts of rainfall,

Photo 5.5: *The inner caldera of Suswa Volcano.* On the left of the photograph is the raised central block of the inner caldera floor, completely surrounded by a caldera wall, 60 m or more high, and marked by the depression in the middle of the photograph. At the background is the caldera wall of the outer caldera.

Photo 5.6: *A grove of phreatophyte vegetation of papyrus, indicating presence of sub-surface waters.* This type of vegetation contrasted on the imagery from the surrounding ground, and could be delineated, thus affording mapping of points of sub-surface water concentrations, using the imagery.

and thus the available recharge to the surface and sub-surface waters. These are inferred by considering the location and density of the vegetation, the elevation of the land, and the density of the drainage patterns. Satellite image interpretations provided a static view of the surface and sub-surface water containment, transitory corridors, and potential problem areas. The interpreted results are considered only qualitatively and are ranked into six categories:

(1) The open water systems of lakes Bogoria, Solai, Ol Bolossat, Nakuru, Elmenteita and Naivasha, seen as regulators of river discharge in the area. Lakes Ol Bolossat and Naivasha are a direct source of the water for domestic consumption. Interpretation of the extent of the water surfaces is made using standard FCC and black to dark blue colour hues for clear waters, and light blue to white for turbid waters. Aquatic vegetation in lakes Naivasha, Ol Bolossat, and Olobanita complicated easy recognition of the whole water bodies, because they imparted a green to red hue to the imagery. The vegetation concentrations show near circular features that defined points of water concentration in swamps and at the shores of these lakes. Most swamp vegetation is closely adjusted to micro-relief, and to the water quality, mainly growing in fresh waters. Identification of floristic composition of the phreatophyte vegetation is rather complex, giving varied patterns of red hues, noted at these lakes and at Loboi swamp, and along Ewaso Narok river.

A white hue is imparted by the sediment traps of lakes Solai and Olobanita, the graben depressions in Lake Bogoria Block, and other low sediment accumulational landforms such as at Loboi swamp. The shores of lakes Nakuru and Elmenteita (see Photo 5.9) also give a white hue that resulted in errors in delimiting the actual extent of the water bodies. These areas are complicated by variations in the rainfall patterns that varied with the season. During periods of prolonged dry spells, the lake levels are considerably reduced, sometimes leading to crystallization of alkali salts on the lakes, further complicating image interpretation using the white hues. Automatic recognition of the extent of the actual water surfaces using the dark, blue to white spectral reflectances may thus lead to interpretation errors.

(2) Highland deciduous forests and thick bushes are located at Mau, Kikuyu,

Sattima, Aberdare, Kipipiri, Marmanet, Bahati and Eburru (see Figure 5.1) (all areas above 2000 m a.s.l) and marked by high rainfall (1000 mm - 2000 mm annual average rainfall). These forest areas lie within the rift bounding escarpment, occurring at the plateaus immediately bordering the escarpments, and at the steep faces of the fault scarps or at the slopes of the volcanic massifs. Short fractures at the faces of the escarpments are marked by a high density of short drainage lines, these being areas of percolating runoff, falling down the escarpment. The presence of vegetation at the plateaus bordering the escarpments favour infiltration of runoff to recharge the water table that feeds the springs occurring at the foot of the escarpments. Thus the forested areas, when well watered, are outstanding catchment areas for water resource development at the foot of the escarpment. The spring sources at the foot of the escarpment can be located on satellite imagery by the presence of spots of dense red hue, in contrast to the blue/green to reddish brown hues of the rest of the escarpment. In the field, the spots of dense red hue were mapped as well-developed groves of "mukuyu" trees which confirmed the presence of springs and water points at these locations.

(3) The multi-direction trending fault structures in Menengai, Bahati, Chesauilmet and Kijabe areas are permeable landforms. At Menengai, the fault structures are ring or arcuate faults, within the caldera floor. At Bahati, Chesauilmet and Kijabe, the faults form radial domed structures, often covered by pyroclastics and ashes. These zones fall in areas of transfer fault structures or doming due to magmatic intrusion. Since these areas occur at the junction of the E-W cross structures, and the main rift escarpments, where there is a relatively high amount of rainfall (> 900 mm), they could be areas of recharge into the rift floor aquifers. The fracture zones are mapped on the imagery and are seen forming multi-direction fault structures (see Figure 4.7), unlike the rest of the Rift Valley, which show mainly N18°W to N13°E parallel fault structures.

(4) The plains around Longonot volcano (Ewaso Kedong and Akira), Lake Naivasha (Ndabibi), and Lake Nakuru (Kiwi and Kwa Rodha) are covered by pyroclastics and ashes. These plains show very low drainage density. At the approach

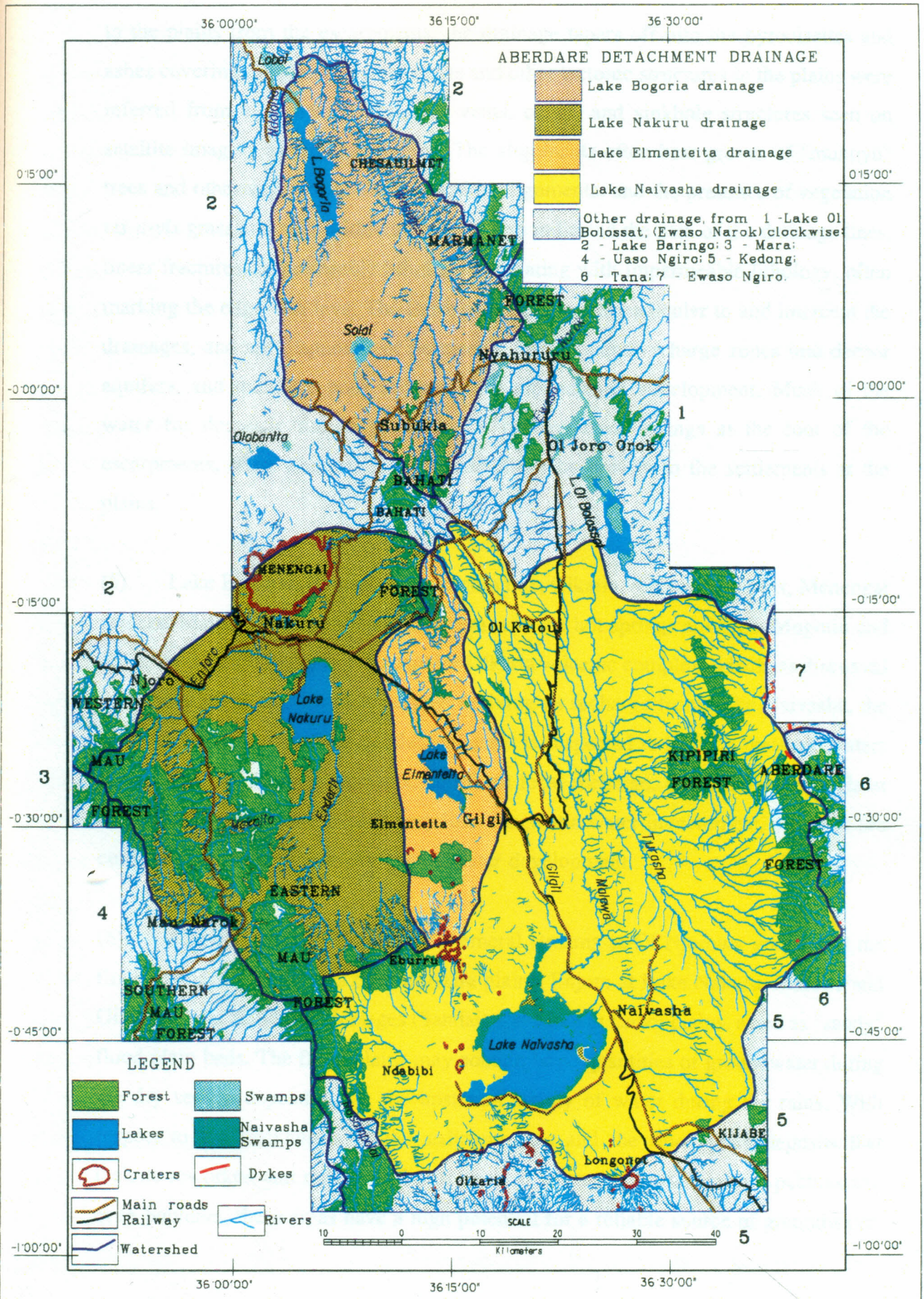

Figure 5.1: Drainage patterns and the extend of the watersheds in the Aberdare Detachment.

to the plains from the escarpments, the drainage tapers off into the pyroclastics and ashes covering the plains. Buried faults and other tectonic structures in the plains were inferred from alignment of volcanic vents, cones, and sinkhole structures seen on satellite imagery as aligned patterns. The alignments often bear groves of "mukuyu" trees and other vegetation. The vegetation alignments, and the presence of vegetation *vis-a-vis* grass and soils within the plains, also indicated the path of the drainage lines, linear fractures, or permeable lithology alternating with impermeable lithology, often marking the edge of a lava. The linear patterns run perpendicular to and intercept the drainages, and are diagnostic of permeable fractures and recharge zones into deeper aquifers, and therefore poor prospects for groundwater development. Much of the water for domestic use in the plains is derived from springs at the foot of the escarpments, from where it is piped and flows by gravity to the settlements at the plains.

(5) Lake Bogoria, Eburru volcanic complex, Olkaria volcanic complex, Menengai caldera, Margaret volcano, Suswa caldera, and the hot springs at Gilgil, Mogotio and Solai, have steam fumaroles. Except for Olkaria volcanic complex, which, as discussed in section 5.3 of this chapter, may be deriving its recharge from Lake Naivasha, the recharge into the rest of the geothermal areas is suspected to be from meteoric waters crossing in from the escarpments, and from local recharge. Since the water table at these areas is high, and there is very little magmatic water involvement, the areas are considered good prospects for groundwater development.

(6) Alluvial deposits along the ephemeral streams at Ol Njorowa gorge, and the flood plains of Ol Njorowa river at Akira plains, Enjoro at Lake Nakuru, Malewa and Gilgil at Lake Naivasha, Waseges (Sandai) and Molo at Loboi plains, acted as "sandy" flood plain beds. The flood plains may contain large quantities of groundwater during the dry season depending on the upstream supply of water during the rains. With respect to the thicknesses of the sediment fans and the flood plain deposits that include reworked and redeposited pyroclastics, volcanic "sands", gravel, pebbles and even boulders, these areas have a high potential for a reliable source of groundwater.

The drainage away from volcanic centres and the immediate faces of the fault scarps is mostly parallel to the fault structures. In most cases, they are small ephemeral streams that are nothing more than seasonal stream gullies, most of which have recently developed due to increased cultivation in the area. Climate and physiography have a strong control on the depositional and sedimentological patterns in the Rift Valley. The absence of any thicknesses of sediments in the Aberdare Detachment, away from the immediate lake environment, is indicative of a dry continental rift. Flexural isostatic uplift on the rift shoulders have had an important effect on the syn-rift sedimentation style. At Mau escarpment, for example, the uplift has created drainage barriers to large drainage systems like Amala and its tributaries, that could be draining into the rift floor but now drain south westerly into the Mara river drainage.

5.2.1 Structural Control on the Drainage Systems

Central Kenyan Rift Valley is marked by step-faulted platforms that are down-stepped towards the Rift floor axis and tilted away from the axis on either side of it. Towards the axis the faulting is intense and culminates in sub-parallel N-S elongate host and graben structures that are more conspicuous in the Lake Bogoria area than in Menengai-Olkaria area, where they have been buried under volcanics. The step-fault platforms appear as ramps formed by major faults arranged in *en echélon* patterns, such that the up-throw and down-throw sides are connected. These major faults branch and terminate within the rift floor. McCall (1967) portrays the rift floor fault systems as a series of anastomosing and bifurcating faults with short segment cross structures. The cross structures obliquely cut the main faults, separating them into isolated individual grabens and horsts that are characterized by antithetic tilt, giving slopes away from the axis of the Rift Valley, towards the west for the western rift margin escarpments and to the east for the eastern rift margin escarpments.

The major rift margin faults have surficial throws of more than 400 m, that have generated major tilted blocks, which, from the area around Menengai and Bahati, are uplifted more than those towards the north or south. Thus, there is a northerly and southerly tilt on the ramps from Menengai-Bahati area. These ramps, assisted by the northerly and southerly

tilts believed to be due to uplift and volcanism in the Central Rift Valley floor, serve to collect drainage from the marginal escarpments and channel it into the rift floor basins. The drainage from Bogoria, Kisanana-Chemasa-Emsoss, Chui-Maryland-Lolderodo, Solai, Subukia and Marmanet escarpments collects along the ramps into Lake Bogoria, north of the uplift. South of the uplift, the ramps collect the drainage from Bahati, Gilgil, southern parts of Kinangop and Sattima escarpments into Lake Naivasha or Lake Elmenteita. Lake Nakuru, however, is served by the Enjoro, Larmudiac, Makalia and Enderit that are channelled along and across step-faults on the Mau escarpment, most of them being diverted north, by the presence of Eburru complex (Figure 5.2).

The major ramp structures, however, direct the major drainage into the widely separated rift floor basins of Turkana and Natron, leaving the Aberdare Detachment lakes with little surface recharge. Uaso Ngiro and Siyapei rivers, for example, drain the Nguruman and part of Mau escarpments into Lake Natron, bypassing Lake Magadi located to the south of the study area. The Molo river drains parts of Mau escarpment into Lake Baringo, bypassing lakes Nakuru and Bogoria in the Central Rift Valley floor. The Kerio river, on the other hand, is assisted by ramps against the Elgeyo escarpment formed by Kamasia and Tugen hills, and flows north into Lake Turkana, instead of south into Lake Baringo or Lake Bogoria. These three drainage systems are the only major rivers draining a substantial area of the rift flanks and enter the rift floor. They do not, however, drain into the basins of the Aberdare Detachment. The three drainage systems also supply a substantial volume of sediments to the lake basins they recharge.

The Kinangop plateau of the Aberdare Detachment is tilted to the north-east, perhaps due to uplift at the Kijabe fracture. The drainage from its back-slope is influenced by this tilt and, for the larger part, flows north-westerly. At Malewa fault scarp, at the foot of which Malewa river flows, cross structures cause the rivers on the eastern part of the northern part of the fault, to be diverted and flow southerly. The fault structurally controls the drainage south of Menengai-Bahati uplift, into Lake Naivasha. The Malewa and its tributaries are channelled down the Bahati and Kinangop escarpments, bypassing Lake Elmenteita. North of the cross structures on the Kinangop plateau, just south of Lake Ol Bolossat, the drainage is the exception to the rift floor drainage which is internal into the Rift Valley. Here the

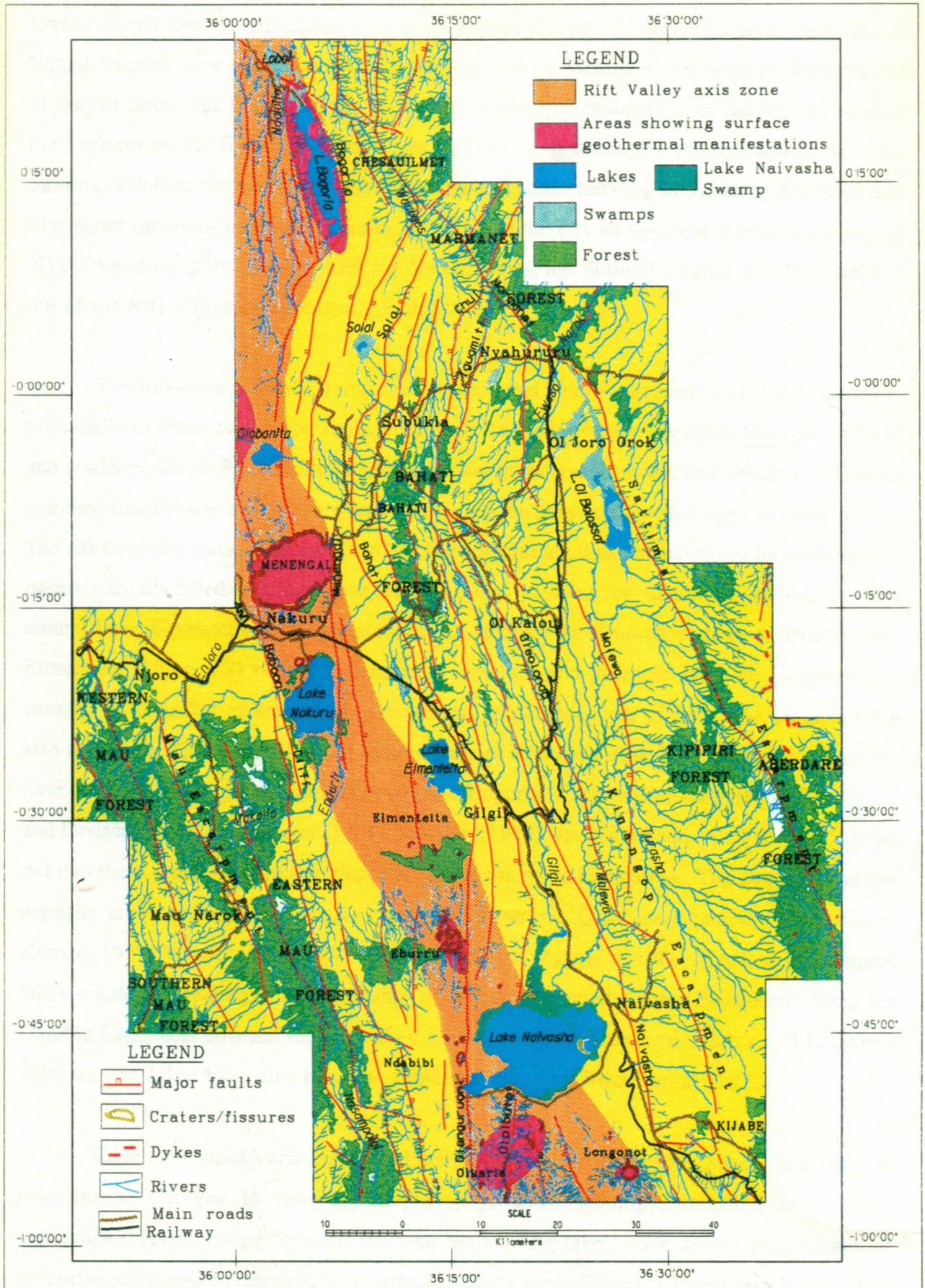

Figure 5.2: Drainage map of the Aberdare Detachment, showing the relationship between the major fault structures, and the drainage patterns. Note the low density of drainage patterns along the axis of the Rift Valley.

Ewaso Narok and its tributaries (also discussed in Chapter 2) drain the area north-east of Bahati fracture zone and Lake Ol Bolossat and part of Sattima escarpment at Olondoto out of the rift floor. The Ewaso Narok drainage is a result of channelling of the drainage due to the back-tilt on the Kinangop escarpment and the ramp structures. At Nyahururu, the main Sattima fault dies out and is replaced by traces of Lariak (trending in the same direction) and Marmanet (trending in N30°W) faults. At this area there is an apparent displacement due to N11°E trending faults, along which the Ewaso Narok has defined a valley in which it flows out of the Rift Valley at Thomson's Falls.

The influence of faults, ramps and caldera and cinder volcanism in the Rift Valley is principally to divert or dam the surface drainage. The voluminous volcanism from the calderas and cinder cones have tended to supply abundant pyroclastics, ashes, and volcanic sediments that now blanket the faulted topography, covering the horst-graben structures in many places. The rift floor depressions in the Aberdare Detachment are thus characterized by shallow lake basins, partially filled with lacustrine sediments that include a few diatomaceous beds exposed around Lake Elmenteita, at Soysambu and Kariandus. The diatomaceous earth around Lake Elmenteita (Photo 5.8) occurs in lenses, in clay, silt and volcanic ash and, in places, are covered in a blanket of ashes and pyroclastics. Some exposures of lacustrine sediments are also seen at the Kedong Valley, the eastern parts of Ndabibi plains, Kiwi plains and along the river channels of the graben structures of Lake Bogoria Block. Nyamweru (1977), Thompson and Dodson (1963), Thompson (1964), Johnson (1969), and Baker and Mitchell (1976) point out that these sediments are thin deposits laid down in the Pleistocene. The larger part of the deposits are volcaniclastic materials deposited after the Quaternary period (Washbourne-Kamau, 1971; Washbourne, 1967). The authors also suggest that the Aberdare Detachment lakes south of Menengai, are remnants of a formerly much larger Pleistocene lake, the Gamble Lake, that covered the rift valley section between Menengai caldera and Longonot volcano. The lakes have also been the subject of study by Butzer *et al.* (1972).

There is a rapid variation of sediment types in the Aberdare Detachment lakes in response to changes in lithology, topography, and hydrology, resulting in complex stratigraphic relationships between the lake basins. The lakes, have a very poor supply of lacustrine sediments in response to the small drainage areas (Figure 5.1) and very low rainfall.

The main graben or half-graben lakes in the Aberdare Detachment area are the closed basins of lakes Bogoria, Solai, Nakuru and Elmenteita. These lakes contain highly saline waters, attributed to solution of peralkaline and natro-carbonate rich volcanic ashes, and recirculation of alkaline groundwater by hot springs. Because of very high evaporation rates and recrystallization of alkaline salts in the basins, there is deposition of salt-impregnated sediments at the lakes, and this complicates stratigraphic relations among the basins. The exceptions to the salinity of the Rift Valley lakes are the more open water systems of lakes Ol Bolossat, discussed in Chapter 2, and Lake Naivasha, and the much smaller Lake Olobanita. Lake Naivasha receive drainage from a relatively large area compared to other lakes in the Aberdare Detachment.

5.2.2 Lake Naivasha (1885 m a.s.l)

Lake Naivasha (1889.3 m a.s.l - 1983 level: Ase *et al.* (1986)) - Plate 5.1, is located in a trough between Eburru and Olkaria/Longonot volcanic massifs. The lake is at the highest part of the Rift Valley floor, from where the floor slopes to the south and north, attaining very low altitudes at lakes Magadi (600 m a.s.l) to the south, and Bogoria (985 m a.s.l) to the north. The Naivasha basin is separated from Elmenteita basin by Eburru volcanics and a very low divide, 2000 m a.s.l, formed by the Gilgil escarpment (Figure 5.3). The lake is flanked by the high escarpments of Mau and Kinangop on the west and east respectively. These escarpments, together with Eburru, receive ample rainfall and form the main catchment areas considered by Clarke *et al.* (1990) as groundwater highs for Lake Naivasha. As seen in Figure 5.1 and 5.2, the principal surface influx to the lake is from the north, down Bahati and Kinangop escarpments, and covers an area of 3319.9 km^2. The runoff from Bahati escarpment is channelled through the Karindo, Murindati and Little Gilgil, tributaries of the Gilgil; whereas that from Kinangop escarpment is channelled through Muruaki, Engare Mugutyu, Kitiri, Makungi and Turasha, tributaries of the Malewa. Malewa is the only perennial river recharging the lake. Gilgil river on the other hand is the only other river reaching the lake by means of surface discharge, but this river, in exceptional periods of prolonged drought, becomes ephemeral at its approach to the lake. The rest of the drainages from Bahati, Kinangop and Mau escarpments, and Eburru, Longonot, and Olkaria volcanic centres do not

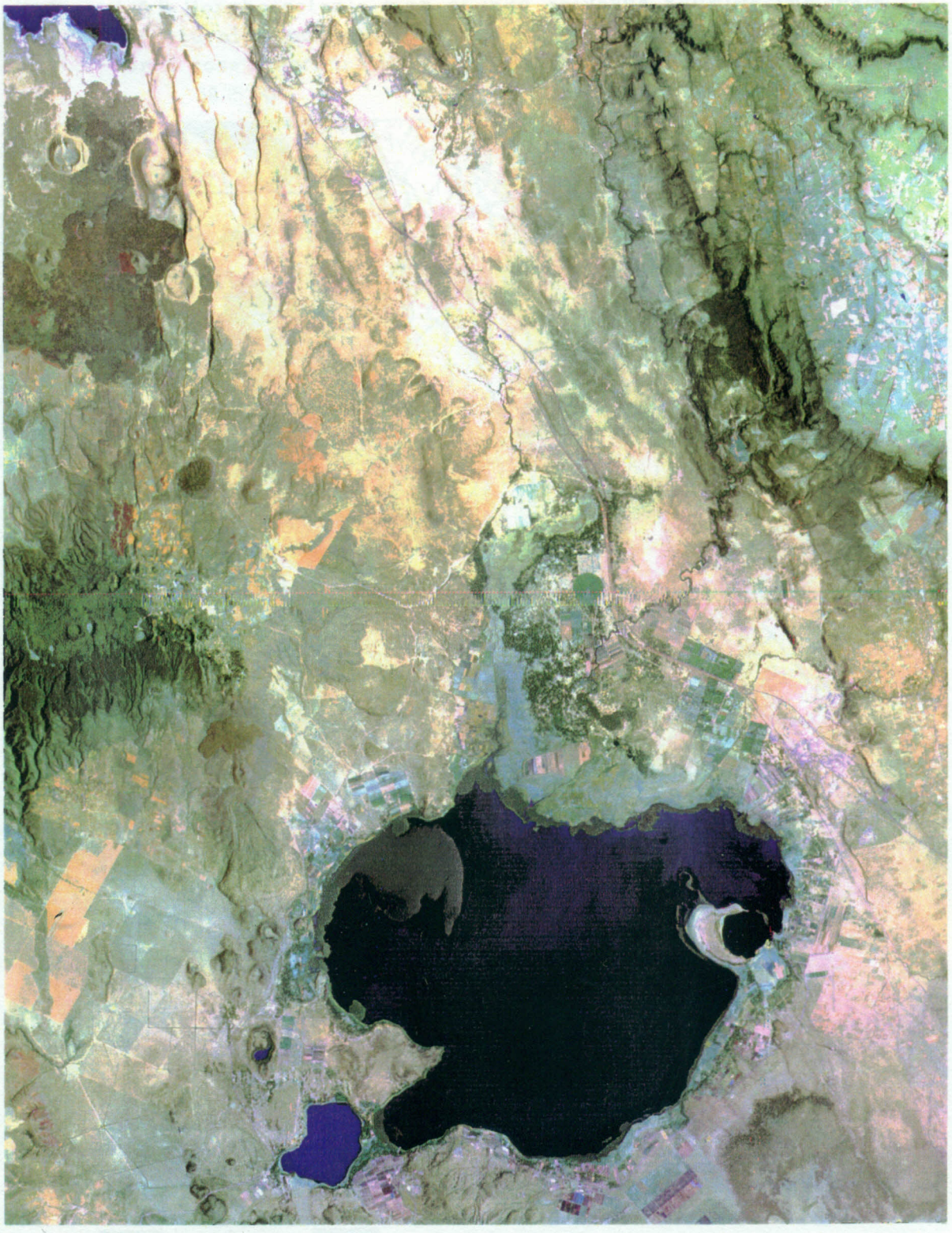

Plate 5.1: FCC of Lake Naivasha area, formed by registering Landsat-5 TM (1/3/1989) bands 5,1,7 in RGB order. Note the water hyacinth and *salvina molesta*, around the fringes of the lake, and a large part of the north west of the lake. Note also the line of volcanic centres on the western part of the area. Refer to Figure 5.3 for morphostructural interpretation.

Figure 5.3 Morphotectonic map of lake Naivasha, showing the main structural trends and the drainage patterns. Refer to Figure 5.4 for a rose diagram of the fault azimuths

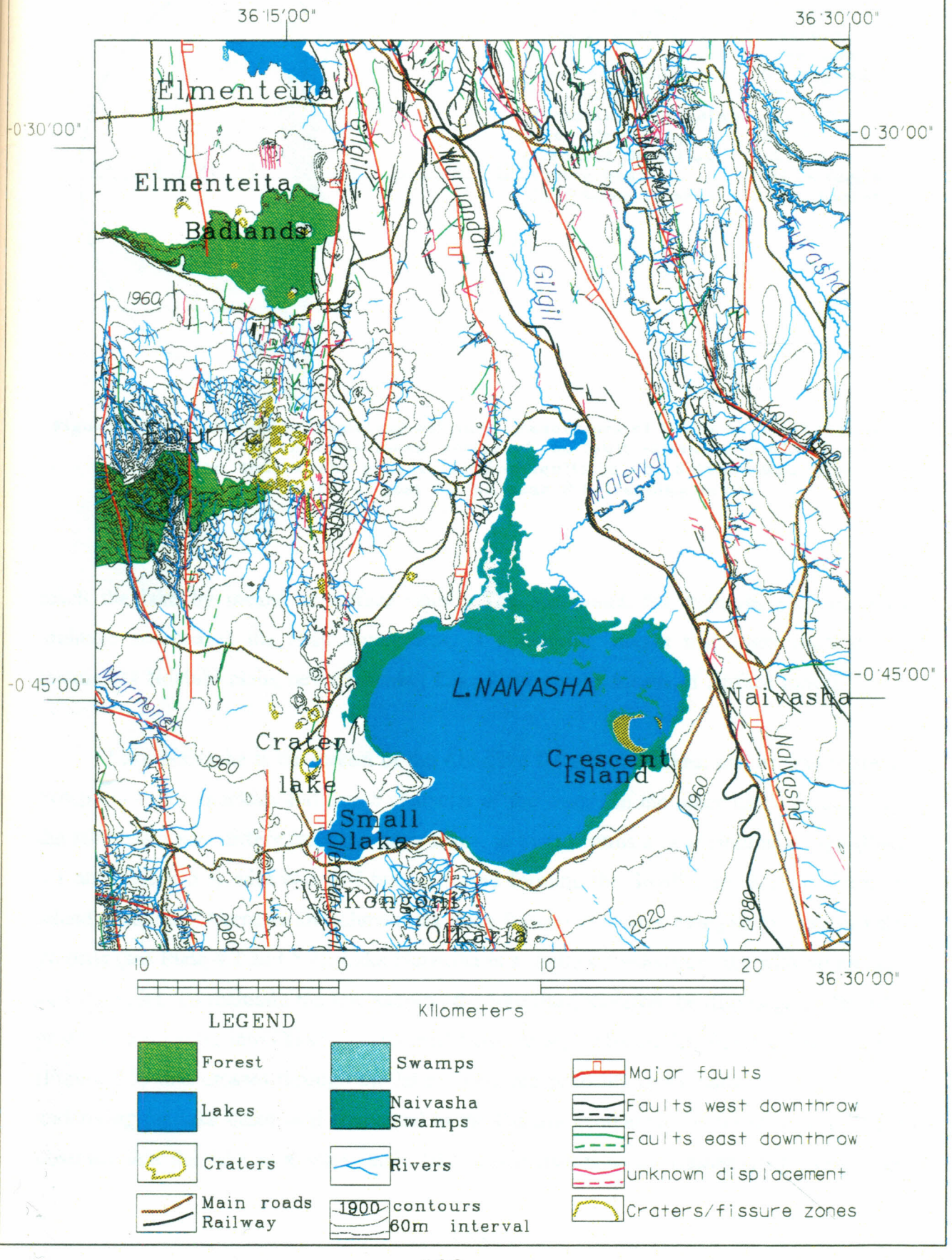

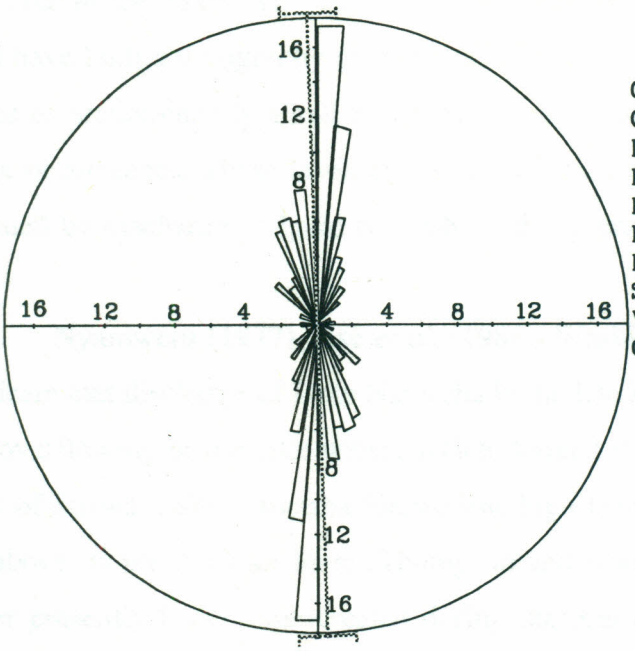

Calculation Method ... Frequency
Class Interval ..... 5 Degrees
Data Type ..... Bidirectional
Rotation Amount ..... 0.0 Degrees
Population 426
Maximum Percentage .. 16.0 %
Mean Percentage ..... 2.8 %
Standard Deviation ..... 3.25 %
Vector Mean ..... 358.19 degrees
Confidence interval ..... 5.56 Degrees

Figure 5.4: Rose diagram depicting azimuth frequencies of faults in the Lake Naivasha area. Note that the mean vector of the fault azimuths is N1.8°W and differ from that of the general trend of faults in the Sattima-Mau Block due to the contribution of post 0.3 Ma, near N-S trending faults.

reach the lake by means of surface runoff. The Marmonet, for example, with its main drainage sourced at the Mau escarpment, is a tapering stream that loses itself in the featureless Ndabibi plain, never reaching Lake Naivasha by means of surface runoff.

Lake Naivasha is the largest of the Aberdare Detachment lakes, and its waters are an exception to the brackish and saline character of the waters in the other lakes. Structurally, the lake basin also differs from the other lakes, in that it forms a near circular trough (Plate 5.1 and Figure 5.3) with two half buried craters forming the Small Lake and the Crescent Island. The other Aberdare Detachment lakes are formed in narrow elongate grabens or half-grabens (see Plate 4.1 and 5.2). Lake Naivasha is a shallow freshwater lake with no modern surface outlet. To maintain the low salinity, the lake must therefore be discharging. The lake probably discharges into Olkaria geothermal field, through Muruandati-Baxia-Ololbutot fault (Figure 5.3) that crosses through the lake. There are probably other buried fault structures underlying the lake basin, and connected to the Olkaria geothermal reservoir. Baker (1986) observes that the lake is a water table lake which maintains its freshness by sub-surface

discharge into permeable pyroclastics of Longonot and Olkaria volcanics that have dammed the lake to the south. The volcanics have been erupted intermittently since the Pleistocene, and have built a topography characterized by ash/pyroclastic domes (Plate 5.1) and acid lava piles of predominantly alkali-rhyolites (comendites) with some peralkaline and intermediate rock occurrences. These lavas and ashes are well exposed in Ol Njorowa gorge which was created by discharge of Lake Naivasha, subsequent to its initial damming.

Nyamweru (1977), Ase *et al.* (1986), Washbourne-Kamau (1971) and Kamau (1974) indicate that discharge of Lake Naivasha in the late Pleistocene was through the gorge created by overflowing of the lake waters which drained towards the Kedong Valley through north-east of Suswa. Lake Naivasha Pleistocene high levels is predicted to have been at about 120 m above its present lake level (Thompson and Dodson, 1963). The gorge in which Kedong river presently flows, was created during the draining of the lake. Presently, water-created channel sections seen north-east of Suswa, east of Longonot, and in the Akira plain (south of Longonot) reveal evidence of flooding during the draining of Lake Naivasha. In these sections, lacustrine sediments are seen overlying earlier erupted pyroclastics. Subsequent eruptions from Longonot overly these lacustrine sediments. The earlier channels are buried under these later pyroclastics, and other than at the Ol Njorowa gorge and at Kedong Valley, are not easily traced. The draining of Lake Naivasha is thus an older process than the latest ash-producing Longonot eruptions. Scott (1980) indicates that most of the ashes and pyroclastics from Longonot post-date the draining of Lake Naivasha, suggested to have last occurred at 12000-5600 B.P. Richardson and Richardson (1972) and Kamau (1974) also give the same dates for the draining of the lake, and suggest that after the creation of the gorge, its channels south of the gorge were re-filled by tephra from eruptions of Longonot and perhaps Suswa after 5600 B.P.

The lake has had a history of fluctuations which have been recorded since 1860 (Richardson, 1966). In general, as indicated by Richardson and Richardson (1972), there has been an overall fall in the water level since 1917. The annual rainfall and evaporation figures from meteorological station around the lake, although fluctuating over the years and showing significantly low volumes in the ten year drought cycle, reveal no overall decrease or increase in precipitation. Yet, in recent years the lake has shown significant drops during prolonged

droughts, especially in the year immediately following the ten year drought cycle of 1965, 1976, 1984 and 1993, when most rainfall stations in the study area recorded less than 700 mm of total annual rainfall. In 1994, for example, following the drought of 1993, there was a significant drop in the lake levels of all Aberdare Detachment lakes, except Lake Bogoria. In this period, large sections of Lake Naivasha lake bed were exposed, with the resulting changes causing significant ecological imbalance in the lake and affecting the fishing industry. In this period, the entire crater rim of the Crescent Island, whose eastern section is always under water, was exposed.

Short term lake level fluctuations are thus a response to severe climatic fluctuations, ecological changes and demographic activities affecting evapotranspiration and surface discharge into the lake. Direct evaporation from the lake is also high, with significant increases during the dry season. The lake, over the years, has supported a thriving vegetation of fever acacia (Naivasha thorn - *Acacia xanthophloea*) and papyrus, protecting the lake from evapotranspiration. This vegetation cover now consists of no more than isolated groves of fever acacia, and patches of papyrus at the lake shore. Increased land use in the catchment areas, significant direct water consumption from the lake for irrigation, and damming of Turasha river to serve Nakuru Town, may also be contributing significantly to the overall water balance in the lake with a net deficit during prolonged droughts. The fresh waters of the lake support an increasing horticultural industry on the banks of the lake. This may also be providing mineral rich leachates into the lake from fertilizer applications. The lake currently supports a thriving water hyacinth (see Plate 5.1 and Figure 5.3) as a result of the leachates. A fresh water weed, *Salvina molesta*, is also seen floating on the lake, occurring in large concentrations at the lake-shores along with the water hyacinth, both of which increase evapotranspiration from the lake.

Other than the climatic changes and land use/land cover changes affecting Lake Naivasha, the cause of the water level changes in the lake is also of geological interest. The Lake Naivasha level changes are perhaps also activated by poor land use and exploitation of the Olkaria geothermal field. In the Ndabibi plain, bordering the lake to the west, and on the slopes of Mau escarpment, rich volcanic soils are cultivated for wheat, maize and used for grazing, leading to disturbance of the soil structure. These soils are formed on a blanket of

pyroclastics and ashes covering buried faults discussed in section 5.1.2 for the area around Longonot. The land use activities, apart from increasingly exposing the soil to wind erosion have in recent years resulted in accelerated erosion from surface runoff, most of which follow depressions along the buried faults. In places, pools of runoff water develop along depressions on the fault line, with the resulting weight causing the soils to sink into the underlying gushes, thus leading to development of sinkhole structures along, the fault line. Subsequent runoff is under, and along these exposed gushes. Many of the streams draining the steep Mau escarpment have cut deep, steep-walled gorges several tens of metres deep. These runoff from the Mau escarpment immediately percolate into pyroclastics and ashes at the Ndabibi plain where also the drainage lines terminate at the fault lines. Because of the sudden lowering of water-head at the sinkholes, there is accelerated erosion leading to deeper cutting into the face of the escarpment. The drainage off Mau escarpment thus terminate at the fault lines on the Ndabibi plain and probably flows along the fault structures, either south into the Suswa geothermal reservoir or north into the nearby Eburru geothermal reservoir.

Within the Eburru geothermal reservoir, and along the fissures on the eastern parts of Eburru volcanic centres, there are a number of steam fumaroles. The absence of hydrogen sulphide and other magmatic gases in solution in these steam fumaroles point to steam sources from sub-terranian levels and recharge from meteoric waters. This supports the view that percolation of runoff from Eburru volcanic complex, and the Mau escarpment are the recharge waters into the underlying thermal sources at Eburru. Meteoric waters from Mau escarpment may not be crossing into Lake Naivasha or Olkaria reservoir beyond the west downthrown Gilgil-Ol Obonge-Olenguruoni-Lolonita-Loirogwe major fault structure, along which are aligned recent volcanic centres (see Plate 5.1 and Figure 5.3). The aligned sinkholes in the Ndabibi plain, west of this major fault structure, also point to buried faults that are structural barriers to groundwater that could be flowing into Lake Naivasha. These buried fault structures on the main belong to the post 0.3 Ma fault system, giving a fault azimuth vector mean of N1.8°W (Figure 5.4) and may be acting as conduits, structurally controlling the groundwater flow in a direction parallel to the fault lines. At depth, and underlying Suswa and Eburru, are hydrothermal convective cells which draw sub-terranian water, heating it and forcing it up to the surface where it is manifested as steam fumaroles.

5.2.3 Crater Lake

West of Lake Naivasha is the Crater Lake occurring in a small water-filled crater (Photo 5.7) just 15 m above the level of Lake Naivasha. Being in a confined crater, the lake has no surface recharge, other than that from direct rainfall. Its waters are green, algae rich, with its volume slightly fluctuating with the seasons. The water is relatively deep and confined by underlying non-porous agglomeratics rock. The main mass of the crater is agglomeratic, composed of welded pyroclastic with large clasts of comendite, basalt, and obsidian, probably broken from the plug that initially blocked the crater vent. The crater is faulted on its eastern side with the down-throw to the east. On satellite imagery (Plate 5.1), another major fault is observed forming the Gilgil-Ol Obonge-Olenguruoni-Lolonita-Loirogwe fault structure, a linear feature traced south to the escarpment at Kongoni, and into Olkaria Hill. To the east of the lake and close to the shores of Lake Naivasha are other fault scarps forming a couple of low raised blocks. The Small Lake, south-west of Lake Naivasha, is formed in a graben between these blocks. The fault lines are pointers to possible tectonic involvement through the fault structures, and to connection of discharge of the Small Lake and Lake Naivasha into Olkaria reservoir. Presently, the Small Lake is completely cut off from the main lake.

5.2.4 Lake Elmenteita (1776 m a.s.l)

Lake Elmenteita is a closed basin situated in a complex fault bound trough (Plate 5.2 and Figure 5.4). To the east of the trough is the low west downthrown Gilgil escarpment; which separates this lake from Lake Naivasha. To the west are a series of smaller east downthrown fault scarps of which the Lion Hill is the largest and separates the lake from Lake Nakuru. To the south are the Eburru volcanics and a number of striking faulted pyroclastic cones and very recent basaltic flows and cones forming the Elmenteita "badlands". Some of these cones lie on Gilgil-Ol Obonge-Olenguruoni-Lolonita-Loirogwe fault line.

Photo 5.7: *Crater Lake, at Crater Lake volcano, Naivasha.* This lake is saddled in a crater, very close to the southwestern shore of Lake Naivasha and lies 15 m above Lake Naivasha. The walls of the crater and the vegetation protect it from evaporation. A dense algae growth gives the lake a green colour.

Photo 5.8: *Kariandus diatomaceous deposit.* The open cast mine reveal the thickness of the diatomaceous earth deposits in the Elmenteita Pleistocene lake basin. Also exposed is a buried river channel defined by the V-shape valley. The deposits here, indicate a turbulent water laid sediment deposition.

The lake owes its existence to surface influx and springs from Bahati step-fault ramp with increments from Meroronyi, Mbaruk and Kariandus rivers and, as seen in Figure 5.1, these rivers drain a very small catchment area (499.5 sq.km). The rivers are fed by warm springs recharged by waters percolating in from the Bahati and Gilgil escarpments. The rivers show a considerable decrease in their volume downstream, due to losses underground through the fault lines along which they flow, and only the Kariandus river recharges the lake all year round. The lake water is highly saline due to high rates of evaporation, insufficient recharge, and concentration of alkali salt solutions brought in by the warm springs.

Around the lake are diatomaceous deposits (Photo 5.8) dated at 0.4 Ma (Thompson and Dodson, 1963) and exposed due to faulting which must have occurred after their deposition. The diatomite deposits are mined at Kariandus on the eastern side of the lake and at Soysambu to the south-western side. Presently the lake is floored by rather coarse, salt impregnated sediments. On the imagery, this lake contrasts from the other lakes because of silting, possibly resulting from increased sediment load due to erosion of the poorly consolidated soils around the lake. These soils are now increasingly exposed by agricultural activities around the lake, since mid-1980's when the area opened for agricultural settlements. During the rainy period preceding the 1993/1994 dry spell, for example, large volumes of soil and debris were washed into the lake. In this dry period, and in the 1984/85 drought, the lake also showed considerable decrease in its volume (Photo 5.9), and actually dried up in the month of February, 1985.

5.2.5 Lake Nakuru (1758 m a.s.l)

Lake Nakuru lies in a graben between Lion Hill fracture zone in the east and a series of east downthrown step-fault scarps leading to the Mau escarpment to the west (Plate 5.2 and Figure 5.5). The lake is elongate in the N-S direction in the trend of the axial rift faults (Figure 5.5) and dammed to its north by Menengai caldera. It is a shallow soda lake, rich in algae, and has in the recent past, attracted millions of flamingos, for which the lake is famous. These flamingoes, however, have now migrated to other lakes because of the frequent drying up of the lake in the past few years. In the February-April 1994 period, for example, the lake

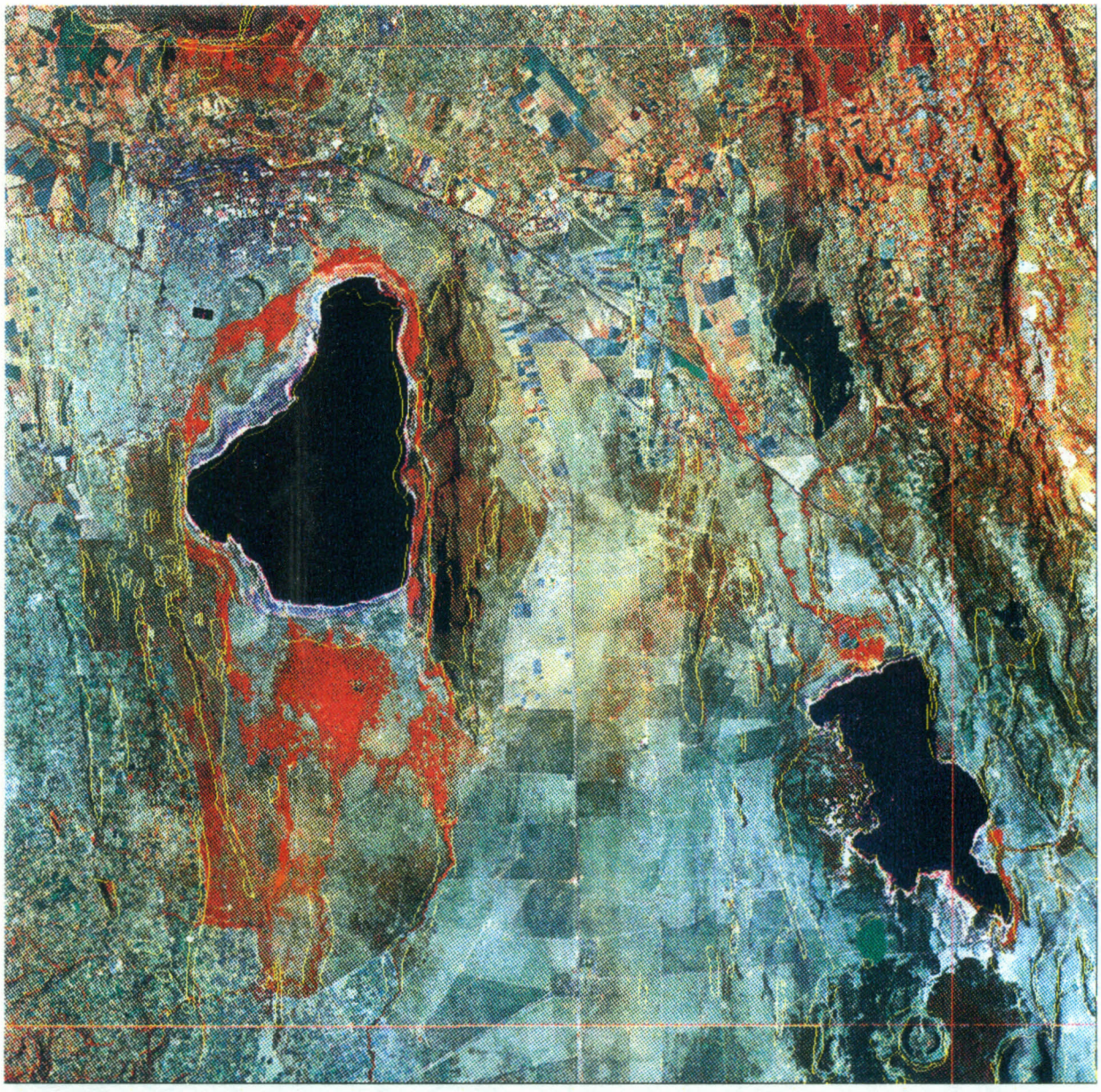

Plate 5.2: linear rectified image of Lake Nakuru-Lake Elmenteita area, showing lithology (yellow lines) as digitized from geological maps of the area. Note the volcanoes of Elmenteita "Badlands" (south east corner) and the edge of Menengai caldera (north west corner). Note also the grid of latitudes and longitudes.

Figure 5.5: Structural elements of lake Nakuru-lake Elmenteita area, interpreted from Landsat-5 TM imagery and existing geological maps (see Figure 5.6 for rose diagram of the fault azimuths.

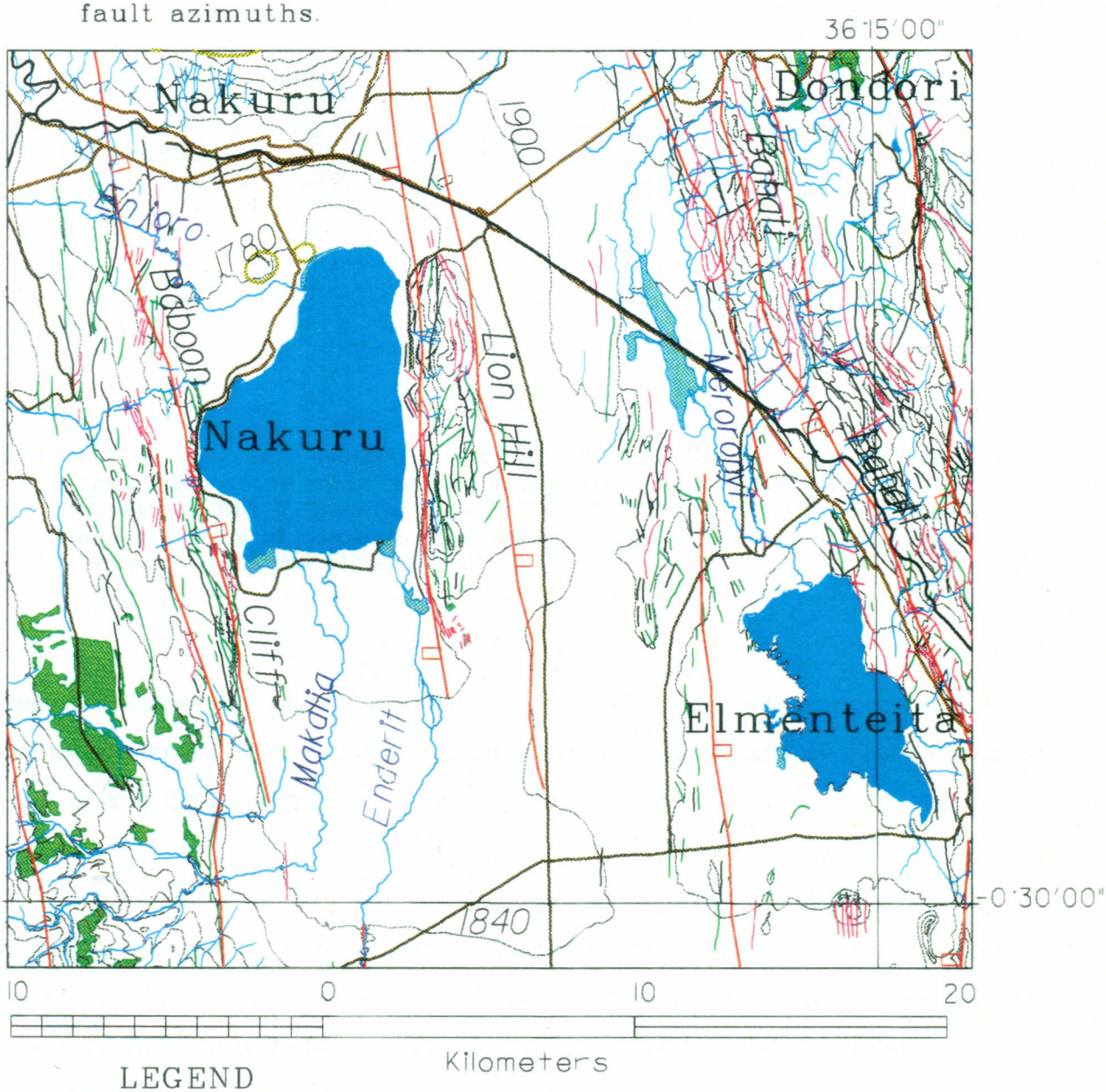

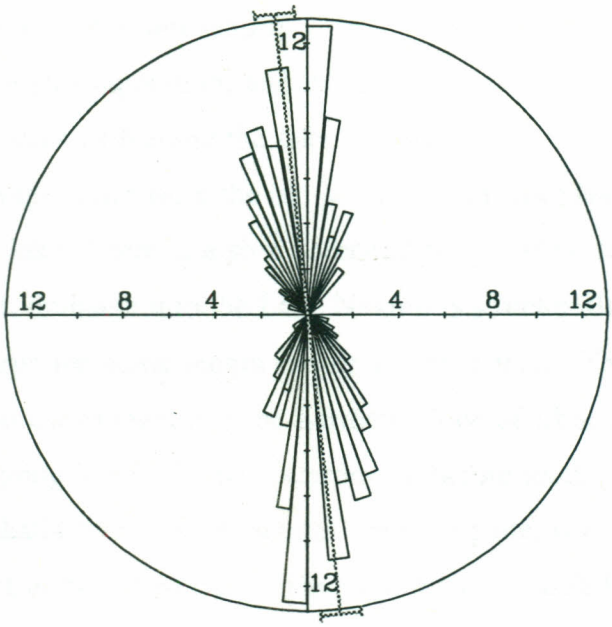

Calculation Method ... Frequency
Class Interval ..... 5 Degrees
Data Type ..... Bidirectional
Rotation Amount ..... 0.0 Degrees
Population 579
Maximum Percentage . 11.9 %
Mean Percentage ..... 2.9 %
Standard Deviation ..... 3.17 %
Vector Mean ..... 353.38 Degrees
Confidence Interval ..... 4.03 Degrees

Figure 5.6: Rose diagram depicting azimuth frequencies of faults in the Lake Nakuru area. The vector mean of the fault azimuths is N6.6°W and differ from the perceived N18°W general trend of faults in the Sattima-Mau Block due to the contribution of the near N-S trend of post 0.3Ma faults located between Lake Nakuru and Lake Elmenteita.

waters completely crystallised to a blanket of soda. There has also been increased sediment influx into the lake in recent years as seen in the waters of Makalia river contributing to the migration of the flamingoes.

Recharge to the lake is from a drainage area of 1675.4 km^2 and is mainly by direct rainfall and increments from surface runoff through Enjoro, Makalia, Larmudiac and Enderit rivers that drain the Mau escarpment (Figure 5.1). Because of the porous nature of pumice and ash formations in the Mau escarpment and because of their high permeability, the surface runoff from the escarpment is poor. Most of it sinks into the ground, assisted by the forest cover at the highest parts of the escarpment, before reaching the main streams or the lake itself. Large sections of the catchment area are, however, under increased cultivation on the poorly consolidated soils, exposing them and leading to increased soil erosion and accelerated surface runoff during the rains. Surface infiltration and percolation of water into the water table has been reduced, no longer maintaining the springs that feed the rivers and the lake.

The lake is a closed basin and its water is highly saline, never filling to more than a couple of metres deep. Fluctuations in the lake are rapid, with the lake becoming slightly deeper in the wet season. During prolonged drought, its waters are greatly reduced Plate 5.2 through evaporation, and its surface increment is poor, or non-existent, due to drying up of the streams feeding the lake. In this period, the only surface increment into the lake is from sewage water from the old sewage treatment plant of Nakuru Town, just to the north-east of the lake. There is also a perennial supply from small springs, off Lion Hill. For the greater part, drainage into the Lake Nakuru is structurally controlled, following the base of the fault scarps for some length before crossing them. The Githanguin river deeply incises parts of Mau escarpment and the northern slope of Eburru, close to the escarpment and drain north, aligning itself with the escarpment, before joining the Enderit as a tributary. The Enderit and Makalia rivers, have angular drainage patterns on the Kiwi plain, suggesting their structural control by buried faults. The Enjoro river also follows several angular bends as it flows down the fault scarps on the Mau escarpment area. At these fault lines, aided by porous pyroclastic cover, the runoff loses occur into the ground. The percolating runoff is believed to be the recharge water to an aquifer underlying the lake (Dindi, 1995 - personal communication). As indicated by Dindi, the aquifer is confined and separated from the saline waters of the lake by a salt impregnated clay. The underlying groundwater is thus under low artesian pressure.

Enjoro, Larmudiac, Makalia and Enderit rivers are the only drainage systems that reach the lake when carrying runoff. The rest of the drainages rising from Eburru, Bahati and the rest of the Mau escarpment, carry runoff only during prolonged rainfall, but never reach the lake by means of surface runoff. These drainages are short and quickly taper off on their approach to Kiwi and Bahati plains that lie along the axis of the Rift Valley.

5.2.6 Lake Bogoria (985 m a.s.l)

Lake Bogoria is also a narrow soda lake lying in a trough formed between a fault-fragmented, eastward sloping Kipngatip plateau of phonolite lava to its west, and Lake Bogoria fault scarp (Lake Hannington fault) immediately to its east (Photo 5.10). Lake Bogoria escarpment rises to 1634 m at Sirken Hill, (750 m above the lake shoreline).

Photo 5.9: *The dry lake bed of Lake Elmenteita.* This lake showed significant drop in the 1993/94 dry period when as seen in the photograph, large sections of the lake bed were exposed. It previously dried-up in 1985. At the background is the Gilgil escarpment that separates this lake from Lake Naivasha.

Photo 5.10: *Lake Bogoria escarpment.* At the Background is the N30°W running Lake Bogoria escarpment with Lake Bogoria at its foot. The lake receives water increment from hot springs and geysers around the lake. The lake is home to hundreds of thousands of flamingoes.

The main escarpment conforms to the trend of Marmanet escarpment (N30°W). The fragmented Kipngatip plateau is part of the Lake Bogoria Block, discussed in Chapter 4, where for the most part, the fault lines trend N-S. The area surrounding the lake is mainly covered by intermediate to basic lavas with associated sediments and pyroclastics of Tertiary to Quaternary age.

Lake Bogoria is replenished and sustained by a number of springs, most of which emerge along the N-S fissures at the shores of the lake. Some of the springs are hot and boiling (Photo 5.10). Emsoss warm spring water flows in from the south through fissures on the Emsoss escarpment (trend, N38°E). The larger part of the drainage area, 1075.5 km^2, is occupied by Waseges river, which closely follows the foot of Marmanet escarpment and collects numerous short tributary springs on its north westerly flow. This river diverts its course at Chesauilmet fracture zone and cuts its way eastward, down the Ngusero, Waseges and Sandai fault scarps where it has formed the Sandai Gorge. At the foot of Sandai escarpment, it lends itself into the Loboi plain where it has built a great deltaic sediment fan. At the plain it cuts through the fan and flows southward as the Sandai river through the Kisibor swamp, into Lake Bogoria. The constructive sediment fan outwash, and the presence of a remnant fault host block just to the east of Kisibor swamp, has helped channel the waters of the Waseges into the lake.

The lake waters are highly saline and contain sodium carbonate, chloride and fluoride. There is a supply of low saline waters from the hot springs due to decomposition (solution) of alkaline igneous rocks and recirculation of groundwater by the hot springs. The alkaline and peralkaline igneous rocks in the Rift Valley contain sodium metasilicates, and their decomposition provide the sodium salts in this lake. There is no surface outlet from the lake, and its location in a semi-arid environment, in a confined depression, 750 m below the escarpment, means that there is high evaporation, contributing to concentration of the salts.

Unlike the other lakes under study in the Aberdare Detachment (all of which showed significant drops in their water levels in the 1984/85 and 1993/94 drought periods), Lake Bogoria maintained its water level during this drought periods. This is attributed to the fact that its main surface influx is from the hot and warm springs close to the lake. Recharge into

the aquifers that feed the springs is from deep percolation of runoff from the Marmanet escarpment and the surrounding areas and from the Bahati fracture zone. This runoff percolates into the ground through intervening faults, as noted in the area north of Olobanita. There is also evidence of drainage disappearing through sinkholes in the Kisanana-Koisomo area, probably to replenish the groundwater table that feeds the springs recharging the lake.

The drainage on the western side of the lake is structurally controlled, following the troughs between the fault scarps or the base of the fault scarps. This drainage, that would have flowed into the lake, flows north, quite close to the lake, into Loboi plain and Lake Baringo. The Molo river, for example, collects water from the Mau escarpment as far south as Elburgon forest and flows parallel to the lake, structurally controlled by Molo fault scarp into Lake Baringo. Ndoloita hot spring on the other hand flows parallel to the lake, just 1.5 km to the west of the lake, controlled by the Ndoloita fault scarp, and takes its waters into the Loboi swamp about 0.5 km from the northern end of Lake Bogoria. From the swamp the river flows north into Ngarua swamp where it joins the Molo, into Lake Baringo, 23 km north of Lake Bogoria.

The Molo, Waseges and Perkerra rivers have deposited a thick sediment load in the Loboi flood plain. The sediments are pebbly and stratified deltaic silts, washed in from the neighbouring cliffs and the southern parts of Kamasia range. Some silts, over which some irrigation is taking place, have been transported from as far south as Molo, by the Molo river. On the satellite imagery of Lake Bogoria area (Plate 4.1), the sediments are easily delineated. Despite the presence of relatively thick sediments on the Loboi plain, there is a total lack of any similar sediments in Lake Bogoria itself. The thin deposit present in the lake are associated with sediments and pyroclastics, indicated by Bosworth *et al.* (1986) and Hackman (1988) to be of Tertiary to Quaternary age. The lake is also a comparatively recent feature. The fact that no major river takes its waters directly into the lake, largely contributes to the lack of sediments in the lake. The Waseges which could provide the main sediment load, silts into Kisibor swamp, never carrying any sediments into Lake Bogoria.

5.3 GEOTHERMAL MANIFESTATIONS IN THE ABERDARE DETACHMENT

Noble and Ojiambo (1976) have reviewed the early detailed geological mapping geared towards locating the lithology, structures and fault patterns which control the occurrence of geothermal reservoirs in the Kenyan Rift Valley. They review some of the earliest written descriptions of thermal springs in the Rift Valley and suggest that the steam fumaroles have their origin from a juvenile source trapped beneath volcanic rocks. Torfeson (1987) indicate that xenoliths of syenite found in ignimbrites and in agglutinate lava of Longonot, Menengai and Suswa reveal the presence of the same type of magmatic intrusions. These volcanoes are also domed, with Menengai and Suswa showing a radial tendency of the fracture zones (active arcs) along the caldera floors. The active arcs are zones of geothermal manifestations in the form of steam fumaroles. The radial tendency suggests a rise of the central parts of the volcanoes above a shallow level intrusion. Olkaria and Eburru volcanic complexes are also domed, possibly due to similar magmatic intrusions as at Menengai and Suswa. The doming implies up-flow zones, linked to high level intrusions that are the heat sources for the geothermal reservoirs. Baker (1986) and Lambiase (1989) have interpreted a positive gravity anomaly which they associate with axial rift volcanism and shallow magma intrusion.

Exploration with the purpose of obtaining a better understanding of the sub-surface geology, geothermal reservoirs and their boundaries requires a thorough evaluation involving integration of geochemical, gravity, electromagnetic, seismic and magnetotelluric data sets structured in a GIS database. This could help in evaluating the contribution of porosity, tectonism, permeability, fluid content, temperature and geothermal alterations, to the properties of the geothermal reservoirs.

The distribution of geothermal resources in the Aberdare Detachment is related to major fault zones and fractures associated with cinder and caldera volcanism in the rift floor. High enthalpy steam vents and true hot and boiling springs sometimes under pressure are seen in fissures and zones of acid rocks of Eburru and Olkaria, and in the fissures of Lake Bogoria. Scattered warm springs are also seen rising from underneath lavas and fissures in these areas and along the foot of the escarpments to the east of the Rift Valley axis. These geothermal manifestations are most conspicuous at Eburru, Olkaria, Maji Moto near Mogotio,

Lake Bogoria, Mt. Margaret and the crater floors of Menengai and Longonot. In most instances they are aligned along N-S trending faults located in these areas. At Menengai, Longonot, Margaret and Suswa caldera, the geothermal activity is confined to the caldera walls and craters and along ring fractures and volcanic vents on the caldera or crater floor.

Some areas around the fumaroles and the steaming ground show surface alterations of volcanic rocks and soils to clay minerals. This is evident at Olkaria, Eburru and Menengai crater floor. In the absence of the steam fumaroles, these altered zones could be used to locate fossil geothermal centres. Noble and Ojiambo (1976) indicate that warm ground can also be located in the field by the presence of a grass, *Fimbristylis exilis*, which is found growing in soils of up to 75°C. This grass is identified in those areas that showed clay mineral alterations at Eburru, Olkaria and Menengai. In other locations, steam fumaroles of up to 40°C were seen rising from fractures within the rift floor grid faults. These were mainly located along the axis of the Rift Valley floor and to the east of it. The locations were confined to the area east and north of Olobanita swamp and along well-defined fissures at the foot of the west downthrown eastern rift margin fault scarps of Sattima, Subukia, Solai, Emsoss and Marmanet.

There is significant geothermal activity at Olkaria and Eburru, which is not surprising, since these areas are the sites of the most recent multi-volcanic eruptions, dating just over 200 years. At Eburru, the geothermal activity consists of steam fumaroles and steaming ground confined to a shallow, down-faulted block lying between the peak of Ol Doinyo Eburru to the west, and the line of a fault that runs into the main Gilgil fault to the east (Plate 5.1 and Figure 5.3). Along the southern parts of the Gilgil fault are aligned small craters, observed on the satellite imagery of the area. From one of these craters, the youngest Ol Obonge lava (on the south-eastern slopes of Eburru volcanic complex) has been extruded. At Olkaria, the geothermal activity is concentrated along, and to the east of the fault line on which Crater Lake, Olenguruoni, Olkaria and Lolonita volcanoes are aligned. The surface evidence of the steam fumaroles are here most conspicuous along Ololbutot fissure and within exposed dykes at Ol Njorowa gorge.

The geology of Olkaria is marked by complex volcanic and tectonic activities. Early eruptions are composed of vent and fissure comendites and large quantities of pumiceous

pyroclastics that are exposed as bedded tuffs, pyroclastics and ashes in Ol Njorowa Gorge. Bedding is cut by dykes that are exposed at the gorge (Photo 5.11). Thompson and Dodson (1963), and Odongo (1982), indicate that the bedded volcanics originally erupted from Longonot. The dykes link comendite plugs that have a N-S trend, similar to that of the rift floor faults. The emplacement of pumice cones, rhyolite domes, comendite lavas and dyke intrusions in Olkaria area followed the phase of rift floor plateau trachyte faulting. The most recent volcanism is along the N-S Ololbutot fissure (Photo 5.12) and was initially associated with white to grey pumiceous ash eruptions that left behind a line of phreatic explosive vents along the fissure. The phreatomagmatic explosive event was followed by an upsurge of intrusive magma and extrusion of pumiceous obsidian that now form the youngest lava flow, the Ololbutot lava.

Despite good sections at Ol Njorowa gorge, complex eruptions make it difficult to distinguish marker horizons within the area. Onacha (1989) has attempted to correlate the rocks at Olkaria area with those of Suswa using geoelectric properties of rocks. His interpretations suggest a horst-graben geoelectric structure for the area with a wide variation in electrical properties of the rocks between different sounding stations. The suggested horst-graben structure model lead to questions about the link between Suswa, Olkaria, and Eburru geothermal prospects. Keller (1972) observes that the horst-graben structures are found at different depths and are separated from one another by oblique E-W horst structures, concealed under the pyroclastics. If, as suggested by Keller (1972), all the geoelectric structures were smoothened, Olkaria and Eburru prospects could be considered as individual dome structures, due to intrusion at depth rather than horst-graben structures due to faulting.

Electrical resistivity soundings made in Olkaria and interpreted by Hochstein (1971) show that most of the area has high resistivity in the sub-surface and decreasing resistivity with depth. Keller (1972) has delineated major lateral resistivity variations by interpreting dipole sounding. The interpretation suggests that the decrease in resistivity with depth is confined to areas with geothermal manifestations. Bhogal (1980), using a dipole method, estimated the width of the Olkaria field to be 8 km and its depth about 3-4 km. Skinner (1977) estimates this depth at about 2.5 km along the axis of the rift. The 8 km width of the Olkaria geothermal prospect thus suggests a confined geothermal reservoir.

Photo 5.11: *Dyke intrusions at Ol Njorowa Gorge.* The gorge, 160 m deep in places exposes acid lava dykes of comendite, obsidian and rhyolite, forming sills or cutting through the volcanic ash. At the dykes area, steam fumaroles are emitted.

Photo 5.12: *Ol' lolbutot Fissure.* This open fissure is within a phreatomagmatic eruptive centre and can be traced along a line of similar centres running N-S in the Olkaria area. The youngest of the lavas in the area flew out of the fissure (Photo 5.9). The fissure dies out towards Lake Naivasha and is one of the possible underground discharge area for the lake.

From the electrical resistivity data analysis carried out by Meidav (1972), Furgerson (1972), Bhogal (1980), and Onacha (1989), for the Olkaria area, four geoelectric units are identified: (1) a resistive overburden, (2) a resistive cap-rock, both correlating to Quaternary lavas and volcanic sediments, (3) a conductive unit (3-15 Ωm) correlating to Tertiary pyroclastics intercalated with tuffs, rhyolites and trachytes, and (4) an electrical "basement" (50-200 Ωm) correlating to Miocene volcanics. The two conductive units are attributed to permeable layers that are part of a confined convective hydrothermal cell, the geothermal reservoir. From data obtained from the Kenya Power Company Ltd at the Olkaria Power Station, drilled wells reveal two production zones, one between 750 m and 900 m, rich in steam and corresponding to the conductive unit (3-15 Ωm). The other reservoir is between 1100 m and 1300 m, rich in water and corresponds to the electrical "basement" (50-200 Ωm). The production area demonstrates the presence of a considerable geothermal resource between 900 m and 2600 m below the surface. The shallowest production well, is well OW-12 (901 m deep). Cores and cuttings from one of the wells, Well OW-18, show that the rocks are mainly trachytes and rhyolites with intercalations of minor basalts and varying thicknesses of pyroclastics and ashes. The Olkaria geothermal field, which is presently under exploitation, started production in 1981.

The water table in Olkaria area, as suggested by Clarke *et al.* (1990) is high in the production area. The shallower geothermal reservoir could be attributed to the interaction of meteoric waters with steam migrating vertically through fault structures from the second deeper geothermal reservoir, up to the surface. There is no information about the water table up to depths of 300 m at the adjoining Longonot-Akira plain and at Ndabibi plain which are to the east and west respectively. The mode and regions of recharge of the geothermal reservoirs in Olkaria and areas of outflow from the geothermal field are therefore speculative. Mahon (1972) and Burgess (1986) suggest a possibility of an influx, to the sub-surface, of deep geothermal waters underlying an extensive area of the Rift Valley. Furgerson (1972) recognizes the field as having two geothermal anomalies of similar electrical properties, separated by a NNE-SSW discontinuity of characteristic doming or horst structure, interpreted as lying along the axis of the rift floor. The rift floor axis area shows a reduced drainage pattern (Figure 5.2) and fault structures (Figure 4.7). Clarke *et al.* (1990) recognize the need for a thorough water balance study to be certain of the areas of inflow into the fields. They

suggest that the recharge into the Olkaria geothermal field is from the Mau catchment and should be ample to sustain geothermal energy production in the geothermal fields around the catchment area. Torfeson (1987) also predicts recharge of the Suswa reservoir as being from the bordering Kikuyu and Mau escarpments and rules out inflows from Lake Naivasha.

The present study observes that the drainage from the Mau escarpment is terminated at the fault line striking perpendicular to the east-flowing drainage on the Ndabibi plain and disappears underground through the fault. The drainage probably flows south along the fault lines to feed the Suswa reservoir located further south. Similarly, drainage from Kinangop and Kikuyu escarpments flows west towards the rift floor, but is terminated along the N-S striking fault line and flows south along these structures to the Kedong Valley. The fault structures were mapped from the satellite imagery and were confirmed in the field as having strong control on the drainage from the escarpments. There are therefore doubts as to whether the escarpment catchments are the source of the recharge into the Olkaria geothermal reservoir.

It is observed in the present study that the trend of geothermal manifestations in the Aberdare Detachment area are aligned along fractures that extend from the area around Lake Elmenteita to Mt. Suswa, and confined to zones at Eburru , Olkaria, Longonot and Suswa - all centres of Recent rift floor volcanic activities. There is also a concentration of these manifestations at the fault zones extending from Menengai crater to Lake Bogoria and confined to zones at Menengai crater, Olobanita, Maji Moto (Mogotio) and Lake Bogoria. The interpretation made for the Eburru prospect shows that recharge into the reservoir is from runoff crossing in from the Mau escarpment and migration of deep meteoric waters along the more than 100 km long Gilgil-Ol Obonge-Olenguruoni-Lolonita-Loirogwe fault line. The length of the fault line suggests very deep faulting. The surface runoff crossing from the Mau escarpment in the west and the Gilgil escarpment to the north percolate through the deep faults, where at depth it is heated. There is also local recharge from Eburru catchment. Since the lines of steam fumaroles on Eburru complex coincide with the fault structures cutting through the complex. The deep fault zones are the permeable zones of complex fluid migration to the surface.

The Olkaria geothermal prospect on the other had is bordered to its west by the Gilgil-

Ol Obonge-Olenguruoni-Lolonita-Loirogwe fault line which, however, does not cross the reservoir and is unlikely to be a conduit for the recharge waters into the reservoir. Instead, it is seen as a barrier to the runoff from the Mau escarpment. This runoff, instead of crossing into Olkaria reservoir, flows along the fracture to feed the Eburru reservoir to the north and probably also flows south to feed the Suswa reservoir. The Olkaria reservoir is bordered to the east by another fault barrier to the fluid flows, the Kijabe-Malewa Oleolondo fault and other buried fault lines such as the Nguruine fault that run parallel to one another. Most of the drainage crossing in from the Kikuyu and Kinangop escarpment catchment areas, south of the Karati river, drains on the surface to the Kedong Valley, or percolates into the ground through volcanic formations and fault structures, where it flows south to feed Margaret reservoir or the Magadi reservoir located in the area further south. The drainage from this part of the Kikuyu and the South Kinangop escarpments is therefore unlikely to be the recharge waters of the Olkaria reservoir. It is suspected that deep meteoric waters from Bahati and North Kinangop escarpments feed the reservoir through the more than 70 km long Muriandati-Baxia-Olkaria East fault line, crossing through Lake Naivasha (Figure 5.3). There are fault structures within the Olkaria geothermal manifestations area such as Ololbutot fault line that is traced north to the neck of the Small Lake in Lake Naivasha and south to Ol Njorowa gorge. The trends of the Muriandati-Baxia-Olkaria East and Ololbutot faults crossing through Lake Naivasha, point to an hydraulic connection between the lake and the Olkaria geothermal reservoir, and possibly deeper percolation from the lake to the Suswa reservoir which is on the same line as the Olkaria reservoir and located to the south.

Recharge of the Menengai reservoir is mainly from the Crater Stream crossing in from the Bahati catchment in the east. The runoff from this stream flows south along the foot of Menengai fault after crossing the escarpment, and immediately percolates into the caldera fracture zone, never staying for any length of time on the surface. There is also recharge of the Menengai reservoir from runoff within the crater, which, during periods of rainfall, crosses from the central caldera floor "cone" and from the internal slopes of the caldera walls and collects at the caldera fracture zone. These zones are covered by eroded volcaniclastic materials that display high porosity and permeability of the unconsolidated deposits, implying deep percolation of surface runoff within the crater.

In the other geothermal localities, of Olobanita, Maji Moto (Mogotio) and Lake Bogoria, geothermal manifestations are also related to deep fracture zones where vertical migration of fluids is envisaged. Hydraulic connection within these areas and with the Menengai prospect is suspected. Most of the recharge waters is groundwater percolation from the Bahati, Solai-Subukia and Marmanet catchments. The runoff crosses in from these escarpments and either crosses westwards down the escarpments or flows northwards along the foot of the escarpment. Since, as indicated before, there is a shallow intrusive magma body suspected to be located at the axis of the Rift Valley, the surrounding rock is hot, providing the heat for the meteoric waters.

* * * *

CHAPTER 6

SUMMARY AND CONCLUSIONS

6.1. RESULTS AND DISCUSSIONS FOR LAND COVER AND STRUCTURAL-GEOLOGICAL MAPPING

The first objective of this study was to create a Geographic Information System (GIS) database with which to integrate raster and vector data sets. It sought to use vector database and image analysis to establish a methodology of data integration and registration. The software product, Microstation, linked to an Informix relational database in an Intergraph GIS system, was used to develop drainage, geographical, and structural coverages for the area. Structure, lithology, topography and geography are the four themes addressed. Selected graphics of various maps were linked to descriptive data via the GIS database, resulting in topological intelligence.

Topographic relief, represented by contours, faults, lithologic divisions and drainage patterns, as discussed in Chapter 4, are transformed and designed into a GIS database. Their relationship to that of land use and land cover patterns were interrogated and modelled more effectively using the database. The relationship between the data sets was re-confirmed through integration with remote sensing data and by ground truth survey. The GIS was found to be suited in analysing and querying spatially related data. This thesis has used it to study the interaction between the faults systems and the drainage patterns. The GIS was used to transform and link geologic structures with their orientation and location in space and to correlate them to hydrologic resources. A drainage network analysis that helped determine the discharge of the water resources and the location of geothermal resources was also carried out. Through the GIS, 2-dimensional (2-D) digital terrain models (DTM) of the topography of the study area were produced and their illustrations presented throughout this thesis.

The geological and structural units shown in geological maps and reports of the Aberdare Detachment, are based on the smallest measurable linear dimension on the maps, of approximately 1 mm, and at the mapping scale of 1 : 125,000, they represent mapping

ground units of 125 m. Landsat-5 TM's smallest mapping unit is, however, a pixel of 30 m resolution and that of SPOT's multispectral data 20 m. Therefore, satellite mapping approach has potentially more information due to its smaller mapping units than those shown on the geological maps. In this study satellite imagery were therefore used to extrapolate on the structures and to redefine some of the rock unit boundaries shown on the geological maps. The 30' quadrants used for the Kenya Geological maps were mapped at diverse dates and by different geologists and show boundary discrepancy in adjoining maps. A mosaic of these maps, such as that produced in this study by digitizing, shows this discrepancy in unit boundaries of adjacent maps. Correction of these discrepancies may require extensive field checks. Extrapolation of units in the existing geological maps were made by registering the digitized maps onto the imagery. This way, the discrepancy in maps boundary units in the quadrants were corrected by referring to remote sensing units. This type of discrimination was a deliberate bias and helped to optimize field work. The mapping approach was thus found to be cost effective and time efficient.

Representative spectral values and areas with units which showed significant tonal contrast and texture were interpreted and selectively examined in the field to determine the underlying geological units. In certain localities, more detail showed on the image than was presented in the geological maps. The identification of small mapping units was enhanced by a high contrast between surficial materials, especially between the lava flows and the ashes. This afforded one to make finer lithological mapping such as that shown for the Menengai Caldera, discussed in Chapter 3.

Image classification and characterization of land use categories, when integrated with vector data, provided a good perspective of the study parameters. The data showed high prospect in analysis of drainage patterns and in detection of geomorphic and landscape units and structures in the Aberdare Detachment area. Registration of GIS image files, produced by the classification, onto the GIS vector files containing relevant topological information was used in the interpretation. The GIS was used to extract and represent specific types of non-spectral knowledge parameters. Some of these parameters, such as elevation (contours), structures, geology, and drainage patterns were designed as layers of mapped information in the GIS.

6.1.1 Land cover Characteristics and Classification

The second objective aimed to interpret satellite imagery, and to use it for land cover classification. It also sought to examine the effectiveness, suitability and capacity of satellite data for land use pattern analysis and for structural and geological mapping of the Aberdare Detachment. Methods of satellite remote sensing, and benefits realised from the analysis of photographic SPOT and Landsat-TM image products, are discussed in Chapter 2. The technique adopted in the study of the Olobanita-Nyahururu cultural and biotic environment shows some image indicators and land cover characteristics that provided a good perspective of the study area. It produced thematic maps containing some degree of generalized information due to uncertainties in interpretation of some spectral reflectance. However, it proved to be a quick and rapid method by which to obtain reliable land use and land cover data for mapping and inventorying. From the digitally treated Landsat-5 TM data discussed in Chapter 3, land cover types, structures and some surface geological units were mapped and show that the remote sensing methods create unique opportunities for investigating the earth's environment.

The standard FCC's presented hues of green for the bare ground, green/blue hue for the less vegetated areas and various shades of brown to red for the vegetated terrains which were used to select training samples for classification. In the classification of Nakuru-Menengai area, informative value of satellite imagery about the study parameters was high. PC's 1,2,3, contained most information for characterization of land use categories. The image exhibited clear sensitivity to regular patterns of crop fields and other land cover types. These indicators provided a good perspective of land use, and as seen in Plate 3.3 and Table 3.9, the estimate in classification was promising.

On a regional scale, the wide view provided by the imagery allowed for demarcation of the eastern escarpment, the western escarpment and the Rift Valley floor. Geometric shapes, forms and patterns were also exploited in delineating structural features in the rift floor. The study area was characterised by geomorphological features, geological formations and structures, hydrological patterns, geothermal manifestation, vegetational characteristics and agricultural patterns that were effectively studied using the satellite imagery. Good ground

resolution of the data showed details of the land, with the synoptic view suggesting NNE, NE and NW striking linear patterns of fault scarps and associated grabens and plateaus.The faults were recognized from a series of dark near parallel lineaments enhanced by the shadow effect resulting from the sun azimuth (3° - 5°) at the time of imaging. The near vertical slopes on the escarpments and the sub-meridian, near north-south trend associated with faulting and tectonic activities in the Rift Valley, also greatly enhanced the linear features in the rift floor.

The third objective of this thesis aimed to evaluate the land resources of the area (such as vegetation, hydrology, settlement patterns and demographic pressure). Many of the land cover features observed in the Aberdare Detachment were reflected in the vegetation and soil cover type. The composition of residual soils in the area reflected the chemistry of the underlying formations, and in the areas where there was limited human influence, the soil types and the vegetation cover were used to define remote sensing units. Comparisons were made with digitized ancillary data and field checks made to attach a meaning to the remote sensing units which provided a threshold of information for the supervised radiometric signature classification.

The classification was used to assess the extent of anthropogenic changes in the Aberdare Detachment. Multidate imagery was used to ascertain the consistency of the image features used to delineate the land use unit boundaries. In naming the units, ancillary data from geological, structural, and topographic maps, and the land system atlas were used. The use of ancillary data sets can, justifiably be regarded as a deliberate bias. It could, however, not be avoided, as designing of existing data into a GIS database and using the database for integration was the aim of this research effort. Extensive ground truth survey was carried out to supplement the collateral information mentioned above and to verify the image classification. The field work served to determine the accuracy of existing interpreted geological units and structures. All the data sets were compiled and integrated to produce the synthetic, thematic maps and structural maps presented in this thesis.

In the section of the Aberdare Detachment, such as at Bahati, Subukia, Kinangop plateau, around Lake Naivasha, Ndabibi and Njoro, intense cultivation was observed. These areas showed frontal massive boundary change, greatly influencing the overall radiometric

signature, making it difficult to use the imagery to delineate lithological features. Land evaluation, as discussed in Chapters 2, 3 and 5 as shown in various illustrations in this thesis, indicated that the natural forests in escarpment areas of Mau, Bahati, Ol Bolossat and Marmanet have been intensively cleared to give way to cultivation. Larger plantations of especially coffee, tea and sisal were easy to delineate from images of all seasons, since boundary change and green vegetation reflectance defining these fields was distinct. In the large fields of maize and wheat, however, there were variations in the images of different periods due to various stages of growth of the crops and inconsistency of the areas occupied by the crops. It was therefore difficult to characterise these crops, and real time imagery would be required for their specific mapping. In the small scale mixed farms, a mixed reflectance occurred, making it difficult to define individual fields. The areas, however, provided a good perspective of the land development process in the Aberdare Detachment, and thus their environmental impact. Questions are, for example, raised about the environmental friendly usage of Lake Naivasha waters and the need for conservation of the catchment areas to maintain an ecological balance in the lake. As discussed in Chapter 5, land use activities have a great influence in the hydrological regimes of the area, and to some extent modify the land morphology, and thus control on the drainage.

The presence of human settlement has also resulted in increased infrastructures and development of commercial centres, with Nakuru, Naivasha and Nyahururu the largest. The contrasting spectral reflectance of these urban centres can be exploited by town planners and engineering geologists to determine the direction of expansion of the town relative to the availability of construction materials, drinking water, disposal sites, and areas of possible geological hazard provided by buried fault lines.

6.1.2 Errors in Radiometric Signature Classification

Errors in radiometric signature classification were related to observations made on imagery of different periods. The solar azimuth was different for images of different periods with the differences carrying errors related to differential illumination and shadow effects. However, low sun angle illuminations were instrumental in enhancing subtle geologic features

especially those with steep slopes on the ground. Seasonally related temporal changes offered significant errors. Cloud cover, burnt areas, cultivated areas, and flush vegetation growth in response to plentiful precipitation were some of the changes observed in multidate imagery, implying that single images could not wholly be relied on for land cover classification. Multidate image registrations were found to be particularly sensitive to the predominantly small and localized land cover changes in the small scale settlements. Variation in climatic patterns in the area over short distances also contributes to difficulties in identifying and grouping mapping units. It was difficult to use the same colour identifiers to pick out and map the same remote sensing units throughout the study area. Dry season Landsat-5 TM and SPOT imagery, however, provided a good spatial aggregation, greatly increasing discrimination of remote sensing units and geological structures, especially in the uncultivated areas.

6.2 CONCLUSIONS AND RECOMMENDATIONS

The following conclusions and recommendations are made from this study:

1. From the satellite imagery, it was possible to identify several types of geologic features such as lava flows, fault structures and volcanic centres in the Rift Valley floor. Lithologic information in the form of radiometric signatures and topographic style was obtained for Menengai crater and used to map the lava flows in the crater. The lava flows were mapped from the lobate patterns and tonal contrast due to abrupt topographic changes, vegetation changes and rock-type changes. In the less vegetated uncultivated areas of the Aberdare Detachment the remote sensing units correspond to lithologic units and were detectable by visual analysis of satellite imagery. In the Gilgil, Lake Elmenteita and Eburru areas, grouping of rock units was possible due to sharp boundaries and differences in lithology defined by vegetation which showed distinctive colours, especially of the young lavas. The data could thus be used in updating some geologic information in the existing geologic maps. Here, the digitized map data can be registered onto the imagery and the imagery used to extrapolate on the unit boundaries using image hues based on radiometric signatures and geomorphological information.

2. Producing structural maps by image analysis and integration with existing data increases accuracy of mapping of fault elements. From the radiometric signatures it was possible to define and extrapolate fault structure in the Kedong Valley of Longonot area, Ndabibi plain and the Gilgil-Eburru area. This was coupled with field data after recognizing potential sinkhole areas from the grooves of trees mapped from the red tones on the imagery. The synoptic view provided by the imagery and the GIS capability to overlay and mosaic data, gave another dimension of analysing map information from the Aberdare Detachment. Offset direction of the shear fault zones along the edge of the major Sattima escarpment at the Marmanet-Loboi fault zone and major trends of the fault structures were thus recognised. The regional perspective enabled the structures to be extended over large areas and also into the adjoining 30' quadrangle areas with minimal ground control.

3. Radial drainage patterns were found to be confined to the Rift Valley floor volcanic centres. Except for the radial drainage patterns originating from Kipipiri volcano, the rest of the drainage from the other volcanic centres are ephemeral, defining gullies down the slopes of the volcanic centres and terminating at the foot of the cones. Therefore this drainage has no immediate influence on the Rift Valley lakes, but it could be contributing to the meteoric waters recharging the aquifers underlying the volcanic centres. Angular drainage patterns were more conspicuous in the Kiwi plain, Olobanita plain and Kwa Rodha. In these areas many of the faults are buried under a blanket of ashes and pyroclastics and the angular drainage lines were used to map the fault lines. It is in these areas and in the intervening plains within the rift floor that the drainage from the escarpments was terminated. The drainage patterns were used in redefining the rock unit boundaries and the drainage termination areas. Parallel drainage patterns were confined to the main escarpment faces, running down the slopes or along the faults or in the grabens, between the horst blocks.

As presented in this thesis, GIS modelling can provide cartographic ability to view graphic element representation and to address questions such as those relating to structural control on the drainage and the land cover types. From the maps of various themes, and from visual comparison between vector data and raster data of processed images, there is a strong

structural control both on the drainage patterns and on the lake basins. The GIS database can now be used for further structural and drainage pattern analysis, and detection of geomorphic and landscape units in the Aberdare Detachment area. New information can be developed by combining and comparing the raster GIS and vector GIS with other data, for example, gravity data, aeromagnetic data etc. Draping satellite information on the vector data and its incorporation into the database is an essential element if the present GIS is to be used for land use analysis. The database can be used in:

(a) utilization of satellite imagery potential for monitoring and updating of land cover data, and for further database design.

(b) continual building and analysis of the present data. There is potential to incorporate new techniques of data processing and implementation of new processing systems and dissemination of information.

Since remote sensing data is a record of the land surface, the data can be used for updating the GIS and it is thus an essential element for dynamic analysis and time dependent changes of land use, for the reliability of a GIS. Remote sensing data is also cost effective when looking at large areas. It complements field data and allows for comparison with existing survey maps by overlying registered imagery on the digital graphics of the maps. Thus, a GIS set-up, used in conjunction with knowledge of the data, allowed the making of better decisions. In the methodology applied, the use of remote sensing data is quite appropriate for data gathering, lake level changes monitoring, and for structural studies. Although satellite data provide surface clues as to the nature of sub-terranian structures, it is limited as a tool for studying sub-terranian water flows and stocks. Other methods beyond the scope of this study such as use of tracer elements, electrical resistivity sounding and seismic profiling can provide substantial sub-surface information for a complete modelling and analysis of the nature of the sub-terranian connection between the lakes and the geothermal fields. With the potential for fresh water below the clay underlying Lake Nakuru (Dindi, 1995 personal communication), for example, boreholes can be located to intercept the fresh water, before it reaches the saline portions of the basin. This can be done at the shores of the lake, or at the base of the alluvial fans, or at the edge of the depressions on the flood plains close to the lake.

The results of this study proved useful in mapping the structures of the area. From in-depth analysis and land use capability study and follow-on studies, the results and the synthesized structural maps can be used to refine the understanding of the structural patterns, geology, soils and land use potential in the study area. Despite uncertainties in interpretation of some spectral reflectance, remote sensing data was found to be a quick means to obtain reliable land use and land cover data for mapping. The land cover units in Nakuru-Menengai area, for example, were used as a proxy to infer human activities. The inconsistency in reflectance of Bahati forest in this interpretation on the other hand, reflects a rapid increase in population, resulting in deforestation for subsistence cultivation. Knowledge of the current land use patterns, location, extent, quality, and accessibility is thus needed for the rational planning of the area.

The spectral classification discussed in Chapter 3 may not have been able to classify all samples without uncertainty. Different types of non-spectral knowledge parameters, especially registration of GIS files containing relevant information onto the classification image were used to eliminate the uncertainty. Some of the specific types of non-spectral knowledge parameters such as elevation (contours), structures, geology, and drainage patterns are discussed in Chapter 4. These vector GIS data were incorporated into the classified GIS image files to create thematic maps.

The test of the classification was made on a single data set and utilizing an image obtained 6 years prior to this study. Further testing in different areas and with other imagery would be useful in validating the results. Since spectral signatures and therefore the identifying parameters of any class varies from one scene to another, the method used here would benefit from real time data so that the training samples can readily be verified. Frequent satellite overpasses give fresh data for analysis and allow for selection of time periods when discrimination of land cover types is optimal, thus providing a monitoring function, which is the strongest argument for satellite imaging. Atmospheric conditions during the rains may need off-nadir observation or radar imaging mode which can also be used in mapping structural features. The concept of different levels of land use and land cover details from imagery may also benefit from spatial resolution quality of different imaging system. More work with real time data is required, and if later confirmed, the data can be used at

operational stages for monitoring. There is need for reliable resource inventories and updates of land cover maps that require the benefit of the satellite mapping techniques.

It is the author's hope that this thesis, the database, and its related map products will form part of a growing body of knowledge that will contribute to improved land use decisions and resource management activities in the region. The main draw back in this process, however, is the lack of hardware and software in Kenya for data capture and manipulation. There are also organisational and legal issues related to acquiring archive data.

* * * *

REFERENCES

American Society of Photogrammetry, (1960), *Manual of Photographic Interpretation*, Am. Soc. Photogram., Washington D.C.

American Society of Photogrammetry, (1975), *Manual of Remote Sensing; Interpretation and Applications*, Am. Soc. Photogram., Washington D.C., 2144 pp.

Andrews, H. C. and Hunt, B. R. (1977), *Digital Image Restoration*, Prentice-Hall, Englewood Cliffs: New Jersey.

Ase, L. E.; Sernbo, K. and Per, S. (1986), Studies of Lake Naivasha, Kenya, and its drainage area, *Stockholms Universitet Naturgeografiska institutionen* **106**, 91 Stockholm.

Baker, B. H. (1986), Tectonics and volcanism of the southern Rift Valley and its influence on rift sedimentation, *Geol. Soc. special publication* **No. 25**, pp. 45-57.

Baker, B. H and Mitchell, J. G. (1976), Volcanic Stratigraphy and Geochronology of the Kedong-Olorgesailie area and the evolution of the south Kenya Rift Valley, *Journal Geol. Soc. London* **Vol. 132**, pp. 407-484.

Baker, B. H.; Mohr, P. A. and Williams, L. A. J. (1972), Geology of the Eastern Rift System of Africa, *Geol. Soc. Am. Spec. Paper*, pp. 136-167.

Baker, B. H.; Williams, L. A. J.; Miller, J. A. and Fitch, F. J. (1977), Sequence and Geochronology of the Kenya Rift Volcanics, *Tectonophysics* **Vol. 11**, pp. 191-212.

Baker, B. H. and Wohlenberg, J. (1971), Structure and evolution of Kenya Rift Valley, *Nature (London) Phys. Sci.* **Vol. 229**, pp. 538-542.

Bhattarai, K. D. (1983), Mineral exploration by remote sensing techniques in Nepal, *Adv. Space Res.*, **Vol. 3**, No. 2, pp. 49-54.

Bhogal, P. S. (1980), *Electrical resistivity survey method of geophysical prospecting and its application to geothermal exploration in the Kenya Rift Valley*, Unpublished PhD Thesis, Department of Physics, University of Nairobi, Nairobi, Kenya.

Bosworth, W.(1985), Geometry of propagating continental rifts, *Nature*, **Vol.316**, pp. 625-627.

Bosworth, W. (1986a), Comments on Detachment Faulting of the Evolution of Passive Continental Margins, *Geology*, **Vol. 14**, pp. 890-891.

Bosworth, W. (1986b), Off axis volcanism in the Gregory Rift, East Africa: Implications for models of continental rifting, *Geology*, **Vol. 15**, pp. 397-400.

Bosworth, W.; Lambiase, J. and Keisler, R. (1986), A new look at the Gregory's Rift: The Structural Style of the continental rifting, *EOS*, PP. 576-578.

Burgess, C. F. (1986), *Kenya Rift Valley Geothermal project: Hydrogeology and Geothermics of the Magadi-Longonot sector*, BGS Report WD/05/86/5, KP&L, Ministry of Energy, Nairobi, Kenya.

Burgess, C. F.; Rosendahl, B. R.; Sander, S.; Burgess, C. A.; Lambiase, J.; Derksen, S. and Meader, N. (1987), The structural and stratigraphic evolution of lake Tanganyika. A case study of continental rifting, *American Association of Petroleum Geologists*.

Burrough, P. A. (1986), *Principles of Geographic Information Systems for Land Resources Management*, Clarendon Press, London.

Butzer, K. W.; Isaac, G. L.; Richardson, J. L. and Washbourne-Kamau, C. (1972), Radiocarbon dating of East Africa lake levels, *Science*, No. 175, pp. 1069-1076.

Carter-Bonham, C. F. (1994), *Geographic Information Systems for Geoscientists: modelling with GIS*, Pergamon, Ontario.

Chorowicz, J. (1992), The role of ancient structures in the genesis and evolution of the East African Rift. *Bull. Soc. Geol. France*, **Vol. 163,** No. 3 pp. 217-227.

Chorowicz, J. (1990), Dynamics of the different basin types in East African Rift, *Journal of African Earth Sciences*, **Vol. 10**, No. 1/2, pp. 271-283.

Chorowicz, J; Fournier, J. L. and Vidal, G. (1987), A model for rift development in East Africa, *Geological Journal*, **Vol. 22**, Thematic issue, pp. 495-513.

Chorowicz, J.; Guezlane, M.; Rudant, J. P. and Vidal, G. (1988), Analysis of the Aswa Fault zone in Kenya from Landsat MSS and MOMS-01 space imagery: Influence of Precambrian heritage on the Gregory Rift structures, *C.R. Acad. Sc. Paris*, **T. 307**, series II, pp. 83-88.

Clarke, M. C. G.; Woodhall, D. G.; Allen, D. and Darling, W. G. (1990), *Geological, volcanological and hydrological controls on the occurrence of geothermal activity in the area surrounding Lake Naivasha, Kenya*, Ministry of Energy, Nairobi, Kenya, 138 pp.

Cole, M. M.; Owen-Jones, E. S.; Custance, N. D. E. and Beaumont, T. E. (1974), Recognition and interpretation of spectral signature of vegetation from aircraft and satellite imagery in western Queensland, Australia, *Symposium European Earth Resources. Satellite Experiments, 1974 Proc. European Space Research Organization* **Spec. Pub. 100**, pp. 243-287.

Curran P. J. (1985), *Principles of Remote Sensing*, Longman Scientific and Technical, New York, 282 pp.

Delvaux, D.; Levi, K.; Kajara, R.; and Sarota, J. (1992), Cenozoic Paleostress and kinematic evolution of the Rukwa-North Malawi Rift Valley (East African Rift System). *Bull. Cetres Rech.* Explor. - Prod. Elf Aquatine. **Vol. 16**, No. 2, pp. 383-406.

D'Hoore, J.L. (1977), *Soil diagnosis through remote sensing in earth observation systems for resource management and environmental control*, Ed. Clough D. J., Plenum Press, London.

Drury, S. A. (1987), *Image Interpretation in Geology*, Allen and Unwin, London.

Elachi, C. (1980), Spaceborne Imaging Radar: Geologic and Oceanographic Applications, *Science*, **Vol. 209**, pp. 1073-1082.

Elmasri, R. and Nevathe, S. B. (1989), *Fundamentals of Database Systems*, Cummings, Redwood, Canada.

ERDAS Field Guide, (1990), National Centre for Geographic Information and Analysis, Second Edition Version 7.5, ERDAS Inc. Atlanta, USA.

Fairhead, J.D. (1976), The structure of the lithosphere beneath the Eastern Rift deduced from gravity studies, *Tectonophysics*, **Vol. 30**, pp. 269-298.

Fairhead, J. P.; Mitchell, J. G. and Williams, L. A. J. (1972), New K/Ar determination on rift volcanics of southern Kenya and their bearing on age of rift faulting, *Nature*, **Vol.238**, 83, pp. 66-69.

Fernandez, R. N. and Rusinkiewicz, M. (1993), A conceptual design of a soil database for a Geographic Information System, *Inter. Journal Geographic Information Systems*, **Vol. 7**, No. 6, pp. 525-539.

Fillippone, W. R. (1986), Practical applications of remote Sensing, *Geophysics the leading Edge of Exploration*, **Vol. 6**, No. 12, 1987, pp. 16-22.

Fitton, I. and Upton, B. G. J. (1987), Alkaline igneous rocks, *Special Publication of the Geological Society of London*, No. 30.

Furgerson, R. B. (1972), *Electrical resistivity survey of the Olkaria prospect, Kenya*, Geothermal exploration project, EAP&L, Ministry of Energy, Nairobi, Kenya.

Gaudiet, J. J. and Falconer, A. (1982), *Remote sensing for tropical freshwater bodies: The problem of floating islands on lake Naivasha*, Regional Remote Sensing Centre, Nairobi.

Gibbs, A. O. (1984), Structural evolution of extensional basin margins, *Geological society of London Jou.*, **Vol. 141**, pp. 609-620.

Girdler, R. W.; Fairhead, J. D.; Searle, R. C. and Sowerbutts, W. T. C. (1969), Evolution of Rifting in Africa, *Nature*, **Vol. 224**, pp. 1178-1182.

Goetz, A. F. H.; Billingslay, F. C.; Gillespie, A. R.; Abram, M. J.; Squires, R. L.; Shoemaker, E. M.; Luchitta, I. and Elston, D. P. (1975), *Application of ERTS images and image processing to geologic problems and geologic mapping in North Arizona*, Jet Propulsion Lab.

Goetz, A. F. H. (1976a), Remote Sensing geology - Landsat and beyond, *Caltech/JPL Conference on image processing technology, Data Sources and software for commercial and scientific purposes, Jet Propulsion Lab.*, **Spec. Publ. 43-30**, pp. 8-1 to 8-8.

Goetz, A. F. H (1976b), *Applications of remote sensing for resources exploration, present and future*, Jet Propulsion Lab.

Goetz, A. F. H. (1989), *Spectral remote sensing in Geology*, in Asrar, G., *Theory and applications of remote sensing*, John Wiley, New York, pp. 491-523.

Gregory, J. W. (1896), *The Great Rift Valley*, John Murray, London.

Griffiths, P. S. and Gibson, I. L. (1980), The geology and petrology of the Hannington trachyphonolite formation, Kenya Rift Valley. *Lithos*, **Vol. 13**, pp. 43-53.

Grimaud, P.; Richert, J. P.; Rolet, J.; Teircelin, J. J.; Xavier, J. P.; Morley, C. K.; Coussement, C.; Karanja, S. W.; Renaut, R. W.; Guern, G; le Turdu, C.; and Michel-Noel, G. (1994). Fault geometry and extension mechanisms in the Central Kenya Rift Valley, East

Africa. A 3D remote sensing approach. *Bull. Centres Rech.* Explo. - Prod. Elf Aquatine. **Vol. 18,** No. 1, pp. 59-92.

Hackman, B. D. (1988), *Geology of the Baringo-Laikipia area*, Report No. 104, Mines and Geology Department, Nairobi, Kenya.

Harris, R. (1987), *Satellite Remote Sensing, an Introduction*, Routlede and Kegan Paul, London.

Haukwa, C. B. (1986), *Interpretation of well measurements for exploration areas and reservoir changes in Olkaria East field*, Paper for Kenya Power Company, Scientific and Technical Review meeting, KP&L, Ministry of Energy, Nairobi, Kenya.

Haydn, R.; Dalke, G. W.; Henkel, J. and Bare, J. E. (1982), Application of the IHS Color Transform to the Processing of Multisensor Data and Image Enhancement. *Proceeding of the International Symposium on Remote Sensing of Arid and Semi-Arid Lands*, Cairo, Egypt, January 1982, pp. 599-616.

Hochstein, M. P. (1971), *Reinterpretation of a Resistivity Survey of the Kenyan Rift Valley between lakes Naivasha and Bogoria, Kenya.* Unpublished report to the UNDP/EAP&L Project.

Hunt, G. R. (1977), Spectral signatures of particulate minerals in the visible and near infrared, *Geophysics*, **Vol. 41**, pp. 501-513.

Ilyin, A. V.; Glukhovsky, M. Z.; Koslov, V. V.; Moralev, M. V. and Startzev, A. L. (1983), The application of space imagery to geology and mineral exploration in the U.S.S.R. - A case history, *Adv. Space Res.*, **Vol. 3**, No. 2, 1983, pp. 19-26.

Jutz, S. L. and Chorowicz, J. (1993), Geological mapping and detection of the oblique extensional structures in the Kenyan Rift Valley with a SPOT/Landsat-TM datamerge. *International Journal Remote Sensing*, **Vol. 14**, No 9, pp. 1677-1688.

Johnson, R. W. (1969), Volcanic Geology of Mount Suswa, Kenya. *Philosophical transactions of the Royal Society, London,* Series A, **Vol. 265**, pp. 383-412.

Kagasi, J. (1983), *The volcanic petrology and geological structures of Mt. Margaret and Kijabe Hill area, Kenya Rift Valley*, Unpublished Masters Thesis, Department of Geology, University of Nairobi, Nairobi, Kenya, 194 pp.

Kamau, C. (1974), *The lake Naivasha Basin*, Unpublished Report, Geography Department, University of Nairobi, Nairobi, Kenya.

Kartikeyan, B.; Majumder, K. L. and Dasgupta, A. R. (1995), An expert system for land cover classification, *IEEE Transactions on Geoscience and Remote Sensing*, **Vol. 33**, No. 1, pp. 58-66.

Keller, G. V. (1972), *Electrical Resistivity Survey of the Kenya Rift Valley.* Unpublished Report to the UNDP/EAP&L Project.

Khan, M. A., Swain, C. J. and Bishop, W. W. (1987), Structure of Kenya Rift from seismic refraction, *Nature*, **Vol. 325**, No. 6101, pp. 239-242.

Kowalik, W. S. and Glenn, W. E. (1987), Image processing of aeromagnetic data and integration with Landsat images for improved structural interpretation, *Geophysics*, **Vol. 52**, No. 7, pp. 875-884.

Labovitz, M. L.; Masuoka, E. J.; Bell, R; Siegrist, A. W. and Nelson, R. F. (1983), The application of remote sensing to geobotanical exploration for metal sulphides - result from the 1980 field session at Mineral Virginia, *Economic Geology*, **Vol. 78**, pp.750-760.

Lambiase, J. J. (1989), The Framework of African Rifting During the Phanerozoic, *Journal of African Earth Sciences*, **Vol. 8**, No. 2/3/4, pp. 183-190.

Leat, P. T. (1984), Geological evolution of the trachytic caldera volcano Menengai, Kenya Rift Valley. *J. Geol. Soc., London*, **Vol.141**, pp 1057-1069.

Lo, C. P. (1986), *Applied Remote Sensing*, Longman Scientific and Technical, New York, 393 pp.

Mahon, W. A. J. (1972), *The general geochemistry of the Rift Valley of Kenya; Lake Baringo to Lake Magadi and the Geochemistry of Olkaria, Eburru and Lake Hannington Geothermal Prospects*, Unpublished Paper to Technical Review Meeting, UNDP, Nairobi, Kenya.

Mason, J. E. (1967), *Geothermal occurrence and investigations in Central Rift Valley, Kenya* Unpublished Report, Mines and Geology Department, Nairobi, Kenya.

Matheson, F. J. (1966), *Geology of the Kajiado area*, Report No. 70, Geological Survey of Kenya, Nairobi Kenya, 51 pp.

McCall, G. J. H. (1967), *Geology of the Nakuru - Thomson's Falls-Lake Hannington area*, Report No. 78, Geological survey of Kenya, Nairobi, Kenya, 122 pp.

Meidav, T. (1972), *Further Interpretation of Resistivity data and Recommendation for follow-up work, Kenya Geothermal Exploration Project.* Unpublished Report to the UNDP/EAP&L Project.

Microstation II-32/pc 2D Graphics Training Course Guide, (1991), Intergraph Corporation, Huntsville, Al, USA.

Microstation I-32 2D Graphics Training Course Guide, (1992), Intergraph Corporation, Huntsville, Al, USA.

Microstation GIS Environment/ImageStation Imager-2 (MGE/ISI) User's Guide (1992), Intergraph Corporation, Huntsville, Al, USA.

Microstation GIS Environment Projection Manager (MSPM) operator training Guide (1991), Intergraph Corporation, Huntsville, Al, USA.

Microstation GIS Environment Terrain Modeler (MSM) reference manual, (1991), Intergraph Corporation, Huntsville, Al, USA.

Miller, J. B. (1975), Landsat images as applied to petroleum exploration in Kenya, *NASA Earth Resources Survey Symposium, NASA TM X 58168*, **Vol. 1-B**, pp. 605-624.

Morley, C. K.; Nelson, R. A.; Patton, T. L. and Munn, S. G. (1990), Transfer Zones in the East African Rift System and their relevance to Hydrocarbons Exploration in Rifts, *The American Association of Petroleum geologists Bulletin*, **Vol. 74**, No. 8, pp. 1234-1253.

Nash, W.P.; Carmichael, I. S. E.; and Johnson, R. W. (1969), The Mineralogy and Petrology of Mt Suswa, Kenya. *Journal of Petrology*, **Vol.10**, pp. 409-439.

Naylor, W. I. (1972), *Geology of the Eburru and Olkaria Geothermal prospects*, UNDP/EAP&L, Geothermal Exploration Project, Ministry of Energy, Nairobi, Kenya.

Nderitu, J. G. (1993), *A Comparative Study of Resistivity Models from Menengai and Olkaria Geothermal Prospects*. Unpublished Masters Thesis, Department of Geology, University of Nairobi, Nairobi, Kenya, 177 pp.

Ndombi, J. M. (1981), The structure of the shallow crust beneath Olkaria geothermal field, Kenya, deduced from gravity studies, *Journal Volcanology, Geothermal Resources*, **Vol. 9**, pp. 237-251.

Noble, J. W and Ojiambo, S. B. (1976), Geothermal Exploration in Kenya, *Proceedings of 2nd UN Symposium on development and use of Geothermal Energy*, UNDP/EAP&L Project, Nairobi, Kenya, **Vol. 1.**, pp. 189-204.

Norconsult, A.S. (1977), *Remote Sensing for Transport Planning and Highway Engineering: Pilot Project in North Kenya and South Sudan*, Report for Ministry of Transport and Communication, Nairobi, Kenya.

Nyambok, I. O. (1985), Evolution of the East African rift system with special emphasis on the central rift of Kenya: a new model, *Kenya Journal of science and Technology*, **series A**, 6(2), pp. 83-90.

Nyamweru, C. K. (1977), The Ol Njorowa Gorge, Lake Naivasha Basin, Kenya. In *Desertic Terminal lakes: Proceedings from international conference on Desertic Terminal Lakes, Weber State College Ogden, Utah 84408 May 2-5, 1977*, pp. 297-307.

Nyamweru, C. (1980), *Rifts and Volcanoes: A Study of the East African Rift Systems*, Nelson Africa.

Odhiambo, B.D.O. (1988), *A Geobotanical study around the Fluorite Mineralization in Kerio Valley, Kenya.* Unpublished Masters Thesis, Department of Geology, University of Nairobi, Nairobi, Kenya, 107 pp.

Odongo, M. E. O. (1982), Petrography of well samples from the Olkaria Geothermal Field - Its use as a tool in geothermal resources development, *Proceedings of the regional seminar on geothermal energy in East and South Africa, UNESCO/USAID, Nairobi, Kenya*, pp. 76-79.

Onacha, S. A. (1989), *An Electrical Resistivity Study of the area between Suswa and Olkaria Geothermal Field, Kenya*, Unpublished Masters Thesis, Department of Geology, University of Nairobi, Nairobi, Kenya, 181 pp.

Onywere, S. M. (1990), *Application of remote sensing techniques in geological mapping of the Nairobi - Kajiado - Machakos area*, Unpublished Masters Thesis, Department of Geology, University of Nairobi, Nairobi, Kenya, 126 pp.

Onywere, S. M. and Gaciri, S. J. (1993), Application of satellite remote sensing techniques in land use and land cover pattern analysis of Nakuru-Nyahururu area, *Proceedings of the International Geoscience and Remote Sensing Symposium (IGARSS'93): Better understanding of the earth environment*, 18-22 August 1993, Kogakuin University, Tokyo, Japan, pp. 927.

Pratt, W. K. (1977), *Digital Image Processing*, John Wiley and Sons, New York.

Pulfrey, W. (1960), *Shape of the Sub-Miocene erosion level in Kenya*, Bulletin 3, Geological Society of Kenya, Nairobi, Kenya.

Richards, J. A. (1986), *Remote sensing digital image analysis*, Springer-Verlay, New York, 281 pp.

Richardson, J. L. (1966), Changes in level of Lake Naivasha, Kenya, during postglacial times, *Nature, London*, **Vol. 209**, No. 5020, pp. 290-291.

Richardson, J. L. and Richardson, A. E (1972), History of an African Rift Lake and its climatic implications, *Eclo. Monogr.*, **421**, pp. 499-534.

Saad, M. A. (1979), *The Use of Landsat Imagery and Computer Compatible Tapes for the study of Temporal Change in a portion of the Meghna River Bangladesh*, Visiting International Scientists Program (VISP) Remote Sensing Institute, SDSU - USA.

Sabins, F. F. Jr. (1986), *Remote Sensing, Principles and Interpretation*, Second Edit. W. H. Freeman and Company, New York.

Saggerson E. P. (1991), *Geology of Nairobi area*, Report No. 98. Geological Survey of Kenya, Nairobi, Kenya.

Scott, S. C. (1980), The Geology of Longonot Volcano, Central Kenya; A question of volumes, *Phil. Trans. Roy. Soc. London.*, **Vol. 296**, 1420, pp. 437-465.

Scott, S. C. and Bailey, D. K. (1986), Co-eruption of contrasting magmas and temporal variations in magma chemistry at Longonot, Central Kenya, *Bulletin of Volcanology.*

Scott, R. M.; Webster R., and Lawrence, C. J. (1971), *Land System Atlas of Western Kenya*, Christchurch Hampshire England.

Short, M. N. (1982), *Landsat Tutorial Workbook: Basics of Satellite Remote Sensing*, US Government Printing Office, Washington D.C., 553 pp.

Siegel B. S.; and Gillespie, A. R. (1980), *Remote Sensing in Geology*, John Wiley and Sons, New York.

Skinner, N. J. (1977), Recent Geophysical Studies of the Kenya Rift Valley. *Contemp. Phys.* pp. 455-470

Smith, M. and Mosley, P. (1993), Crustal heterogeneity and basement influence on the development of the Kenya Rift, East Africa. *Tectonics,* **Vol. 12,** No. 2, pp 591-606.

Sutherland, D. S. (1974), Petrography and Mineralogy of peralkaline silicic rocks, *Bulletin Volcanology*, **Vol. 38**, pp. 517-547.

Swain, C. J., Afthab Khan, A., Wilton T. J., Maguire, P. H. K, Griffiths, P. H. (1981), Seismic and gravity surveys in the lake Baringo, Tugen Hills area, Kenya Rift Valley. *J. Geol. Soc. London*, **Vol. 138**, pp. 93-102.

Thomas, I. L; Benning, V. M and Ching, N. P. (1987), *Classification of Remotely Sensed Images*, Adam Hilger, Bristol, 268 pp.

Thompson, A. O. and Dodson, R. G. (1963), *Geology of Naivasha area*, Report No. 55 Geological Survey of Kenya, Nairobi, Kenya, 80 pp.

Thompson, A. O. (1964), *Geology of Kijabe area*, Report No. 67, Geological Survey of Kenya, Nairobi, Kenya, 52 pp.

Tobin, D. G.; Ward, P. L. and Drake, C. l. (1969): Micro-earthquakes in the rift valley of Kenya, *Geological Society of America Bulletin*, **Vol. 80**, pp. 2043-2046.

Torfeson, H. (1987), *Geothermal and Geological Survey of Mt. Suswa*, Unpublished Technical Report KEN/82/002, UNDP/DTCD, Nairobi, Kenya, 64 pp.

Washbourne-Kamau, C. K. (1971), Late Quaternary Lakes in the Nakuru-Elmenteita basin, Kenya, *Geographical Journal*, **Vol. 137**, pp. 522-535.

Washbourne, C. K. (1967), Lake Levels and Quaternary Climates in the Eastern Rift Valley of Kenya. *Nature*, **Vol. 216**, pp. 672-763.

Wendlandt, R. F. and Morgan, P. (1982), Lithosphere thinning associated with rifting in East Africa, *Nature, London*, **Vol. 298**, pp. 734-736.

Williams, L. A. J.; MacDonald, R. and Leat, P. T. (1983), Magmatic and structural evolution of the central part of the Kenya Rift, *Proceedings of the Regional Seminar on Geothermal Energy in Eastern and Southern Africa*, UNESCO/USAID, Nairobi, Kenya, pp. 61-67.

Wilsher, W.; Neicker, I; Wullshleger, N.; Herbert, R.; de Wit, M. J.; and Vitali, E. (1993), Towards Intelligent Spatial Computing for earth Sciences, *South Africa Journal of Sciences*, **Vol 89**, pp. 315-323.

* * * *

APPENDICES

Appendix 2.1: Records of various fault azimuths in the Aberdare Detachment.The azimuths are in degrees (bearing reading) measured from the north. Rose diagram plots are shown at the end of the records.

(a) 288 records of fault azimuths in Lake Bogoria Block.

7.2	23.3	157.2	17.5	21.1	10.1	133.9	0.1	156.7	3.7
12.7	14.7	14.5	6.8	165.6	171.3	136.2	160.1	19.6	0.4
170.9	0.0	177.0	3.4	25.6	154.6	160.1	159.4	0.0	2.1
177.7	29.2	38.6	4.1	0.1	144.6	71.0	32.7	0.0	167.2
12.1	13.2	169.2	1.9	11.3	26.2	53.9	158.2	0.0	157.5
2.7	168.7	159.1	12.8	176.5	142.0	10.9	0.9	174.0	65.8
147.5	24.0	174.0	4.1	7.8	16.8	8.3	169.7	2.4	32.7
4.2	0.0	1.0	1.1	18.0	156.9	2.7	162.6	23.5	169.4
22.4	166.3	0.0	2.4	1.4	0.1	172.2	17.6	10.6	30.6
17.3	173.8	13.2	41.1	13.6	174.1	154.1	0.0	4.9	12.4
0.0	162.6	15.4	4.5	14.0	160.5	145.0	176.5	133.9	3.9
174.8	3.9	14.4	5.5	12.7	0.8	165.6	1.8	173.7	3.2
165.3	0.0	171.7	1.7	27.0	148.9	24.6	4.6	171.5	170.6
1.4	22.6	167	0.9	24.0	172.4	127.4	0.0	7.1	0.4
1.2	171.1	4.0	9.9	11.1	154.3	15.6	177.0	7.5	9.9
164.6	173.1	1.6	10.6	6.8	16.0	162.6	1.4	4.3	7.1
47.8	177.4	15.9	163.8	6.1	163.1	0.7	166.1	23.3	1.7
166.9	177.8	14.1	158.0	24.7	172.8	17.1	1.0	43.2	8.7
154.6	0.6	140	155.2	172.3	5.3	156.3	19.1	175.8	7.0
13.1	40.1	169.7	10.4	174.2	0.6	29.5	7.6	171.1	0.1
33.1	15.2	0.0	160.4	10.3	159.2	24.7	7.5	27.0	164.2
2.3	8.2	176.0	171.5	7.8	10.2	0.4	21.4	8.7	9.4
3.9	142.9	16.0	176.4	166.6	6.4	153.9	30.0	10.6	161.1
0.0	7.9	162.3	163.2	175.9	4.3	160.0	131.4	6.9	7.1
170.5	11.3	13.6	157.2	12.4	8.4	164.6	165.1	161.1	1.8
165.4	163.7	17.6	177.1	23.4	8.4	6.4	0.9	4.9	6.4
26.8	154.5	157.2	1.5	1.0	153.7	0.0	6.5	12.7	2.9
15.2	138.2	158.2	3.4	16.5	9.8	161.7	172.2	152.7	177.0
149.6	11.8	28.1	3.6				16.6		
6.8	14.5	1.0							

(b) 579 records of fault azimuths in the Lake Nakuru area

170.1	158.7	21.3	108.3	0.6	168.4	1.2	21.6	141.5	128.4	21.5	138.7
11.3	160.3	24.1	169.6	21.1	178.3	176.2	20.3	5.4	39.7	148.1	96.9
173.7	173.3	46.2	4.9	175.0	170.0	18.9	153.6	8.1	36.9	3.5	130.1
149.6	164.9	26.2	174.2	149.0	156.8	24.9	29.9	22.5	133.8	3.5	4.8
170.5	146.8	141.2	8.4	140.3	8.9	27.1	12.4	167.2	158.1	0.9	164.7
153.8	157.5	128.8	0.2	174.9	0.4	120.7	30.3	169.2	36.4	19.5	169.8
16.9	158.2	148.7	170.5	118.3	172.2	3.4	175.0	137.1	35.4	24.8	151.5
6.7	175.3	148.3	159.9	154.5	3.2	0.4	4.0	112.7	152.1	1.1	169.6
142.5	171.0	168.4	1.8	158.3	160.2	2.3	4.1	105.9	21.9	8.7	156.1
6.2	171.6	27.9	149.8	145.2	172.2	26.0	17.4	163.8	15.2	7.1	159.5
172.3	168.2	151.4	137.6	160.7	163.3	134.3	170.3	173.8	11.7	171.0	162.4
147.6	173.3	1.6	153.7	139.3	15.0	4.6	170.7	10.4	149.2	11.9	171.5
27.1	137.8	179.2	176.3	162.5	122.2	1.0	168.8	178.7	170.9	179.1	5.8
126.5	143.8	160.1	150.6	13.5	169.9	20.3	4.0	161.4	170.5	2.2	38.5
123.0	12.2	6.3	36.2	149.2	167.7	29.2	6.4	158.9	120.1	4.7	2.2
0.5	154.7	5.4	9.6	5.2	171.4	51.3	14.7	0.9	172.5	1.0	14.5
4.8	174.9	172.6	3.4	11.3	176.0	29.9	46.6	29.3	164.6	178.9	6.9
174.0	168.9	171.0	162.0	2.2	159.4	3.6	174.6	141.8	54.7	137.3	9.0
161.7	172.0	5.2	179.6	175.0	171.7	171.1	172.7	8.9	149.3	24.7	8.1
160.3	3.5	21.0	1.8	173.5	168.4	159.1	3.9	107.8	143.8	163.3	2.1
164.9	155.2	1.0	161.2	4.5	165.1	172.9	125.6	89.4	10.8	8.0	163.5
165.3	70.1	4.9	2.0	14.0	163.0	163.0	12.6	7.7	141.9	165.7	5.1
176.3	17.1	12.7	178.2	6.3	19.3	174.3	162.4	4.3	7.4	122.0	11.8
167.6	44.3	59.1	5.1	169.0	167.1	3.0	155.3	132.4	120.1	141.7	13.7

22.4	30.2	174.3	173.7	13.7	141.6	4.8	76.2	159.4	144.7	151.1	171.3
11.6	5.0	154.6	115.8	7.8	161.6	102.1	166.6	152.6	171.2	13.0	8.7
13.6	172.8	35.8	69.8	24.9	155.3	109.7	51.0	62.1	22.1	177.8	176.8
7.8	169.2	39.3	151.8	169.2	165.6	2.3	145.6	15.5	169.4	27.7	15.1
139.9	161.5	10.4	166.2	17.5	172.4	156.5	128.4	18.9	0.9	17.5	156.7
136.3	48.5	24.7	138.9	3.5	35.5	26.2	137.1	156.3	11.1	7.2	8.7
3.6	0.4	176.7	149.6	161.6	156.3	27.2	150.8	156.3	166.7	155.9	2.3
2.1	173.4	162.8	154.7	15.4	145.6	32.6	160.3	9.8	0.4	2.4	4.0
175.2	25.4	160.0	146.1	0.5	139.7	24.8	160.6	163.8	175.0	21.1	6.7
160.7	170.1	149.8	168.0	0.9	6.1	106.4	151.9	164.2	154.9	158.9	155.5
157.6	168.4	162.0	5.1	161.7	160.6	2.1	151.3	15.6	159.9	5.2	162.7
153.2	149.9	41.4	166.7	155.9	151.8	167.0	154.1	15.6	146.0	0.4	172.8
155.3	156.5	1.0	161.5	171.7	154.7	172.8	141.8	171.5	4.4	20.0	129.9
156.6	5.6	159.9	38.7	21.8	160.6	157.8	149.2	140.8	1.1	173.6	176.3
36.1	7.3	49.8	44.5	16.2	145.7	126.0	142.0	171.9	13.4	9.1	2.8
32.6	172.4	4.6	126.3	0.9	161.9	34.0	115.9	64.7	169.9	3.3	5.3
50.7	163.8	140.4	132.6	29.5	39.4	147.1	22.9	80.2	178.3	12.2	
40.4	7.1	163.7	164.0	11.7	27.2	147.8	0.8	156.9	6.7	162.7	
167.7	153.2	135.8	23.2	156.5	32.5	25.8	10.3	136.2	175.0	40.7	
172.4	5.4	7.0	168.6	160.8	165.6	1.8	157.2	138.3	171.0	2.9	
169.2	16.9	11.9	145.2	170.4	158.6	123.6	171.3	159.9	157.0	3.6	
171.9	21.4	168.3	22.2	1.1	153.4	151.5	173.9	150.7	18.8	151.1	
134.0	143.9	166.9	157.9	174.8	145.4	20.0	26.7	151.4	166.0	37.4	
153.7	164.0	139.9	5.4	7.5	157.8	149.8	163.4	166.7	30.5	156.6	
152.5	152.1	167.6	3.6	140.8	129.1	170.7	6.8	172.5	175.0	167.0	

(c) 426 records of fault azimuths in the Lake Naivasha area

0.4	175.2	156.3	176.6	161.3	164.0	29.4	169.4	3.3	51.6
157.4	45.5	161.5	0.5	39.5	21.9	42.2	174.3	1.9	4.8
3.9	28.8	11.8	1.8	173.5	78.2	41.8	85.7	20.5	132.3
175.1	36.5	3.4	33.2	22.2	93.0	25.6	2.7	112.8	172.7
174.9	165.5	5.9	159.0	0.3	9.3	125.7	8.2	39.6	10.2
5.2	142.6	178.5	3.1	175.2	3.4	137.4	159.8	32.9	36.5
14.9	2.4	9.9	16.1	151.5	2.4	121.9	91.8	172.1	158.8
1.0	166.2	30.5	173.1	19.9	157.6	156.1	165.4	0.6	82.9
16.6	24.1	20.8	37.2	70.0	13.6	160.3	167.5	134.8	169.1
13.3	169.8	6.7	147.3	173.4	3.8	149.5	90.6	47.9	174.5
46.8	171.7	179.2	159.9	113.0	0.5	0.1	150.7	160.9	145.1
169.4	178.2	162.7	70.7	117.6	2.1	39.7	2.5	27.1	20.4
1.9	145.9	48.3	57.4	151.9	155.8	18.9	161.0	4.8	171.9
161.2	20.7	5.9	171.9	157.1	3.2	177.2	162.7	15.4	173.2
179.4	176.5	6.3	153.9	114.2	152.6	118.6	154.7	156.6	48.6
7.1	6.3	4.2	137.3	8.2	22.1	155.5	156.4	8.1	133.2
148.1	0.9	5.6	76.5	19.7	6.6	133.6	1.7	0.6	2.2
85.0	170.5	14.9	116.25	160.8	7.7	125.5	140.0	15.2	138.9
4.3	178.5	176.0	140.8	142.1	46.6	41.9	159.5	96.6	144.4
6.6	176.5	0.5	55.9	173.4	27.2	167.8	4.0	89.2	169.6
27.8	174.3	13.8	17.0	157.0	165.5	170.3	17.4	75.5	0.2
20.8	27.4	136.9	32.4	31.4	157.6	172.4	10.7	63.5	7.9
10.8	61.8	5.1	123.5	155.0	31.6	168.7	126.7	173.2	130.9
26.6	50.9	4.9	4.5	131.9	48.4	158.9	8.4	8.1	10.5
173.9	4.9	4.0	162.6	138.5	174.6	120.1	174.5	173.8	8.2
13.8	41.7	5.5	30.9	132.9	81.2	8.9	162.3	177.5	38.8
4.3	142.8	8.2	17.2	136.6	3.7	147.1	106.6	176.2	5.6
7.9	148.1	151.3	13.4	171.9	5.3	24.0	162.0	174.4	165.9
25.4	150.5	175.1	19.3	155.2	13.7	155.7	0.6	3.2	100.2
166.1	150.5	10.3	24.6	16.0	0.8	164.7	7.9	0.8	143.7
24.1	176.6	10.2	128.6	132.7	171.2	16.3	2.7	14.4	161.8
7.3	43.1	4.2	38.5	168.9	175.2	162.8	3.2	13.7	
13.6	146.6	0.7	6.7	169.2	153.7	163.3	2.2	12.0	
11.6	174.6	0.5	155.9	134.3	178.0	172.5	6.7	13.4	
4.2	130.9	18.2	160.9	3.6	171.2	0.7	154.7	6.6	
160.1	4.7	6.9	65.3	146.4	167.8	14.7	3.6	4.2	
168.4	5.9	2.5	158.5	140.3	0.4	142.5	14.1	19.9	
164.1	0.5	85.2	134.6	154.0	147.6	172.6	35.6	6.5	
112.2	3.7	12.0	166.3	5.4	1.0	15.2	4.5	0.6	
4.4	2.1	177.2	172.0	40.4	52.0	164.2	0.6	9.6	
143.3	1.2	157.9	168.9	24.3	129.6	6.4	164.4	167.4	
135.7	5.5	8.8	32.8	8.2	163.9	3.6	134.3	10.0	
35.9	5.8	5.4	63.1	7.7	2.2	6.1	167.8	59.7	
131.2	166.2	172.8	24.9	69.2	163.6	162.7	166.		

(d) 688 records of fault azimuths in the Solai-Subukia block (Olobanita Nyahururu area)

31.1	135.0	7.6	12.5	175.0	15.7	29.0	21.7	5.2	18.7	26.9	20.9
24.1	24.4	179.0	2.5	0.8	44.5	24.0	32.0	7.7	20.5	40.0	35.2
6.6	171.1	0.5	165.4	101.2	23.0	13.3	170.6	34.8	52.6	17.7	7.7
25.6	32.8	.4	14.1	172.2	30.6	17.0	174.0	149.9	29.5	69.4	130.2
14.1	5.5	14.5	145.5	2.2	157.8	2.1	0.0	161.4	24.7	19.8	135.9
25.5	97.7	21.6	2.0	2.1	19.8	30.1	4.5	162.1	29.6	17.5	8.3
19.3	15.1	12.4	0.8	9.5	26.9	20.5	0.9	169.3	179.2	107.2	24.3
24.7	118.5	28.5	172.6	138.0	19.1	14.4	4.5	4.2	140.7	72.5	61.4
21.8	114.3	164.4	48.4	4.5	20.9	24.6	4.2	19.0	10.4	172.6	63.1
90.9	17.7	17.6	21.5	45.3	11.3	130.8	4.3	32.6	134.7	50.8	54.8
5.1	174.1	23.6	8.8	175.1	18.5	23.6	13.1	1.6	133.3	41.3	48.6
9.1	2.4	2.2	6.6	4.7	102.0	122.9	160.0	27.6	27.2	66.2	74.1
18.5	5.3	5.7	137.7	37.4	12.3	13.1	142.9	24.2	17.7	170.7	75.5
132.8	21.3	3.2	102.0	12.6	16.9	44.0	175.1	15.8	26.8	166.7	2.8
22.2	161.1	16.4	121.0	1.0	13.2	11.2	0.5	17.3	28.5	53.3	32.2
14.9	178	14.3	162.5	2.0	40.1	119.2	42.1	6.9	13.7	138.7	33.5
153.7	172.1	168.3	177.7	15.6	28.8	4.6	28.2	162.5	12.3	37.0	12.8
21.6	179.2	174.2	166.6	4.5	0.9	23.5	55.9	18.9	8.2	67.5	15.8
30.9	154.4	171.4	142.4	5.0	48.3	20.7	4.6	0.8	6.2	11.8	88.8
38.3	2.2	171.0	10.7	177.6	170.7	9.7	20.2	17.7	17.1	176.3	70.6
36.7	6.0	17.2	9.6	8.7	25.4	15.6	150.6	39.2	14.1	41.8	7.3
27.3	21.2	172.7	116.0	25.0	149.3	23.5	11.2	34.8	36.8	13.8	92.4
30.0	22.1	22.3	163.7	22.8	87.4	11.9	12.3	0.8	32.5	145.6	16.8
60.2	157.0	41.6	4.7	13.3	172.5	10.2	168.8	125.4	27.2	66.7	19.7
28.7	11.6	12.3	164.0	26.1	29.3	14.8	43.0	16.8	17.3	169.7	27.9
4.2	37.6	4.2	143.3	2.1	14.5	24.8	29.1	163.0	24.2	53.0	78.0
0.6	158.1	13.6	3.5	2.0	20.8	42.7	3.5	20.0	86.3	21.6	123.2
10.6	37.6	2.0	5.0	22.9	11.2	30.4	23.6	39.1	17.8	156.0	58.5
111.0	179.1	7.3	3.5	36.4	0.6	8.1	28.6	1.9	41.0	18.5	58.7
139.6	21.5	0.0	5.4	1.0	27.2	25.3	7.6	19.6	16.2	140.5	31.9
131.5	78.9	22.0	18.4	166.9	25.3	16.0	33.7	21.1	24.3	1.2	27.3
34.8	86.9	24.7	163.8	165.1	20.1	13.8	11.8	23.2	21.3	4.8	150.5
40.8	27.0	32.8	175.1	178.0	20.4	13.5	171.8	8.4	36.8	2.2	21.2
110.8	152.4	41.2	15.4	161.5	14.3	32.6	22.4	26.7	153.0	3.8	175.1
120.9	4.7	32.9	5.0	18.0	23.1	9.3	9.2	70.7	110.0	0.4	166.4
29.6	0.8	56.5	161.9	0.9	6.0	3.4	30.1	159.2	130.0	3.5	0.9
24.2	6.7	0.6	0.5	6.4	27.5	42.7	59.3	158.5	175.2	147.6	1.0
19.2	112.4	166.2	17.6	15.7	10.6	7.6	38.8	165.9	13.3	24.2	10.0
21.2	172.1	19.5	2.8	40.9	32.1	19.1	19.1	26.5	163.3	174.3	0.5
67.5	17.1	26.0	39.3	26.8	178.0	27.9	13.7	7.7	0.4	171.9	157.0
24.3	8.9	6.6	171.1	175.7	24.1	36.0	17.8	19.7	0.5	13.9	4.8
26.1	152.1	177.5	4.4	0.4	24.1	0.4	174.4	24.2	145.1	24.2	42.1
12.4	144.2	5.8	13.9	21.1	23.2	12.4	9.9	75.8	170.0	13.8	47.6
19.4	56.0	147.0	178.0	155.1	3.6	10.2	1.8	56.1	47.2	16.0	2.2
3.5	168.8	0.4	170.4	25.6	17.0	23.5	20.1	26.5	152.2	24.9	157.5
135.8	2.4	28.1	25.7	13.2	25.3	14.6	16.8	19.2	148.0	172.8	1.8
146.2	4.0	147.6	25.1	151.5	32.2	15.1	29.5	11.7	126.0	16.5	9.7
99.0	17.5	1.2	9.9	28.1	1.7	37.1	23.6	51.6	174.1	5.2	9.4
0.7	168.3	121.5	179.2	151.1	0.5	30.2	21.6	178.6	100.1	21.9	27.5
151.6	168.4	2.8	125.7	8	30.5	0.5	19.8	7.3	4.1	43.6	29.5
157.6	0.0	149.6	10.5	168.9	18.9	17.4	16.9	6.6	116.5	141.7	27.0
0.8	154.2	155.4	22.3	27.1	27.0	12.3	63.1	29.7	0.9	163.6	18.0
41.4	172.8	157.4	6.1	32.1	34.0	18.5	25.5	26.5	12.9	132.9	5.1
69.9	1.8	167.1	34.9	9.0	17.51	29.1	53.6	23.4	2.3	41.1	18.9
0.4	142.9	5.7	7.1	2.2	71.0	46.7	113.5	103.8	147.1	155.9	157.0
178.2	147.2		167.4	6.6	158.6	138.4	163.6	144.3	5.7	164.9	22.8
145.2	159.8		126.9		159.9	169.2	13.6	145.7	15.3	133.9	0.5
144.8	156.6		118.4			138.5		22.0	9.6	159.4	167.0

Rose diagrams accompanying the tables (pp. 176-179) of records of faults azimuth in the Aberdare Detachment.

(a) Rose diagram depicting azimuth frequencies of faults in the Lake Bogoria Block.

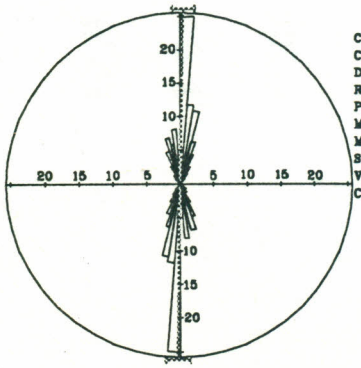

Calculation method ... Frequency
Class Interval .....5 Degrees
Data Type ..... Bidirectional
Rotation Amount ..... 0.0 Degrees
Population 286
Maximum Percentage . 23.8 %
Mean Percentage ..... 4.2 %
Standard Deviation .... 5.20 %
Vector Mean ..... 0.96 Degrees
Confidence Interval .... 4.12 Degrees.

(b) Rose diagram depicting azimuth frequencies of faults in the Lake Nakuru area. These fault trends reflect the general azimuth of faults in the Sattima-Mau Block.

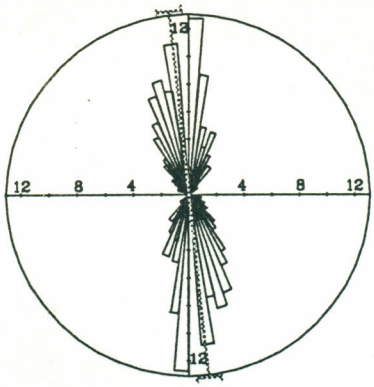

Calculation Method ... Frequency
Class Interval ..... 5 Degrees
Data Type ..... Bidirectional
Rotation Amount ..... 0.0 Degrees
Population 579
Maximum Percentage . 11.9 %
Mean Percentage ..... 2.9 %
Standard Deviation ..... 3.17 %
Vector Mean ..... 353.38 Degrees
Confidence Interval ..... 4.03 Degrees

(c) Rose diagram depicting azimuth frequencies of faults in the Lake Naivasha area.

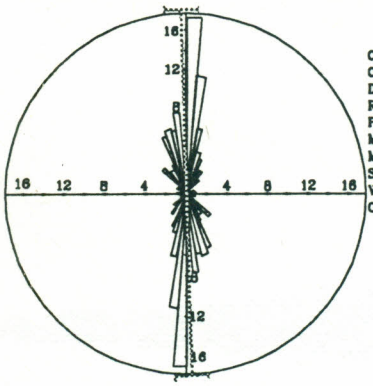

Calculation Method ... Frequency
Class Interval ..... 5 Degrees
Data Type ..... Bidirectional
Rotation Amount ..... 0.0 Degrees
Population 426
Maximum Percentage .. 16.0 %
Mean Percentage ..... 2.8 %
Standard Deviation ..... 3.25 %
Vector Mean ..... 356.19 degrees
Confidence Interval ..... 5.56 Degrees

(d) Rose diagram depicting azimuth frequencies of faults in the Solai-Subukia Block.

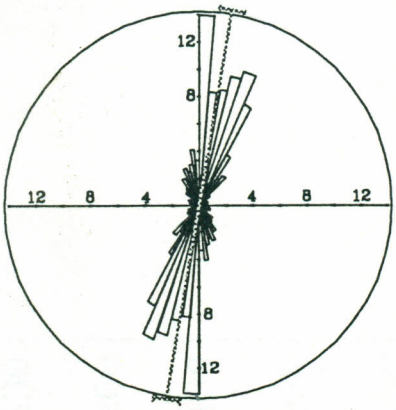

Calculation Method .. Frequency
Class Interval ..... 5 Degrees
Data Type ..... Bidirectional
Rotation Amount ..... 0.0 Degrees
Population 688
Maximum Percentage . 13.4 %
Mean Percentage ..... 2.9 %
Standard Deviation ..... 3.30 %
Vector Mean ..... 10.30 Degrees
Confidence Interval ..... 4.11 Degrees

Appendix 3.1

Image Histograms of original TM data of Nakuru–Menengai area (Image File TMS4.LAN). The data represent the statistics of unstretched bands and show a plot of pixel values (digital number–DN) representing discrete values on a grey scale.

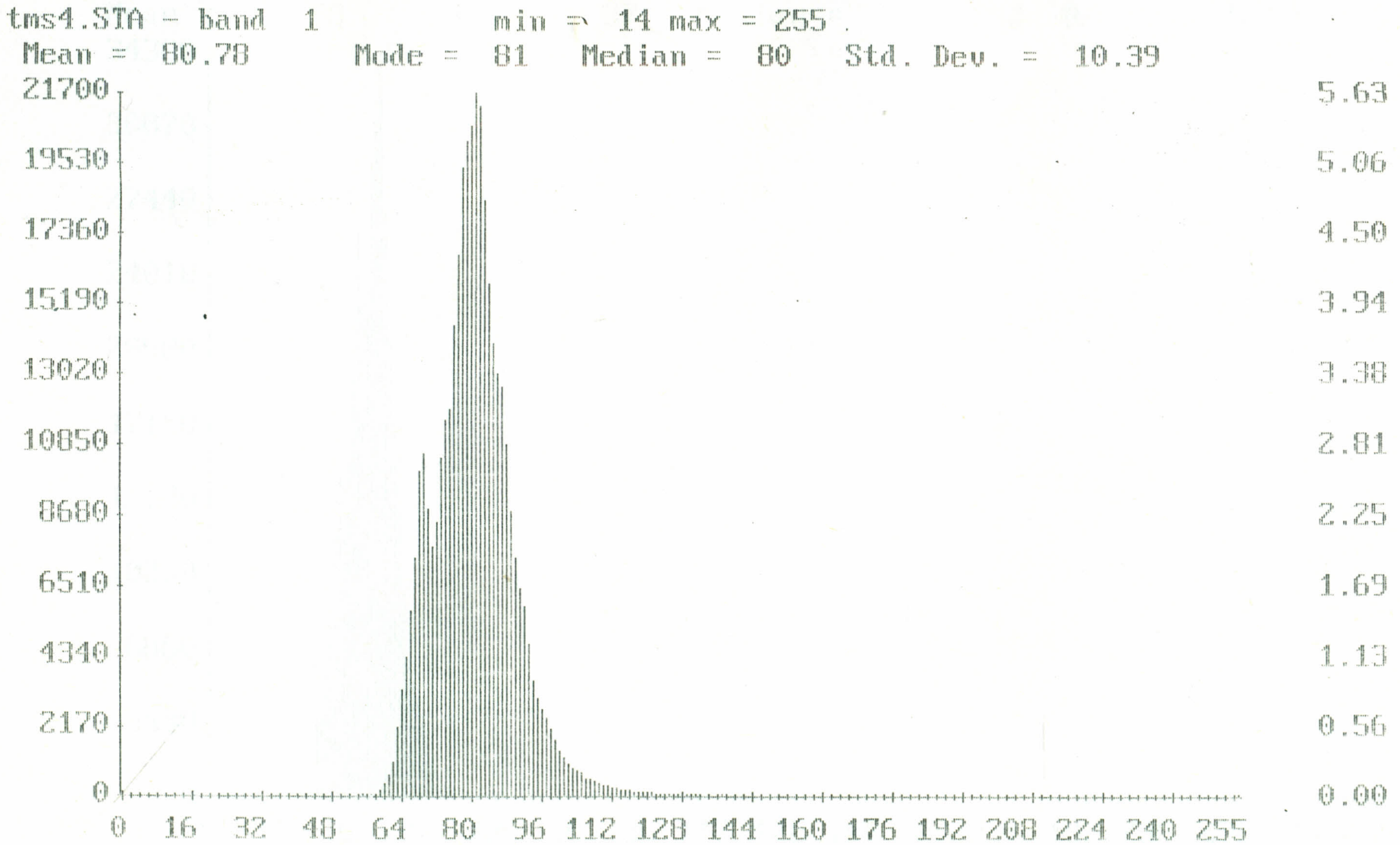

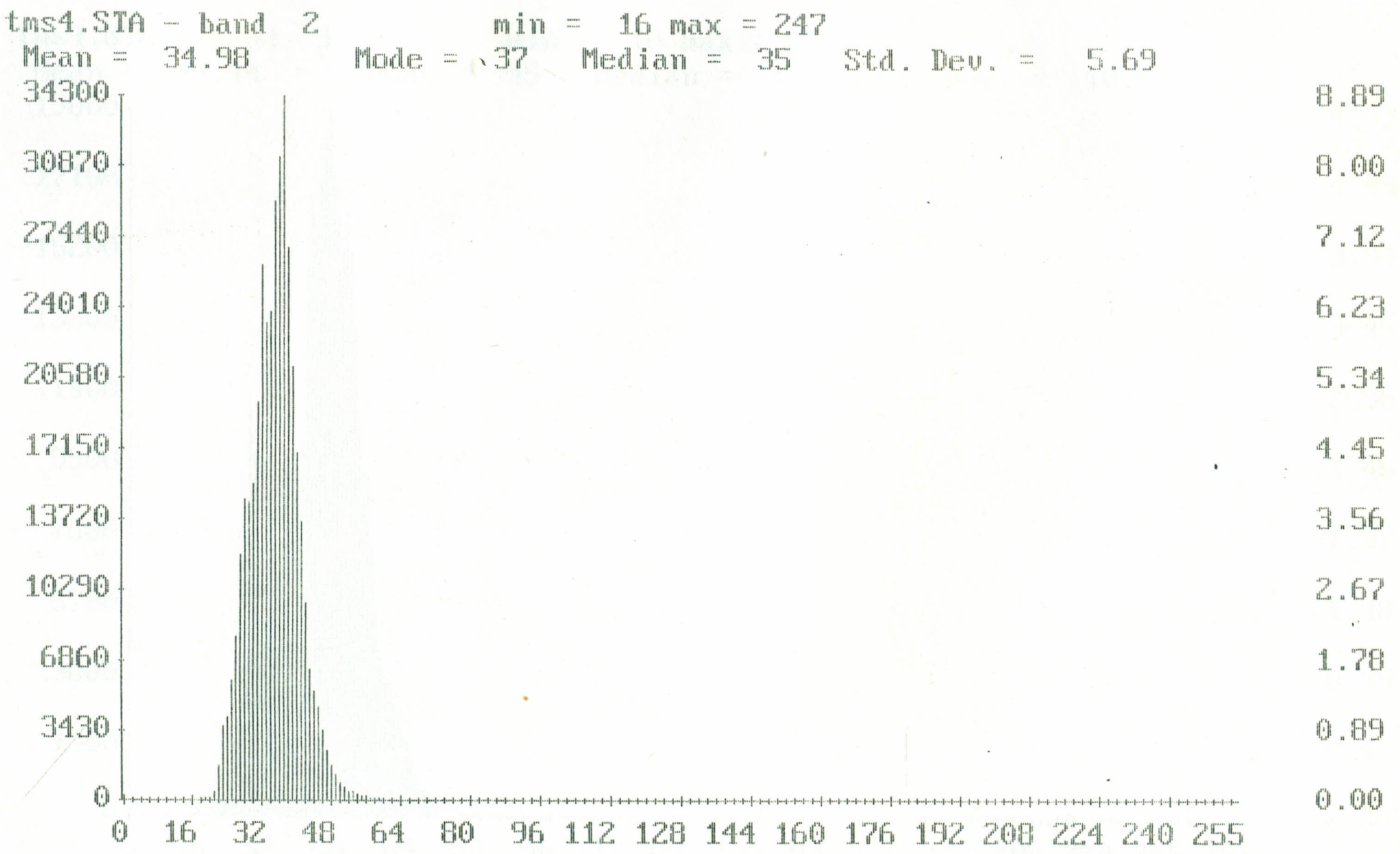
tms4.STA - band 2
min = 16 max = 247
Mean = 34.98
Mode = 37
Median = 35
Std. Dev. = 5.69
34300
30870
27440
24010
20580
17150
13720
10290
6860
3430
0
8.89
8.00
7.12
6.23
5.34
4.45
3.56
2.67
1.78
0.89
0.00
0 16 32 48 64 80 96 112 128 144 160 176 192 208 224 240 255

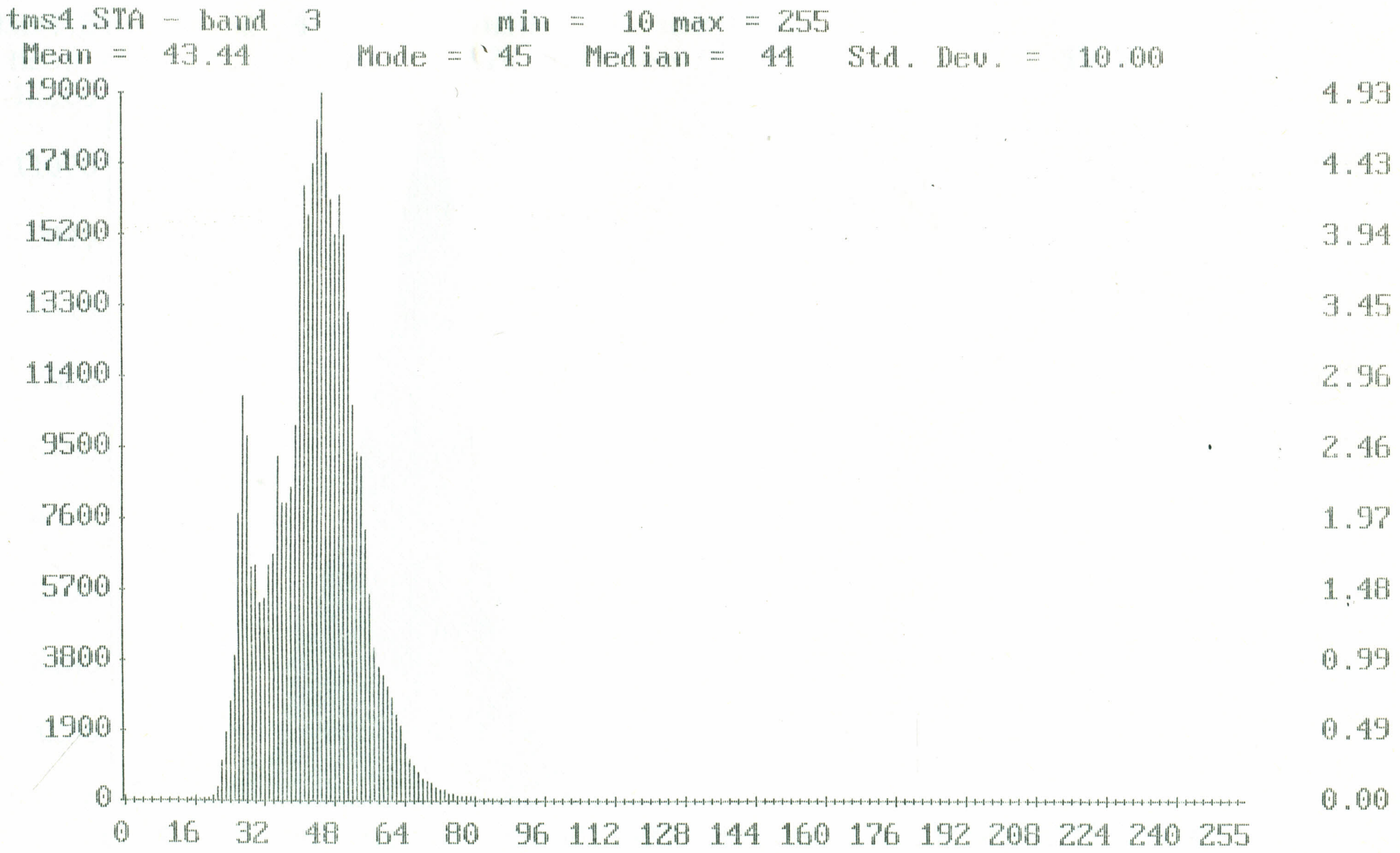
tms4.STA - band 3
min = 10 max = 255
Mean = 43.44
Mode = 45
Median = 44
Std. Dev. = 10.00
19000
17100
15200
13300
11400
9500
7600
5700
3800
1900
0
4.93
4.43
3.94
3.45
2.96
2.46
1.97
1.48
0.99
0.49
0.00
0 16 32 48 64 80 96 112 128 144 160 176 192 208 224 240 255

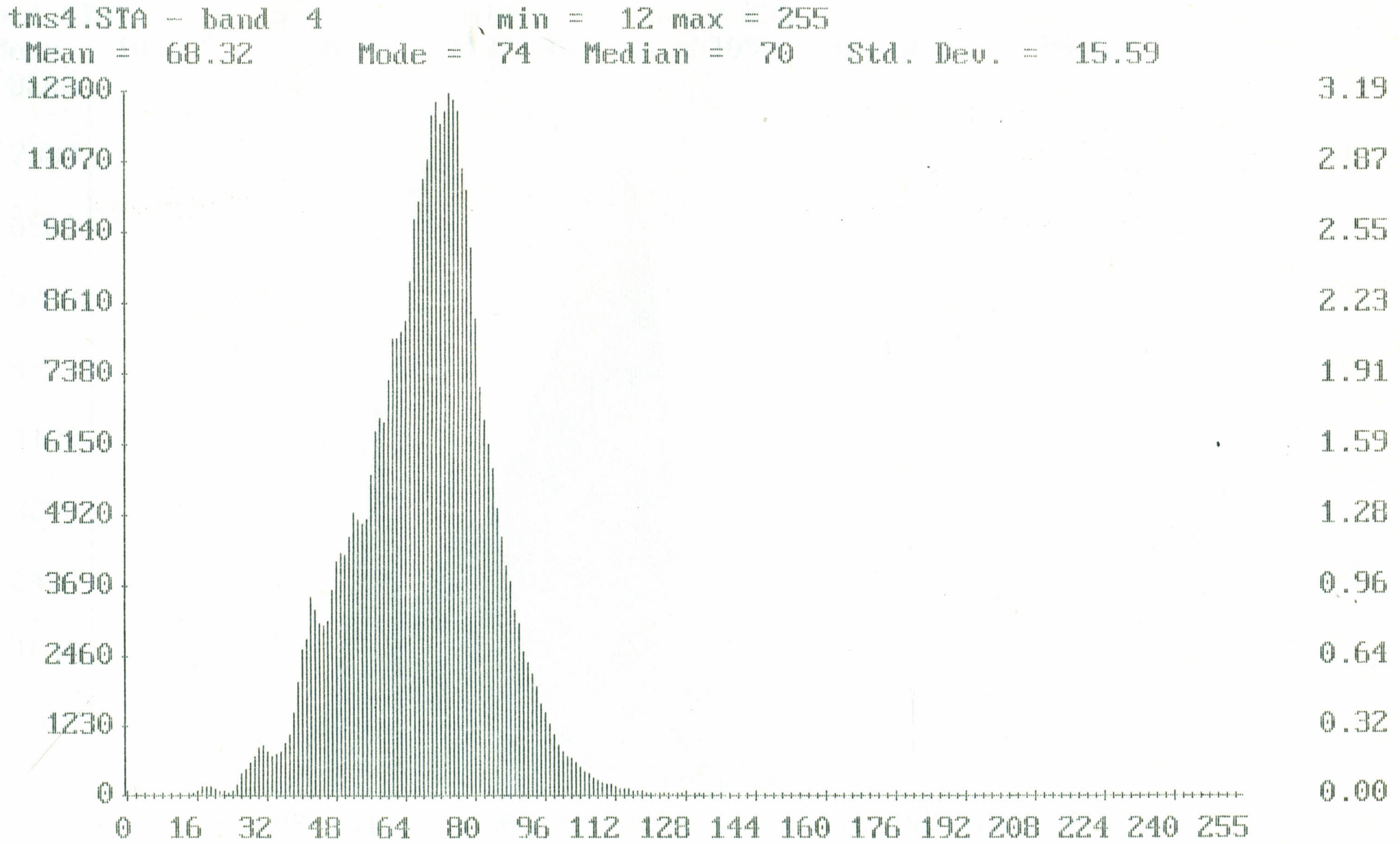
tms4.STA - band 4
min = 12 max = 255
Mean = 68.32
Mode = 74
Median = 70
Std. Dev. = 15.59
12300
11070
9840
8610
7380
6150
4920
3690
2460
1230
0
3.19
2.87
2.55
2.23
1.91
1.59
1.28
0.96
0.64
0.32
0.00
0 16 32 48 64 80 96 112 128 144 160 176 192 208 224 240 255

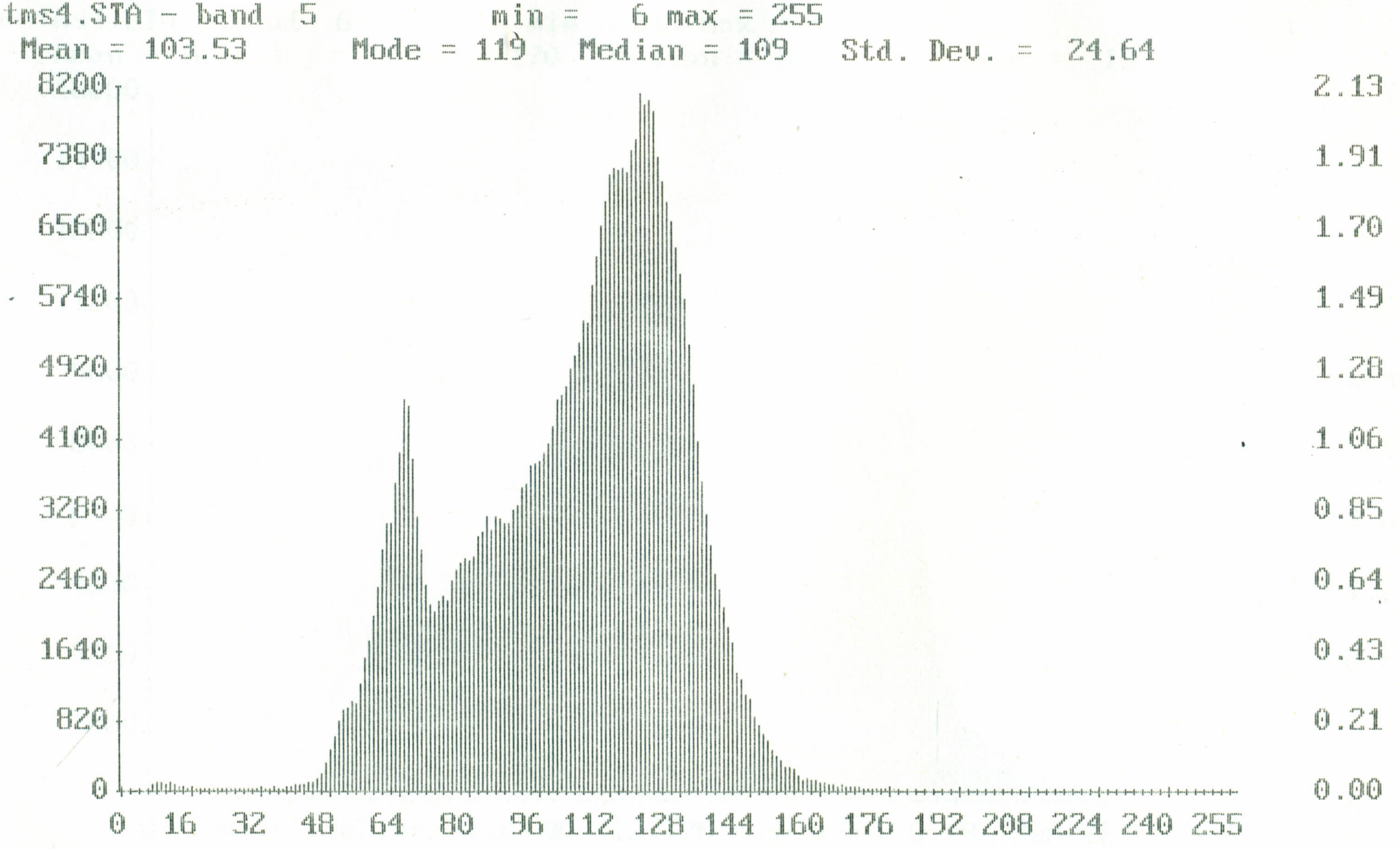
tms4.STA - band 5 min = 6 max = 255
Mean = 103.53 Mode = 119 Median = 109 Std. Dev. = 24.64
8200
7380
6560
5740
4920
4100
3280
2460
1640
820
0
2.13
1.91
1.70
1.49
1.28
1.06
0.85
0.64
0.43
0.21
0.00
0 16 32 48 64 80 96 112 128 144 160 176 192 208 224 240 255

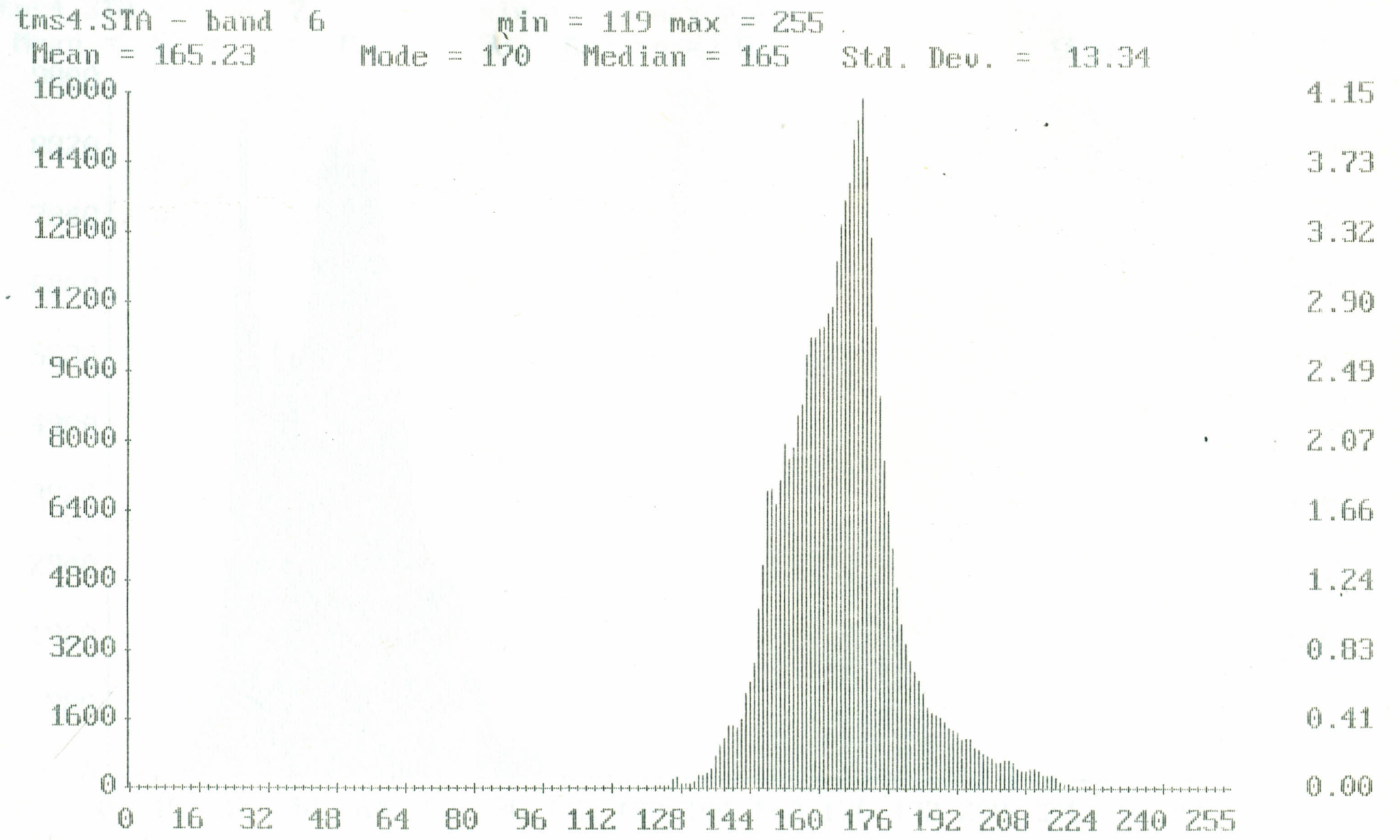
tms4.STA - band 6
min = 119 max = 255
Mean = 165.23
Mode = 170
Median = 165
Std. Dev. = 13.34
16000
14400
12800
11200
9600
8000
6400
4800
3200
1600
0
4.15
3.73
3.32
2.90
2.49
2.07
1.66
1.24
0.83
0.41
0.00
0 16 32 48 64 80 96 112 128 144 160 176 192 208 224 240 255

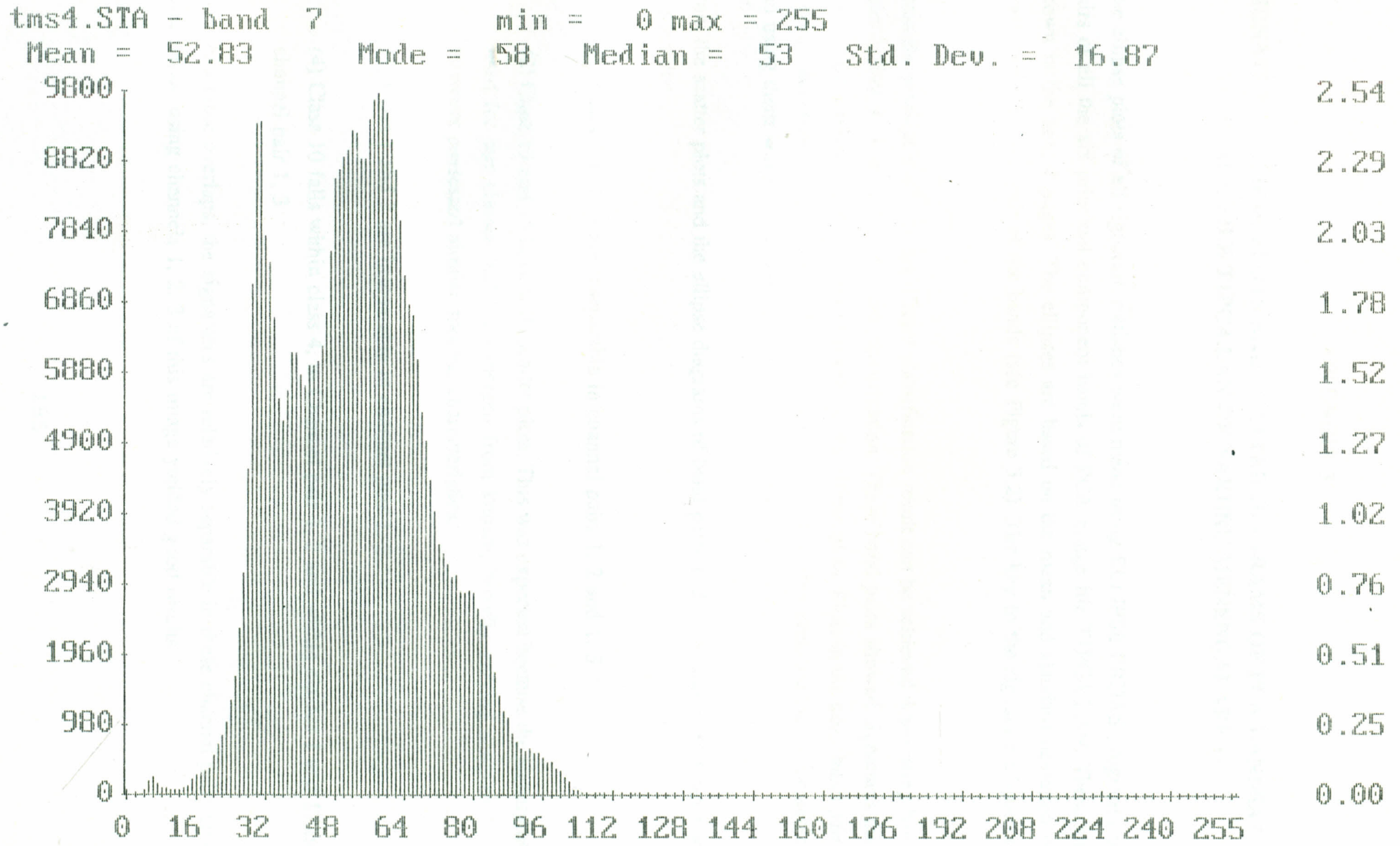
tms4.STA - band 7
min = 0 max = 255
Mean = 52.83
Mode = 58
Median = 53
Std. Dev. = 16.87
9800
8820
7840
6860
5880
4900
3920
2940
1960
980
0
2.54
2.29
2.03
1.78
1.52
1.27
1.02
0.76
0.51
0.25
0.00
0 16 32 48 64 80 96 112 128 144 160 176 192 208 224 240 255

APPENDIX 3.2

SIGNATURE ELLIPSE PLOTS AND SCATTER DIAGRAMS OF PCA LANDSAT-5 TM IMAGE FILE T1PCA.LAN OF NAKURU-MENENGAI AREA.

The ellipse plots of all signature statistics were made using ELLIPSE ERDAS program and pairs of all the six principal component bands of PCA image file T1PCA.LAN. These are shown in the next 4 pages. The ellipses are based on the mean and standard deviation of every signature in a pair of the bands (see Figure 3.2). The key to the signature ellipses is given in Table 3.9.

From the result of the plots, significant classification result can be achieved when using band pairs 1, 2 or 1, 3 or 1, 4 or 2, 3 for classification. These band pairs showed signatures that represented a relatively distinct set of pixels on the ellipse plots. Plots in the other band pairs overlap, and show a wide scatter. The class signatures in this other plots are thus inseparable, and using them will result in unpredictable result in the classification.

From the scatter plots and the ellipse diagrams of band pairs 1, 2; 1, 3; and 2, 3; it can also be seen that:

(1) Class 5 and 14 are inseparable in channel pairs 1, 2 and 1, 3.

(2) Class 13 and 15 have wide scatter plots. This was expected because the signatures used for this classes had been merged from known, broadly varying samples that however possessed similar spectral characteristics.

(3) Class 1 and 2 are inseparable in channel pair 1, 2

(4) Class 10 falls within class 4, in Channel pair 1, 2 and within classes 1 and 17 in channel pair 1, 3

Other than these overlaps, the signatures are relatively separable in these channel pairs and classification using channels 1, 2, 3 of this image yielded good results.

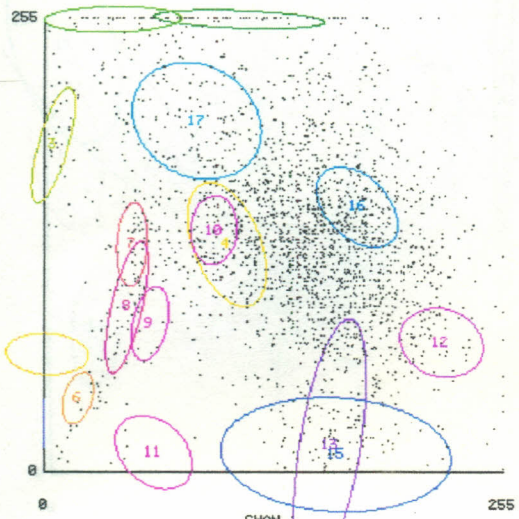

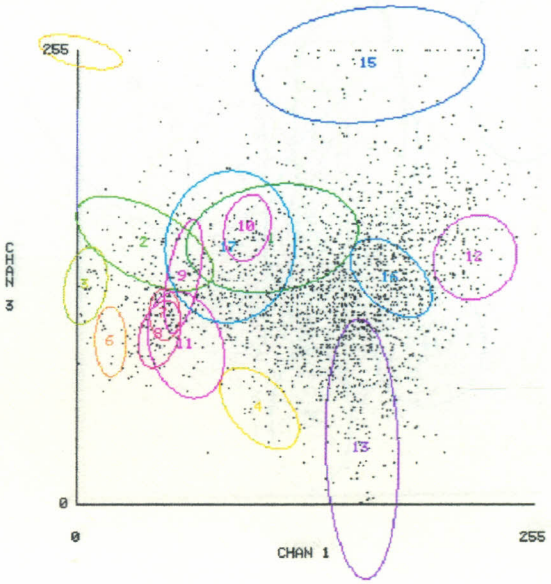

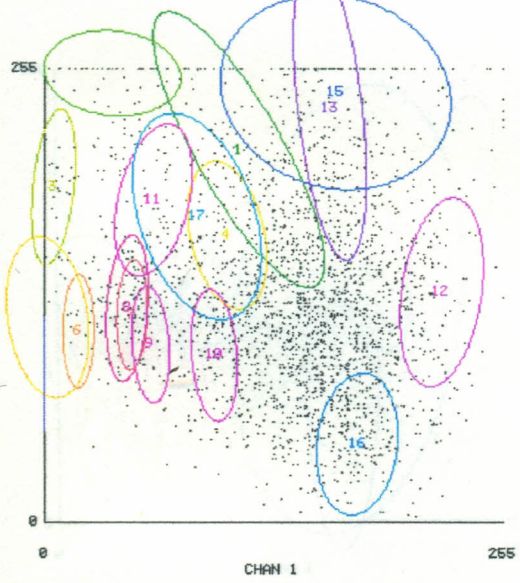

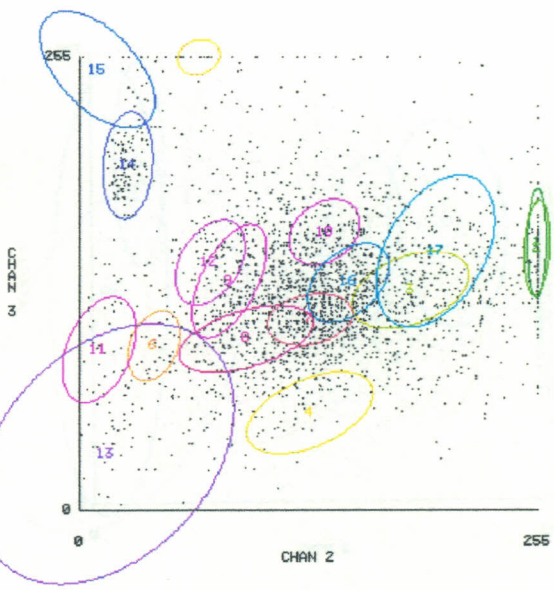

14-s67
15-s915
16-s1718
17-s2123

DATA : TIPCA.LAN
STAT : PCASIG.SBD
NAME : PCASIG.NAM

CHAN	MIN	MAX
1	0.0	255.0
2	0.0	255.0
3	0.0	255.0
4	0.0	255.0
5	0.0	255.0
6	0.0	255.0

2025

SIGNATURE ELLIPSE PLOT OF T1PCA

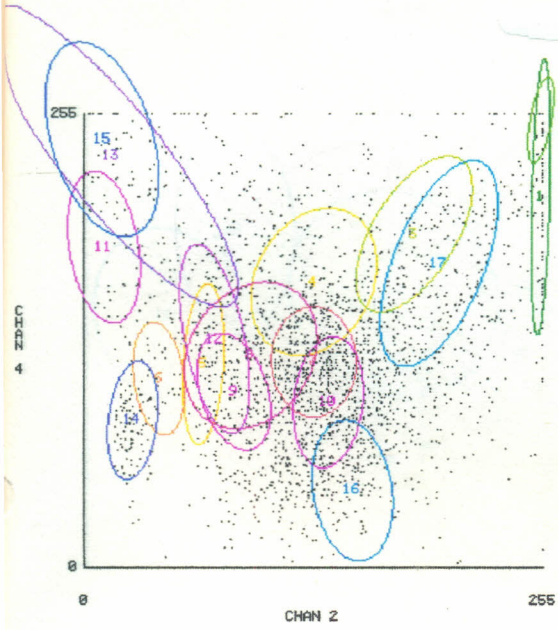

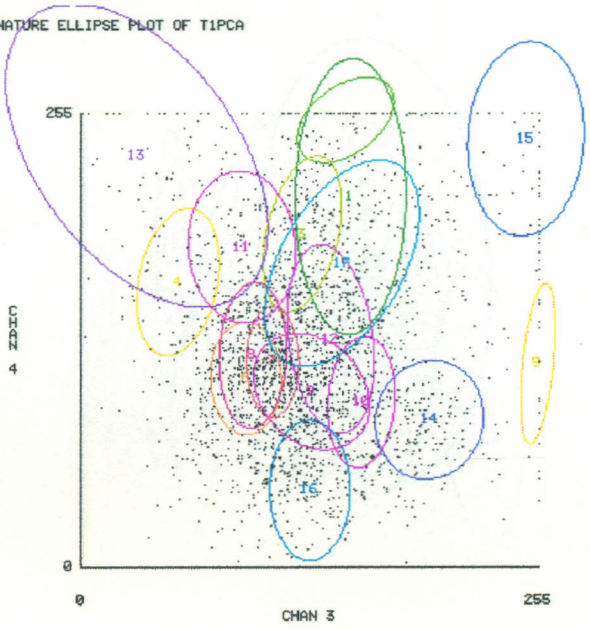

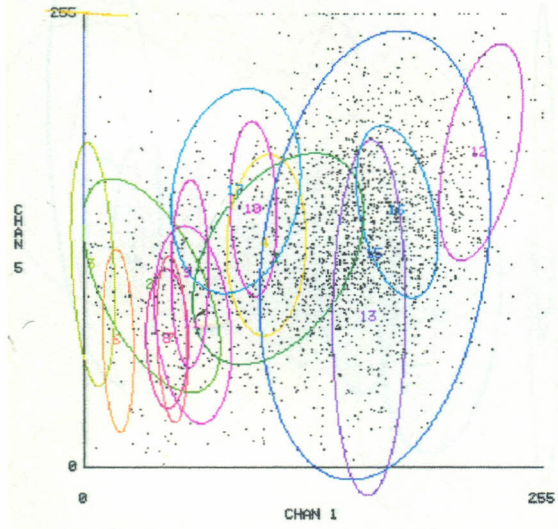

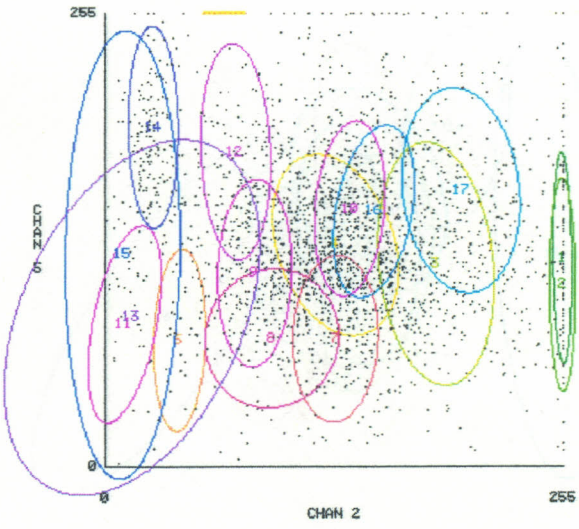

14-s67
15-s915
16-s1718
17-s2123

DATA : T1PCA.LAN
STAT : PCASIG.SBD
NAME : PCASIC.NAM

CHAN	MIN	MAX
1	0.0	255.0
2	0.0	255.0
3	0.0	255.0
4	0.0	255.0
5	0.0	255.0
6	0.0	255.0

162025

SIGNATURE ELLIPSE PLOT OF T1PCA

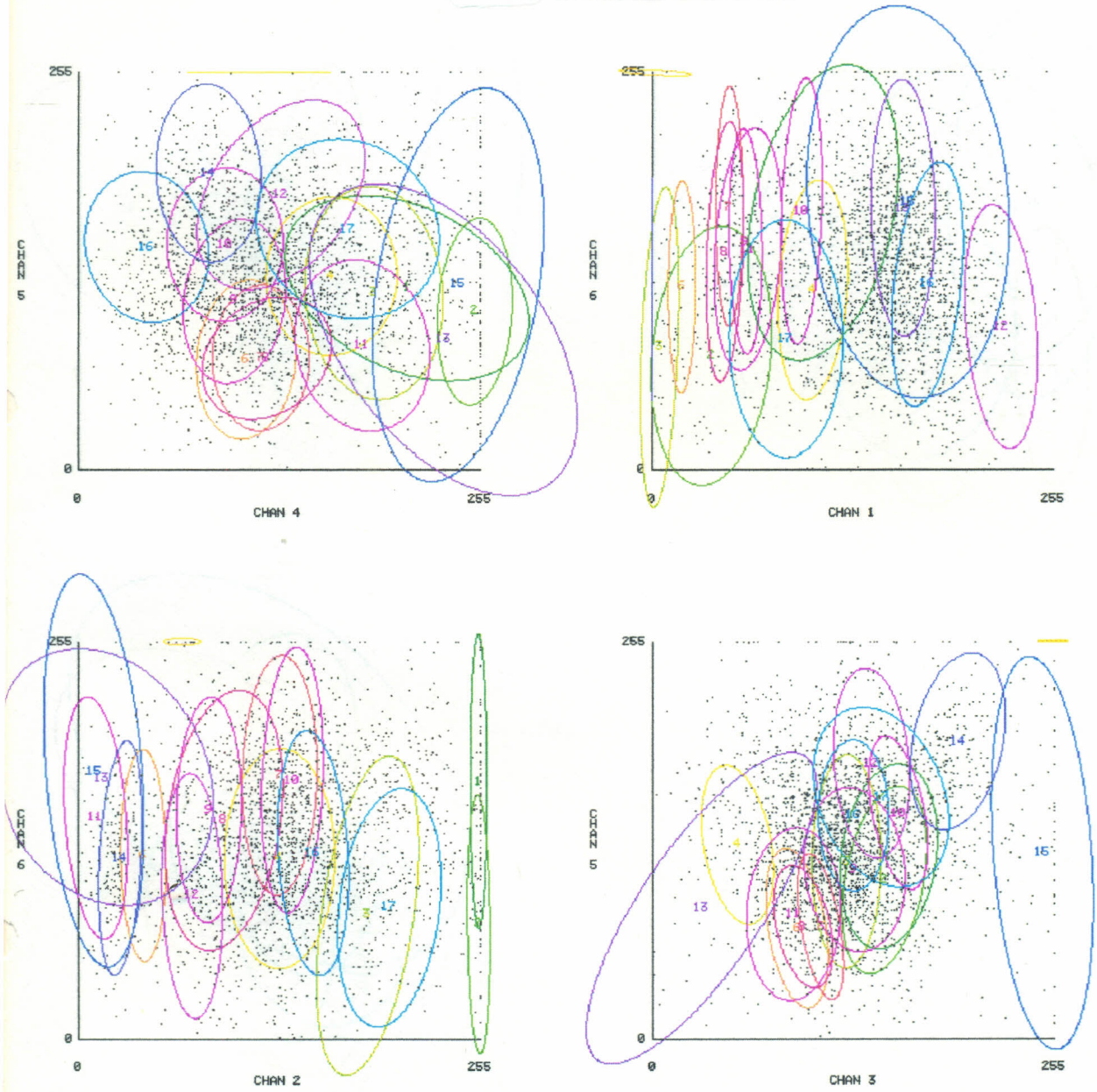

14-s67
15-s915
16-s1718
17-s2123

DATA : T1PCA.LAN
STAT : PCASIG.SBD
NAME : PCASIG.NAM

CHAN	MIN	MAX
1	0.0	255.0
2	0.0	255.0
3	0.0	255.0
4	0.0	255.0
5	0.0	255.0
6	0.0	255.0

5162025

SIGNATURE ELLIPSE PLOT OF T1PCA

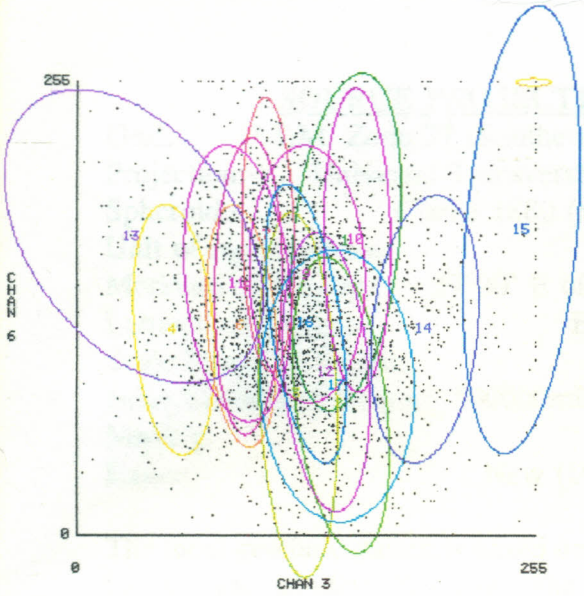

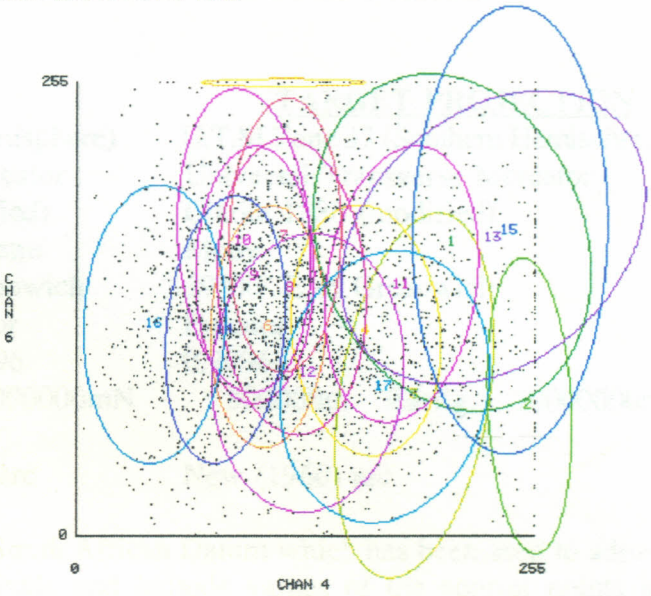

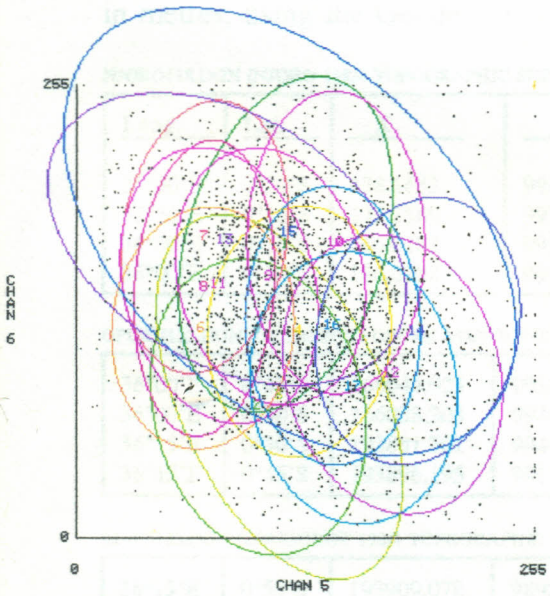

14-s67
15-s915
16-s1718
17-s2123

DATA : T1PCA.LAN
STAT : PCASIG.SBD
NAME : PCASIG.NAM

CHAN	MIN	MAX
1	0.0	255.0
2	0.0	255.0
3	0.0	255.0
4	0.0	255.0
5	0.0	255.0
6	0.0	255.0

5162025

APPENDIX 4.1

PROJECTION PARAMETERS OF 1:50000 TOPOGRAPHIC AND 1:125000 GEOLOGIC MAPS USED TO CREATE GIS DESIGN FILES OF TOPOLOGY, LITHOLOGY AND STRUCTURE OF THE STUDY AREA.

	SOURCE PROJECTION	TARGET PROJECTION
Grid:-	U.T.M. Zone 37 (Southern Hemisphere)	U.T.M Zone 37 (Southern Hemisphere)
Projection:-	Universal Transverse Mercator	Universal Transverse Mercator
Spheroid:-	Clarke 1880 (modified)	Clarke 1880 (modified)
Unit of measurement:-	Metre	Metre
Meridian of Origin:-	39°00' E of Greenwich	39°00' E of Greenwich
Latitude of Origin:-	Equator	Equator
Scale Factor at Origin:	0.9996	0.9996
False Co-ords of Origin:-	500000mE, 10000000mN	500000m East'g, 10000000m North'g
Datum:-	New (1960) arc	New (1960) arc

The local geodetic datum is based on the South African Datum which has been used to adjust the Kenyan geodetic network. The longitude and latitude values of the control points in degrees, minutes and seconds (d:m:s units) were converted to cartesian coordinate values (x,y) in metres, using the Geodetic Calculator.

NJORO118.DGN (NJORO 118/4 TOPOGRAPHIC SHEET)

Long.	Lat.	X	Y
35°50'E	0°30'S	138.1683	9944.6504
35°50'E	0°15'S	138.1580	9972.3252
36°00'E	0°15'S	166.0187	9972.3319
36°00'E	0°30'S	166.0282	9944.6637

NKRU119.DGN (NAKURU 119/3 TOPOGRAPHIC SHEET)

Long.	Lat.	X	Y
36°00'E	0°30'S	166028.208	9944663.910
36°00'E	0°15'S	166018.714	9972331.859
36°15'E	0°15'S	193873.005	9972337.963
36°15'E	0°30'S	193881.701	9944675.917

OPURU133.DGN (OL DOINYO OPURU 133/1 TOPOGRAPHIC SHEET)

36°00'E	0°45'S	166044.025	9916995.546
36°00'E	0°30'S	166028.208	9944663.710
36°15'E	0°30'S	193881.701	9944675.917
36°15'E	0°45'S	193896.195	9917013.855

NGSHA105.DGN (NGELESHA 105/1 TOPOGRAPHIC SHEET)

36°00'E	0°15'N	166018.717	10027668.141
36°00'E	0°25'N	166024.341	10046113.572
36°15'E	0°25'N	193878.158	10046103.399
36°15'E	0°15'N	193873.005	10027662.037

LONG133.DGN (LONGONOT 133/4 TOPOGRAPHIC SHEET)

36°15'E	0°55'S	193909.078	9898572.467
36°15'E	0°45'S	193896.195	9917013.855
36°30'E	0°45'S	221742.490	9917030.567
36°30'E	0°55'S	221754.198	9898592.891

NVSHA133.DGN (NAIVASHA 133/2 TOPOGRAPHIC SHEET)

36°15'E	0°45'S	193896.195	9917013.855
36°15'E	0°30'S	193881.701	9944687.059
36°30'E	0°30'S	221729.318	9944687.059
36°30'E	0°45'S	221742.490	9917030.567

GGIL119 (GILGIL 119/4 TOPOGRAPHIC SHEET)

36°15'E	0°30'S	193881.701	9944675.917
36°15'E	0°15'S	193873.005	9972337.963
36°30'E	0°15'S	221721.415	9972343.534
36°30'E	0°30'S	221729.318	9944687.059

KJBE134.DGN (KIJABE 134/3 TOPOGRAPHIC SHEET)

36°30'E	0°55'S	221754.198	9898592.891
36°30'E	0°45'S	221742.490	9917030.567
36°35'E	0°45'S	231023.375	9917035.782
36°35'E	0°55'S	231034.692	9898599.266

KNGOP134.DGN (KINANGOP 134/1 TOPOGRAPHIC SHEET)

36°30'E	0°45'S	221742.490	9917030.567
36°30'E	0°30'S	221729.318	9944687.059
36°45'E	0°30'S	240291.396	9944693.895
36°45'E	0°45'S	240303.687	9917040.821

NDRWA120.DGN (NDARAGWA 120/1 TOPOGRAPHIC SHEET)

36°30'E	0°15'S	221721.415	9972343.534
36°30'E	0°10'S	221719.951	9981562.356
36°35'E	0°10'S	231001.590	9981563.516
36°35'E	0°15'S	231003.005	9972345.273

NHURU105.DGN (NYAHURURU 105/4 TOPOGRAPHIC SHEET)

36°15'E	0°00'	193870.106	10000000.000
36°15'E	0°15'N	193873.005	10027662.037
36°30'E	0°15'N	221721.415	10027656.466
36°30'E	0°00'	221718.781	10000000.000

MNGAI119.DGN (MENENGAI 119/1 TOPOGRAPHIC SHEET)

36°00'E	0°15'S	166018.717	9972331.859
36°00'E	0°00'	166015.554	10000000.000
36°15'E	0°00'	193870.106	10000000.000
36°15'E	0°15'S	193873.005	9972337.963

SKTEK133.DGN (SAKUTIEK 133/3 TOPOGRAPHIC SHEET)

36°10'E	0°55'S	184626.093	9898565.226
36°10'E	0°45'S	184612.818	9917007.930
36°15'E	0°45'S	193896.195	9917013.855
36°15'E	0°55'S	193909.078	9898572.467

KJBE67.DGN (KIJABE GEOLOGY)

36°30'E	1°00'S	221760.930	9889374.048
36°30'E	0°30'S	221729.318	9944687.059
36°43'E	0°30'S	245859.581	9944695.854
36°43'E	1°00'S	245888.445	9889391.636

NKRU78.DGN (NAKURU GEOLOGY)

36°00'E	1°30'S	166028.208	9944663.710
36°00'E	0°00'	166015.554	10000000.000
36°30'E	0°00'	221718.781	10000000.000
36°30'E	0°30'S	221729.318	9944687.059

NJORO86.DGN (MOLO GEOLOGY)

35°49'E	0°30'S	145598.268	9944654.081
35°49'E	0°00'	145584.836	10000000.000
36°00'E	0°00'	166015.554	10000000.000
36°00'E	0°30'S	166028.208	9944663.710

KPPRI120.DGN (KIPIPIRI 120/3 TOPOGRAPHIC SHEET)

36°30'E	0°30'S	221729.318	9944687.059
36°30'E	0°15'S	221721.415	9972343.534
36°40'E	0°15'S	240284.021	9972346.952
36°40'E	0°30'S	240291.396	9944693.895

OROK119.DGN (OL JORO OROK 119/2 TOPOGRAPHIC SHEET)

36°15'E	0°15'S	193873.005	9972337.963
36°15'E	0°00'	193870.106	10000000.000
36°30'E	0°00'	221718.781	10000000.000
36°30'E	0°15'S	221721.415	9972343.534

SOLAI105.DGN (SOLAI 105/3 TOPOGRAPHIC SHEET)

36°00'E	0°00'	166015.554	10000000.000
36°00'E	0°15'N	166018.717	10027668.141
36°15'E	0°15'N	193873.005	10027662.037
36°15'E	0°00'	193870.106	10000000.000

MAU132.DGN (MAU NAROK 132/2 TOPOGRAPHIC SHEET)

35°55'E	0°45'S	156758.570	991689.087
35°55'E	0°30'S	156742.312	9944659.405
36°00'E	0°30'S	166028.208	9944663.710
36°00'E	0°45'S	166044.025	9916995.546

KPPRI12.DGN (NYERI GEOLOGY)

36°30'E	0°30'S	221729.318	9944687.059
36°30'E	0°10'S	221719.951	9981562.356
36°43'E	0°10'S	245851.028	9981565.288
36°43'E	0°30'S	245859.581	9944695.854

NVSHA55.DGN (NAIVASHA GEOLOGY)

36°00'E	1°00'S	166066.169	9889327.358
36°00'E	0°30'S	166028.208	9944663.710
36°30'E	0°30'S	221729.318	9944687.059
36°30'E	1°00'S	221760.930	9889374.048

NYHRU78.DGN (LAKE HANNINGTON GEOLOGY)

36°00'E	0°00'	166015.554	10000000.000
36°00'E	0°25'N	166024.341	10046113.572
36°15'E	0°25'N	193878.158	10046103.399
36°30'E	0°00'	221718.781	10000000.000

MAU96.DGN (MAU GEOLOGY)

35°52'E	0°45'S	151186.947	9916985.127
35°52'E	0°30'S	151170.424	9944656.764
36°00'E	0°30'S	166028.208	9944663.710
36°00'E	0°45'S	166044.025	9916995.546

APPENDIX 4.2

GIS ATTRIBUTE DATA OF LITHOLOGY OF THE ABERDARE DETACHMENT AREA

litho_value	litho_class	litho_category	lithology	litho_description	keywords	period	symbol
100	sedimentary		alluvium	alluvium in lake and swamp basins		recent	Ql_6
100b	sedimentary		talus	screes and rock fall	superficial	recent	Ql_5
111	sedimentary		volcanic_ soil	superficial deposits	superficial	recent	Qv
103	igneous	extrusive	trachyte	glassy, ropy,blocky flows (Upper Menengai series	flow	recent	Qvt_1
106	sedimentary		silt	stratified deltaic saline beach deposits	beach/saline/stratifie d	recent	Ql_4
107	sedimentary		silt	trona impregnated silt bordering soda lakes	beach/saline/stratifie d	recent	Ql_3
104	sedimentary		silt			recent	Ql_2
109	sedimentary		gravel/tuff/s ilt/sand	the silt is diatomaceous	diatomaceous	recent	Ql_1
114	sedimentary		silt/sand/gra vel	lacustrine deposits	lacustrine	recent	Ql
112	sedimentary		tuff	pumiceous tuff of Menengai series	pumiceous	recent	Qvf_2
113	sedimentary		pyroclastic	pyroclastic and sediments of Rongai plain and Mau slopes		recent	Qvf_1

219b,c	sedimentary		tuff	pumiceous tuff and sediments	pumiceous	recent	Qvf
105	igneous	extrusive	basalt	basalt forming cinder cones (lake Elmenteita)	vent	recent	Qvb
120	igneous	extrusive	trachyte			recent	Qvt
121	igneous	intrusive	obsidian			recent	Qvr
417i,ii,iii,iv	igneous	extrusive	trachyte	sequential lava flow	flow	pleistocene	Plt_5
122	igneous	intrusive	obsidian			pleistocene	Plr_2
123i,ii,iii,iv	igneous	extrusive	rhyolite	sequential lava flows	flow	pleistocene	Plr_1
124i,ii,iii,iv	igneous	extrusive	phonolite	sequential lava flows	flow	pleistocene	Plp_3
125	igneous	extrusive	trachyte			pleistocene	Plt_4
126	igneous	extrusive	basalt			pleistocene	Plb_5
127	igneous	intrusive	comendite			pleistocene	Plr
127a	sedimentary		pyroclastic	stratified pyroclastic sediments of Ol Jorowa Gorge	stratified	pleistocene	Pll3
128	igneous	extrusive	phonolite			pleistocene	Plp_2
220	igneous	extrusive	tuff	late valley filling of tuff unconformable to Bahati tuff		pleistocene	Plv_5
221	igneous	extrusive	tuff	reddish brown unstratified lapilli tuff	lapilli/unstratified	pleistocene	Plv_4
222	igneous	extrusive	tuff	unstratified lapilli tuff with green welded tuff (Larmudiac)	lapilli/unstratified/welded	pleistocene	Plv_3

223	sedimentary		tuff/silt/gravel/sand	water laid tuff, lacustrine/fluviatile gravel,silt, diatomaceous silt	lacustrine/diatomaceous	pleistocene	Pll_2
215	sedimentary		pyroclastic	Mau volcanic ash with poorly consolidated basal tuff altered to clay	ash/clay	pleistocene	Plf_5
217	igneous	extrusive	tuff	basal agglomeratic lapilli tuff	lapilli/agglomerate	pleistocene	Plv_2
210	igneous	extrusive	tuff	eutaxitic welded tuff	eutaxitic/welded	pleistocene	Plv_1
211	igneous	extrusive	trachyte			pleistocene	Plt_3
212	igneous	extrusive	phonolite	Kalelwa hill phonolite		pleistocene	Plp_1
213	sedimentary		pyroclastic	volcanic ash of Tindiret	ash	pleistocene	Plf_4
214	sedimentary		pyroclastic	volcanic ash and tuff of Mogotio	ash	pleistocene	Plf_3
129	igneous	extrusive	tuff	welded tuff	welded	pleistocene	Plv
626	sedimentary		pyroclastic	pyroclastic sediments		pleistocene	Plf_2
130	igneous	extrusive	basalt			pleistocene	Plb_4
627i,ii,iii,iv	igneous	extrusive	trachyte	sequential lava flows	flow	pleistocene	Plt_2
628	sedimentary		pyroclastic	pyroclastic sediments		pleistocene	Plf_1
131	igneous	extrusive	basalt			pleistocene	Plb_3
216	igneous	extrusive	basalt	mafic basalt of Londiani	mafic	pleistocene	Plb_2
230	igneous	extrusive	basalt	faulted vesicular olivine basalt of Elmenteita	vesicular/olivine	pleistocene	Plb_1
231, 231b	sedimentary		pyroclastic	pyroclastic with agglomeratic tuff	agglomerate	pleistocene	Plf

232	sedimentary			lake beds of Kariandus and Soysambu with graded pumice tuff & diatomite	diatomaceous	pleistocene	Pll_1
240	sedimentary			lacustrine sediments and graded tuff	lacustrine	pleistocene	Pll
241	igneous	extrusive	trachyte	Gilgil phonolitic trachyte	phonolitic	pleistocene	Plt_1
242	igneous	extrusive	phonolite	Ronda hill phonolite		pleistocene	Plp
243	igneous	extrusive	basalt	porphyritic olivine basalt (Mbaruk basalt)	porphyritic/olivine	pleistocene	Plb
244	igneous	extrusive	trachyte	porphyritic trachyte	porphyritic	pleistocene	Plt
310	igneous	extrusive	trachyte	trachyte and quartz trachyte of Londiani and Kilombe	silicic	pliocene	Tvt_3
311	igneous	extrusive	phonolite	Nyando valley phonolite		pliocene	Tvp_5
312	igneous	extrusive	phonolite	Tindiret phonolite		pliocene	Tvp_4
313	igneous	extrusive	basalt	Maji Mazuri basalt		pliocene	Tvb_6
314	igneous	extrusive	basalt	alkaline basalt of Molo plateau	alkaline	pliocene	Tvb_5
320	sedimentary			sediments of Londiani and Maji Mazuri		pliocene	Tl_1
410	igneous	extrusive	tuff	eutaxitic welded tuff	eutaxitic	pliocene	Tvf_{12}
411	sedimentary		pyroclastic	black volcanic ash of Elbergon	ash	pliocene	Tvf_{11}
412	igneous	extrusive	tuff	grey and bleached agglomeratic lapilli tuff	lapilli	pliocene	Tvf_{10}
413	igneous	extrusive	tuff	pale grey eutaxitic welded tuff	eutaxitic	pliocene	Tvf_9

414	igneous	extrusive	tuff	pink to dark friable eutaxitic tuff	eutaxitic	pliocene	Tvf_8
415	igneous	extrusive	tuff	purple and grey devitrified tuff	devitrified	pliocene	Tvf_7
416	igneous	extrusive	tuff	basal eutaxitic tuff	eutaxitic	pliocene	Tvf_6
419	igneous	extrusive	tuff	clay-stone tuff with plant remain	clay	pliocene	Tvf_5
420	igneous	extrusive	tuff	welded vitreous tuff and ignimbrite	vitreous	pliocene	Tvf_4
421	igneous	extrusive	tuff	vitric pumice tuff, ignimbrite and welded tuff	vitreous	pliocene	Tvf_3
423	igneous	extrusive	trachyte	phonolitic trachyte	phonolitic	pliocene	Tvt_2
424	igneous	extrusive	trachyte	quartz trachyte and fragmental trachyte	silicic	pliocene	Tvt_1
425	igneous	extrusive	phonolite/trachyte	analcitic phonolite and subordinate trachyte	analcitic	pliocene	Tvp_3
426	sedimentary		silt/sand/gravel	lacustrine sediments of graded tuff and pumice sediments	lacustrine/tuff/pumiceous	pliocene	Tl
427	igneous	extrusive	basalt	olivine basalt (Turasha basalt)	olivine	pliocene	Tvb_4
610	igneous	extrusive	basalt	vesicular olivine basalt(Laikipia basalt)	vesicular/olivine	miocene	Tvb_3
611	igneous	extrusive	phonolite	trachytic phonolite (Sattima series)	trachytic	miocene	Tvp_2
612	igneous	extrusive	basalt	Laikipia basalt		miocene	Tvb_2
613	igneous	extrusive	tuff	welded tuff	welded	miocene	Tvf_2

615	igneous	extrusive	phonolite	fissile black grey analcitic phonolite	analcitic	miocene	Tvp_1
616	igneous	extrusive	phonolite	porphyritic phonolite (Rumuruti phonolite)	porphyritic	miocene	Tvp
617	sedimentary		pyroclastic	tuffaceous sediments of Samburu plateau		miocene	Tvf_1
618	igneous	extrusive	basalt	porphyritic olivine basalt	porphyritic/olivine	miocene	Tvb_1
620	igneous	extrusive	basalt	porphyritic olivine basalt (Samburu series)	porphyritic/olivine	miocene	Tvb
621	igneous	extrusive	tuff	graded pumice tuff intercalations in olivine basalt (Samburu series)	pumiceous	miocene	Tvf
625	igneous	extrusive	trachyte	trachyte of the younger Aberdare volcanic vents	vent	miocene	Tvt

The litho_centroid value was linked to the attribute data via unique identifiers, MS-link, generated by the GIS system. The columns 'lithology' and 'keywords', were first created in separate tables and later joined to other data using the litho_value as the link element to the MS-links.